Universitat Autònoma de Barcelona

Quatsomes as a novel nanocarrier for clinical delivery of small RNA

Ariadna Boloix Amenós

ADVERTIMENT. L'accés als continguts d'aquesta tesi doctoral i la seva utilització ha de respectar els drets de la persona autora. Pot ser utilitzada per a consulta o estudi personal, així com en activitats o materials d'investigació i docència en els termes establerts a l'art. 32 del Text Refós de la Llei de Propietat Intel·lectual (RDL 1/1996). Per altres utilitzacions es requereix l'autorització prèvia i expressa de la persona autora. En qualsevol cas, en la utilització dels seus continguts caldrà indicar de forma clara el nom i cognoms de la persona autora i el títol de la tesi doctoral. No s'autoritza la seva reproducció o altres formes d'explotació efectuades amb finalitats de lucre ni la seva comunicació pública des d'un lloc aliè al servei TDX. Tampoc s'autoritza la presentació del seu contingut en una finestra o marc aliè a TDX (framing). Aquesta reserva de drets afecta tant als continguts de la tesi com als seus resums i índexs.

ADVERTENCIA. El acceso a los contenidos de esta tesis doctoral y su utilización debe respetar los derechos de la persona autora. Puede ser utilizada para consulta o estudio personal, así como en actividades o materiales de investigación y docencia en los términos establecidos en el art. 32 del Texto Refundido de la Ley de Propiedad Intelectual (RDL 1/1996). Para otros usos se requiere la autorización previa y expresa de la persona autora. En cualquier caso, en la utilización de sus contenidos se deberá indicar de forma clara el nombre y apellidos de la persona autora y el título de la tesis doctoral. No se autoriza su reproducción u otras formas de explotación efectuadas con fines lucrativos ni su comunicación pública desde un sitio ajeno al servicio TDR. Tampoco se autoriza la presentación de su contenido en una ventana o marco ajeno a TDR (framing). Esta reserva de derechos afecta tanto al contenido de la tesis como a sus resúmenes e índices.

WARNING. The access to the contents of this doctoral thesis and its use must respect the rights of the author. It can be used for reference or private study, as well as research and learning activities or materials in the terms established by the 32nd article of the Spanish Consolidated Copyright Act (RDL 1/1996). Express and previous authorization of the author is required for any other uses. In any case, when using its content, full name of the author and title of the thesis must be clearly indicated. Reproduction or other forms of for profit use or public communication from outside TDX service is not allowed. Presentation of its content in a window or frame external to TDX (framing) is not authorized either. These rights affect both the content of the thesis and its abstracts and indexes.

Quatsomes as a novel nanocarrier for clinical delivery of small RNA

PhD thesis presented by

Ariadna Boloix Amenós

To obtain the degree of

PhD for the Universitat Autònoma de Barcelona (UAB)

PhD thesis carried out in the Translational Research in Child and Adolescent Cancer Research Group, at Vall d'Hebron Research Institute (VHIR), and at the Nanomol Group, at the Institute of Materials Science of Barcelona (ICMAB-CSIC)

Thesis affiliated to the Department of Biochemistry and Molecular Biology from the UAB, in the PhD program of Biochemistry, Molecular Biology and Biomedicine

Universitat Autònoma de Barcelona, September 17th 2019

Directors

Dr. Miguel F. Segura Ginard | Dra. Nora Ventosa Rull

PhD Candidate
Ariadna Boloix Amenós

Tutor
Dr. José Miguel Lizcano de Vega

"Cal tenir aspiracions elevades,

expectatives moderades

i necessitats petites".

Heinrich Von Stein

A la meva família de sempre

i a la que es contrueix dia a dia.

Acknowledgments

Aquesta tesi no l'hauria pogut realitzar sense l'ajuda de molta gent que en sigui o no conscient ha influït en el seu desenvolupament.

Voldria agraïr especialment als meus directors de tesis, al Dr. Miquel Segura i la Dra. Nora Ventosa per confiar en mi durant els quatre anys que he estat duent a terme el projecte Smarty. Moltessímies gràcies Miquel per donar-me l'oportunitat de formar part del grup, per fer-me descobrir la ciència com una forma de viure, per ensenyar-me no només els coneixements que he adquirit sinó també l'esperit crític i la teva capacitat resolutiva. Moltes gràcies Nora a tu també per obrir-me les portes del teu laboratori, per premetre'm ampliar la meva visió de la ciència i de les possibilitats que tenim entre mans. També t'he d'agraïr que em contagiessis la teva il·lusió i passió pel projecte, així com els ànims que m'has anat donant al llarg d'aquests anys.

Agraeixo també al Dr. Sánchez de Toledo i la Dra. Soledad Gallego la seva predisposició per aproximar-nos a la clínica fent-nos adonar de la importància de la nostra recerca, així com de la oportunitat que ens han ofert de ser conscients de la necessitat de seguir investigant. Gràcies també pels vostres consells i aportacions científiques que sovint ens ajuden a ser més pràctics i a no perdre el sentit de la nostra investigació.

Moltes gràcies també al Servei de Microscòpia de la UAB, principalment al Martí, per la realització de les imatge de cryo-TEM.

Voldria agrair també al Dr. Lorenzo Albertazzi i la Natalia Feiner per col·laborar amb nosaltres per entendre millor els sistemes emprats en aquesta tesi.

Finalment, moltes gràcies als membres i ex-membres d'ambdós grups Oncologia Pediàtrica i Nanomol, per ensenyar-me, aconsellar-me i estar al meu costat aquests anys.

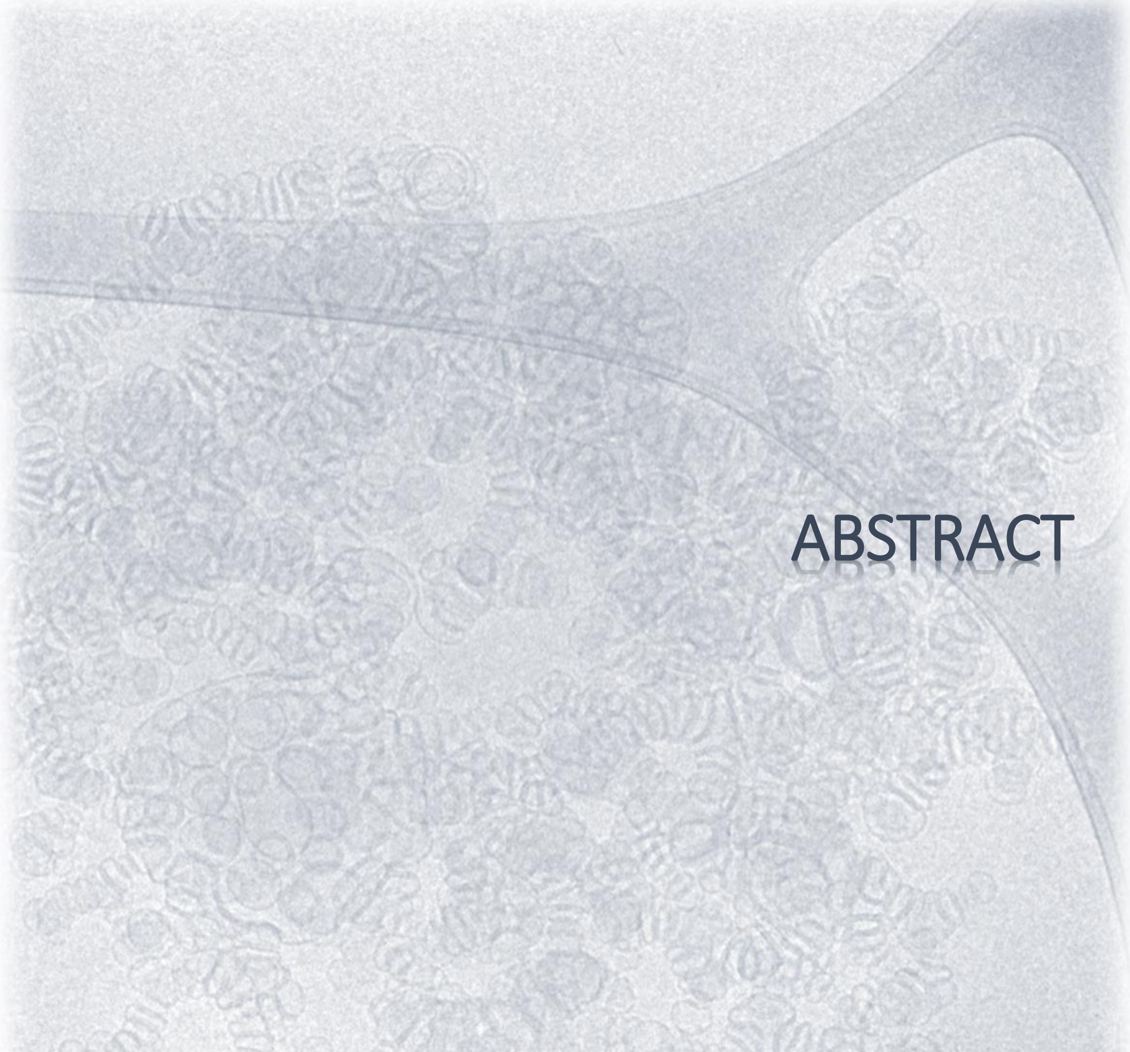

ABSTRACT

Abstract

Current medicines are directed to modify the functionality of proteins, which represent only 2% of human transcribed genome. However, the possibility of targeting the transcriptome, i.e. ~ 70% of the genome, using RNA-based therapies will expand significantly the number of druggable targets. MicroRNA (miRNA), endogenous small non-coding RNAs, could be used to target the transcriptome interfering in the translation and stability of target mRNA genes. Nevertheless, miRNA-based therapies have not reached the market due, in part, to suboptimal biodistribution and short half-life in bloodstream. Nanomedicine promises the precise delivery of nucleic acids into tumours with reduced off-target toxicities. Hence, conjugation of miRNA to nanoparticles could be a good strategy to test anti-tumour effects of miRNAs *in vivo*. However, there is still a lack of a standard formulation for their clinical administration.

In this thesis, the tumour suppressive miR-323a-5p was selected as a proof of concept for miRNA-based therapies to treat high-risk neuroblastoma (NB) tumours. To move forward this discovery to clinical applications and to overcome the current challenges for delivering small RNA for cancer treatment, we have designed and synthetized a clinical formulation based on novel nanoparticles, called Quatsomes (QS). QS are non-liposomal lipid nanovesicles prepared using the DELOS-SUSP technology. Compared to other nanoparticles, such as liposomes, QS are small unilamellar vesicles with high homogeneity and positive charge, which grants an excellent long-term colloidal stability and the efficient entrapment of small RNA (sRNA) in their surface. New QS-based formulations were designed to optimize the complexation of potentially-therapeutic small RNA (i.e. miR-323a-5p and siCCND1) which can halt the progression of cancer cells. QS-miR-323a-5p and QS-siCCND1 complexes showed efficient miRNA complexation, enhanced resistance to nucleases, high transfection efficiency and intracellular accumulation of mature miRNA forms. From the functional point of view, treatment of NB cells with miR-323a-5p nanoconjugates induced downregulation of bona fide miR-323a-5p targets, such as CCND1 or CHAF1A, at mRNA and protein level and induced a reduction in tumour cell viability.

In summary, the results achieved in this thesis support the application of QS-sRNA nanoconjugates as a potential tool for the treatment of human disease.

Resum

Les teràpies actuals estan dirigides a modificar la funcionalitat de les proteïnes, les quals només representen el 2% del genoma humà transcrit. No obstant, la possibilitat de dirigir-les a actuar sobre tot el transcriptoma, aproximadament un 70% del genoma, mitjançant l'aplicació de teràpies basades en ARN pot augmentar significativament el nombre de dianes terapèutiques. Els microARN (miARN), petits ARNs endògens no codificadants, podrien ser utilitzats per atacar el transcriptoma interferint en la traducció i l'estabilitat del ARNm diana. No obstant, les teràpies basades en miARN encara estan lluny de la seva aplicació clínica degut, en part, a que presenten una biodistribució subòptima i a una vida mitja curta en el torrent sanguini. El camp de la nanomedicina promet millorar el lliurament precís d'àcids nucleics als tumors diana reduïnt-ne els efectes adversos. Per tant, la conjugació dels miARN amb nanopartícules podria ser una bona estratègia per obtenir els efectes antitumorals dels miRNAs *in vivo*. No obstant, encara és necessari el descobriment d'una formulació de referència capaç d'aministrar miARN a la clínica.

En aquesta tesi, el miR-323a-5p, el qual té propietats supressores de tumors, es va seleccionar com a prova de concepte de les teràpies basades en miARN per tal de tractar el neuroblastoma (NB) d'alt risc. Per implementar-ho a la clínica, en aquesta tesi s'han dissenyat i sintetitzat unes nanopartícules basades en una nova formulació clínicament administrable anomenada Quatsomes (QS), capaç de transportar petits ARN per al tractament del càncer. Els QS són nanovesícules lípidiques no liposomals preparades mitjançant la tecnologia DELOS-SUSP. En comparació a altres nanopartícules, com els liposomes, els QS són petites nanovesícules unilamel·lars amb una alta homogeneïtat i càrrega positiva, la qual que els atorga una excel·lent estabilitat col·loïdal a llarg termini i la capacitat de conjugar-se de forma eficient amb petits ARNs en la seva superfície. Concretament, les noves formulacions de QS dissenyades s'han optimitzat per millorar la seva capacitat de complexació de petits ARN potencialment terapèutics (com ara el miR-323a-5p i el siCCND1), els quals s'ha observat que poden frenar la progressió de les cèl·lules canceroses de neuroblastoma. Els conjugats de QS i miARN van demostrar una eficient complexació del petit ARN, resistència a les nucleases, una elevada eficiència de transfecció i la posterior acumulació del miARN madur a nivell intracel·lular. Des del punt de vista funcional, el tractament de les cèl·lules de NB amb els nanoconjugats QS-miR-323a-5p va induir la modificació dels gens diana del miR-323a-5p, com són CCND1 o CHAF1A, a nivell de ARNm i proteïnes i van induir una reducció de la viabilitat de les cèl·lules tumorals.

En conclusió, els resultats aconseguits en aquesta tesi donen suport a l'aplicació dels nanoconjugats basats en QS i petits ARN com a eina potencial per al tractament de malalties humanes.

Resumen

Las terapias actuales están dirigidas a modificar la funcionalidad de las proteínas, las cuales representan solo el 2% del genoma humano transcrito. Sin embargo, la posibilidad de dirigirlas hacia todo el transcriptoma, aproximadamente el 70% del genoma, utilizando terapias basadas en ARN puede ampliar significativamente el número de dianas terapéuticas. Los microARN (miARN), son pequeños ARN no codificantes endógenos, que podrían usarse para atacar el transcriptoma interfiriendo en la traducción y la estabilidad del ARNm diana. No obstante, las terapias basadas en miARN no han llegado aún al mercado debido, en parte, a una biodistribución subóptima y una vida media corta en el torrente sanguíneo. La nanomedicina permite la administración de ácidos nucleicos de una forma más precisa en tumores, reduciendo así los posibles efectos adversos. Por lo tanto, la conjugación de miRNA a nanopartículas podría ser una buena estrategia para obtener los efectos antitumorales esperados del miARN *in vivo*. A pesar de sus ventajas, todavía se requiere el desarollo de una formulación de referencia para su administración clínica.

En esta tesis, el miR-323a-5p, con propiedades antitumorales, se seleccionó como prueba de concepto de las terapias basadas en miARN para tratar tumores de neuroblastoma (NB) de alto riesgo. Para implementar este descubrimiento a la clínica, en esta tesi se ha diseñado y sintetizado una formulación basada en nanopartículas novedosas, llamadas Quatsomas (QS), para administrar pequeños ARN para el tratamiento del cáncer. Los QS son nanovesículas lipídicas no liposomales preparadas con la tecnología DELOS-SUSP. En comparación con otras nanopartículas, como los liposomas, los QS son pequeñas vesículas unilamelares de alta homogeneidad y carga positiva, lo que les garantiza una excelente estabilidad coloidal a largo plazo y la capacidad de conjugarse eficiente con pequeños ARN en su superficie. Concretamente, las nuevas formulaciones diseñadas están basadas en optimizar los QS para mejorar su capacidad de complejación con pequeños ARN potencialmente terapéuticos (como es el caso del miR-323a-5p y de siCCND1) que pueden detener la progresión de las células cancerosas. Los conjugados QS-miR-323a-5p y QS-siCCND1 mostraron una complejación del ARN eficiente, mayor resistencia a las nucleasas, alta eficiencia de transfección y acumulación intracelular de las formas maduras del miARN. Desde el punto de vista funcional, el tratamiento de las células NB con los nanoconjugados de QS-miR-323a-5p indujo la regulación negativa de los genes diana del miR-323a-5p, como CCND1 o CHAF1A, a nivel de ARNm y proteína e indujo una reducción en la viabilidad de las células tumorales.

En conclusión, los resultados de esta tesis respaldan la aplicación de nanoconjugados basados en QS y pequeños ARN como potencial herramienta para el tratamiento de enfermedades humanas.

Table of contents

ACKNOWLEDGMENTS .... **I**

ABSTRACT .... **III**

RESUM .... **V**

RESUMEN .... **VII**

TABLE OF CONTENTS .... **IX**

LIST OF FIGURES .... **XIV**

LIST OF TABLES .... **XVIII**

ABBREVIATIONS .... **XX**

1. INTRODUCTION **3**

- 1.1. RNA-BASED THERAPIES 3
- 1.2. SMALL RNA 4
  - *1.2.1. microRNA (miRNA) 4*
  - *1.2.2. MicroRNA in paediatric cancer 8*
  - *1.2.3. Role of miRNA in neuroblastoma 9*
    - 1.2.3.1 . Pathogenesis of Neuroblastoma 9
    - 1.2.3.2 Mechanisms of miRNA deregulation in Neuroblastoma 10
    - 1.2.3.3 MiRNA act as oncogenes or tumour suppressors in NB 11
  - *1.2.4. MiRNA as a therapeutic tool in Neuroblastoma 14*
  - *1.2.5. Advantages and limitations of the use of miRNA as therapeutic tools 15*
- 1.3. RNA DELIVERY SYSTEMS 18
  - *1.3.1. Viral vectors 18*
  - *1.3.2. Non-viral vectors 19*
    - 1.2.3.1 Inorganic nanoparticles 20
    - 1.2.3.2 Organic nanoparticles 20
  - *1.3.3. Advantages and limitations of nanoparticles for drug delivery 28*
- 1.4. USE OF MIRNA AS THERAPEUTIC TOOLS IN CLINICAL TRIALS 33

2. HYPOTHESIS AND OBJECTIVES **39**

3. MATERIALS AND METHODS **43**

- 3.1 MATERIALS 43
  - *3.1.1 Lipids and surfactants 43*
  - *3.1.2 Neuroblastoma cell lines 43*
  - *3.1.3 sRNA 44*

3.2 METHODS 46
3.2.1. Cell transfection of lipoplexes 46
3.2.2. microRNA functional high-throughput library screening 46
3.2.3. Cell proliferation assays with lipoplexes 48
3.2.4. Cell cycle analysis 49
3.2.5. Cell death assay 49
3.2.6. Western Blot 49
3.2.7. In silico miRNA-target analysis 52
3.2.8. Quantitative real-time PCR (qPCR) 52
3.2.9. 3' UTR Luciferase Reporter Assay 54
3.2.10. Nanoparticles preparation 55
3.2.10.1. Quatsomes synthesis by DELOS-SUSP 55
3.2.10.2. Synthesis of Quatsome-based vesicular systems prepared by sonication 60
3.2.10.3. MKC micelles synthesis by self-assembly 61
3.2.10.4. Nanoparticles purification by diafiltration 61
3.2.10.5. Nanoparticles concentration by diafiltration 63
3.2.11. Physicochemical characterization of QS 63
3.2.11.1. Dynamic Light scattering (DLS) measurements 63
3.2.11.2. Morphology by Cryo-TEM 65
3.2.11.3. Membrane components concentration by gravimetric analysis. 66
3.2.11.4. pH stability and buffering capacity 67
3.2.11.5. Fluorescent characterization by UV-Vis 68
3.2.12. QS-sRNA and MKC micelles complexes formation with miRNA 69
3.2.13. Complexation efficiency of miRNA in QS 72
3.2.14. Cell Proliferation assays with QS-miRNA complexes 73
3.2.15. Internalization of QS-miRNA complexes in NB cells 73
3.2.16. QS$_4$-miRNA complexes stability in presence of serum 74
3.2.17. RNAse A protection assays 74
3.2.18. FRET analysis 74
3.2.19. Statistical analysis 76

4. RESULTS 79

4.1. TUMOUR SUPPRESSOR MIR-323A-5P IS A POTENTIAL THERAPEUTIC TOOL FOR NB 79
4.1.1. Identification of miRNA with tumor-suppressive functions in NB by a functional high-throughput screening 79
4.1.2. Restoration of miRNA located at 14q32 reduces cell viability in NB cell lines 80
4.1.3. Ectopic expression of miR-323a-5p halts cell cycle progression and induces apoptosis in NB . 82
4.1.4. MiR-323a-5p target cell cycle and survival genes 83

4.1.5. CCND1, CHAF1A and INCENP silencing mostly reproduces miR-323a-5p overexpression effects 85
4.2. Quatsomes are good nanocarriers for the delivery of small RNAs 87
New designed Quatsomes for miRNA transfection in vitro 87
4.2.1. Selection of the Quatsomes as small RNA nanocarriers 87
4.2.2. QS are capable of complexing small RNA 101
4.2.3. miR-497-5p is efficiently transfected by QS$_0$-miR-497-5p and QS$_1$-miR-497-5p complexes ... 103
4.2.4. QS$_{0-1}$-miR-497-5p complexes do not modify the expression of miR-497 direct targets 104
Innovative engineered Quatsomes for intracellular delivery of sRNA 107
4.2.5. Synthesis and physicochemical characterization of QS with different pH sensitive behaviour 107
4.2.6. High efficiency of QS-miRNA complexes formation 110
4.2.7. QS$_{1-4}$-miRNA complexes not impair cell viability 114
4.2.8. QS-miRNA formulations efficiently internalized into SK-N-BE(2) cells 115
4.2.9. QS-miR-323a-5p are efficiently transfected and raise intracellular levels of miR-323a-5p 118
4.2.10. Only QS$_4$-miR-323a-5p modulates miR-323a-5p target expression 119
4.2.11. QS$_4$ is also a suitable delivery system for sRNA delivery 125
4.2.12. QS$_4$-miRNA complexes are stable in biological fluids and protect miRNA from RNAses 127
4.3. Cellular dynamics of QS$_4$-miRNA demonstrated miRNA release from QS$_4$ 131
4.3.1. QS labelling for in vitro and in vivo tracking 131
4.3.2. ^{Dil}QS present similar complexation efficiency than plain QS 135
4.3.3. Fluorescent QS$_4$-miRNA complexes demonstrated FRET efficiency 138
4.3.4. miRNA is released from QS$_4$ after transfection 140

5. DISCUSSION 147

5.1. The present and the future of RNA-based therapies 147
5.2. Finding tumor-suppressive miRNAs in NB 148
5.3. Clinical delivery of microRNAs 151
5.4. Quatsomes as a nanomedical-delivery platform 152
5.4.1. QS as a nanocarriers for protein-based medicinal products 153
5.4.2. QS as potential nanocarriers for small RNAs 153
Selection of QS membrane components 154
QS physicochemical properties impact on cellular uptake and viability 155
QS complexation efficiency with sRNA 157
QS and QS-miRNA complexes are biocompatible 160
Study of QS-miRNA mechanism of cellular uptake 161
Tuning QS for cargo release 168
5.4.3. Road into clinics of QS nanocarrier 171
Scaling-up QS production 171

QS suitability to deliver other sRNAs.......... 172
Integrity of QS-miRNA complexes in biological fluids 172
Biodistribution of QS-miRNA complexes.......... 173
Specific tumour targeting of QS nanocarrier.......... 176

6. CONCLUSIONS 181

7. REFERENCES.......... 185

8. PUBLICATIONS.......... 203

9. ANNEXES 207

List of figures

FIGURE 1. SCHEMATIC CLASSIFICATION OF NON-CODING RNAS(NCRNAS). 3

FIGURE 2. MIRNA BIOGENESIS MACHINERY IN EUKARYOTES.. 7

FIGURE 3. PROPOSED STRATEGIES USING MIRNA-BASED THERAPIES AGAINST CANCER. 15

FIGURE 4. CLASSIFICATION OF NANOPARTICLES USED FOR DRUG DELIVERY DEPENDING ON THE NATURE OF THEIR CHEMICAL COMPOSITION 19

FIGURE 5. DENDRIMER STRUCTURE. 22

FIGURE 6. SCHEMATIC REPRESENTATION OF LIPID-NANOVESICLES STRUCTURE AND THEIR FUNCTIONALIZATION CAPABILITIES AS A NANOCARRIER. 23

FIGURE 7. EXPERIMENTAL DESIGN AND STATISTICS ANALYSIS OF THE MICRORNA HIGH-THROUGHPUT SCREENING. 47

FIGURE 8. PROTEIN TRANSFER SET UP. 50

FIGURE 9. MIR-323A-5P PREDICTED BINDING SITES FOR EACH OF THE SELECTED TARGET GENES. 55

FIGURE 10. SCHEMATIC REPRESENTATION OF THE LAB-SCALE SET-UP AND IMAGE OF THE REACTOR USED FOR THE DELOS-SUSP EXPERIMENTS. 56

FIGURE 11. DEPRESSURIZATION OF AN EXPANDED LIQUID ORGANIC SOLUTION-SUSPENSION (DELOS-SUSP) PROCEDURE FOR VESICLE PREPARATION. 57

FIGURE 12. IMAGE OF THE VIBRACELL SONICATOR USED FOR NANOSRUCTURES PREPARATION. 61

FIGURE 13. IMAGE OF THE DIAFILTRATION SYSTEM FOR QS PURIFICATION. 62

FIGURE 14. SCHEMATIC REPRESENTATION OF THE HYDRODYNAMIC DIAMETER (D_H) GIVEN BY DLS TO INDICATE THE SIZE OF NANOPARTICLES. 64

FIGURE 15. SCHEMATIC REPRESENTATION OF FRET. 75

FIGURE 16. FUNCTIONAL HIGH-THROUGHPUT MIRNA SCREENING IDENTIFIED SEVERAL TUMOR-SUPPRESSIVE MIRNA. 80

FIGURE 17. OVEREXPRESSION OF MIRNA LOCATED AT 14Q32 REDUCED CELL PROLIFERATION IN MULTIPLE NB CELL LINES. 81

FIGURE 18. MIR-323A-5P INDUCES CELL CYCLE ARREST AT G0/G1 PHASE AND APOPTOSIS IN SK-N-BE(2) CELLS. 82

FIGURE 19. MIR-323A-5P MODIFY MULTIPLE TARGET GENES INVOLVED IN CELL CYCLE ARREST AT G0/G1 PHASE AND APOPTOSIS IN SK-N-BE(2) CELLS. 83

FIGURE 20. MIR-323A-5P MODULATE THE EXPRESSION OF MULTIPLE CANCER-RELATED, CELL CYCLE AND CELL ADHESION GENES. . 84

FIGURE 21. MIR-323A-5P MODULATE THE EXPRESSION OF PREDICTED MIR-323A TARGETS GENES. 84

FIGURE 22. MIR-323A-5P MODULATE THE EXPRESSION OF DIRECTED MIR-323A TARGETS GENES. 85

FIGURE 23. MIRNA TARGET-KNOCKDOWN PARTIALLY REPRODUCES THE ANTITUMORAL EFFECTS OF MIR-323A-5P. 86

FIGURE 24. REPRESENTATION OF QUATSOMES (QS) STRUCTURE AND THEIR MEMBRANE COMPONENTS. 88

FIGURE 25. SCHEMATIC REPRESENTATION OF THE STEPS DONE FOR QS SAMPLES PREPARATION, DIAFILTRATION AND CONCENTRATION. 89

FIGURE 26. REPRESENTATIVE IMAGES OF VIALS SHOWING THE MACROSCOPIC APPEARANCE OF CHOL:MKC AND CHEMS:MKC SYSTEMS. 90

FIGURE 27. QS_0 SYSTEMS PRODUCED AT MOLAR RATIOS 1:0.75 AND 1:1 OF CHEMS:MKC DIAFILTRATED. 91

Figure 28. Yields of the preparation of QS_0 using initial molar ratios of Chems:MKC of 1:0.75 and 1:1. 92

Figure 29. Macroscopic images of the vials containing Chol:MKC-based QS_1 produced by DELOS-SUSP.. 93

Figure 30. Comparison of the physicochemical properties of diafiltered QS_1, produced by DELOS-SUSP using initial molar ratios of Chol:MKC of 1:1.5, 1:2 and 1:3, and the nanostructures produced by sonication using a molar ratio of Chol:MKC of 1:1.. 94

Figure 31. Comparison of the yields of each process and the final yield (DELOS-SUSP or sonication and diafiltration) developed for QS_1 systems at molar ratios 1:1.5, 1:2 and 1:3, between the sterol and the surfactant, and the nanostructures produced by sonication. 95

Figure 32. QS prepared at high concentrations presented different physicochemical properties and macroscopical appearance. 97

Figure 33. Comparison of the polidispersity and the morphology of QS_1 prepared at different starting concentrations (7.5, 5 and 3.6 mg/mL) and then concentrated by diafiltration (5X or 10X) 98

Figure 34. Physicochemical properties (hydrodynamic diameter and Z-potential) of QS_1 at diferent membrane components concentrations over time.. 99

Figure 35. QS_0 physicochemical properties after purification and after concentration (8X) by diafiltration over time. 100

Figure 36. Schematic representation of QS-miRNA complexes produced by electrostatic interactions between positive charges of the MKC surfactant located outside the QS membrane and the negative charges from the miRNA backbone. 101

Figure 37. QS_1 has a higher miRNA complexation capacity than QS_0. 102

Figure 38. QS_{0-1}-miRNA complexes presented similar morphology. 102

Figure 39. $QS_{0/1}$-miR-497-5p complexes transfect miR-497-5p in NB cells. 103

Figure 40. Schematic illustration of miR-497-5p targets functions in cancer cells when miR-497-5p is overexpressed. 104

Figure 41. QS-miR-497-5p complexes did not modify miR-497-5p targets expression. 105

Figure 42. Membrane components used for the preparation of various QS systems (A) and schematic representation of the various compositions of QS prepared (B). 107

Figure 43. QS presented good physicochemical properties over time, such as small size, positive charge and slightly acidic-neutral pH after purification by diafiltration.. 108

Figure 44. QS_{2-4}, composed by Dc-Chol, had a higher yield than QS_1 after their purification. 109

Figure 45. All QS_{1-4} prepared are SUVs and presented spherical morphology. 109

Figure 46. QS prepared with the sterol DC-Chol maintain the pH sensitive behavior after QS formation............ 110

Figure 47. QS-miRNA complexes present different morphology and lamellarity. 111

Figure 48. High miRNA complexation efficiency of Quatsomes (QS) prepared with DC-Chol derivative sterol. 113

Figure 49. miRNA is released from QS_{1-4}, after previous complexation, through SDS treatment. 114

Figure 50. High cellular viability of SK-N-BE(2) cells after QS_{1-4} treatment at different concentrations (Table 20) or after QS_{1-4}-miR-Control complexes transfection at various loadings QS_{1-4}-miRNA (I-VIII). 115

Figure 51. QS-miRNA complexes are efficiently internalized in NB cells but only few QS_1-miRNA complexes colocalize with lysosomes after 24 h post-transfection. 116

Figure 52. QS-miRNA complexes remain into NB cells cytosol after 48 h post-transfection. 117

Figure 53. miRNA transfected with QS_4 are in the NB cells cytosol after 72 h post-transfection........ 118

Figure 54. miR-323a-5p transfected with various QS formulations and lipoplexes increase intracellular miR-323a-5p expression levels. 119

Figure 55. Inducible expression of QS-miR-323a-5p complexes, modify miR-323a-5p targets expression at mRNA after QS_4-miR-323a transfection in chemoresistant NB cells (SK-N-BE(2)), as well as lipoplexes. 120

Figure 56. Inducible expression of QS-miR-323a-5p complexes, modify miR-323a-5p targets expression at protein level after QS_4-miR-323a transfection in chemoresistant NB cells (SK-N-BE(2)), as well as lipoplexes........ 121

Figure 57. Inducible expression of QS_4-miR-323a-5p complexes increase miR-323a-5p expression levels in SK-N-BE(2) cells and modify direct miR-323a-5p targets expression at mRNA and protein level........ 122

Figure 58. Schematic illustration of miR-323a-5p targets functions in cancer cells where miR-323a-5p is downregulated (A) and with restored levels (B). 123

Figure 59. Inducible expression of QS_4-miR-323a-5p complexes modify indirect miR-323a-5p targets expression at protein level. 123

Figure 60. miR-323a-5p transfection with naked miRNA or complexed with MKC micelles did not modify the indirect miR-323a-5p targets expression at protein level in SK-N-BE(2) cells. 124

Figure 61. Inducible expression of QS_4-miR-323a-5p complexes reduce SK-N-BE(2) cellular proliferation. 125

Figure 62. Inducible expression of QS_4-siCCND1 complexes modify direct siCCND1 targets expression at mRNA level. 125

Figure 63. Inducible expression of QS_4-siCCND1 complexes modify direct and indirect siCCND1 targets expression at protein level and reduce SK-N-BE(2) cells proliferation. 126

Figure 64. QS_4-miRNA complexes are stable in serum.. 127

Figure 65. QS_4 protects miRNA from nuclease degradation. Gel electrophoresis of QS_4-miRNA complexes incubated with RNAse A. 128

Figure 66. Excitation and emission spectra of DiI (green) and Cy5 (magenta) fluorophores. 132

Figure 67. Physicochemical properties of the indicated QS_4 labelled with DiI fluorophore, at different dye concentrations (8, 23 and 70 µM), are similar for non-labelled QS_4 after diafiltration.. 134

Figure 68. Optical properties of $^{DiI}QS_4$ at different DiI loadings, in comparison to DiI optical properties in ethanol. 135

Figure 69. $^{DiI}QS_4$-miRNA complexes presented similar morphology and lamellarity despite being labelled with DiI at different concentration in QS_4 surface. 136

Figure 70. High miRNA complexation efficiency of DiI labelled or non-labelled Quatsomes (QS_1) prepared in PBS. 137

Figure 71. High miRNA complexation efficiency of DiI labelled QS_4 compared to plain QS_4. 138

Figure 72. Complexes of miRNA labelled with Cy5 and QS_4 labelled with DiI at three different concentrations (8 µM, 23 µM and 70 µM) produce FRET 139

Figure 73. QS_4-miRNA complexes remain stable prior to cell transfection. 141
Figure 74. QS_4-miRNA complexes are separated after overnight transfection in SK-N-BE(2) cells 141
Figure 75. QS_1-miRNA complexes remain attached after overnight transfection in SK-N-BE(2) cells. 142
Figure 76. MiR-323a-5p expression levels correlated with clinical parameters 149
Figure 77. Schematic representation of the different sizes of MKC surfactant micelles compared to Quatsomes (QS) 154
Figure 78. miRNA complexation efficiency of QS_0 using different buffers in complexes formation. 158
Figure 79. Schematic representation of the charges involved in the QS-miRNA complexation process by electrostatic interactions. 159
Figure 80. Principal internalization pathways used for nanocarriers in mammalian cells. 162
Figure 81. Intracellular trafficking of nanoparticles using the principal internalization pathways. 163
Figure 82. Intracellular trafficking followed by the principal cellular uptake pathways and the pharmacological inhibitors to block the internalization or endosomes maturation to lysosomes. 167
Figure 83. Hypothesis of the pH dependent mechanism employed by QS_4 to release the miRNA into cytosol after deprotonation of DC-Chol tertiary amine. 170
Figure 84. Hypothesis of the reason why QS_1 did not release the miRNA in the cytosol. 170
Figure 85. Principal extracellular barriers of administered NP for drug delivery and their excretion routes before reaching the tumour. 174
FIGURE A1. BOTH QS_0 SYSTEMS PRODUCED AT MOLAR RATIOS 1:0.75 AND 1:1, BETWEEN THE STEROL AND THE SURFACTANT, HAD GOOD PHYSICOCHEMICAL PROPERTIES AFTER DELOS-........201
FIGURE A2. COMPARISON OF THE PHYSICOCHEMICAL PROPERTIES OF QS_1 AT MOLAR RATIOS 1:1.5, 1:2 AND 1:3, BETWEEN THE STEROL AND THE SURFACTANT, PRODUCED BY DELOS-SUSP AND THE NANOSTRUCTURES PRODUCED BY SONICATION (AT MOLAR RATIO 1:1)........201
FIGURE A3. PHYSICOCHEMICAL PROPERTIES (HYDRODYNAMIC DIAMETER (A) AND z-POTENTIAL (B)) OF QS_1 OVER TIME AFTER DELOS-SUSP PREPARATION........202
FIGURE A4. QS PRESENTED GOOD PHYSICOCHEMICAL PROPERTIES OVER TIME, SUCH AS SMALL SIZE, POSITIVE CHARGE AND SLIGHTLY ACIDIC-NEUTRAL PH AFTER DELOS-SUSP PREPARATION........202

List of tables

Table 1. MicroRNAs with therapeutic potential demonstrated *in vivo* in neuroblastoma mouse models. 12

Table 2. Advantages and drawbacks of the nanomedicines used for nucleic acids delivery. 31

Table 3. Selected list of miRNA therapeutics currently in clinical trials. 34

Table 4. Human synthetic miRIDIAN miRNA mimics obtained from Dharmacon Inc. 44

Table 5. siRNA purchased from Sigma-Aldrich. 45

Table 6. Primary antibodies list and conditions used for Western Blot. 51

Table 7. Secondary antibody conditions used for Western Blot. 51

Table 8. TaqMan probes purchased for RT-qPCR of miRNA expression levels. 52

Table 9. List of primer sequences of genes used for RT-qPCR. 53

Table 10. 3'UTR luciferase reporter cloning. 54

Table 11. Compositions used for the preparation of various Quatsomes (QS) systems by DELOS-SUSP method. 58

Table 12. Compositions used for the preparation of various Quatsomes (QS) systems labelled with different concentrations of DiI (^{DiI}QS) by DELOS-SUSP method. 60

Table 13. Composition used to prepare Quatsomes nanostructures (NS) by sonication. 61

Table 14. Yield and real concentrations of various QS systems after DELOS-SUSP preparation, diafiltration or concentration. 67

Table 15. Protocol for the preparation of QS_0-sRNA complexes at different loadings of sRNA in QS. 69

Table 16. Protocol for the preparation of $QS_{1\text{-}4}$-sRNA complexes the indicated loadings of sRNA in QS. 69

Table 17. Concentrations of the QS and miRNA solutions used for the preparation of QS nanoconjugates with different loading of miRNA. 70

Table 18. Concentrations of the QS and siRNA solutions used for the preparation of QS nanoconjugates with different loading of siRNA. 71

Table 19. Concentrations and volumes of the MKC micelles and miRNA solutions used for the preparation of nanoconjugates of miRNA loaded in MKC micelles. 71

Table 20. QS and miRNA concentrations for cell viability assays. 73

Table 21. Neuroblastoma cell lines characteristics. 81

Table 22. Chemical description of the ^{DiI}QS samples used for monitoring cellular dynamics of QS-miRNA complexes. 133

TABLE A1. POLIDISPERSITY INDEX OF QS_1 PREPARED AT DIFFERENT INITIAL CONCENTRATIONS AFTER DELOS-SUSP, DIAFILTRATION AND THEN CONCENTRATION..203

TABLE A2. POLIDISPERSITY INDEX STABILITY OVER TIME OF QS_0 PREPARED AFTER DELOS-SUSP, DIAFILTRATION AND THEN CONCENTRATION...203

TABLE A3. OLIDISPERSITY INDEX STABILITY OVER TIME OF $QS_{1\text{-}4}$ REPARED AFTER DELOS-SUSP AND DIAFILTRATION........203

ABBREVIATIONS

A	**AAV**	Adenoassociated virus
	AD	Administration
	AGO	Argonaute (also called EIF2C2)
	ASO	Antisense oligonucleotides
	ATP	Adenosine 5'-triphosphate
B	**BAK**	Benzalkonium chloride
	BCL-2	B-Cell CLL/Lymphoma 2
	Bp	base pair
	BSA	Bovine serum albumin
C	**CCND1**	Cyclin D1
	cDNA	Complementary DNA
	Chems	Cholesteryl hemisuccinate
	CHFA1A	Chromatin Assembly Factor 1 Subunit A
	CHEK1	Checkpoint Kinase 1, also called CHK1
	CDC25A	Cell Division Cycle 25A
	CDK4/6	Cyclin Dependent Kinase 4/6
	Chol	Cholesten-3β-ol or Cholesterol
	CLL	**C**hronic lymphocytic leukaemia
	CMC	Critical micellar concentration
	CO_2	Carbon dioxide
	CPC	Chromosomal passenger complex
	Cy5	Cy5-labelled miRNA
D	**DC-Chol**	Cholesteryl N-(2-dimethylaminoethyl)carbamate
	DELOS-SUSP	Depressurisation on an Expanded Liquid Organic Solution-SUSPension
	DGCR8	(dsRNA)-binding protein DiGerorge Syndrome critical region
	D_h	Hydrodinamic diameter
	DiI	1,1’-dioctadecyl-3,3,3’,3’-tetramethyl-indocarbocyanine perchlorate
	DlinDMA	1,2-dilinoleyloxy-N,N-dimethyl-3-aminopropane
	DLS	Dynamic light scattering
	DNAse	Deoxyribonuclease
	DMSO	Dimethyl sulfoxide
	DODAP	1,2-dioleoyl-3-dimethylammonium propane
	DODMA	1,2-dioleyloxy-N,N-dimethyl-3-aminopropane
	DOGS	Dioctadecyl amido glycil spermine
	DOGSDSO	1,2-dioleoyl-sn-glycerol-3-succinyl-2-hydroxyethyl disulfide ornithine
	DOPC	1,2-Dioleoyl-sn-Glycero-3-Phosphocholine
	DOPE	1,2-Dioleoyl-sn-glycero-3-phosphoethanolamine
	DOSPA	2,3-dioleoyloxy-N-[2-(sperminecarboxamido)ethyl]-N,N-dimethyl-1-propanaminium
	DOTAP	1,2-dioleoyl-3-trimethylammonium-propane
	DOTMA	1,2-di-O-octadecenyl-3-trimethylammonium propane
	DOX	Doxorubicin
	DPPC	Dipalmitoylphosphatidyl choline

D	**DSPE**	1, 2-Distearoyl-sn-glycero-3-phosphoethanolamine
	DsRNA	Double-stranded RNA
E	**ECL**	Enhanced chemiluminescence
	ECO	1-aminoethyl)iminobis[N-(oleicylcysteinyl-1-amino-ethyl)propionamide]
	EGF	Epidermal growth factor
	eiF4	Eukaryotic initiation factor 4F
	EPR	Enhanced Permeability and Retention
	EtBr	ethidium bromide
	EtOH	Ethanol
F	**FBS**	Foetal bovine serum
	FDA	Food and Drug Administration
	FG	Gas filter
	Fw	Forward
G	**GalNAc**	N-acetyl-D-galactosamine
	GD_2	Disialoganglioside GD2
	GFP	Green Fluorescent Protein
	GTP	Guanosine-5’-triphosphate
H	**hATTR**	Hereditary TTR-mediated amyloidosis
	HRP	Horseadish Peroxidase
	HDACi	Histone deacetylase inhibitors
I	**iD**	Identification
	ID	Intradermal
	IMDM	Iscove’s modified Dulbecco’s Medium
	INCENP	Inner centromere protein
	ITS	Insulin-Transferrin-Selenium Supplement
	IV	Intravenous
K	**Kb**	kilobase
L	**LNA**	Locked nucleic acids
	lncRNA	Long non-coding RNA
M	**MPS**	Mononuclear phagocyte system
	miRbase	miRNA database
	miRNA	microRNA
	MKC	Benzyldimethyltetradecylammonium Chloride
	MNA	MYCN amplified
	MOCHOL	Cholesteryl-4-([2-(4-morpholinyl)ethyl]amino)-4-oxoburanoate
	mRNA	messenger RNA
	MTAB	Myristyl trimethyl ammonium bromide
	Mut	Mutated
N	**NA**	Not amplified
	NaOH	Sodium hydroxide
	NB	Neuroblastoma

N	**NP**	Nanoparticles
	NS	Nanostructures
	ncRNA	non-coding RNA
	Non-MNA	MYCN non amplified
	NT	Non-transfected
O	**o/n**	Overnight
P	**PA**	Partial amplification
	PBS	Phosphate buffered saline
	PCR	Polymerase chain reaction
	PDI	Polydispersity index
	PEG	Poly-(ethylene glycol)
	piRNA	Piwi-interacting RNA
	PIWI	P element-induced wimpy testes
	Pol II	RNA polymerase II
	POPC	1-palmitoyl-2-oleoyl-sn-glycero-3-phosphocholine
	pRb	Phospho-Rb
	pre-miRNA	**P**recursor miRNA
	pri-miRNA	**P**rimary miRNA
	PVDF	Polyvinylidene difluoride
	P-bodies	Processing-bodies
Q	**qPCR**	Quantitative PCR
	QS	Quatsomes
	QS_1	Quatsomes composed of Chol:MKC
	QS_2	Quatsomes composed of (10%DC-Chol/90%Chol):MKC
	QS_3	Quatsomes composed of (50%DC-Chol/50%Chol):MKC
	QS_4	Quatsomes composed of DC-Chol:MKC
R	**RanGTP**	GTP-binding nuclear proteina RAN
	RBPs	RNA-binding proteins
	RES	Reticuloendothelial system
	RGD	Arg-Gly-Asp
	RIPA	Radioimunoprecipitation assay
	RISC	RNA-Induced Silencing Complex
	RNA	Ribonucleic acid
	RT	Room temperature
	RT-qPCR	Real time-quantitative PCR
	Rv	Reverse
S	**SC**	Subcutaneous
	SD	Standard deviation
	sRNA	Small non-coding RNA (also called sncRNA)
	SDS	Sodium dodecyl sulfate
	SEM	Standard error of the mean
	sRNA	small RNA
	siRNA	Small interfering RNA
	SUV	Small unilamellar vesicles

T	**TBS-T**	Tris buffered saline Tween
	Tm	Melting temperature
	TRBP	TAR RNA-binding protein (also called TARBP2)
W	**WEE1**	WEE1 G2 Checkpoint Kinase
	wt	wild type
X	**XPO5**	Exportin 5

1. INTRODUCTION

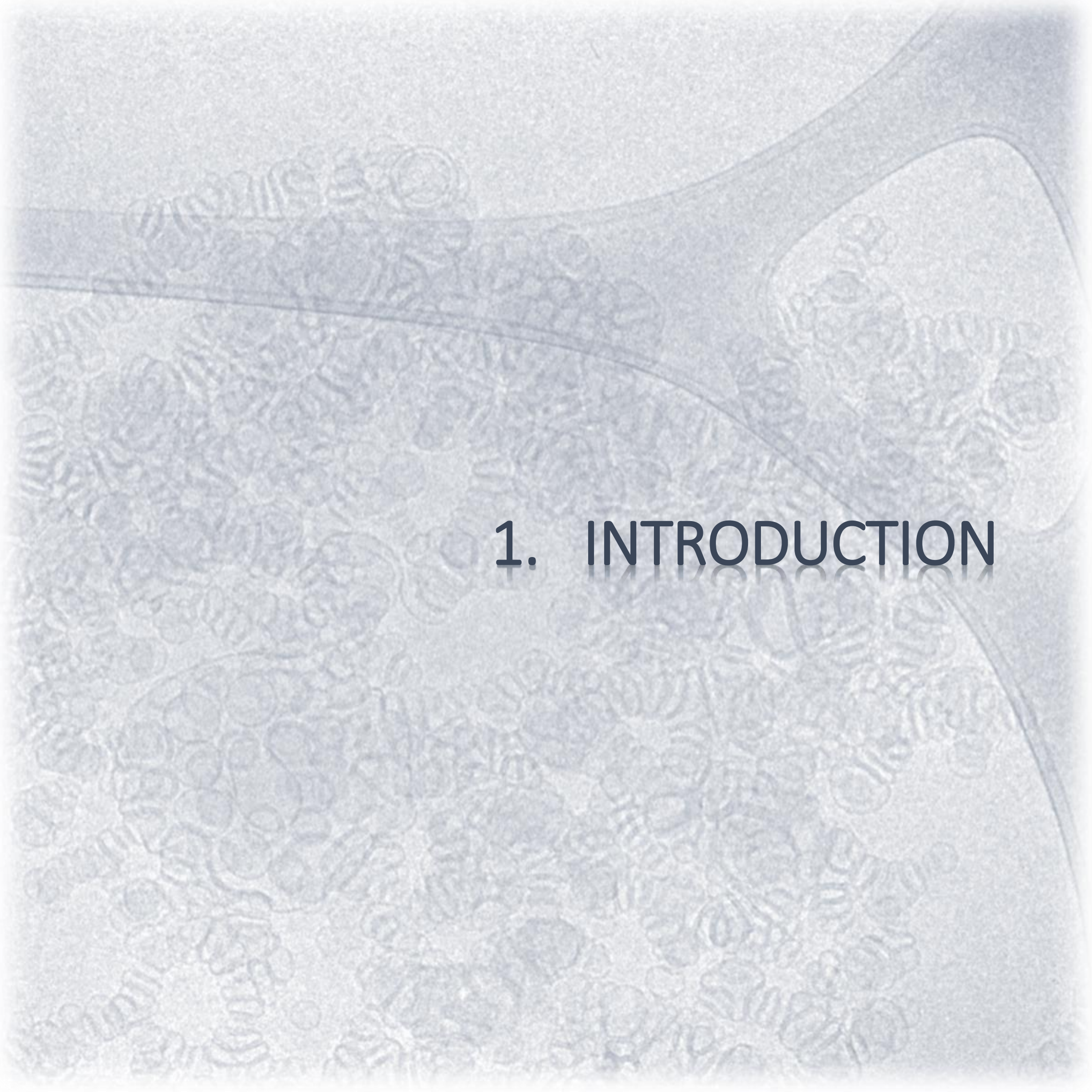

1. INTRODUCTION

1.1. RNA-based therapies

Most of the current medicines are directed to target proteins, which means that only 0.05% of the human translated genome has been drugged. Therefore, RNA-based therapies are emerging therapeutic alternatives that broaden the druggable targets having the capacity to act over the whole transcriptome. It is well known that only 1.5% of the human genome encodes proteins and that 10-15% of them are disease-related[1]. Most of the disease-related proteins are difficult to target or are termed undruggable, because these molecules lack a distinctive motif for small molecules binding. However, targeting directly mRNA, activities of proteins difficult to target or undruggable might be modulated, before or during their biogenesis. Besides, ~ 70% of the human genome is transcribed into non-coding RNA; hence targeting them will expand the number of druggable targets[2]. Non-coding RNA (ncRNA) are classified depending on their size into small non-coding RNA (sncRNA), shorter than 200 nt, and long non-coding RNA (lncRNA), longer than 200 nt (Figure 1). Both are gene expression modulators at the transcriptional or post-transcriptional level[3,4].

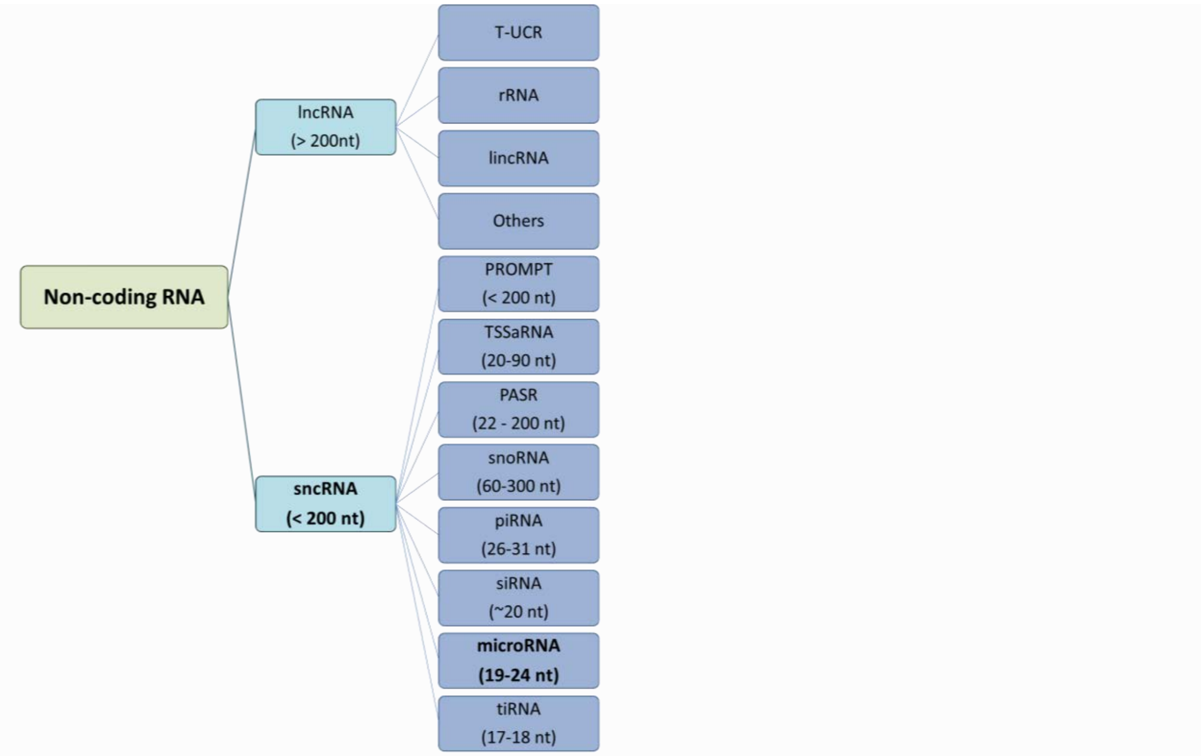

Figure 1. Schematic classification of non-coding RNAs(ncRNAs). The ncRNA can be long non-coding RNA (lncRNA), which comprise RNAs longer than 200 nucleotides (nt), such as transcribed ultraconserved regions (T-UCR), ribosomic RNA (rRNA), long intergenic RNA (lincRNA) and others. Small non-coding RNA (sncRNA) are shorter than 20 nt and are classified in promoter upstream transcripts (PROMPT), TSS-associated RNA (TSSaRNA), promoter-associated small RNA (PASR), small nucleolar RNAs (snoRNA), PIWI-interacting RNAs (piRNA), microRNA (miRNA) and transcription initiation RNAs (tiRNA). Adapted from Esteller[1].

1.2. Small RNA

Small non-coding RNA (sncRNA or sRNA) are RNA with 20-30 bp in length that are considered key regulators of gene expression. Approximately twenty years ago, the discovery of RNA interference and the development based on high-throughput sequencing techniques, generated a depth knowledge on the sRNA classes, their functionalities and their use as RNA-based therapies for gene silencing[5]. At least three classes of sRNA are encoded in human genome, which are microRNA (miRNA), piwi-interacting RNA (piRNA) and small interfering RNA (siRNA) (Figure 1). Essentially, siRNA and miRNA are similar in terms of size, molecular characteristics, biogenesis and functions, but differ into their therapeutic approaches[6]. Despite miRNA and siRNA share the processing pathway used for the post-transcriptional repression of their target genes, they differ on their mechanism of action and their molecular origins. Whereas the structure and the sequence of mature miRNA depends on the structure of the primary miRNA transcript and the recognition of miRNA precursor by nuclear processing machinery, siRNA are produced from dsRNA introduced exogenously or from endogenous RNA. The transfection of short, 21-23 nucleotides in length, exogenous double-stranded siRNA silence the expression of a specific gene by the degradation of their complementary host mRNA. The uptake of siRNA is mediated by RNA-Induced Silencing Complex (**RISC**) complex, which after siRNA unbounding, the antisense or guide strand binds to their homologous host mRNA[7]. The fully complementary of siRNA with the host mRNA causes a direct cleavage of the mRNA target by the endonuclease Argonaute (**AGO**) and the silencing of its target genes[7,8].

1.2.1. microRNA (miRNA)

MicroRNA (miRNA) are small endogenous RNA of 20-22 nucleotides in length that directly interact with partially complementary mRNA targets in the 3’ untranslated region in order to induce the translation repression or the mRNA target cleavage[9]. A single mRNA may be regulated by multiple miRNAs and one single miRNA may regulated hundreds of mRNA in the same or different pathways. For this reason, miRNA play an essential role in a wide range of biological processes, such as cell proliferation, differentiation, apoptosis and metabolism among others. In consequence, deregulation of miRNA expression levels has been associated to the development of human diseases, such as cancer. Computational predictions and genome-wide studies estimated that at least 50% of the transcriptome is subject to miRNA regulation[10]. In some cases, miRNA can also interact with DNA or proteins. For example, it was reported that miR-373 has binding sites in the promoter of genes such E-cadherin and CSDC2 (cold shock domain-containing protein C2). These elements are functional since the ectopic expression of miR-373 was able to induce the expression of those genes[11].

On the other hand, it has been reported in a leukemia cell model that miR-328 is capable of interact with the translational regulator poly(rC)-binding protein hnRNP E2, which exerts a decoy activity that interferes with the function of this regulatory protein[12].

Biogenesis of microRNA

MiRNA can be encoded in introns of protein-coding genes or in non-coding transcripts, and in exonic regions[13,14]. MiRNA are generally transcribed by RNA polymerase II (Pol II) obtaining a primary miRNA (**pri-miRNA**) form larger than 1Kb, which is constituted by three different parts: a stem of 33-35bp, a terminal loop and single-stranded RNA segments in 5' and 3' ends (Figure 2). Pri-miRNA contains in the stem-loop structure the miRNA sequence of a single miRNA or a cluster of several miRNA, which are transcribed together. Then, pri-miRNAs are capped in the 5' end, spliced and polyadenylated in the 3' end after their association with the **microprocessor complex**. This complex contains a RNase III enzyme Drosha, its cofactor the double-stranded RNA (dsRNA)-binding protein DiGerorge Syndrome critical region (DGCR8) and other auxiliary factors, such as DEAD box RNA helicases and p72 (also known as DDX5 and DDX17, respectively). Drosha is a nuclear protein of ~ 160 KDa composed by two RNAse III domains, that interact specifically with double-stranded RNA (dsRNA) to induce the pri-miRNA cleavage. However, Drosha is necessary for the miRNA processing, it is not enough for substrate interaction. DGCR8 is a protein of ~ 90 KDa located at the nucleoplasm and nucleolus that facilitate the pri-miRNA recognition while interacts with Drosha using their conserved C terminus end. Alterations in both Drosha or DGCR8 genes are associated to lethality or defects in the early stages of embryogenesis in mice and humans. The auxiliary factors DDX5 and DDX17 are RNA-binding proteins that interact with Drosha and/or the pri-miRNA to interfere in the stability and the localization of the microprocessor complex[13]. Next, pri-miRNA are cropped in the microprocessor complex by Drosha in the stem-loop to release a small RNA hairpin-shaped called precursor miRNA (**pre-miRNA**) of ~ 65-70 nucleotides in length[14,15]. This biogenesis pathway is called **canonical** and differs only by the Drosha-mediated digestion in the nucleus with the **non-canonical** miRNA biogenesis, in which pre-miRNAs are generated by mRNA nuclear splicing machinery[16,17].

To become a functional miRNA, the pre-miRNA forms must be exported to the cytoplasm by the RanGTP-dependent nuclear transport receptor Exportin 5 (**XPO5**) (Figure 2). After the translocation through the nuclear pore complex, GTP is hydrolysed inducing the disassembly of the complex and the pre-miRNA release into the cytosol. XPO5 recognizes dsRNA of >14 bp in length that have a short 3' overhang inducing their export but also protect the pre-miRNA from nucleolytic attack.

In the cytoplasm, the miRNA processing is controlled by the RNase III endonuclease **DICER,** which binds to the 5’ phosphorylated end of the pre-miRNA and cleaves it near the terminal loop (22 nucleotides away from the 5’ end) generating a **mature miRNA** duplex of 18-25 nucleotides in length composed by the 5p and 3p strands. DICER may have DICER homologues with different roles. While DICER-1 is required for miRNA biogenesis, DICER-2 is devoted to siRNA production. Like Drosha, DICER interacts with the cofactors TAR RNA-binding protein (TRBP) or dsRBD PACT that also mediates the cleavage of the pre-miRNA. Although their mechanism of action is not fully understood, TRBP is required for siRNA and miRNA functions, by acting as a biosensor selecting the dsRNA to be loaded into the RISC complex. Mutations in these cofactors have been reported in human cancers and their loss of function leads to DICER protein destabilization and decreased miRNA levels[13,16].

The small RNA duplex generated by DICER is then unwound and loaded in the RNA-Induced Silencing Complex (**RISC**). RISC complex is formed by the proteins EIF2C2, also known as Argonaute or **AGO**, Dicer and RNA-binding proteins (TRBP or TARBP2). AGO proteins are highly conserved RNA binding proteins, composed by four domains, called the amino-terminal domain, the PAZ domain, the MID domain and the P element-induced wimpy testes (PIWI) domain. **AGO** proteins adopt a bilobate structure composed by PAZ and MID-PIWI domains that are ubiquitously expressed. PIWI domain binds with the miRNA guide at its 5’ end and using their active site cleaves mRNA target between the positions 10 and 11. On the other hand, PAZ domain is bound to the 3’ end of the guide miRNA strand. The thermodynamically stability of the two ends of the duplex mature miRNA during the AGO loading step, determine the guide strand, which will become the mature miRNA after their retaining into the RISC complex. Indeed, the strand with unstable terminus at the 5’ side get used to be the *guide strand*, while the other strand called *passenger strand* is discarded to generate a mature RISC able to complementary target the mRNA for gene silencing in the processing-bodies (P-bodies). In some cases, the passenger strand is cleaved by the multimeric endonuclease complex C3PO, instead of being unwound from the miRNA duplex. Modifications in AGO proteins, such as phosphorylation, hydroxylation and ubiquitination, results in higher AGO stability proteins, their inclusion in P-bodies or in translational repression. Interestingly, AGO proteins are more stable when the miRNA are loaded into their structure[18-20]. Among AGO proteins, AGO2 are the only ones that matched perfectly to human target mRNA, but all of them are capable to incorporate miRNA and siRNA to repress the mRNA translation and decay the mRNA target.

Finally, mature miRNA can bind to the complementary target mRNA through 7-8 nucleotides located at the 5'-end of the miRNA (commonly termed **seed sequence**) with perfectly or imperfectly complementarity to their target sequence[15]. Nucleotide positions 2 to 7 at the 5' end of the mature miRNA, commonly called **miRNA seed**, are crucial for the target recognition. While the first nucleotide of the RNA guide is usually unpaired, the downstream nucleotides of miRNA seed contribute to base pairing with the mRNA target[14,16]. Once miRISC complex is bound to the 3'-UTR of mRNA target genes, target proteins levels are reduced owing to the inhibition of mRNA translation and/or mRNA degradation (Figure 2). In some cases, miRNA may inhibit the initiation of translation by interfering the eukaryotic initiation factor 4F (eiF4F), affecting the ribosomal subunits recruitment and/or impairing the post-initiation translational ribosomal complex[17]. Less frequently, the miRNA binding to gene promoters may induce the activation of transcription or miRNA can regulate gene expression by binding to RNA-binding proteins (RBPs) which act as transcriptional activators or repressors[14].

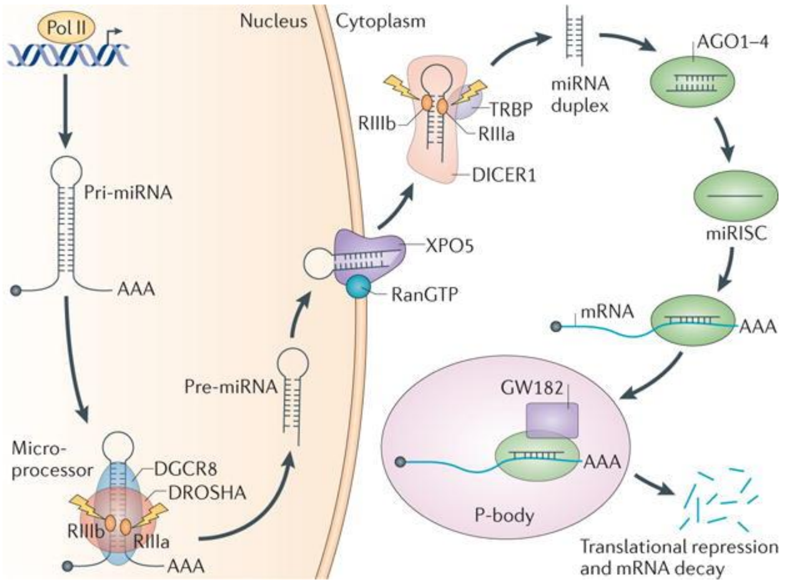
Pol II
Nucleus
Cytoplasm
Pri-miRNA
AAA
Micro-
processor
DGCR8
DROSHA
RIIIb
RIIIa
AAA
Pre-miRNA
XPO5
RanGTP
RIIIb
TRBP
RIIIa
DICER1
miRNA
duplex
AGO1–4
miRISC
mRNA
AAA
GW182
AAA
P-body
Translational repression
and mRNA decay

Figure 2. MiRNA biogenesis machinery in eukaryotes. Adpated from Ha et al.,[13].

MiRNA families, clusters and nomenclature

Many of the animal miRNA are phylogenetically conserved, ~55% of the *C.elegans* miRNA have homologues in humans, which means that miRNA have had important roles throughout evolution. Approximately 50% of mammalian miRNA loci are found in close proximity to other miRNA (< 10kb). When this happens, these miRNA are considered a **miRNA cluster**, which could be transcribed as a single polycistronic unit or are overlapped in the host transcripts, within introns or exons, depending on the host gene splicing[13,16]. Despite miRNA in clusters are transcribed together, they form different mature miRNA that are regulated independently at post-transcriptional level.

MiRNA specificity to target genes is given by the seed sequence of the miRNA. In consequence, miRNA that contain identical seed sequences regulate almost the same set of target genes, because they belong to the same **miRNA family**. It was reported that human genome contains 34 miRNA families phylogenetically conserved from C.elegans and 196 miRNA families conserved among mammals. However, some miRNA belonging to the same family share a common evolutionary origin but present a different miRNA seed sequence, such as happen with the miR-200 superfamily[21,22]. Furthermore, the human genome encodes paralogs loci, which encodes miRNA belonging from the same family but due to the gene duplication their target genes barely overlap (i.e. miR-17-92 family)[23,24].

The miRNA nomenclature has evolved through the last years. MiRNA found in early genetic studies was named as their target genes (such as let-7 or lin-4)[25], whereas most miRNA discovered by cloning or sequencing techniques were named with numbers (for example miR-34). When two miRNA from the same family are produced by gene duplication and are located in the same chromosome, are called miR-34b and miR-34c, whereas if both miRNA are located in separate chromosomal loci numeric suffixes are added at the end of miRNA names (i.e. miR-329-1 and miR-329-2). On the other hand, each pre-miRNA generates two strands, the 5' strand and the 3' strand. They are called miR-34a-5p and miR-34a-3p respectively. However, the guide strand of the miRNA (miR-34a-5p) is usually more abundant and more biologically active than the passenger strand (i.e. miR-34a-3p)[26-28].

In the latest catalogue of miRNA database (miRbase; *www.mirbase.org*;[29]) 2588 miRNA have been identified in humans, although the function of many of them remains to be determined[13].

1.2.2. MicroRNA in paediatric cancer

Since miRNA have crucial roles in biological processes, alterations in miRNA expression and function are common in human diseases and have been implicated in cancer initiation, progression and metastasis[17]. It was reported that miRNA are often downregulated in tumoral cells compared with normal tissues, suggesting that miRNA biogenesis machinery may be impaired in cancer[30]. In 2002, it was reported the first evidence of miRNA deregulation associated to cancer development. Calin and colleagues described that in chronic lymphocytic leukaemia (CLL) the chromosomal region 13q14, which contains miR-15 and miR-16, was deleted in more than 50% of cases[31]. In consequence, miRNA expression was lost or reduced in 68% of CLL tumours[32]. In contrast to adult cancers, childhood and adolescent cancers are not frequently associated to environmental factors, because their causes are linked to genetic or epigenetic alterations[33]. It is well known that paediatric cancers and adult cancers present differences in aetiology, incidence and risk factors, but they are often treated with the same multimodal therapies[34]. For this reason, the general miRNA downregulation found in cancer may have a significant impact in paediatric cancers development. In the recent years, the advances in childhood cancers treatments and supportive care have improved the survival rate of these patients until approximately 80% but progresses in several childhood cancers are varied and significantly more limited[34]. For example, nowadays, 40% of children diagnosed with acute myelogeneous leukemia, 66% of high-risk neuroblastoma patients and more than 95% of children diagnosed with brainstem glioma die from these diseases[35]. Hence, the determination the miRNA role and the impact of miRNA deregulation on paediatric cancers can improve the knowledge required to diagnose and to treat children patients.

1.2.3. Role of miRNA in neuroblastoma

1.2.3.1 . Pathogenesis of Neuroblastoma

Among childhood cancers, neuroblastoma (NB) is the third most common extracranial solid tumour in children. Moreover, NB is the most common malignancy diagnosed in the first year of life and 90% of tumours are diagnosed in children who are < 10 years of age [36]. Generally, NB is diagnosed during the first five years of children life. It represents 8-10% of all diagnosed childhood cancers in Europe and USA and are the cause of 15% of paediatric cancer-related deaths[37]. Despite being the most common extracranial tumour in children, NB incidence is low (10.5 cases per million in North America and Europe) and therefore, it is considered an orphan disease.

NB is an embryonal neuroendocrine tumour of the sympathetic nervous system which is originated in the neural crest lineage cells. NB is frequently located in the adrenal glands but may also be found in sympathetic ganglia of the cervical region, thorax, abdomen and pelvis[38]. The most common presentation of NB is an abdominal mass[39]. The clinical and pathological characteristics, such as age at diagnosis, disease stage, MYCN oncogene amplification, tumour histology and DNA ploidy are used to stratify NB patients into risk groups. Patients of low and intermediate risk have good survival rates (>90% for low-risk and >70% for intermediate-risk), while high-risk NB patients have a poor prognosis and require intensive treatments. Despite these multimodal therapeutic approaches, ~60% of children will not be cured[37].

It is well known that NB is a highly heterogeneous tumours that can spontaneously regress or differentiate to benign tumours. However, it may also progress to aggressive metastatic disease.

1.2.3.2 Mechanisms of miRNA deregulation in Neuroblastoma

In the last ten years has suggested that the dysregulation of miRNA may play a key role in the pathogenesis of NB[40]. Chen and Stallings demonstrated that in different genomic subtypes of NB many miRNA are deregulated[41]. Stallings and their colleagues observed that chromosomal alterations (such as loss of distal chromosome 1 or gain of 17q) and MYCN amplifications result in the miRNA deregulation in NB[42]. In 20% of NB cases MYCN is amplified, which correlates to undifferentiated, more aggressive phenotype and poor clinical prognosis in NB patients[43]. For example, it was described that MYCN protein can bind directly to the promoter of miR-17-5p-92 cluster, inducing the up-regulation of this clustered miRNA[38]. Another example that produced a differentially expression of miRNA was the loss of heterozygosity on the long arm of the 14q32 chromosome[44]. The loss of heterozygosity was analysed in 54 primary NB samples using microsatellite markers on 14q32, in which 31% of tumours showed the loss of heterozygosis at one or more of the markers[45]. Other studies demonstrated that miRNA located in 14q32 chromosome suffer a differentially expression. Gattolliat and their colleagues observed in a comparative genomic hybridisation array that 50 of 851 human miRNA were differentially expressed in high-risk relatively to the low-risk NB. Among them, 17 miRNA were downregulated and of these 17, 15 are located on the 14q32.31 locus. These results were validated in a cohort of 214 patients (142 classified as low-risk and 72 as high-risk NB), in which the low expression of 14q32.31 miRNAs, such as miR-487b and miR-410, was associated to poor prognosis[46]. Furthermore, miRNA deregulation may occur by alterations in components implicated in miRNA biogenesis, such as DICER or DROSHA that were observed to be lowly expressed in high-risk NB tumours. In consequence, a reduced overall miRNA expression was observed in advanced stages and correlated with poor outcome in high-risk NB patients. Conversely, the elevated expression of some miRNA has attributed to more positive outcomes, such as the restoration of the tumour suppressor miR-34a due to their antiproliferative effects[38]. However, miR-34a is localized in the short arm of the chromosome 1, which is generally deleted in cancer and, in consequence, miR-34a is lost. This deletion and the low miR-34a expression are most often found in MYCN amplified (MNA) tumours[47].

1.2.3.3 MiRNA act as oncogenes or tumour suppressors in NB

Recently, the importance of miRNA as RNA regulators conduced to assign to miRNA oncogenic or tumour suppressor activities depending on their target genes[14]. Oncogenic miRNA, called **oncomiRs**, promote tumour progression due to genomic amplifications that silence tumour suppressor genes. This was demonstrated by miR-17-92 cluster, also called oncomiR-1, which acting in combination with MYC favour NB progression[48]. Similarly, the inhibition of miR-380-5p reduced tumour growth in MYCN-dependent tumours by inducing TP53-mediated cell death[49]. After the discovery of oncomiR, other miRNA with **tumour suppressor** functions were found. In this case, a miRNA loss of function in tumours due to chromosomal rearrangements, deletions or mutations was observed. This has been shown for let-7 family of miRNA which suppress tumour growth acting over oncogenes like MYCN, involved in NB development[50]. Another example is miR-34a, that due to their targeting of MYCN in a p53 dependent manner after their overexpression decreased cell proliferation and increased apoptosis *in vitro* and in NB xenografts[51]. In an attempt to find miRNA that could target overexpressed genes implicated in multidrug resistance in high-risk NB tumours, a functional screening was performed in our laboratory. Several miRNA that reduced cellular proliferation in chemoresistant NB cell lines were found. Among them miR-497 was the best reducing the proliferation of NB cell lines and inducing apoptosis in MYCN-amplified cell lines *in vitro* and *in vivo*[52].

To date, numerous preclinical studies in NB using miRNA have been conducted but any of them have reached the market yet. The miRNAs with therapeutic effects in NB preclinical models have been highlighted in Table 1.

Table 1. MicroRNAs with therapeutic potential demonstrated *in vivo* in neuroblastoma mouse models.

miRNA	Types	Deregulation	Validated target(s)	Therapeutic approach	Function/processes	Reference(s)
miR-17-5p-92 cluster	Oncogene	Up	TGFβ-signalling, p21 and Bim	Inhibition	↓ Cell proliferation, ↓ cell adhesion, apoptosis and cell cycle arrest	48,53
miR-152	Oncogene	Up	CHUK, CUL5 and GADD45A	Inhibition	Neuroblast differentiation, ↓ migration/invasion and apoptosis	54
miR-181a/b	Oncogene	Up	ABI1	Inhibition	↓ Cell viability, ↓ invasion and ↓ migration	55
miR-296-5p	Oncogene	NA	Bax	Inhibition	↓ Cell proliferation and apoptosis	56
miR-338	Oncogene	Up	PTPRT	Inhibition	Neuroblast differentiation and apoptosis	54
miR-380-5p	Oncogene	Up	p53	Inhibition	Apoptosis	49
miR-558	Oncogene	Up	HPSE, HIF-2α	Inhibition	↓ colony formation, ↓ Cell proliferation, ↓invasion, ↓metastasis, ↓angiogenesis	57-60
Let-7	Tumour suppressor	Down	MYCN via LIN28B axis	Restoration	↓ Cell proliferation, ↓ cell colony formation, ↓cell viability and cell cycle arrest	61
miR-9	Tumour suppressor	Down	trkC, MMP14	Restoration	↓ Cell proliferation, ↓ angiogenesis, ↓ metastasis and apoptosis	62,63
miR-27b	Tumour suppressor	Down	PPARγ	Restoration	↓ Cell proliferation and inflammatory response	64
miR-34a	Tumour suppressor	Down	NMYC, BCL-2, E2F3, TIMP2,	Restoration	Cell cycle arrest, apoptosis, DNA repair and ↓ angiogenesis	65 66 51,67,68
miR-125a/b	Tumour suppressor	Down	trkC	Restoration	↓ Cell proliferation, apoptosis	62
miR-138	Tumour suppressor	Down	Bax, Bcl-2, calpain and caspase-3	Restoration	↓ Tumour growth, ↓ colony formation and apoptosis	69
miR-141	Tumour suppressor	Down	FUS	Restoration	↓ Cell proliferation, ↓ migration and cell cycle arrest	70
miR-145	Tumour suppressor	Down	HIF-2α	Restoration	↓ Cell growth, ↓ invasion, ↓ metastasis and ↓ angiogenesis	71

miRNA	Types	Deregulation	Validated target(s)	Therapeutic approach	Function/processes	Reference(s)
miR-183	Tumour suppressor	Down	HDACi, MYCN	Restoration	Apoptosis and ↓ colony formation	72
miR-184	Tumour suppressor	Down	AKT2	Restoration	Apoptosis	73,74
miR-200a	Tumour suppressor	Down	AP-2γ	Restoration	↓Cell proliferation	75
miR-200b	Tumour suppressor	Down	ZEB1	Restoration	Neuroblast differentiation, ↓ migration/invasion and apoptosis	54
miR-204	Tumour suppressor	Down	MYCN	Restoration	↓ Cell proliferation and tumorignesis	76
miR-205	Tumour suppressor	Down	CREB1	Restoration	↓ Cell growth, ↓ invasion, ↓ migration and apoptosis	77
miR-335	Tumour suppressor	Down	SOX4, TNC	Restoration	↓ colony formation, ↓cell proliferation, ↓ invasion and ↓ metastasis	78
miR-337-3p	Tumour suppressor	Down	MMP14	Restoration	↓ Cell growth, ↓ invasion, ↓ metastasis and ↓ angiogenesis	79
miR-362-5p	Tumour suppressor	Down	(PI3K)-C2β	Restoration	↓ Cell proliferation, ↓ invasion and ↓ migration	80
miR-363	Tumour suppressor	Down	AMDM15, MYO1B	Restoration	↓ colony formation, ↓cell proliferation, ↓ invasion and ↓ metastasis	78
miR-410	Tumour suppressor	NA	VEGF-A, NIPBL	Restoration	↓ Cell proliferation, ↓ migration and ↓ angiogenesis	81
miR-542-3p	Tumour suppressor	Down	Survivin	Restoration	↓ Cell viability, ↓ cell proliferation and apoptosis	82
miR-542-5p	Tumour suppressor	Down	Unknown direct targets	Restoration	↓ Cell proliferation, ↓ invasion, ↓metastasis and ↓ survival	83
miR-584-5p	Tumour suppressor	Down	MMP14	Restoration	↓ Cell growth, ↓ invasion, ↓ metastasis and ↓ angiogenesis	84
miR-591	Tumour suppressor	NA	NA	Restoration	↓ colony formation, ↓ Cell proliferation,	58

NA: Not available. Adapted from Boloix et al.,[40] and Verimisso et al.,[85].

1.2.4. MiRNA as a therapeutic tool in Neuroblastoma

MiRNA-based therapies can be designed to inhibit or mimic the function of miRNA. These strategies are based on (Figure 3):

- **Therapies that inhibit oncogenic miRNA**: MiRNA can be blocked individually using antisense oligonucleotides (ASO), including locked nucleic acids (LNA), anti-miRNA oligonucleotides, morpholinos, miR-sponges and antagomirs or antimirs[86]. ASO are synthetic single stranded molecules that inhibit in a competitive manner miRNA molecules by their annealing to the mature forms and competing for the miRNA and mRNA target interaction. Anti-miRNA oligonucleotides have a perfect complementarity to the target miRNA that inhibit their binding to mRNA targets or induce their degradation by RNAse H[87]. On the other hand, antimiRs are small, synthetic molecules structurally similar to ASO that have a complementary sequence to their target mature miRNA[47]. LNA are a chemical modified new generation of antimirs, which form a thermodynamically strongest duplex with complementary mRNA known. Moreover, the good properties observed of LNA antagomirs imply a reduction of antimir nucleotides to shorter 8-mer-oligonucleotides, called “tinyLNA”. Finally, miR-sponges are RNA transcripts that act as miRNA decoy preventing the binding to one or multiple target mRNA[87].

  A different approach is the use of miRNA-masking synthetic antisense oligonucleotides, called miR-mask or target protectors, which perfectly bind to the mRNA target blocking the miRNA accession to mRNA target. This perfectly binding confers to miR-mask a high specificity that reduced their off-target effects, but this may reduce their possibility to affect multiple target genes[14].
- **Restoration therapies of tumour suppressor miRNA:** The genomic loss or downregulation of miRNA with tumour suppressor functions can be restored using miRNA mimetics or mimics or by gene therapy[1]. MiRNA mimics are synthetic double-stranded RNA with identical guide strand as endogenous mature miRNA that needs to be restored, while the passenger strand is fully complementary to the guide strand[86].

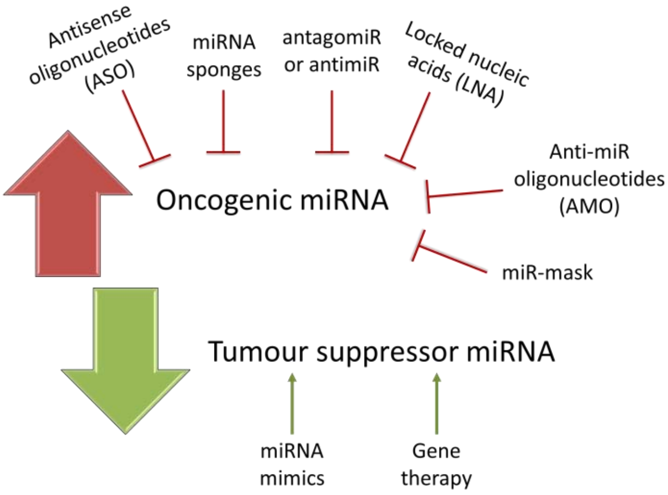

Figure 3. Proposed strategies using miRNA-based therapies against cancer. The objective of these approaches is the downregulation of high expressed oncogenic miRNA (red arrow) or the upregulation or mimicking the downregulated tumour suppressor miRNA (green arrow). Modified from Gambari et al., [86].

Concomitantly, miRNA-based therapies to inhibit or to restore miRNA functions present an important limitation related to their potential degradation by RNAses in serum or in endocytic compartments. For this reason, ASO, LNA, antimiR and miRNA mimics have been chemically modified in the 2’-OH-ring to increase their stability in front of nucleases, specificity and binding affinity to mRNA. Some of these modifications are the incorporation of phosphorothioate nucleotides, 2’-O-methyl groups (2’-OMe), sugar molecules with 2’-fluor residues or methoxyethyl groups or a methylene linkers. Although in some cases, these modifications enhanced the miRNA stability, binding affinity and reduced immunogenicity[6,88], sometimes the phosphortioate bonds can promote the binding of serum proteins and reduce their efficacy[6]. Moreover, for miRNA mimics, the modifications in both strands need to be different to ensure the proper loading of the guide strand into the RISC complex and the degradation of the passenger strand[88].

1.2.5. Advantages and limitations of the use of miRNA as therapeutic tools

The potential therapeutic effects of miRNA-based therapies observed in NB preclinical models have awaken the researcher’s interest in the last years. The use of miRNA as therapeutic tools presents several advantages useful for cancer therapy:

- MiRNA can **target multiple target genes** by acting over multiple mRNA simultaneously affecting different components of a single molecular signaling pathway or even different pathways. This minimizes the possibility of compensatory effects[40].

- Unlike mRNA or pre-miRNA, mature miRNA mimics are already **functional gene products** and do not require additional transcriptional regulation to carry out their functions[40].
- MiRNA do not reach **a "plateau"** response after their repetitive use in tumour cells, like occur with chemotherapeutic treatments. On the other hand, the radio- or chemoresistance observed with cytostatic drugs is not produced with miRNA-based therapies, which in turns may **sensitize the tumoral cells** to conventional treatments. Therefore, miRNA can improve targeted therapies, modulating targets involved in tumour development, restoring the sensitivity to conventional drugs or using in combination with current treatments[14].
- MiRNA are stable in frozen tissues and in formalin-fixed and paraffin-embedded tissue samples. This allows their extraction from clinical biopsies and their quantification by standardized methods such as quantitative PCR at any point during a patient's treatment[40].
- Finally, the major advantage of the therapeutic use of miRNA and other small molecules, such as siRNA, is that they can **broaden the number of druggable targets (~70% of the whole genome),** acting over RNA molecules which do not end up in protein production[6].

Although miRNA-based therapies are potential alternatives for the NB treatment, they still have some limitations to reach the clinic:

- The multiple target genes regulation by a selected miRNA can induce **unwanted or toxic effects**[89].
- The use of pre-miRNA mimics may induce a **saturation or insufficiency** of the enzymes involved in miRNA processing and, consequently, an inefficient efficacy. To overcome this hurdle, the use of mature miRNA mimics can avoid the miRNA processing enzymes saturation, because they have not to be processed[90].
- One of the challenges in developing miRNA-based therapies is to identify the best miRNA candidate for each cancer type[47].
- Finally, the major limitation of the use of miRNA as a therapeutic tool is their clinical administration due to **poor biodistribution**, **rapid clearance** and **lack of efficient delivery**[91]. Thereby, miRNA must move intact through bloodstream, achieve the target tissue, traverse different biological barriers, go through the cell membrane and, finally, enter in the cytoplasm of target cells[88]. Even though local delivery of miRNA modulators is achieved via direct injection at the site of action, this approach is limited to few cancer types (including sarcomas, mesotheliomas or brain tumours, but not for NB) and not enable the exposure of all tumour cells to the miRNA-based therapy. Therefore, systemic delivery of miRNA-based therapies is a most attractive therapeutic tool.

- However, their administration has *in vivo* barriers to overcome:
    1. Naked miRNA are rapidly **degraded by nucleases**, such as RNAse A, in the bloodstream in less than thirty minutes. This degradation reduces the miRNA half-life.
    2. One of the major disadvantages is the **poor biodistribution** of miRNA to not high perfused tissues because they are rapidly concentrated in the liver, where can be effective but are also **metabolized** and excreted rapidly by the **renal clearance**. Consequently, miRNA have **short half-life** that restrict the miRNA therapeutic efficacy in less irrigated tissues[92]. The high metabolism and excretion are caused by miRNA physicochemical properties. As well as other sRNA molecules, miRNA naked have a hydrophilic poly-anionic backbone with high molecular weight (~ 14KDa), that allow the easy miRNA solubility after their administration raising the miRNA plasma levels rapidly but, likewise they raise they are quickly decreased.
    3. MiRNA *in vivo* administration may activate the **innate immune response** mediated by type I interferon and proinflammatory cytokines[89] and can be triggered by TLR or macrophages leading to miRNA degradation[6] and unwanted toxicities[90].
    4. The major challenge of miRNA administration is their **deliver into target tumour** site with efficient penetration. Despite miRNA molecules do not present an active targeting to tumour sites, the enhanced permeability and retention effect (EPR effect) may facilitate the miRNA accumulation. EPR effect is described in passively targeted molecules which are extravasated into tumours due to the leaky vasculature and endothelial gaps (ranging from one to hundreds of nanometers)[93].
    5. Upon the tumour tissue is reached, the hydrophilic nature, negative charge and high molecular weight of miRNA backbone is responsible to the **poor penetration** in target tissues and their **low internalization** into tumoral cells because miRNA are unable to cross the cellular membrane[94].
    6. Once inside the cells, if it is the case, miRNA naked tend to be **degraded into lysosomes** due to their entrance by endocytic pathways. For this reason, **endosomal escape** is required for miRNA to reach the cytoplasm[92].

In consequence these disadvantages induce a low efficacy of these miRNA at target sites, which have made difficult the use of miRNA-based therapies in *in vivo* models and, in consequence, their entrance in clinical trials[95].

1.3. RNA delivery systems

The major role of a delivery system is to enhance the cellular uptake and the release of sRNA into target tissues. Moreover, the delivery systems are engineered to protect these oligonucleotides from premature nuclease degradation, increase their pharmacological effectiveness and reduce toxicity[6]. In general, the optimal nanocarriers should be safe, low immunogenic, high versatile, able to release their cargo and able to be prepared in a simple manufacturing low cost preparation/purification method[90]. Considering the similarities among small RNA, such as miRNA or siRNA, in terms of structure, physicochemical properties, intracellular target site to achieve and functions, similar delivery technologies can be applied for different types of sRNA[96].

The RNA delivery systems are classified in viral vectors and non-viral vectors.

1.3.1. Viral vectors

Until the 90s, viral vectors were the most common carriers used for gene therapy[97]. Researchers have used the process of virus infection as a delivery carrier to internalize nucleic acids inserted inside the virus capsid through endocytic pathways and release their content like happen with the viral genome. This process demonstrated high transduction efficiencies *in vitro* and *in vivo* and cell specificity when targeting moieties were added into viral capsid[92]. The most common viruses that successful deliver these nucleic acids are lentivirus, adenovirus and adenoassociated virus (AAVs). Lentivirus are less safe than adenovirus because lentivirus integrate their genome within the host cells’ genome, leading to higher risk of mutations and oncogenesis[92]. However, the systemic administration of AAV-miR-26 in mice displayed high transduction efficiencies in hepatocytes, downregulation of miR-26 target genes (e.g. Cyclin D2 and E2) and suppressed tumorigenesis in liver cancer with undetectable toxicity. Although in a murine model of more aggressive liver tumours, the AAV-miR-26 treatment did not have the expected outcomes[98]. Despite several viral vectors efficiently deliver miRNA into tumours and regulate target gene expression, their translation into clinics is slowed down due to different safety issues[96], such as genomic integration in the host genome, mutagenesis[99], immunogenicity or the activation of competent virus replication[100]. In addition to safety problems, viral vectors exhibited other problems, such as small cargo capacity and difficulties in large-scale production[87], which prompted the interest on the development of non-viral carriers able to deliver sRNA[97].

1.3.2. Non-viral vectors

Non-viral vectors have emerged as a potential alternative to viral vectors due to their less immunogenic effects, their easy control on their molecular composition and simplified manufacturing and purification[101]. Even though non-viral delivery systems usually had low transfection efficiencies and short duration on target gene expression, the rational design of new systems to deliver sRNA using nanotechnology has improved their clinically efficiency[92]. Recent developments in the nanotechnology field offer new possibilities to resolve the present issues and barriers in drug delivery. Thus, nanoparticles (NP) are nanostructured entities with controllable size, shape, surface and biological behaviour[89]. These NP can be used for the delivery of chemical and biological actives because they can be loaded and transport multiple cargos, such as drugs, nucleic acids, or targeting ligands among others. For this reason, NP are also called nanocarriers. Moreover, nanocarriers can improve sRNA biodistribution because they can extend miRNA half-life protecting them from premature degradation by nucleases; can avoid their elimination by renal clearance; increase their cellular uptake and improve their delivery into the specific cellular compartment, enhancing their efficacy over target genes and reducing potential side-effects, such as the stimulation of the innate immune response[102]. Furthermore, NP can enhance the absorption of miRNA into the selected tissues, when these NP are functionalized with targeting moieties[103]. In addition, some NP allow the control of their pharmacokinetics profile and cargo release, reducing the frequency of administration or the dosage needed[89].Non-viral nanocarriers are usually classified depending on their chemical composition in inorganic NP or organic NP[104] (Figure 4). Both systems have been used to load and transport sRNA in *in vitro* or *in vivo* studies.

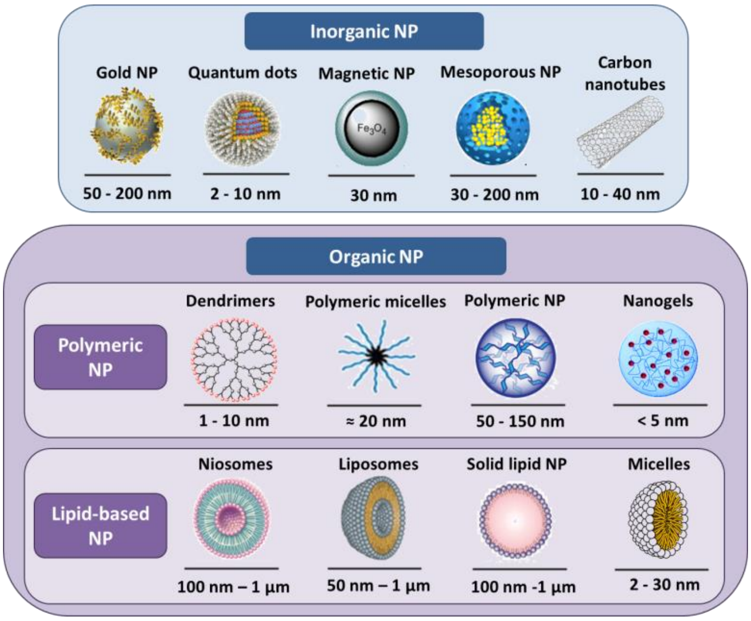
Inorganic NP
Gold NP
Quantum dots
Magnetic NP
Mesoporous NP
Carbon nanotubes
Fe_3O_4
50 - 200 nm
2 - 10 nm
30 nm
30 - 200 nm
10 - 40 nm
Organic NP
Polymeric NP
Dendrimers
Polymeric micelles
Polymeric NP
Nanogels
1 - 10 nm
≈ 20 nm
50 - 150 nm
< 5 nm
Lipid-based NP
Niosomes
Liposomes
Solid lipid NP
Micelles
100 nm – 1 µm
50 nm – 1 µm
100 nm -1 µm
2 - 30 nm

Figure 4. Classification of nanoparticles used for drug delivery depending on the nature of their chemical composition. Adapted from Gu et al., [105]; Khodabandehloo et al.,[106].

1.2.3.1 Inorganic nanoparticles

Inorganic nanoparticles have been widely employed in biomedical field for several applications, such as drug delivery, imaging agents, biosensors and tissue engineering[106]. The inorganic materials that compose a drug delivery system offer the potential to develop a NP with a controlled size and morphology and with biocompatible[106], non-immunogenic and non-toxic properties. Moreover, they can be easily produced in a cost-effective method and can be scaled-up[92]. Inorganic NP may be made with different inorganic materials, such as gold, silver, silica, cerium oxide, hafnium oxide, iron oxide, metal, quantum dots, nanoshells[100]… Gold NP (AuNP) are the inorganic NP most frequently used for disease diagnosis. In particular, gold NP are used as suitable nanocarriers for bioimaging applications taking the advantages offered by the miRNA dysregulation in cancer, which are considered promising biomarkers for early diagnosis[106]. Magnetic NP are mainly used for diagnostic purposes; however, inorganic NP used to deliver miRNA for cancer treatment are still in preclinical stages. For example, silica-based NP with a disialoganglioside GD2 (GD_2) antibody were engineered to specifically deliver miR-34a into neuroblastoma tumours. Systemic administration of anti-GD_2-coated NP with miR-34a inhibited tumour growth in orthotopic NB models due to an increased apoptosis and reduced vascularization[68]. Despite inorganic NP have been considered good nanocarriers for nucleic acids, due to the good previous results in preclinical studies, they have still several concerns to be translated into the clinic. Some of them are the low encapsulation efficiency, poor storage stability, poor endosomal escape[90] and the long-term toxicity and carcinogenesis[107].

1.2.3.2 Organic nanoparticles

Organic nanoparticles are characterised to be composed of organic materials, such as lipids and polymers, usually with a bigger diameter compared to inorganic NP (from 10 nm to micrometres). Moreover, they present diverse advantages, mainly related to their biocompatibility and biodegradability. The more widely used organic NP for sRNA delivery are lipid-based nanocarriers and polymeric nanocarriers[108].

i. Non-lipid or polymer-based nanovesicles

Polymeric nanovesicles

Polymeric carriers are one of the most extensively used RNA delivery systems. Polymeric NP are solid, submicronized (10-1000 nm) colloidal particles made up of cationic polymers with amine groups that forms a matrix or scaffold. Normally, polymeric nanocarriers present high biocompatibility, biodegradability and the ability to control their cargo release[108]. Their positively charged polymers facilitate their easy interaction with the negatively charged phosphate groups of nucleic acids to form complexes called polyplexes. Traditionally, polymeric NP are classified into natural or synthetic polymers[90]. Natural polymers include polysaccharides, such as chitosan, peptides and proteins; whereas some examples of synthetic polymers are polyethyelenimines (PEI), poly(lactic-co-glycolic acid) or dendrimers.

Chitosan is the most studied natural cationic polymer for drug delivery due to their biocompatibility, biodegradability and safety structure[90]. For example, Deng and their colleagues co-encapsulated miR-34a and doxorubicin (DOX) into complexes of chitosan and hyaluronic acid in order to treat triple negative breast cancer. Even though, the co-delivery of miR-34a with DOX cannot improve the chemosensitivity and side effects of DOX, but synergistic anti-tumoral activity was observed[109].

Nevertheless, while PEI was initially considered the gold standard polymeric transfection reagent for DNA *in vitro*, in the last ten years has also been introduced as a sRNA or RNA transfection reagent. Upon nucleic acids conjugation, PEI maintains their positive charge that allows that PEI polyplexes enter inside the cells by endocytosis. The high delivery efficiencies of nucleic acids observed with PEI are caused by the “proton sponge” effect that permits the endosomal escape of polyplexes[110]. The endosomal escape is a well-known mechanism which is produced when some agents can avoid the reduction on endosomes pH and induce a destabilization in the endosomal membrane, which allow the release of the entrapped molecules to the cytosol before being digested in the lysosomal compartment. However, this mechanism is a bottleneck in the nanoparticles field. Despite these polymeric nanocarriers are efficient and highly used *in vitro*, their application *in vivo* is limited due to high toxicity. Currently, *in vivo*-jet PEI is a commercially available delivery system formed by PEI that is being tested to deliver sRNA in preclinical studies. *In vivo*-jet conjugated with miR-22 was tested in a breast carcinoma mouse model and showed impairment of tumour growth and metastasis by inducing cellular senescence[111].

Furthermore, in order to take advantage of the proton sponge escape ability of PEI, a new class of polymeric nanocarriers for sRNA were developed. Pluronic® amphiphilic copolymers were combined with PEI-siRNA polyplexes to improve the release of nucleic acids from polymeric NP (PM) and reduce the instability and toxic effects derived from the cationic charges of PEI. In this study, PM loaded with AKT2 siRNA internalized into MDA-MB-231-ALDH1A1:tdTomato and MCF-7- ALDH1A1:tdTomato breast cancer stem cells (CSC) and they did not colocalize in the endosomes. Further, PM-AKT2 siRNA reduced the metastatic potential of cancer stem cells reducing the cell invasion and impairment the colonies formation in CSC. Moreover, the tail vein injection of the PM-siRNA nanosystem in a patient derived xenograft (PDX)-bearing athymic mice confirmed the arrival of PM-siRNA into tumour parenchyma in less than 4 hours[112].

Hence, alternative polymeric materials are frequently used in preclinical stages to deliver sRNA, like N-acetyl-D-galactosamine (GalNAc), Poly(lactide-co-glycolide) (PLGA) and cyclodextrin. The GalNAc–siRNA and GalNAc–miRNA conjugates, called respectively ALN-PCSsc (from Alnylam Pharmaceuticals), and RG-101 (from Regulus), were finalized successfully phase I of clinical trials. PLGA polymer has been widely used in preclinical studies due to their biodegradable sutures and low toxicity but their neutral charge implies low loading rates of sRNA. Cyclodextrin also entered in clinical trials, but the trial was terminated owing to dose-limiting toxicity[101].

Finally, dendrimers, which consist of an hyperbranched core unimolecular structure were also tested for sRNA delivery. In particular, dendrimers composed of poly(amidoamines) or poly(propylenimines), have shown high efficiency release of nucleic acids *in vivo* using the proton sponge effect. The major advantage of dendrimers is that can carry multiple cargos in the core or conjugated to the terminal periphery groups of the dendrimer structure (Figure 5). Furthermore, dendrimers can have a controlled release of their cargo[113]. The most commonly used is poly-amidoamine (PAMAM); however, their cationic charge is often associated to toxicity[47]. For this reason, modified polymers are being explored to solve toxicity issues[90].

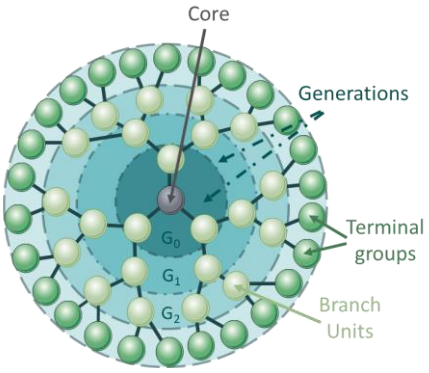

Figure 5. Dendrimer structure. Adapted from Ma et al.,[114].

Polymersomes

Polymersomes have been designed for a broad range of applications but are usually employed for targeted delivery of active biomolecules. Polymersomes are artificial vesicles formed by copolymer chains self-assembled to form amphiphilic membranes with an aqueous core[115]. Compared to liposomes, polymersomes have similar physicochemical properties in terms of size and lamellarity, but their membrane is thicker (i.e. between 5-50 nm, while in liposomes is about 3-5 nm). Although polymersomes stability is higher compared to liposomes, due to their polymeric membrane, their lower permeability and low lateral fluidity, which may reduce their delivery efficiency[116].

To improve their cargo release, such as sRNA, in the cytosol or tumoural microenvironment, pH-sensitive polymersomes have been developed[115]. For example, polymersomes composed by pH-sensitive imidazolic groups functionalized with folic acid presented high colloidal stability and high encapsulation efficiency of ds-DNA and siRNA molecules. Moreover, polymersomes silenced luciferase activity and Hsp90 protein expression after siRNA transfection in B16-F10-luc-G5 cells[117].

Micelles

Micelles are multi-molecular self-assembled nanosized colloidal particles with a hydrophobic core and hydrophilic shell. Micelles can be composed by amphiphilic polymers, lipids (like 1, 2-Distearoyl-sn-glycero-3-phosphoethanolamine (DSPE)) or surfactants[103]. Polymeric micelles are highly stable and biocompatible colloidal particles formed by amphiphilic block co-polymers with a size between 10-100nm[118]. Unlike polymeric NP, lipid micelles are smaller ($D_h < 20$ nm) but are less stable *in vivo* or in physiological fluids[119]. Micelles can load hydrophobic drugs inside their core improving their bioavailability because they protect them from biological environments[113]. Hydrophilic molecules, like sRNA, can be carried outside the micelles. However, sRNA loading outside the micelles may expose sRNA to nucleases degradation after i.v. injection. Moreover, i.v. administration in the bloodstream might cause premature non-desired destruction of the micellar structure.

ii. Lipid-based nanovesicles

Lipids are the most widely used materials to deliver nucleic acids *in vitro* and *in vivo*. Frequently, lipid-based nanocarriers are classified into liposomal or non-liposomal vesicles[90]. The most well-known liposomal nanovesicles are liposomes and solid-lipid nanoparticles. However, a wide variety of non-liposomal lipid-based nanovesicles are being developed. Nanovesicles are colloidal spheroidal structures composed by at least one closed bilayers. Nanovesicle bilayers are formed by the self-assembly of amphiphilic molecules, as it is representd in Figure 6.

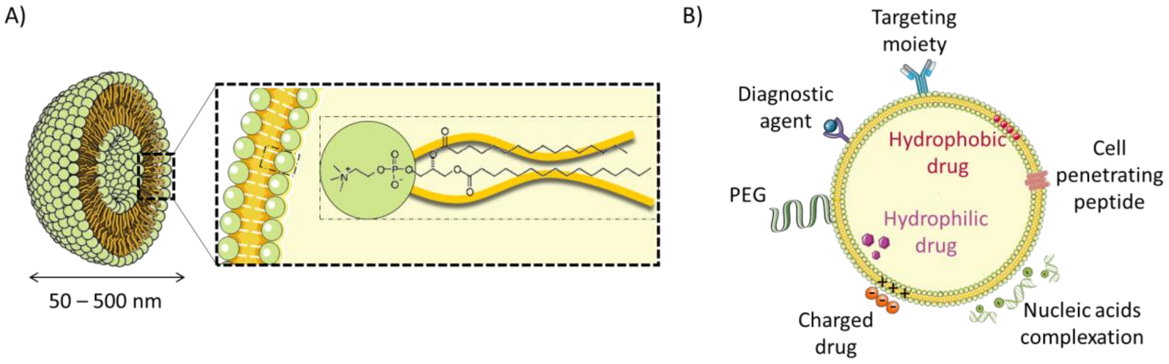

Figure 6. Schematic representation of lipid-nanovesicles structure and their functionalization capabilities as a nanocarrier. Adapted from Torchilin et al.,[120].

Liposomes

Liposomes are probably the most used nanosystems for nucleic acids delivery. The first nanoparticles approved by Food and Drug Administration (FDA) as a drug delivery system was Doxil®, which contains doxorubicin encapsulated in liposomal vesicles[102]. Liposomes are also widely used to deliver sRNA, like Patisiran®, which was the first siRNA approved for commercialization in 2018[121].

Liposomes are spherical self-closed structures formed by one or several concentric phospholipid or lipid bilayers (hydrophobic bilayer) with an aqueous core[90]. Liposomes can form unilamellar or multilamellar vesicles that may contain single or multiple types of lipids. Lipids are composed of three parts: the amine head group, the linker group and the hydrophobic tails, usually two. The amine head group determines the kind of interaction produced with sRNA, which can be by electrostatic interactions when lipids are positively charged or encapsulating them into the aqueous core, the cellular uptake and the endosomal escape capacity[122]. The encapsulation of sRNA molecules in their aqueous core protect them from degradation by nucleases and enhance their internalization through membrane fusion or receptor-mediated endocytosis[89].

Liposomes are nanovesicles composed of phospholipids with a size range between 50-450 nm[120]. Moreover, their similar components to cellular membranes make them highly biocompatible and biodegradable. In addition, their versatility may allow their functionalization through hydrophobic molecules inserted in their membrane, which might be further functionalized with other functional molecules, such as poly-(ethylene glycol) (PEG) molecules or targeting moieties (Figure 6) that extend their circulation time or do a specific tissue delivery, respectively[89]. Despite the mentioned advantages, liposomes present several drawbacks after their *in vivo* administration, such as the accumulation in the reticuloendothelial system (RES), leading to rapid renal clearance and short half-life in serum, poor biodistribution due to the lack of target tissue specificity and reduced efficacy into selected tissues[89]. Moreover, liposomes have in general a very low shelf-stability, which is very problematic in pharmaceutical formulations.

Liposomes can be divided depending on the preparation method, size (small, intermediate or large), lamellarity (uni-, oligo- or multilamellar vesicles) or composition[123]. Furthermore, liposomes are classified depending on their composition into cationic liposomes, ionizable liposomes, neutral liposomes, negative liposomes and lypopolyplexes.

Cationic liposomes

Cationic liposomes are usually formed by cationic lipids with quaternary amines and neutral lipids. The most commonly used cationic lipids are 1,2-dioleoyl-3-trimethylammonium-propane (DOTAP), 1,2-di-O-octadecenyl-3-trimethylammonium propane (DOTMA), 2,3-dioleoyloxy- N-[2-(sperminecarboxamido)ethyl]-N,N-dimethyl-1- propanaminium (DOSPA) and dioctadecyl amido glycil spermine (DOGS). Typically, cationic lipids are used in combination with neutral lipids, also called as helper lipids. Helper lipids are used to improve the transfection efficiency of nucleic acids and enhance the stability of colloidal dispersions[124]. Moreover, helper lipids, including 1,2-Dioleoyl-sn-glycero-3-phosphoethanolamine (DOPE) and Cholesterol (Chol), present fusogenic properties that can induce their fusion with cellular membrane caused of the membrane lipids shift from the more stable lamellar phase to the hexagonal (H_{II}) phase. This transition promotes the cellular or endosomal membrane perturbation and liposomal cargo releases in the cytosol[122]. Nowadays, several lipid transfection reagents are commercially available. For example, Lipofectamine 2000® (Thermo Fisher Scientific), DharmaFECT (Dharmacon), Fugene (Promega), RNAiMAX (Thermo Fisher Scientific) and Lipofectin (Thermo Fisher Scientific)[125].

Cationic liposomes are between 100-300nm in size, protect sRNA from nucleases degradation, increase the sRNA half-life and their arrival into cells. Their physicochemical properties allow the lipoplexes formation by the sRNA encapsulation inside their hydrophilic core or their binding directly by electrostatic interactions between their cationic lipids with the negatively charged sRNA[90]. Their positive charge facilitates their uptake by cellular membranes[87], but may induce a significant toxicity and hypersensitivity *in vivo* due to the activation of the innate immune response by type I and II interferon[89]. Moreover, cationic lipoplexes tend to internalize inside the cells via "clathrin-mediated endocytosis", in which nucleic acids arrive into endosomes and need to destabilize the endosomal membrane to escape to cytosol before endosomal fusion with lysosomes. Hence, to avoid lipoplexes degradation in lysosomes, lipoplexes must induce a "flip-flop" of lipids from the endosome's membranes and liposomes membrane, which consequently release the liposomes cargo into cytosol[124]. Thereby, important issues to consider, especially to use lipoplexes by intravenous administration is their instability in physiological fluids, their toxicity by immunological reaction and uneven transfection efficiencies depending on the cellular type[90,123]. Despite these facts, Wang et al. demonstrated the in vitro efficacy of cationic liposomes with DOTMA to deliver miR-122 specifically in liver to treat hepatic cancers, among other diseases. Wu and their colleagues also shown the potential of the tumour suppressor miR-29b to treat non-small lung cancer using DOTMA lipoplexes in a xenograft mouse model[126].

Neutral liposomes

Neutral liposomes are formed by neutral lipids, some examples are 1,2-Dioleoyl-sn-Glycero-3-Phosphocholine (DOPC), 1,2-Dioleoyl-sn-glycero-3-phosphoethanolamine (DOPE), Chol or polysorbate 20, among others. The neutral charge of these liposomes confers them less cytotoxicity and form less aggregates in physiological fluids compared to cationic liposomes. However, their neutral charge reduce the entrapment efficiency[87], the internalization efficiency and the arrival and delivery to tumour sites[47]. It is reported that neutral liposomes, instead of being accumulated in the liver like cationic liposomes, are highly uptaken by lungs[87]. This property was used by Trang and their colleagues to facilitate the delivery of miR-34a and let-7 from a neutral lipid emulsion into orthotopic lung tumours [127], but this selective biodistribution reduce their medical applications.

Ionizable liposomes

Ionizable liposomes are new engineered pH-sensitive liposomes formed with ionizable lipids that often have tertiary amines that become protonated at acidic pH but remain neutral at physiological pH. Examples of ionizable lipids are 1,2-dioleoyl-3-dimethylammonium propane (DODAP) and 1,2-dioleyloxy-N,N-dimethyl-3-aminopropane (DODMA). However, to form stable liposomes, they should be combined with helper and neutral lipids, such as Chol and saturated phosphatidylcolines, which increase their membrane stability and transfection efficiency[90]. The most well-known pharmacologically-advanced case of a miRNA encapsulated in ionizable neutral liposomes is MRX34. MRX34 is composed by miR-34a and amphoteric liposomes named SMARTICLES® [128]. SMARTICLES® are formed by 1-palmitoyl-2-oleoyl-sn-glycero-3-phosphocholine (POPC), DOPE, cholesteryl hemisuccinate (Chems) and cholesteryl-4-([2-(4-morpholinyl)ethyl]amino)-4-oxoburanoate (MOCHOL). These liposomes are anionic at physiological pH that present a charge and a pH-tunable character. SMARTICLES® present an average size of approximately ~130nm, avoiding the liver metabolism and improving their biodistribution and stability in serum after i.v administration[129]. Moreover, Chems can be protonated in the low tumoral pH or inside the endosomes, which lead to a positive surface of SMARTICLES which promotes tumor cell interaction and endosomal cargo release[130]. Functionally, MRX34 induces tumour regression in Hep3B and HuH7 orthotopic murine models of liver cancer[128] and enhanced their anti-tumor activity when co-administrated with sorafenib[131]. However, the NCT02862145 clinical study was halted in 2016 because of multiple immune related serious adverse events[132].

Anionic liposomes

In general, drug delivery by anionic lipids is not very efficient. The negatively charged head group of lipids prevents the nucleic acid conjugation due to repulsive electrostatic forces with the phosphate backbone of nucleic acids. Considering that cationic liposomes can be inactivated in presence of serum, are unstable upon storage and present high cytotoxicity, anionic liposomes were considered an alternative. Commonly used anionic lipids are naturally found in cellular membranes, such as phosphatidic acid, phosphatidylglycerol or phophatidylserine. In consequence, lipoplexes with a negative charge present low clearance and phagocytosis by macrophages uptake, which lead to high biocompatibility[133]. The main disadvantages of negative liposomes are their less cargo entrapment efficiency and the low cellular uptake.

Solid-lipid NP

A new class of biodegradable solid lipid NP developed to deliver sRNA, are stable nucleic acid lipid particles (SNALP). SNALPs are usually formed by cationic lipids (1,2-dilinoleyloxy-N,N-dimethyl-3-aminopropane, DlinDMA) to improve the internalization, induce the endosomal escape and conjugate the siRNA; helper lipids (1,2-distear-oyl-sn-glycero-3-phosphocholine, DSPC) to promote the release of siRNA; polyethylene glycosylated lipids (PEG–C–DMA) and Chol, to stabilize the liposome[134]. Despite SNALPs present a nanometric size (< 200nm), an excellent biocompatibility, minimal toxicity and less cost of production compared to polymeric carriers[89], their solid fat and lipophilic core have less efficient encapsulation of hydrophilic molecules, such as sRNA[135]. For this reason, PLK1 siRNA encapsulated in SNALP, also known as TKM-080301, are currently in the Phase I/II of clinical trials for the treatment of hepatic cancer (NCT02191878) and liver metastatic tumours (NCT01437007). Although the favourable toxicity profile at the studied dose and the antitumoral activity in xenograft models, TKM-080301 treatment did not demonstrate an improved overall survival in patients with advanced hepatocellular carcinoma. Moreover, another clinical trial started to evaluate the safety and antitumoral activity of TKM-080301 in patients with neuroendocrine or adrenocortical tumours (NCT01262235) showed antitumoral activity but also some serious adverse effects caused by i.v. infusion of the lipid-carried siRNA [136].

Lypopoliplexes

Lypopolyplexes are systems composed by a mixture of lipids and polymers to address the limitations and combine their advantages. Cheng and their colleagues generated DOTAP liposomes combined with hyaluronic acid and protamine NP to co-deliver miR-34a and three different siRNA to target c-Myc, MDM2 or VEGF in B16F10 melanoma lung metastasis murine models. Moreover, these NP were conjugated with the GC_4 tumour-targeting single-chain antibody fragment (scFv), which is specific for metastatic tumour cells. The intravenous injection of this system inhibited the tumour load in the lungs, primarily when antibody-targeting NP contain miRNA and siRNA simultaneously[137].

Non-liposomal lipid-based nanovesicles

The most important examples types of non-liposomal lipid-based nanovesicles are niosomes, transferosomes, ethosomes, sphingosomes, ufasomes, pharmacosomes, virosomes and Quatsomes. Despite all of them were aimed at expanding the nanoparticles application to biomedical use, only niosomes have been tested to deliver sRNA in preclinical studies. Some of them cannot be useful as a drug delivery system due to their limitation to topical applications (i.e, transferosomes, ethosomes and ufasomes). Moreover, sphingosomes are expensive to produce and have a poor entrapment efficiency. Finally, the potential of pharmacosomes and Quatsomes as a nanocarriers to deliver nucleic acids is still unknown.

Niosomes

Niosomes are non-ionic surfactant vesicles that have gained the scientific attention as drug delivery systems due to their cheaper and more stable components compared to phospholipids[138]. Niosomes are usually formed by the self-assembly of cholesterol, fatty acids, cationic lipids and non-ionic surfactants in aqueous phase[139]. Niosomes have similar properties compared to liposomes because are biocompatible, biodegradable and non-toxic. Besides niosomes have good physicochemical stability in terms of size (i.e. D_h between 100 nm and micrometers), unilamellar or multilamellar morphology and they can entrap both hydrophilic or hydrophobic cargos[140]. An example is Span 80-based cationic niosomes, also named iSPN, which contains the cationic lipid DOTAP and the nonionic surfactant sorbitan monooleate Span-80. Their conjugation with sRNA demonstrated the inhibition of miR-138 and enhanced the osteogenic differentiation of hMSC cells. *In vivo* biodistribution assays demonstrated the high accumulation of niosomes in the lung and liver[141]. This limited biodistribution compromises their applicability for cancer therapy in certain types of cancer.

1.3.3. Advantages and limitations of nanoparticles for drug delivery

Nanomedicine has the potential to improve the opportunities to use RNA-based therapies *in vivo*. However, nanocarriers tested for the delivery of sRNA so far, have still some limitations.

The major difficulties of NP are: i) limited carrying capacity; ii) toxicity and, iii) scaling-up their production. In the most types of NP, their loading depends on the encapsulation capacity inside the membrane, which in some cases is spatially reduced. However, the opportunity given by some nanocarriers, like liposomes to carry their cargo by electrostatic interactions outside or anchored in the lipid membrane may increase their loading capacity. Besides, dendrimers can encapsulate more cargo due to their branched structure[142].

Moreover, NP must be made from biocompatible, well characterized, and easily functionalized materials to reduce their toxicity and ensure their biodistribution[96]. Another important limitation observed in several NP is their high cost of production and purification, which restricted their large-scale preparation for clinical uses. For achieve the clinical application, NP must be prepared at industrial scale following the Good Manufacturing Practice (GMP) production, which ensure pharmaceutical quality, through a tight control of NP physicochemical properties and batch-to-batch reproducibility[100]. For example, the preparation of lipid-based nanovesicles using conventional methods, microfluidic or non-conventional methods presents serious difficulties for its scalability at the industrial level and high production costs are associated. Moreover, the use of phospholipids raises the price of liposomes preparation[138].

The obstacles encountered by NP-sRNA conjugates can be classified in extracellular or intracellular barriers:

- The principal **extracellular barriers** occurred after intravenous administration of NP-sRNA conjugates. Although nanocarriers increase sRNA half-life because protect sRNA from nucleases or enzymatic degradation[91], their physicochemical properties are crucial to predict the NP-sRNA conjugates biodistribution *in vivo*. It is well-known that particle size determines the circulation time of these conjugates. After systemic administration, NP tend to accumulate in spleen and liver where are removed by Kupffer cells using the reticulo-endothelial system (RES). Currently, it is accepted that NP around 50-200nm presented an optimal size for sRNA delivery because they are up taken into tumours by the enhanced permeability-retention (EPR) effect, avoiding their metabolism and degradation in liver or spleen observed in bigger NP and the rapidly renal clearance of smaller NP (D_h< 5 nm). Moreover, larger NP (D_h > 15 µm) tend to accumulate in liver, spleen and bone marrow[113]. In addition, NP size, shape and geometry have a significant impact on cellular internalization, which determinates the NP internalization pathway used[113]. Decuzzi and their colleagues demonstrated that the geometry of NP contributes to opsonization, *in vivo* biodistribution, strength of adhesion and internalization rate in cells[143]. Another important parameter of NP is the surface properties that may induce the NP opsonization in blood circulation. The opsonization process is based on the binding of opsonins, such as immunoglobulins or complement proteins, into NP surface that contribute to macrophages recognition and may reduce NP circulation time by RES clearance. Specifically, NP with size smaller than 8 nm or with cationic charges are more likely filtered by RES clearance. In addition, macrophages may activate the innate immune response to favor the elimination of the nanoconjugates which can have unwanted toxic effects *in vivo*[144].

One of the major concerns about clinical administration of nanomedicines is the full toxicological characterization. The acute toxicity observed in some NP caused by innate immune response activation, inflammation, hemolysis or oxidative stress demands data from the largely unknown chronic toxicity of nanoparticles[100].

Moreover, the passive targeting of NP upon specific tissues or organs do not ensure the arrival of these NP to the targeted cells. One example is the addition of peptides such as Arg-Gly-Asp (RGD), which bind to integrin receptors overexpressed in tumoral cells. In addition, NP must overcome the capillary endothelium through an extravasation process and then go through the extracellular membrane. Hence, achieving therapeutic concentrations in the tumour microenvironment is another limitation because the higher interstitial fluid pressure found nearly to solid tumours may prevent the diffusion of NP[89].

- On the other hand, the most common **intracellular barriers** observed in NP are related to: i) their cellular uptake, ii) the endosomal escape and iii) the cargo release[104]. Generally, nanocarriers have high transfection efficiencies and depending on their physicochemical properties are influenced to internalize using different pathways. To ensure the intracellular sRNA delivery, NP need to cross the cellular membrane. Charged NP tend to internalize using endocytosis, which leads to the sequestration of the NP cargo in endocytic vesicles. Then, the acidification of endosomes and their fusion with lysosomes produce the degradation of sRNA and decreases the efficiency of NP as a delivery system[142]. Therefore, NP must escape from endosomes before their fusion with lysosomes in order to avoid their cargo degradation and to facilitate their release into cytosol. To enhance the endosomal escape, several NP are engineered to induce the endosomal membrane destabilization by flip-flop mechanism, the “proton sponge effect” or the endosomal membrane fusion[145]. Despite some NP have the ability to escape from endosomes, for example cationic liposomes (formed with DOTAP or DOTMA), synthetic cationic polymers (like PEI) or ionizable liposomes (composed by DOPE)[146], the lysosomal degradation of NP is a bottleneck in the use of NP to deliver sRNA.

Finally, it was observed that another challenge still unsolved is to ensure the cargo release from NP surface or encapsulation[102]. For this reason, recently sRNA molecules have been bound in a reversible manner by pH-sensitive (such as Chems or DOTAP), reductively labile (like 1,2-dioleoyl-sn-glycerol-3-succinyl-2-hydroxyethyl disulfide ornithine lipid (DOGSDSO) or enzymatically degradable (such as dipalmitoylphosphatidyl choline (DPPC)) bounds that can be broken easily inside the cells and separate the nanocarrier from the sRNA[147].

The main advantages and disadvantages of the currently used nanomedicines for nucleic acids delivery are summarized in Table 2.

Table 2. Advantages and drawbacks of the nanomedicines used for nucleic acids delivery.

Nanocarrier type		Advantages	DisadvantagesInconvenients
Viral vectors		• High transfection efficiency • Cell specificity • High release	• Low cargo packaging • High cytotoxic • High Immunogenic • Mutagenesis • High production cost • Difficult scale-up
Inorganic NP		• Inert materials • Controlled PQ properties • Biocompatible • Easy scale-up	• Poor storage stability • Low cargo payload • Not biodegradable • Poor endosomal escape • High renal clearance • Long term toxicity (carcinogenesis)
Polymeric NP	**All polymeric NP**	• Controlled PQ properties • High colloidal stability • High cargo payload • High transfection efficiency	• Poor biodistribution • High instability in physiological fluids
	Natural	• Biocompatible materials • Biodegradable	• Cytotoxicity • Poor endosomal escape
	Synthetic	• Endosomal escape by proton sponge effect	• High cytotoxicity and immunogenicity • Limited administration routes • Low biodegradability • Low biocompatibility
	Dendrimers	• Biocompatible materials • Biodegradable • Low cytotoxicity	• Limited administration routes • Poor endosomal escape
Micelles		• High cargo payload • High permeability • Biocompatible materials • Biodegradable • Easy synthesis and scale-up	• Poor stability • Poor endosomal escape • High RES or renal clearance • Cytotoxicity (due to the surfactant)

Nanocarrier type		**Advantages**	**Disadvantages**
Liposomes	**All liposomal NP**	• Controllable synthesis conditions • High cargo payload of hydrophobic or hydrophilic drugs • Biocompatible • Biodegradable	• Poor colloidal stability • Low homogeneity among nanovesicles • High cost of preparation • Problems into large-scale production • Opsonization and immunogenicity
	Neutral	• Low cytotoxicity • Low aggregation to serum proteins	• Low entrapment efficiency • Low cellular uptake • Lysosomal degradation • Pulmonary inflammation
	Cationic	• High entrapment efficiency • High cellular uptake • Enhanced stabilization by electrostatic interactions • Variable endosomal escape	• High aggregation to serum proteins • High cytotoxicity
	Negative	• High cellular uptake • Low cytotoxicity	• Low entrapment efficiencies • High aggregation to serum proteins • High immunogenicity • Poor endosomal escape
	Ionizable	• High endosomal escape • High cellular uptake • High entrapment efficiency • Low cytotoxicity	• High immunogenicity
Solid lipid NP		• High colloidal stability • Excellent biocompatibility • Slow cargo release • Easy scale-up and sterilization	• Low entrapment efficiency • Low hydrophilic cargos loading • Immunogenicity • High water content
Niosomes		• Stable upon storage • Biocompatible • Low cytotoxicity	• Poor physical stability • Sterilization problems • Leaking entrapped cargo

Adapted from Wicki et al.,[100]; Choi & Han[148] and Peer et al.,[103].

1.4. Use of miRNA as therapeutic tools in clinical trials

The interest of miRNA therapeutics has raised over the past 20 years, in which the identification of hundreds of miRNA, their target genes and their relation to human diseases have been in the spotlight[87]. Despite the researcher's interest, the emergence of miRNA therapeutics has not yet translated as new drugs approved by regulatory agencies, even therapeutics based on miRNA are already entering in phase I or II of clinical trials (Table 3). Differentially to miRNA, siRNA-based therapies have been the first gene silencing therapy that reached the market using small RNA. For example, Patisiran (Onpattro®) is a double-stranded siRNA encapsulated in a lipid nanoparticle for the treatment of the polyneuropathy of hereditary TTR-mediated amyloidosis in adults (hATTR) (NCT01960348). To date, various pharmaceutical industries or biotech companies are involved in the clinical research using sRNA. Nevertheless, in the major of them sRNA relies on forms for being administrated locally. However, the local miRNA administration can be used in a reduced number of medical applications, e.g. age-related macular degeneration. For this reason, the systemic administration of sRNA is required. In consequence, the limitations observed with sRNA, such as short half-life and inefficient biodistribution, implies the introduction of the nanomedicine field to achieve a successful deliver of sRNA[149].

The miRNA-based therapies currently in clinical stages are summarized in the Table 3.

Table 3. Selected list of miRNA therapeutics currently in clinical trials.

ame (company)	Therapeutic agent	Delivery system	AD route	Target diseases	Trial details	ClinicalTrials. gov iD or Ref.
Miravirasen (Santaris Pharma A/S and Hoffmann-La Roche)	AntimiR-122	LNA-modified antisense inhibitor	SC	Hepatitis C (chronic infections included)	Single-centre phase I, completed Multicentre phase II, completed Multicentre phase II, unknown Multicentre phase II, completed Single-centre phase II, completed Single-centre phase I, unknown	NCT01646489 NCT01200420 NCT01872936 NCT02452814 NCT02508090 NCT01727934
RG-101 (Regulus Therapeutics)	AntimiR-122	GalNAc-conjugated antimiR	SC	Chronic hepatitis C	Phase I, completed Multiple phase II, halted	[150]
RG-125/ AZD4076 (Regulus Therapeutics)	AntimiR-103/ 107	GalNAc-conjugated antimiR	SC	Patients with type 2 diabetes and non-alcoholic fatty liver diseases	Single-centre phase I, ongoing Single-centre phase I/IIa, ongoing	NCT02612662 NCT02826525
MRX34 (Mirna Therapeutics)	miR-34 mimic	Lipid NP (Smarticles®)	IV	Multiple solid tumours (liver, lymphoma, melanoma)	Multi-centre phase I, terminated Multi-centre Phase I/IIa, whithdrawn	NCT01829971 NCT02862145
Remlarsen or MRG-201 (Miragen Therapeutics)	MiR-29 mimic	-	ID	Cutaneous fibrosis	Multi-centre Phase II, ongoing	NCT03601052
Cobomarsen or MRG-106 (Miragen Therapeutics)	AntimiR-155	LNA-modified antisense inhibitor	IV	Mycosis Fungoides Diffuse Large B-Cell Lymphoma Adult T-Cell Leukemia/Lymphoma	Multi-centre Phase I, ongoing Multi-centre Phase II, recruiting Phase II, not yet recruiting	NCT02580552 NCT03713320 NCT03837457
RG-012 (Regulus Therapeutics)	AntimiR-21	GalNAc-conjugated antimiR	SC	Alport syndrome	Multicentre Phase I, completed Single-centre Phase II, suspended	NCT03373786 NCT02855268
MesomiR-1 or TargomiR (EnGeneIC)	miR-16 mimic	EnGeneIC delivery vehicle	IV	Mesothelioma Non-small cell lung cancer	Multi-centre Phase I, completed	NCT02369198
MRG-110 (Miragen Therapeutics)	AntimiR-92a	-	ID	Heart failure Ischemia	Single-centre Phase I, completed	NCT03603431
MRG-201 (Miragen Therapeutics)	miR-29 mimic	Cholesterol-miRNA duplex	ID	Scleroderma Keloid diseases	Single-centre phase I, completed Multi-centre Phase II, ongoing	NCT02603224 NCT03601052

AD, administration route; iD, identification; GalNAc, *N*-acetyl-D-galactosamine; LNA, locked nucleic acid; SC, subcutaneous; IV, intravenous; ID, intradermal. Adapted from Rupaimoole et al.,[47]; Hanna et al.,[149]; Hydbring & Badalian-Very[151]; Gallant-Behm et al.[152]; Zeisel & Baumert[153].

Among the miRNA-based therapies described in Table 3, it is important to highlight the advances observed wit Miravirsen, MRX34 and RG-101/102 and AZD4076.

Miravirsen (Santaris Pharma) is an LNA-modified DNA phosphorothioate with a complementary sequence to mature miR-122 aimed at treating patients with hepatitis C infection. This is the first miRNA-targeted drug to enter phase II clinical trials[132]. This study demonstrated the safety and effectiveness of the therapy decreasing the number of copies of virus from hepatitis C after dose dependent treatment with Miravirsen[87]. The next step for Miravirsen is advance to a phase II with additional studies of the long-term effects, with more patients and multidrug combinations[47].

MRX34 (miRNA Therapeutics) is composed by a liposomal nanocarrier, Smarticles®, which encapsulates the tumour-suppressor miR-34a mimic (NCT01829971)[154]. MRX34 have also reached the Phase II in clinical trials to treat patients with advanced solid tumours with preliminary evidence of antitumour activity[155]. Despite the significant tumour reduction observed after MRX34 administration in several tumours[47], this study was halted in 2016 due to the multiple immune-related severe adverse effects[132]. As the cause of these immune reactions is unclear, pre-clinical trials will need to be re-designed.

RG-101/RG-012 (Regulus Therapeutics) are two other miRNA-based therapies developed by Regulus Therapeutics to treat hepatitis C infections and Alport nephropathy Syndrome, respectively. Both have an anti-miRNA conjugated to the acetylgalactosamine (GalNAc) polymer, which are antimir-122 for RG-101 and antimir-21 for RG-012. Despite both therapies finished the phase I of clinical trials and RG-101 demonstrated higher efficacy than Miravirsen, the RG-101 was put on hold by the US FDA after a second case of jaundice was reported[47].

AZD4076 or RG-125 (Regulus Therapeutics) is a N-acetylgalactosamine (GalNAc)-conjugated to an anti-miR-103/107 to treat type II diabetes, non-alcoholic fatty liver disease (NAFLD) (NCT02826525) and non-alcoholic steatohepatitis (NASH) (NCT02612662). After one year the study was halted by the AstraZeneca sponsor.

Another nanomedicine that recently completed phase 1 trial are "**TargomiR**" that use a new technology, named EDV nanocells®, with encouraging results in patients with recurrent malignant pleural mesothelioma or non-small cell lung cancer. In brief, TargomiR contain a miRNA in bacterially derived minicells and an antibody as a targeting moiety. In the first human trial of a TargomiR drug, **MesomiR-1** contains the tumour suppressor miR-16 mimic and the antibody against the epidermal growth factor receptor (EGFR) to target lung cancer cells[149]. The safety profile of MesomiR-1 and the early signs of efficacy in malignant pleural mesothelioma patients have supported them to continue the clinical trials of MesomiR-1 in combination with chemotherapy or immune checkpoint inhibitors[156].

Despite the discovery of therapeutic miRNA is one of the most exhilarating approaches for the treatment of human diseases, the application of miRNA into clinics is progressing at a slow pace. It is likely that many of them will fail during the clinical trials, due to many factors such as safety, efficacy, target selection or effective delivery systems. However, it seems that is clear that miRNA will achieve easily the clinics after their administration using an optimized nanocarrier. Besides, among miRNA tested in clinical phases, few of them are developed to treat cancer. In particular, miRNA-based therapies for NB treatment are still in pre-clinical stages[132]. For this reason, in order to improve paediatric cancers treatments such as high-risk NB, further studies are required to implement the miRNA-based therapies using the opportunities given by the nanotechnology field.

2. HYPOTHESIS AND OBJECTIVES

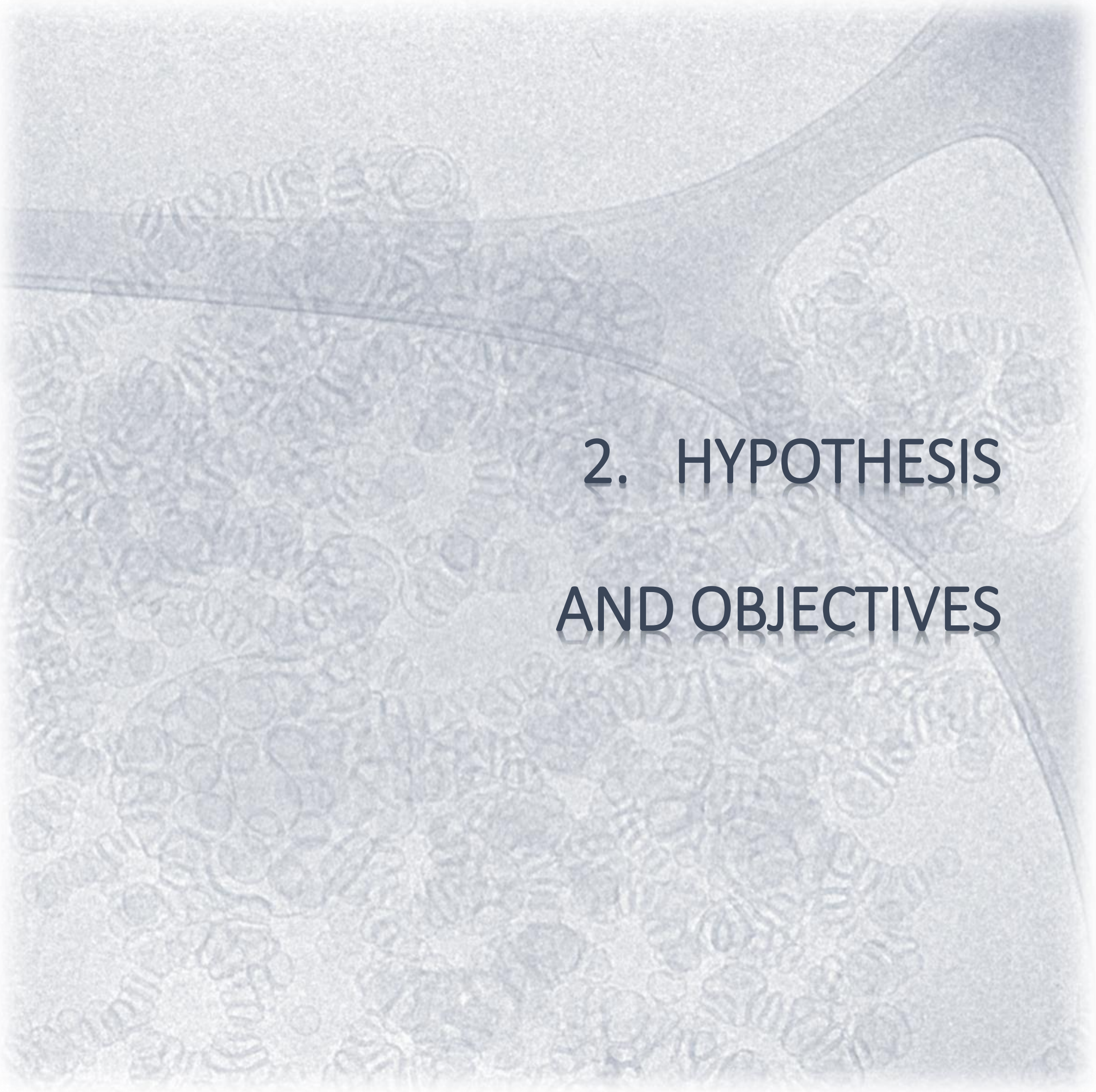

2. HYPOTHESIS AND OBJECTIVES

In recent years, miRNAs have been found to be deregulated in several human diseases and, particularly, in cancer. In neuroblastoma, one of the most aggressive pediatric tumors of the nervous system, the aberrant expression of specific miRNAs has been reported to correlate with stage, progression and patient outcome. For this reason, the use of miRNA restoration therapies represents a novel therapeutic approach.

However, the therapeutic use of RNA molecules such as miRNA, has reached a bottleneck owing to the lack of a standard formulation for clinical administration. To overcome this barrier, the conjugation of miRNA to nanoparticles has been emerging as a promising strategy to use miRNA for clinical applications. Despite the multiple existing nanocarriers (i.e. polymeric particles, metallic nanoparticles, micelles, nanovesicles, etc..) most of them present unsolved drawbacks for clinical administration, such as poor colloidal stability or lower tolerability *in vivo* and difficult production at industrial scale.

Quatsomes (QS) are non-liposomal lipid unilamellar nanovesicles composed by sterols and quaternary ammonium surfactants. These new vesicular formulations have an exceptional stability, a high vesicle-to-vesicle homogeneity and can be produced at large industrial. These non-liposomal nanovesicles are composed by ingredients available in pharmaceutical grade. Hence, our **hypothesis** is that QS have the suitable physic-chemical characteristics to be used as nanocarriers for the intracellular delivery of small RNAs (sRNAs), such as miRNA.

In this framework, the three objectives of this thesis are:

1. **Objective 1.** To select a miRNA with high therapeutic potential for the treatment of high-risk neuroblastoma patients.
2. **Objective 2.** To engineer Quatsomes for the effective transport and intracellular delivery of sRNA.
3. **Objective 3.** To develop a new nanomedicine, composed by a tumour-suppressive microRNA and the Quatsomes nanocarrier, for the treatment of high-risk neuroblastoma.

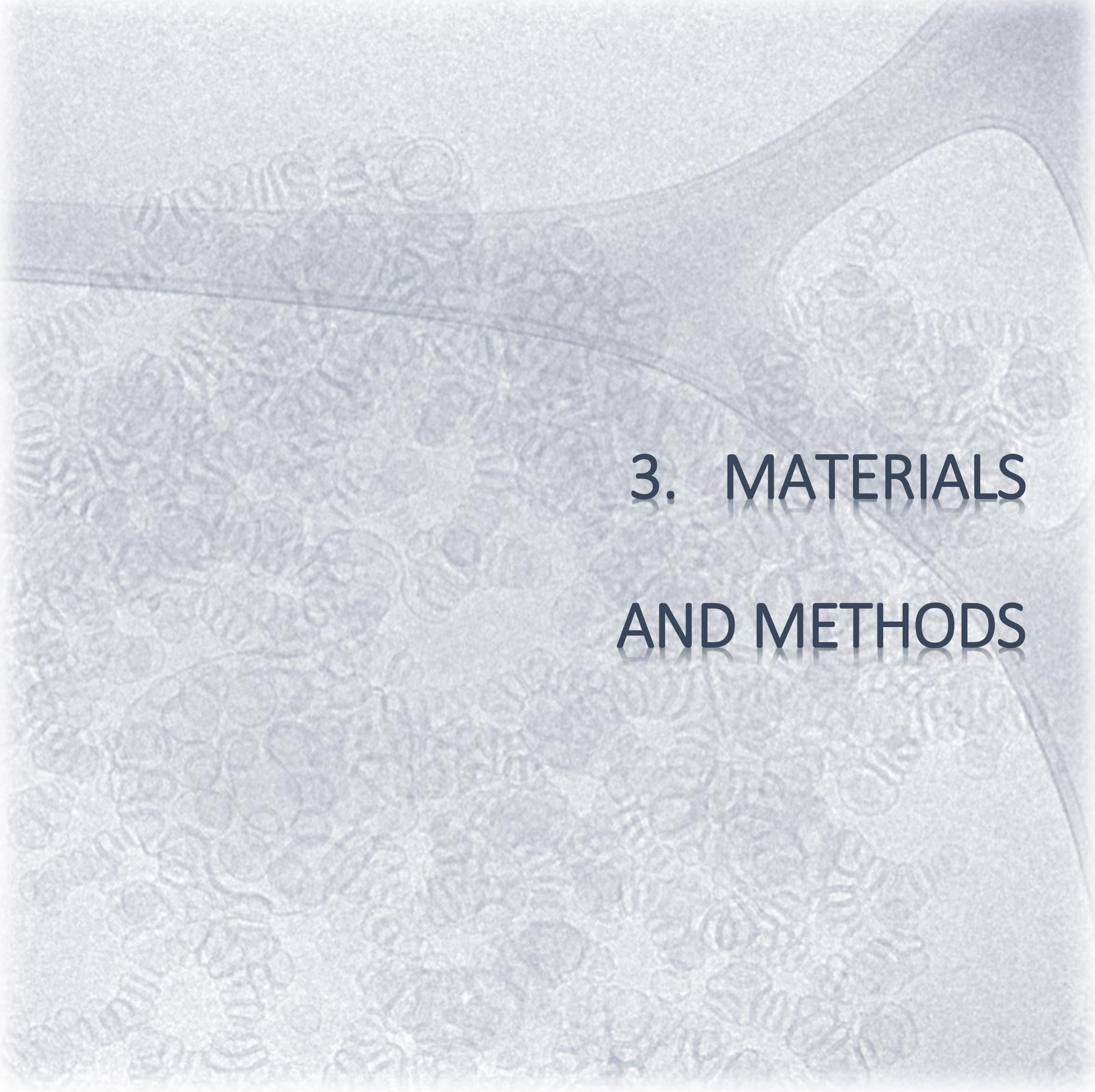

3. MATERIALS AND METHODS

3. MATERIALS AND METHODS

3.1 Materials

3.1.1 Lipids and surfactants

Cholesten-3β-ol (Chol, purity 95%; #A0807) and Sodium hydroxide (NaOH, purity ≥98.0%; # AL6406.1211) were obtained from PanReac (Castellar del Vallès, Spain). Cholesteryl N-(2-dimethylaminoethyl)carbamate (DC-Chol, purity ≥ 98%; #92243) and Cholesteryl hemisuccinate (Chems, purity ≥ 98%; #C6512) were purchased from Sigma-Aldrich (Saint Louis, Missouri, USA). Benzyldimethyltetradecylammonium Chloride (MKC; purity ≥ 99%; #262393) was supplied by AttendBio Research SL (Santa Coloma de Gramenet, Spain). 1,1’-dioctadecyl-3,3,3’,3’-tetramethyl-indocarbocyanine perchlorate (DiI; #D-282), were purchased from Life Technologies (Carlsbad, USA). Ethanol was purchased from Teknochroma (Sant Cugat del Vallès, Spain). Carbon dioxide (purity 99.9%) was acquired from Carburos Metálicos S.A. (Cornellà de Llobregat, Spain). All the chemicals were used without further purification and all solutions were prepared using pre-treated Milli-Q water (Millipore Ibérica, Madrid, Spain).

3.1.2 Neuroblastoma cell lines

SK-N-AS, SH-SY5Y and IMR-32 cell lines were purchased from American Type Culture Collection (ATCC, Manassas, VA, USA), CHLA-90 cell line from the Children’s Oncology Group Cell Culture and Xenograft Repository (Lubbock, TX, USA). SK-N-BE(2) and LA1-5s acquired from Public Health England Culture Collections (Salisbury, UK). All cell lines used in the frame of this thesis are from neuroblastoma origin which were amplified to maintain a stock of cells. For long-term storage, cells were cryopreserved in liquid nitrogen. To ensure the cell integrity during the cryopreservation process, cells were frozen in cellular media supplemented with 10% of Dimethyl sulfoxide (DMSO). Cryovials were placed into propanol-filled cooler that decreases gradually the temperature (-1°C/min). Upon resuscitation, cells had to be thawed quickly with cellular media and centrifuged to replace the DMSO for fresh media. For amplification and maintenance, cells were cultured in Iscove’s modified Dulbecco’s Medium (IMDM; Life Technologies, Thermo Fisher Scientific), supplemented with 10% heat-inactivated foetal bovine serum (FBS) South America Premium, 1% of Insulin-Transferrin-Selenium Supplement (Life Technologies, Thermo Fisher Scientific), 100U/mL penicillin, 100µg/mL streptomycin (Life Technologies, Thermo Fisher Scientific) and 5µg/mL plasmocin (InvivoGen, San Diego, CA, USA). All cultures were maintained at 37°C in a saturated humidified atmosphere of 95% air and 5% CO_2. NB cells were tested for mycoplasma contamination periodically.

3.1.3 sRNA

Small RNA used for miRNA and siRNA transfections used are listed in Table 4 and Table 5, respectively.

Table 4. Human synthetic miRIDIAN miRNA mimics obtained from Dharmacon Inc.

miRNA mimic	miRNA Mimics Catalog Nº	Sequence (Accession)
miRIDIAN microRNA Mimic Transfection Control 1 (C1)	CN-001000-01	UCACAACCUCCUAGAAAGAGUAGA (MIMAT0000039)*
miRIDIAN microRNA Mimic Transfection Control 2 (C2)	CN-002000-01	UCACAACCUCCUAGAAAGAGUAGA (MIMAT0000039)*
miRIDIAN microRNA Mimic Transfection Control with Dy547	CP-004500-01	UCACAACCUCCUAGAAAGAGUAGA (MIMAT0000039)**
Custom miRIDIAN Mimic Transfection Control with Cy5 5' sense	77C-CUSTOM-NM-48	UCACAACCUCCUAGAAAGAGUAGA (HPLC 42 nmol)**
miRIDIAN microRNA hsa-miR-299-3p mimic	C-300656-03	UAUGUGGGAUGGUAAACCGCUU (MIMAT0000687)
miRIDIAN microRNA hsa-miR-323a-5p mimic	C-301085-01	AGGUGGUCCGUGGCGCGUUCGC (MIMAT0004696)
miRIDIAN microRNA hsa-miR-342-5p mimic	C-301083-01	AGGGGUGCUAUCUGUGAUUGA (MIMAT0004694)
miRIDIAN microRNA hsa-miR-380-5p mimic	C-300688-03	UGGUUGACCAUAGAACAUGCGC (MIMAT0000734)
miRIDIAN microRNA hsa-miR-497-5p mimic	C-300765-03	CAGCAGCACACUGUGGUUUGU (MIMAT0002820)
miRIDIAN microRNA hsa-miR-541-3p mimic	C-301230	UGGUGGGCACAGAAUCUGGACU (MIMAT0004920)
miRIDIAN microRNA hsa-miR-654-5p mimic	C-300988-01	UGGUGGGCCGCAGAACAUGUGC (MIMAT0003330)
miRIDIAN microRNA hsa-miR-665 mimic	C-301246-01	ACCAGGAGGCUGAGGCCCCU (MIMAT0004952)

*Based on cel-miR-67 (Control 1) and cel-miR-239 (Control 2), mature sequence, which have minimal sequence identity with miRNA in human, mouse and rat. **Based on the cel-miR-67 miRIDIAN microRNA Mimic Transfection Control 1 labeled with Dy547 or Cy5, which has an absorbance/emission spectra of 557/570 nm or 645/665 nm.

Table 5. siRNA purchased from Sigma-Aldrich.

siRNA	Gener name	Target sequence 5’-3’	Reference
siControl 1 (siCT)	siRNA Control 1	GUAAGACACGACUUAUCGC	157
	siRNA Control 1_as	CAUUCUGUGCUGAAUAGCG	
siCCND1	CCND1	CCUACGAUACGCUACUAUAUU	
	CCND1_as	AAUAUAGUAGCGUAUCGUAGG	
KIF11	KIF11	CUAGAUGGCUUUCUCAGUA	
	KIF11_as	UACUGAGAAAGCCAUCUAG	
INCENP	INCENP	AGUCCUUUAUUAAGCGCAAUU	
	INCENP_as	AAUUGCGCUUAAUAAAGGACU	
CHAF1A	CHAF1A	CUGUCAUGUGGGUUCUGAC	
	CHAF1A_as	GUCAGAACCCACAUGACAG	
CDC25A	CDC25A	GGAAAAUGAAGCCUUUGAG	
	CDC25A_as	CUCAAAGGCUUCAUUUUCC	
FADD	FADD	UGCGUUCUCCUUCUCUGUG	
	FADD_as	CACAGAGAAGGAGAACGCA	

3.2 Methods

3.2.1. Cell transfection of lipoplexes

MiRIDIAN microRNA mimic (see Table 4) were purchased from Dharmacon Inc. Transfection reagents are required because cellular membranes as well as nucleic acids are both negatively charged, which impedes the internalization by electrostatic repulsion. Lipofectamine 2000® (#10696153#; Fisher Scientific) is composed by cationic and neutral lipids that in aqueous media are self-assembled to form positively charged liposomes. The high positive charge of these liposomes allows the entrapment of nucleic acids inside the vesicle's membrane, during the self-assembly process, and the posterior nucleic acids internalization inside the cells. In this thesis, Lipofectamine 2000® was used for the lipoplexes formation with miRNA and their subsequent transfection. The protocol used was adapted from manufacturer's recommendations. Briefly, Lipofectamine 2000® and selected miRNA (see Table 4) or siRNA (see Table 5) at 25nM or 50 nM concentration were mixed with Opti-MEM (#11058021#; ThermoFisher) separately. Lipofectamine 2000 diluted in Opti-MEM and miRNA diluted also in Opti-MEM were combined and incubated 10-15 min to enhance the lipoplexes formation. After incubation time, the lipoplexes were added into cellular media IMDM supplemented with 10% of FBS without antibiotics, which may interfere in cellular transfection. After overnight (o/n) media was changed to remove the lipoplexes and into avoid high toxicity caused by transfection reagents, like Lipofectamine 2000. For 96-well plates transfection, 0.2 µL of Lipofectamine per well in a final total volume of 150 µL, which are composed by 100 µL of cells in cellular media plus 50 µL of lipoplexes. In p60 plates, 8 µL of Lipofectamine was used for SK-N-BE(2) cells transfection, in 4 mL of final volume (3.5 mL of cells in cellular media plus 500 µL of lipoplexes). Transfection efficiency was determined by the fluorescent red staining observed in transfected cells with miRNA Transfection Control labelled with Dy547 and with the explained conditions.

3.2.2. microRNA functional high-throughput library screening

MiRNA functional high-throughput screening was performed with SK-N-BE(2) cells described in Soriano A et al.,[157]. SK-N-BE(2) cells were seeded at 5 x10^3 cells/well in 96-well plates using the MultidropV2 dispenser (Finstruments). Twenty-four hours later, cells were transfected with 25nM of 2048 human miRNA mimics (#CS-001030#, Dharmacon, miRIDIAN® microRNA Library—Human Mimic (19.0), GE Healthcare) using Lipofectamine 2000 (Thermo Fisher Scientific, 0.2 µL per well) by the Robotic Platform Caliper Sciclone (Caliper Life Sciences). Technical triplicates were done per each condition (Figure 7A-B).

After 96-h post-transfection, cells were fixed with 1% glutaraldehyde (#11423488 #; Sigma-Aldrich) and washed with PBS 1X (#10462372#; HyClone) to remove the excess of glutaraldehyde. Then, wells were stained with 0.5% of crystal violet (#C0775#; Sigma-Aldrich) for 20 min. After that an extensive washing with distilled water was performed to remove the excessive dye. When violet crystals were dried, they were dissolved in 15% of acetic acid (#10041250#; Fisher Scientific) and optical density was measured at 590nm using Epoch Microplate spectrophotometer (Biotek).

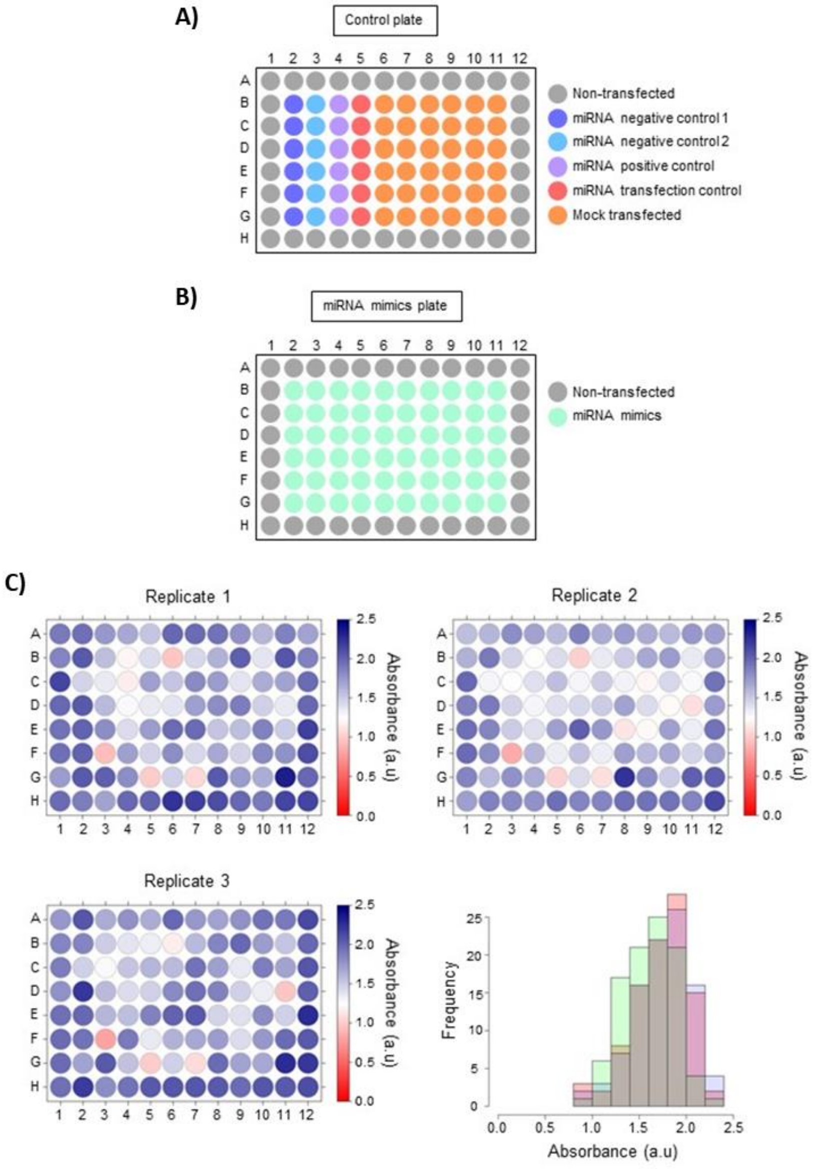

Figure 7. Experimental design and statistics analysis of the microRNA high-throughput screening. SK-N-BE(2) cells were transfected with miRNA mimics (25nM) in 96-well plates. (A) Control plates were transfected with two mimic miRNA negative controls (control 1: cel-miR-67 and control 2: cel-miR-239b), miR-497-5p as a positive control and a mimic miRNA transfection control with Dy547. Mock-transfected cells were transfected with Lipofectamine without miRNA; rows A and H and columns 1 and 12 were non-transfected (NT) cells. (B) MiRNA-mimic plates were transfected with 60 individual miRNA. Rows A and H and columns 1 and 12 were non-transfected (NT) cells. (C) Raw absorbance values from three replicates of miRNA mimics plate 2 and the frequency distribution histograms of absorbance values.

Screening statistics

"R" Statistical Software was used to perform a data quality control and analysis of different factors (e.g. miRNA position, transfection time…) (Figure 7C). The optical density values of each well (mock or miRNA library mimics transfected) was normalized to the median of all non-transfected values of the corresponding replicate plate. To estimate the reduction of cell proliferation caused by miRNA transfection, the mean absorbance of 3 replicates was compared versus the median of all mock values. The statistical significance was evaluated by Student's t test and the p value was adjusted by the false discovery rate "FDR" method. The percentage of proliferation was standardized using the Z score equation $Z = \frac{x-\mu}{\sigma}$ where x is the value of cell proliferation after transfection of each single miRNA, μ is the mean cell proliferation of all miRNA and σ the standard deviation.

Analysis of miRNA expression in human samples

MiRNA expression data from NB tumors was obtained from the Tumor Neuroblastoma Compendium (NRC) dataset. A total of 365 NB samples were obtained and analyzed from patients enrolled by Our Lady's Hospital for Sick Children (Crumlin, Dublin, Ireland), the Children's Oncology Group (Philadelphia, USA), the Ghent University Hospital (Ghent, Belgium), the Academic Medical Center (AMC; Amsterdam, Netherlands) and the University Children's Hospital Essen (Essen, Germany). Tumors were profiled for 430 miRNA plus 36 control small RNA using individual Taqman PCR assays setup in 384-well format and mRNA gene expression profile was performed by Affymetrix GeneChip HG-U133plus2.0. Patient characteristics are listed in and data set has been previously described in a number of publications[158].

3.2.3. Cell proliferation assays with lipoplexes

Proliferation assays were performed with NB cell lines described in Soriano A et al., [157]. Briefly, cells were seeded in 96-well plates at the following confluences: LA1-5s at $1.5x10^3$ cells/well; SK-N-AS at $4x10^3$ cells/well; CHLA-90 at $8x10^3$ cells/well; IMR-32, SK-N-BE(2) and SH-SY5Y at $5x10^3$ cells/well in standard conditions of growing. After twenty-four hours, seeded cells were transfected with the indicated miRIDIAN microRNA mimic oligonucleotides (25 nM or 50nM) using Lipofectamine 2000® (0.2 µL per well) as transfection reagent following the protocol explained before. After o/n transfection, the cellular medium was changed. After 96 hours post-transfection, cells were fixed with 1% glutaraldehyde and washed with PBS 1X. Then, wells were stained with 0.5% of crystal violet and dried violet crystals were dissolved in 15% of acetic acid.

The absorbance of the crystals was measured at 590 nm using Epoch Microplate spectrophotometer. The % of proliferation in NB cells after lipoplexes transfection was normalized to mock-control-transfected cells.

3.2.4. Cell cycle analysis

SK-N-BE(2) (1.4 x 106) cells were reverse transfected with 25 nM of miR-Control or miR-323a-5p mimic in 100-mm dishes (25µL of Lipofectamine/dish). After 96 h, cells were harvested and fixed with cold 70% ethanol and kept at 4°C for at least 24 h. Prior to flow cytometry analyses, cells were washed twice in PBS and resuspended in staining solution [0.19 mM sodium citrate (Sigma-Aldrich), 500 µg/mL propidium iodide (Thermo Fisher Scientific) and 10 mg/mL RNAse DNAse-free (AppliChem)] and incubated overnight. Analysis of DNA content was analyzed using a FACScalibur flow cytometer (BD Biosciences) and data by BD CellQuestTM Pro Software (BD Biosciences).

3.2.5. Cell death assay

SK-N-BE(2) (6 x 104) cells were seeded in 24-well plates and reverse transfected with Lipofectamine 2000 with 25 nM of miR-Control or miR-323a-5p mimic in triplicate. At 96 h post-transfection, cells were stained with 0.05 µg/ml Hoechst 33258 dye and photographed. Apoptosis quantification was made from 4 representative images/well (n=3 replicates/condition). Cells with uniformly-stained chromatin were scored as healthy whereas those that had chromatin fragmentation or condensation were considered apoptotic.

3.2.6. Western Blot

Proteins were extracted using RIPA buffer 1X (#10017003; Fisher Scientific), supplemented with 1X EDTA-free complete protease inhibitor cocktail (#04693159001; Roche, Sant Cugat del Vallés, Spain). Cell lysis was done on ice for 20 min. Lysates were cleared by centrifugation at 14000xg for 15 min at 4°C. Protein samples were stored at -20°C until further use. Protein concentration was determined using Lowry assay (DC protein assay, Bio-Rad) following manufacturer’s instructions.

Thirty µg of protein were prepared in RIPA buffer 1X with loading buffer 1X (NuPAGE LSD sample buffer 4X, Invitrogen), and denaturized by heating the samples at 70°C for 10 min. Before loading the samples in the gel, the proteins were reduced with ditiotreitol (DTT) adding at 1X concentration the NuPAGE^{TM} Sample Reducing agent (10X; #15784202; Fisher Scientific).

Samples were run in precast NuPAGE^{TM} 4-12% Bis-Tris gels (#12020166; Fisher Scientific) in MES-running buffer at 1X (#11509166; Fisher Scientific) and NuPAGE^{TM} Antioxidant (#NP0005; Fisher Scientific) for 1h at 150V at RT.

Proteins were transferred to methanol-activated PVDF membranes using the iBlot Gel Transfer system (#GE10600021; Life Technologies, Thermo Fisher Scientific) for 7 min using the program 3 (at 20V).

Alternatively, when the wet transfer method was used, the membrane sandwich was placed in a transfer tank (see Figure 8) and run at high voltage (110-200V) for 1.5- 2h.

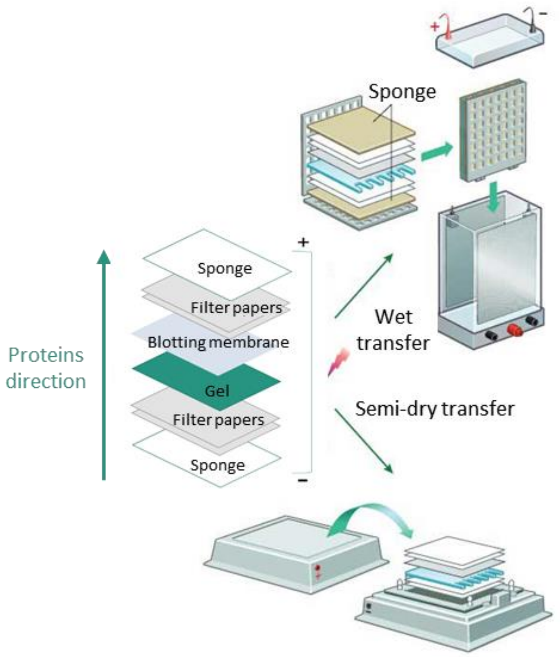

Figure 8. Protein transfer set up. Image adapted from Bio-Rad web page.

After protein transfer, membranes were incubated with blocking solution (Tris-buffered saline with Tween-20 (TBS-T) with 5% bovine serum albumin (BSA) or non-fat milk) for 1h at RT. Next, membranes were incubated overnight at 4°C with the indicated primary antibodies (see Table 6). The secondary antibodies conditions used in this thesis are listed on the Table 7. After three washings with TBS-T of 5 min, membranes were incubated with the corresponding peroxidase-conjugated secondary antibody for 1h and 30 min at RT. Anti-actin-HRP was used as loading control.

EZ-ECL Chemiluminescence detection kit (EZ-ECL; #10340125#; GE Healthcare Fisher Scientific) was used for developing the signal in X-ray films (#16189949#; Fujifilm). Finally, films were scanned for protein levels quantification using ImageJ software[159]. Each analysed protein band intensity was normalised to the loading control.

Table 6. Primary antibodies list and conditions used for Western Blot.

Antibody	Molecular weight (KDa)	Specie	Primary antibody conditions	Company	Catalog number
α-FODRIN	240, 150 and 120 KDa	Mouse	1:3.000 in TBS-T	Millipore	#MAB1622
CHAF1A	145 kDa	Rabbit	1:1.000 in TBS-T + 5% BSA	Cell Signaling	#5480S
KIF11	132kDa	Rabbit	1:2.000 in TBS-T +5% milk	[160]	
INCENP	140 KDa	Rabbit	1:500 in TBS-T +5% milk	[161]	
Phospho-RB	110 kDa	Rabbit	1:1.000 in TBS-T + 5% BSA	Cell Signaling	#8516
WEE1	94 KDa	Mouse	1:2.000 in TBS-T +5% BSA	Santa Cruz	#sc-5285
CDC25A	59 and 54 KDa	Mouse	1:500 in TBS-T +5% milk	Thermo Fisher Scientific	DCS-120
CCNB1	58 KDa	Mouse	1:1.000 in TBS-T + 5% BSA	Millipore	#05-373
CHEK1	56 KDa	Mouse	1:4.000 in TBS-T +5% BSA	Santa Cruz	#sc-8408
E2F2	48 KDa	Rabbit	1:1.000 in TBS-T +5% BSA	Abcam	Ab65222
CCNE1	47 KDa	Mouse	1:1.000 in TBS-T + 5% BSA	Abcam	ab3927
CDK6	36 KDa	Mouse	1:1.000 in TBS-T + 5% BSA	Cell Signaling	#3136
CASP3	35 KDa	Rabbit	1:2.000 in TBS-T + 5% BSA	Cell Signaling	#9662
CCND1	34 kDa	Rabbit	1:1.000 in TBS-T + 5% BSA	Abcam	ab134175
p27	27 kDa	Rabbit	1:1.000 in TBS-T + 5% BSA	Cell Signaling	#3686
FADD	27 KDa	Mouse	1:1.000 in TBS-T +5% milk	Santa Cruz	sc-6035
BCL2	26 KDa	Mouse	1:1.000 in TBS-T +5% milk	Agilent	#M0887
Cleaved CASP3	17 and 19 KDa	Rabbit	1:1.000 in TBS-T + 5% BSA	Cell Signaling	#9664
Tubulin	50 KDa	Mouse	1:5.000 in TBST-T+5% BSA	Sigma-Aldrich	T9026
ACTIN-HRP	45 kDa	Rabbit	1:40.000 in TBS-T+5% BSA	Santa Cruz	sc-1616

Table 7. Secondary antibody conditions used for Western Blot.

Antibody	Specie	Secondary antibody	Company	Catalog number
Anti-Rabbit IgG-Peroxidase	Goat	1:10.000 in TBS-T + 5% BSA	Sigma-Aldrich	#A0545
Anti-Mouse IgG-Peroxidase	Rabbit	1:10.000 in TBS-T + 2.5% milk + 2.5% BSA	Sigma-Aldrich	#A9044

To detect proteins with different molecular weight that could be detected with secondary antibodies from different host species, membranes were incubated with 0.02% of sodium azide (NaN_3) which inactivates the HRP enzyme of the secondary antibodies. When the use of secondary antibodies from different species was not possible, membranes were stripped with the Re-Blot Mild stripping solution for 15 minutes (#2502#; Merck)[162].

3.2.7. In silico miRNA-target analysis

The miRWalk database using five miRNA-target prediction algorithms (DIANA-microT; version 3.0, miRDB, miRWalk[163], miRanda[164] and TargetScan; version 5.1[165]) was used to make the computational miRNA target prediction analysis. The miRNA target search was restricted to the 3'-UTR of target genes and with a minimum complementarity of 7 nucleotides in the seeding region. Probability distribution of random matches was set at 0.05 (Poisson p-value). Target genes with $p \leq 0.05$ predicted by four or all five algorithms were selected as predicted targets. The functional annotations of resulting predicted target lists were performed using the Gene Ontology[166] and the KEGG[167] databases. GSE45547[168] and GSE62564[169] datasets were used for target gene expression analysis in human tumour samples.

3.2.8. Quantitative real-time PCR (qPCR)

Total RNA, including small RNAs, was extracted using the RNeasy Mini kit (Qiagen, Hilden, Germany) and following the manufacturer's protocol. RNA was quantified by Nanodrop spectrophotometer (Thermo Fisher Scientific). For miRNA expression analyses, 12.5 ng/µL were reverse transcribed using Taqman RT kit (#4366596; Thermo Fisher Scientific) following manufacturer's recommendations. Next, quantitative polymerase chain reaction (qPCR) were executed with using TaqMan MiRNA assays using the TaqMan probes indicated in Table 8.

Table 8. TaqMan probes purchased for RT-qPCR of miRNA expression levels.

miRBase ID	Mature miRNA Sequence	TaqMan Assay ID	miRBase Accession Nº
hsa-miR-497-5p	CAGCAGCACACUGUGGUUUGU	001043	MI0003138
hsa-miR-323a-5p	AGGUGGUCCGUGGCGCGUUCGC	002695	MI0000807
RNU44	CCTGGATGATGATAGCAAATGCTGACTGAA CATGAAGGTCTTAATTAGCTCTAACTGACT	001094	NR_002750

For mRNA expression analyses, 500ng of total RNA was reverse transcribed using the Applied Biosystem reverse transcription kit (#10146854) following the manufacturer's protocol. qPCR was performed using 12.5 ng/µL cDNA, 2X Power SYBR Green Master Mix (#10658255; Fisher Scientific) and 0.5 µM of primers indicated in Table 9.

Table 9. List of primer sequences of genes used for RT-qPCR.

Gene	Primer sequence (5' to 3')	Amplicon (bp)
E2F2	Fw: AGGGGAAGTGCATCAGAGTG	84
	Rv: GCGAAGTGTCATACCGAGTCT	
CDK6	Fw: GAACTAGGCAAAGACCTACTTCTGA	130
	Rv: GGTGGGAATCCAGGTTTTCT	
FADD	Fw: AGCGGAGGAGACCAGCTC	96
	Rv: ATGGGCTCTGGTGAAGGAT	
STAT3	Fw: CCCTTGGATTGAGAGTCAAGA	108
	Rv: AAGCGGCTATACTGCTGGTC	
CIT	Fw: ACGTGAAGAAAGTGAAACAGTCC	130
	Rv: CAGAGCCCGTTCTCAATCTT	
INCENP	Fw: AAGAGCAGCAGCGTCTGG	124
	Rv: GAGGTACAAGCTGGAGACTGC	
GSPT2	Fw: TGAGGAATTTACAAACAATGCATAA	114
	Rv: TGGACTTGGACAGAGAAAACAA	
SEPT11	Fw: CGTGGGGAGACCGTCTAA	106
	Rv: TCCTTGAGAAGTAGACTTGTTGACC	
CDC25A	Fw: CCCAGCTCGGATGCTTTCC	82
	Rv: TCACAGGTGACTGGGGTGTA	
FZD6	Fw: CGTCTATGAGCAAGTGAACAGG	114
	Rv: AATTCTGGTCGAGCTTTTGC	
KIF11	Fw: AAAACAACAAAGAAGAGACAATTCC	93
	Rv: CAGATGGCTCTTGACTTAGAGGT	
CHAF1A	Fw: TCA CCC AAT TCA TGA AGA AGC	113
	Rv: GAT CAT ACA GTC GCC CTC CT	
CCND1	Fw: GCT GCG AAG TGG AAA CCA TC	135
	Rv: CCT CCT TCT GCA CAC ATT TGA A	
WEE1	Fw: CACACGCCCAAGAGTTTGC	130
	Rv: GAGGAGTCTGTCGCACATCA	
CHEK1	Fw: GACATTCAGAGGGGCAGGAC	155
	Rv: GCACCTCGGCGGACTG	
L27	Fw: AGCTGTCATCGTGAAGAA	88
	Rv: CTTGGCGATCTTCTTCTTGCC	

qPCR reaction was run in 96-well plates per duplicate in ABI700 Sequence Detection System (Thermo Fisher Scientific) equipment. The protocol followed was an initial denaturing of 95°C for 10 minutes, a denaturing process for 15 seconds at 95°C and the annealing process for one minute at 60°C, these last two steps were repeated during 40 cycles. Gene expression was normalized against L27 or RNU44 housekeeping genes. The relative fold-change relative quantification of gene expression was performed with a comparative $2^{(-\Delta\Delta CT)}$ method[170].

3.2.9. 3' UTR Luciferase Reporter Assay

The 3'-UTR fragments of CHAF1A, KIF11, INCENP, CDC25A, FADD and CCND1 (Table 10; Figure 9) were synthesized by GeneArt Gene Synthesis (Thermo Fisher Scientific) and cloned downstream of the renilla luciferase gene using XhoI/NotI restriction sites in the psi-CHECKTM-2 vector (Promega Corporation). HEK293T cells were seeded in 96-well plates (2 x 10^4 cells/well) and co-transfected 12-14 h later with 50 ng of psi-CHECK2 reporter vectors and 25 nM of miRIDIAN microRNA mimic oligonucleotides using Lipofectamine 2000. Twenty-four hours later, luciferase activity was measured using the Dual-Glo® Luciferase Assay System (Promega Corporation) following the manufacturer's recommendations. Luminescence of each biological sample was measured in an Appliskan (Thermo Fisher Scientific) microplate reader. Renilla luciferase activity was normalized to corresponding firefly luciferase activity.

Table 10. 3'UTR luciferase reporter cloning.

MiRNA	Gene	Fragment of 3'UTR cloned	Binding site
MiR-323a	CHAF1A_3'UTR	+1 to +317	299-305
	KIF11_3'UTR	+786 to +1226	1039-1045
	INCENP_3'UTR	+540 to +1086	789-795
	CDC25A_3'UTR	+774 to +1320	1087-1093
	FADD_3'UTR	+1 to +546	121-127
	CCND1(A)_3'UTR	+642 to +1014	713-720

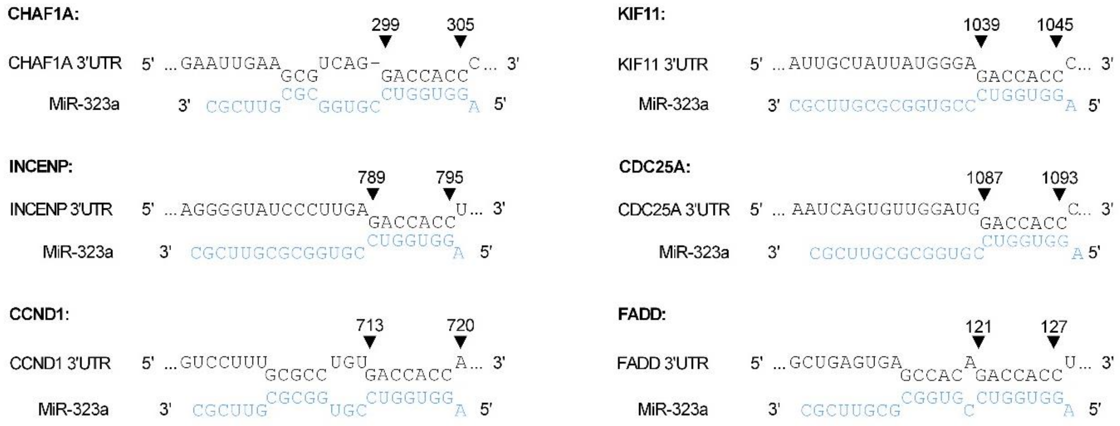
CHAF1A:
299
305
CHAF1A 3'UTR 5' ...GAAUUGAA GCG UCAG- GACCACC C... 3'
MiR-323a 3' CGCUUG CGC GGUGC CUGGUGG A 5'
KIF11:
1039
1045
KIF11 3'UTR 5' ...AUUGCUAUUAUGGGA GACCACC C... 3'
MiR-323a 3' CGCUUGCGCGGUGCC CUGGUGG A 5'
INCENP:
789
795
INCENP 3'UTR 5' ...AGGGGUAUCCCUUGA GACCACC U... 3'
MiR-323a 3' CGCUUGCGCGGUGC CUGGUGG A 5'
CDC25A:
1087
1093
CDC25A 3'UTR 5' ... AAUCAGUGUUGGAUG GACCACC C... 3'
MiR-323a 3' CGCUUGCGCGGUGC CUGGUGG A 5'
CCND1:
713
720
CCND1 3'UTR 5' ...GUCCUUU GCGCC UGU GACCACC A... 3'
MiR-323a 3' CGCUUG CGCGG UGC CUGGUGG A 5'
FADD:
121
127
FADD 3'UTR 5' ...GCUGAGUGA GCCAC A GACCACC U... 3'
MiR-323a 3' CGCUUGCG CGGUG C CUGGUGG A 5'

Figure 9. MiR-323a-5p predicted binding sites for each of the selected target genes. MiR-323a-5p binding sequences within the indicated human genes. Seeding region is flanked by arrows with the indicated nucleotide position within the 3'UTR.

3.2.10. Nanoparticles preparation

The nanoparticles used in this work are Quatsomes (QS), Nanostructures (NS) and MKC micelles, which were prepared by DELOS-SUSP technology, by sonication and by self-assembly in aqueous solution, respectively.

3.2.10.1. Quatsomes synthesis by DELOS-SUSP

Reactor/equipment for QS preparation:

Quatsomes were prepared by the DELOS-SUSP technology using a plant based on a 7.5 mL reactor (Figure 10). The reactor was composed by an external heating jacket, a thermostated syringe pump (model 260D. ISCO Inc., Lincoln, US) and a depressurization valve (V-7). The heating jacket controls the temperature inside the reactor. Moreover, the syringe pump introduces the CO_2 inside the reactor through valve V-4. For QS with fluorophores preparation, a gas filter (FG; 6 µm pores size) is placed before the valve V-7, in order to separate any undesired precipitate from the CO_2-expanded solution. On the other hand, the depressurization valve (V-7) is required to depressurize in a constant pressure the expanded liquid solution into the aqueous phase, which is located after the FG or the reactor. N_2 must been introduced through valve V-6, at a constant pressure of 12MPa. A one-way valve is located after V-6 to prevent the reflux contamination of CO_2 in the N_2 line. Other valves (V-2, V-3 and V-5) divide the CO_2 and N_2 pipelines with other reactors. Finally, there are a pressure indicator (PI) and another one-way valve before the reactor.

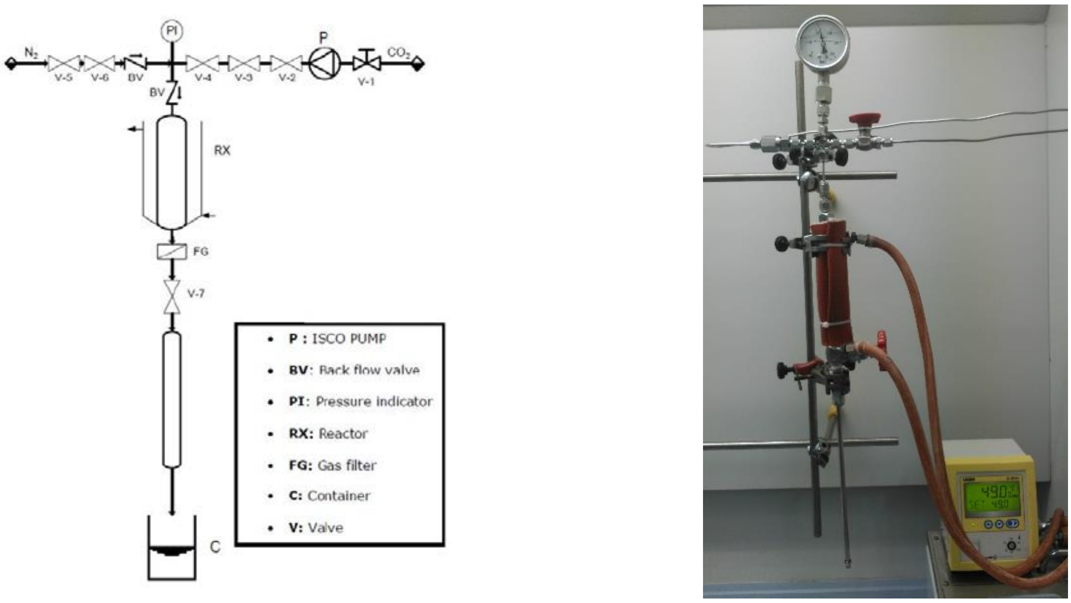

Figure 10. Schematic representation of the lab-scale set-up (left) and image of the reactor (right) used for the DELOS-SUSP experiments.

Experimental procedure for QS preparation:

QS were prepared using the DELOS-SUSP methodology[171]. Briefly, a solution of the desired mixture of sterols (Table 11), such as Chol, Chems or DC-Chol, in ethanol was prepared at a given molarity. This ethanolic solution was let at a temperature of 37-44°C (310.15-317.15K) for 10 minutes. The etOH was used for the sterols dissolution because they are not soluble in water. As represented in step 1 of Figure 11, a known volume of this ethanolic solution, which in this thesis was always 2.88mL, was added to the high-pressure vessel (V=7.05mL) of the lab-scale plant represented in Figure 10. The solution was let 5 minutes for thermal equilibration at 37°C (310.15K), and then compressed CO_2 was added until the desired working pressure (Pw=11.5MPa) was reached, yielding a CO_2-expanded liquid ethanol solution with a molar CO_2 fraction of X_{CO2}=0.60 (step 2, Figure 11). The amount of CO_2, in the expanded solution, is determined by the volume of the high-pressure vessel (7.05 mL), the volume of ethanolic solution (2.88 mL), the working temperature (T_w =37°C or 310.153) and the vapor-liquid equilibrium of ethanol-CO_2 mixtures[172]. The reactor was then maintained at the working pressure and temperature for 1 hour to ensure homogenisation of the organic ethanolic solution and the CO_2, as one-phase inside the reactor. It is very important that all lipids and substances are dissolved in the CO_2-expanded solution at the working conditions of T, P and $X_{CO2.}$ Based on the solubility behaviour of cholesterol derivatives in pressurized ethanol-CO_2 solvent mixtures, reported in the literature[173,174], the concentrations of Chol, Chems and DC-Chol in the CO_2-expanded solution were calculated to avoid undesired precipitation.

Finally, for vesicle formation, the organic solution was depressurised at 11.5MPa of N_2 over an aqueous phase which contained the surfactant MKC (Table 11) dissolved in 24mL of water. The N_2 was used as an embolus to push down the solution expanded inside the reactor onto the aqueous solution maintaining constant the pressure during the depressurization.

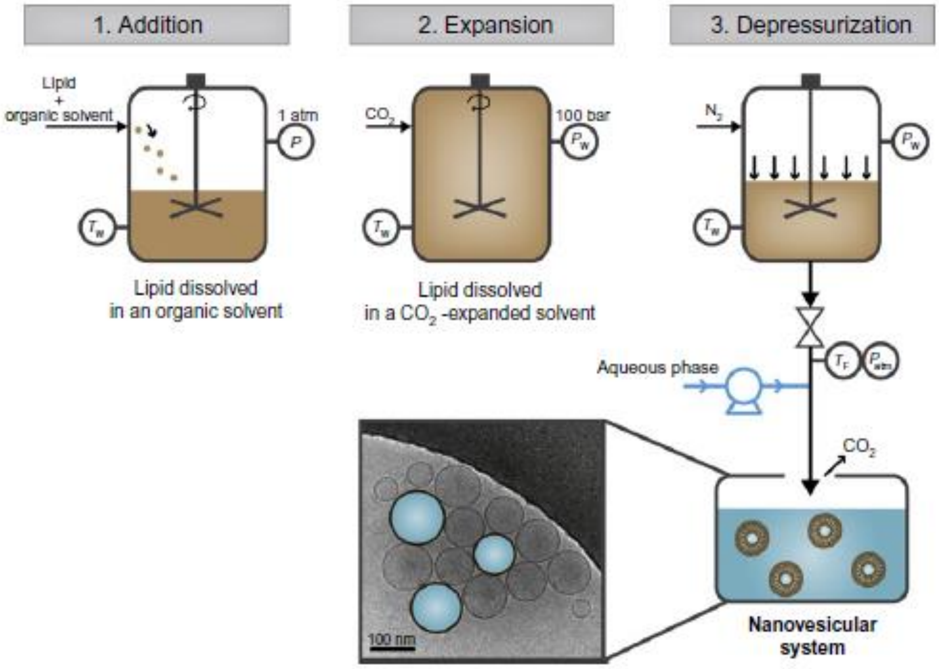
1. Addition
2. Expansion
3. Depressurization
Lipid
+
organic solvent
1 atm
P
T_w
Lipid dissolved
in an organic solvent
CO_2
100 bar
P_w
T_w
Lipid dissolved
in a CO_2 -expanded solvent
N_2
P_w
T_w
T_F
P_{atm}
Aqueous phase
CO_2
100 nm
Nanovesicular
system

Figure 11. Depressurization of an expanded liquid organic solution-suspension (DELOS-SUSP) procedure for vesicle preparation. (1) Addition of an organic solution of the lipid to the vessel at Tw and atmospheric pressure. **(2)** Expansion of the organic solution of the lipid by adding CO_2 until reaching the working molar fraction of CO_2 at Pw and Tw. **(3)** Depressurization of the CO_2-expanded solution over an aqueous flow from Pw to atmospheric pressure. Depending on the hydrophilic or hydrophobic nature of the drug or active substance to be entrapped, it will be dissolved in the initial organic solution **(1)** or in the aqueous phase **(3),** allowing a single step preparation of loaded vesicles. Cryogenic transmission electron microscopy image shows the morphology of vesicles obtained by depressurization of an expanded liquid organic solution-suspension. Pw: Working pressure; Tf: Final temperature: Tw: Working temperature. Figure from Elizondo *et al.,*[175].

The characteristics of the organic and aqueous phase used for the preparation, by DELOS-SUSP, of all QS-based vesicular systems studied in this thesis are given in Table 11.

Table 11. Compositions used for the preparation of various Quatsomes (QS) systems by DELOS-SUSP method.

System	Organic phase	Aqueous phase	Aqueous phase volume	Molar ratio[#]	[Membrane components] (mg/mL)[‡]	% $\frac{DC-Chol}{sterols}$
QS$_0$	Chems (0.068M)	MKC (0.006M)	24 mL	1:0.75	5.5 mg/mL	0%
	Chems (0.069M)	MKC (0.008M)	24 mL	1:1	6.4 mg/mL	0%
QS$_1$	Chol (0.068M)	MKC (0.003M)	24 mL	1:1*	5.6 mg/mL	0%
	Chol (0.068M) + MKC (0.069M)	Water	24 mL			0%
	Chol (0.046M)	MKC (0.008M)	24 mL	1:1.5	4.6 mg/mL	0%
	Chol (0.046M)	MKC (0.011M)	24 mL	1:2	5.5 mg/mL	0%
	Chol (0.068M)	MKC (0.059M)	10mL	1:3	22.8 mg/mL	0%
	Chol (0.068M)	MKC (0.039M)	15 mL	1:3	16.4 mg/mL	0%
	Chol (0.068M)	MKC (0.025M)	24 mL	1:3	10 mg/mL	0%
	Chol (0.047M)	MKC (0.017M)	24 mL	1:3	7.5 mg/mL	0%
	Chol (0.033M)	MKC (0.011M)	24 mL	1:3	5.1 mg/mL	0%
QS$_2$	Chol (0.066M) + DC-Chol (0.006M)	MKC (0.008M)	24 mL	1:1	5.7 mg/mL	9.5%
QS$_3$	Chol (0.037M) + DC-Chol (0.033M)	MKC (0.008M)	24 mL	1:1	6.1 mg/mL	49%
QS$_4$	DC-Chol (0.065M)	MKC (0.008M)	24 mL	1:1	6.5 mg/mL	100%

The organic solution was prepared dissolving the sterols in 2.88mL of ethanol while for the aqueous phase the MKC was dissolved in water in all of cases. [#] Molar ratio is defined as the ratio between the total moles of sterols and the moles of MKC surfactant initially used for the QS preparation. [‡] The membrane components concentration is the theorical concentration defined as the total mass of the sum of the sterols and surfactants mass comprising QS membrane divided by the total volume of the vesicular suspension added in the reactor for QS preparation. * Not QS were formed with this formulation.

After physicochemical characterization, the QS systems used for in vitro experiments were: QS$_0$: (100%Chems): MKC; QS$_1$: (100%Chol/0%DC-Chol):MKC; QS$_2$: (90%Chol/10%DC-Chol):MKC; QS$_3$: (50%Chol/50%DC-Chol):MKC; QS$_4$: (0%Chol/100%DC-Chol):MKC. All of them were prepared at molar ratio 1:1 between the different sterols and the MKC surfactant, except QS$_1$ which was prepared at 1:3 molar ratio.

Experimental procedure for QS labelled with DiI preparation:

To perform FRET experiments between dye labelled QS and labelled Cy5 miRNA, QS labelled with DiI were prepared. Previous studies of Nanomol group, demonstrated the possibility of labelling QS membranes with carbocyanines dyes, like DiI, using DELOS-SUSP methodology[176,177]. A solution stock of known concentration of DiI in ethanol was prepared and the absorbance of five dilutions was measured to determine the volume required for samples preparation. Then, ethanol from the DiI solution stock was evaporated to store DiI at 4°C. In this previous work, various concentrations of DiI were loaded in QS membrane, which was mentioned as DiI loading in QS. The DiI loading (1) was expressed like the relation of DiI moles divided by the moles of the QS membrane components ($(1)\ Loading\ of\ DiI = \frac{moles\ of\ DiI}{moles\ of\ membrane\ components}$). The range of DiI loading in QS tested in previous studies was $0.5 \cdot 10^{-3}$ to $10 \cdot 10^{-3}$ [177]. In this thesis, other QS formulations were labelled with DiI fluorophore, following the same procedure.

In Table 12 are reported the characteristics of the organic and aqueous phase used for the preparation, by DELOS-SUSP, of DiI labelled QS used in this thesis to monitor and study QS-miRNA cellular internalization.

To prepare QS labelled with DiI fluorophore, the lab-scale plant schematized in Figure 10 was used and the same DELOS-SUSP protocol reported before for non-labelled QS was followed. However, a gas filter added in the reactor was used to prevent the mixture of unsolved compounds from the organic phase to the surfactant dissolved in aqueous phase and avoid the contamination of other samples prepared with the same reactor. The procedure to obtain nanovesicles required around 2 hours, after that these vesicles should stabilise one week at RT.

To determine the volume of DiI stock to be added to the organic solution, it was necessary to measure the DiI concentration of the stock ethanolic solution by UV absorbance using a Varian Cary 500 UV-Vis-NIR spectrophotometer (Agilen Technologies). The DiI ethanolic solution was placed into a quartz cell with 1 cm path length and introduced in the spectotrophotometer. Then, the concentration of DiI is calculated using the lambert-Beer Law ($\mathrm{Abs} = \varepsilon \cdot \mathrm{l} \cdot \mathrm{C} \cdot \mathrm{DF}$), where ε is the molar extinction coefficient (ε=148.000 of DiI in etOH at λ=549 nm), l the length of the cuvette, C is the concentration and DF the dilution factor (in this case 1:20)[177].

Table 12. Compositions used for the preparation of various Quatsomes (QS) systems labelled with different concentrations of DiI (^{DiI}QS) by DELOS-SUSP method.

System	Organic phase	Aqueous phase	[Membrane components] (mg/mL)‡	DiI loading (mol/mol)[1]
$^{DiI}QS_1$	Cholesterol (0.033M) + DiI ($5.2 \cdot 10^{-5}$M) in etOH	MKC (0.011M) in water	5.1 mg/mL	$0.4 \cdot 10^{-3}$
	Cholesterol (0.033M) + DiI ($1.6 \cdot 10^{-4}$M) in etOH	MKC (0.011M) in water	5.1 mg/mL	$1.2 \cdot 10^{-3}$
	Cholesterol (0.033M) + DiI ($4.9 \cdot 10^{-4}$M) in etOH	MKC (0.011M) in water	5.1 mg/mL	$3.6 \cdot 10^{-3}$
	Chol (0.061M) + DiI ($1.1 \cdot 10^{-3}$M) in etOH	MKC (0.005M) in PBS	3.9 mg/mL	$3.3 \cdot 10^{-3}$
$^{DiI(8\mu M)}QS_4$	DC-Chol (0.069M) + DiI ($1.3 \cdot 10^{-4}$M) in etOH	MKC (0.008M) in water	6.5 mg/mL	$2.1 \cdot 10^{-3}$
$^{DiI(23\mu M)}QS_4$	DC-Chol (0.069M) + DiI ($3.3 \cdot 10^{-4}$M) in etOH	MKC (0.008M) in water	6.5 mg/mL	$6.3 \cdot 10^{-3}$
$^{DiI(70\mu M)}QS_4$	DC-Chol (0.069M) + DiI ($1.1 \cdot 10^{-3}$M) in etOH	MKC (0.008M) in water	6.5 mg/mL	$19 \cdot 10^{-3}$

The organic solution was prepared dissolving the sterols in 3mL of ethanol while for the aqueous phase the MKC was dissolved in 25mL of water or PBS. # Molar ratio is defined as the ratio between the total moles of sterols and the moles of MKC surfactant initially used for the QS preparation. ‡ The membrane components concentration is the theorical concentration defined as the total mass of the sum of the sterols and surfactants mass comprising QS membrane divided by the total volume of the vesicular suspension added in the reactor for QS preparation. [1]The DiI loading is defined as the moles of DiI divided by the total moles of membrane components used for QS preparation by DELOS-SUSP method ($Loading\ of\ DiI = \frac{moles\ of\ DiI}{moles\ of\ membrane\ components}$).

After fluorometric experiments was done, QS_1 and QS_4 labelled with DiI at the highest concentration (70 µM) was selected for further experiments. These samples are called $^{DiI(P)}QS_1$ and $^{DiI}QS_4$ at 1:1 molar ratio of membrane components for all cases.

3.2.10.2. Synthesis of Quatsome-based vesicular systems prepared by sonication

Quatsome-based nanostructures could also be prepared by sonication according to the following procedure. The membrane components were weight and added directly to 10 mL of an aqueous solution with 10 % of etOH or diluted separately, the sterol in 1 mL of etOH and the surfactant in 9 mL of water (Table 13). The resulting mixture was sonicated at room temperature, using a Vibracell Sonifier titanium probe at 20 KHz for 4 min (Figure 12). After sonication was applied an homogeneous dispersion was obtained.

Table 13. Composition used to prepare Quatsomes nanostructures (NS) by sonication.

System	Solutions prepared before the implementation of ultrasounds	Molar ratio#	[Membrane components] (mg/mL)‡
Quastomes NS	Chol (0.007M) + MKC (0.007M) in water with 10% etOH*	1:1	5.6 mg/mL
	Chol (0.073M) in etOH MKC (0.008M) in water$		

* The final volume of the water with 10% etOH solution is 10mL. $The organic solution was prepared dissolving the Chol in 1mL of ethanol while for the aqueous phase the MKC was dissolved in 9mL of water, obtaining a final volume of 10mL of water with 10% of etOH. # Molar ratio is defined as the ratio between the total moles of sterols and the moles of MKC surfactant initially used for the QS preparation. ‡ The membrane components concentration is the theorical concentration defined as the total mass of the sum of the sterols and surfactants mass comprising QS membrane divided by the total volume of the vesicular suspension added in the ultrasounds for QS preparation.

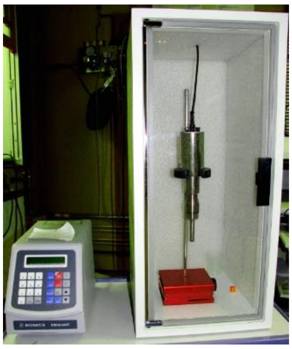

Figure 12. Image of the Vibracell Sonicator used for nanosructures preparation.

3.2.10.3. MKC micelles synthesis by self-assembly

MKC micelles were prepared by the dissolution of MKC surfactant in water (critical micelle concentration or [cmc]= 2.2mM). Briefly, 24 mL of an aqueous solution of MKC (0.008M) surfactant was prepared at room temperature by magnet spindle agitation. The micelles formation was done by the aggregation of MKC molecules among themeselves when they were in contact with an aqueous solution.

3.2.10.4. Nanoparticles purification by diafiltration

After one week of stabilization, all samples were purified by diafiltration using the KrosFlo® Research Iii TFF System (Spectrum Labs from Repligen Corporation; Waltham, Massachusetts, USA). MKC micelles were not purified owing to they were already diluted in water in the preparation process. The diafiltration process is based on a tangential flow filtration to separate and purify solutions or colloidal suspensions, like QS colloidal nanostructures, from permeable molecules (impurities, salts, solvents…). Moreover, this method may be used to concentrate sample formulations.

Diafiltration is based on the same principles than dialysis, but the diafiltration process is faster and more efficient. Depending on the sample volume, different filter columns with a range of surface area (5 cm^2 to 1050cm^2) and different molecular weight of cut-off may be used. Using diafiltration process with the appropriate membrane three aims may be accomplished: i) to change the dispersant medium or buffers; ii) to eliminate the free molecular components, which are not integrated in the colloidal nanostructures, such as QS, and iii) to concentrate the colloidal formulation. In this thesis, the samples were diafiltered using a size-exclusion mPEs Micro Kros filter column (100KDa molecular weight cut-off and a surface area of 20cm^2) to remove the ethanol and non-incorporated MKC surfactant in vesicles. To perform the diafiltration, KrosFlo Research Iii TFF system was set up following the manufacturer's recommendations (Figure 13). Briefly, the sample was introduced in a falcon tube connected with a reservoir falcon, which contained the replacing medium, and the two tubes that recirculates the sample through a rotation pump at a fixed flow rate. The pressure given by the rotation pump pushed the sample through the column and returned it to the original falcon. On the other hand, the pressure difference between inside and outside the membrane permitted the separation of low molecular weight compounds that can go through the membrane pores. During the circulation of the sample, drop by drop the buffer was changed eliminating the previous buffer through the permeate tube (tube which connect the column with the elimination test tube; left part of Figure 13) and introducing the new buffer from the reservoir falcon into the sample falcon (right part of Figure 13). In the present thesis, among 4mL to 15mL of sample was purified at feed speed of 15 mL/min for 6 cycles of recircularization to ensure the fully elimination of the etOH and the non-incorporated components in the vesicles. So that, for 4 mL of initial sample, the sample must circularize until the filtrated buffer volume of the permeate tube achieves 24 mL.

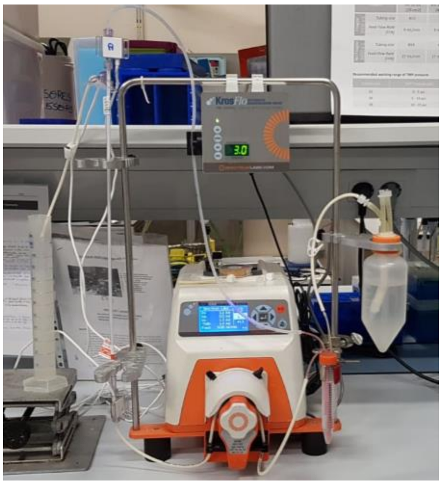

Figure 13. Image of the diafiltration system for QS purification.

3.2.10.5. Nanoparticles concentration by diafiltration

Once samples were purified, QS may be concentrated using the same equipment KrosFlo® Research Iii TFF utilised for diafiltration. After samples were circularized into the column six times their initial volume, the concentration process started. First, the clamp that allowed the introduction of new buffer into the sample, was closed whereas the other clamp that permit the samples removal in the permeate tube was opened. Thus, during the samples recircularization by the rotation pump, QS returned to the samples reservoir while the buffer was eliminated to the system by the permeate tube. The lack of new buffer entrance and the elimination of buffer from the sample, reduced the final volume of the sample and concentrated their components avoiding their removal during the recircularization inside the column. The concentration process finished when the samples reduced their buffer volume x times required for the concentration.

3.2.11. Physicochemical characterization of QS

3.2.11.1. Dynamic Light scattering (DLS) measurements

Particle size, polydispersity and surface charge density of QS were evaluated by the non-invasive dynamic light scattering (DLS) technique. The DLS equipment employed was Zetasizer Nano ZS (Malvern Instruments, Malvern, United Kingdom), which has an incident He-Ne laser light of 4mW, a wavelength of 633nm, a detector angle fixed at 173° with homodyne detection and a thermostatic chamber for the samples.

Particle size and polidispersity:

For hydrodynamic diameter (D_h) and polydispersity index (PDI) measurements, 1 mL of each sample was measured after one week of preparation or purification, as born without modifications or dilution, at 25°C (298.15°K) in tripli°ate. All sizes and particle size distributions have been reported as scattered intensity, which represents the percentage of light scattered into particles in the sample. The most recommendable form to show particle size is as scattered intensity because these data are collected by the detector of DLS in these way without processing or assumptions to calculate it. This technique determines the time-dependent fluctuations of light scattered from particles using a Brownian motion, which occurs from collisions with solvent molecules. Analysing these fluctuations of light scattered, the diffusion coefficient was determined which is, then, converted into the size distribution using the Stokes-Einstein equation.

Stokes-Einstein equation depends on the hydrodynamic radius of the particle, the Boltzmann constant, the temperature and the solvent viscosity. The hydrodynamic radius of the particle is described by the diameter of the sphere with the same translational diffusion coefficient of the particle, which considers the particle "core" size and the particles hydration shell produced by the surface structure, the concentration and the composition of the medium (Figure 14). For this reason, the hydrodynamic diameter (D_h) obtained by DLS is usually larger than measured by other techniques that measure only the core of the particle and not the native environment (e.g. cryo-TEM).

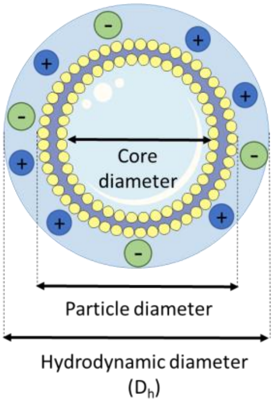

Figure 14. Schematic representation of the hydrodynamic diameter (D_h) given by DLS to indicate the size of nanoparticles.

The Polydispersity index (PDI) is the polydispersity of the Gaussian curve generated from the size distribution of QS sample, that correlates with the monodispersity of the sample. Values of the PDI goes from 0 (very monodisperse sample) to 1 (very polydisperse sample). Values with PDI under 0.3 were considered a colloidal suspension to be monodisperse. In this thesis, to measure the samples by DLS the temperature selected was 25°C (298.15K) and the dispersant mediums used were water for purified samples by diafiltration, water with 10% of etOH for samples prepared after DELOS-SUSP or by sonication, except for $^{DiI}QS_1$ which used PBS or PBS with 10% of etOH, respectively.

Surface particle charge:

Another non-invasive backscattering technique measured with Zetasizer Nano ZS was the Z-potential. Z-potential is the electric potential measured at the double layer distribution of charges from the interface of the particle. The surface charge of particles is distributed in an inner region, called Stern layer with strong bounding to the particle, and an outer region, called diffuse, where the charges are less attached. Z-potential is determined measuring the voltage between two electrodes placed in opposite ends of the cell that contains the sample. When the voltage is applied, particles migrate towards the oppositely charged electrode with determined speed, which will correlate the mobility of the particles to the value of Z-potential by the Henry equation.

The parameters involved in Z-potential determination are the dielectric constant, viscosity of the dispersant and the Henry's function, which was approximately 1.5 for aqueous media according to Smoluchowski[175].

Thereby, Z-potential provides the overall charge of the particle in the dispersant medium, indicating the stability of the colloidal systems due to the repulsion between charges. It is reported that colloidal samples with large values, positive or negative, of Z-potential are generally stable, whereas at Z-potential nearly to neutrality they tend to flocculate[178]. Therefore, large positive or negative surface charge (over than ± 40mV) helps to NP to stabilize and to decrease their aggregation since they repel each other. On the other hand, in this thesis, Z-potential was also used to predict the interactions of QS vesicles with small RNA in the dispersing media PBS, through the positive charge of QS and the negative charge of sRNA. The DLS used has a 633nm laser, which means that samples that absorb or emit at this wavelength can not been determined (e.g. fluorescence samples). In this thesis the DiI fluorophore presents a spectrum of emission and absorption that do not interfere with DLS measurement; thus, that QS samples with DiI fluorophore can be measured also by DLS. In this work, the Z-potential was determined using 800 µL of sample in a DTS1070 disposable folded capillary cuvette at 25°C (298.15K).

Reported values were the average of at least three different samples of hydrodynamic diameters (D_h) ± standard deviation (SD) among samples, PDI ± SD or Z-potential ± SD. Experiments were carried out at least in triplicate. QS colloidal stability over time was determined periodically by DLS after one week, two weeks, one month, three months and six months after sample preparation or purification.

3.2.11.2. Morphology by Cryo-TEM

Cryogenic transmission electron microscopy (Cryo-TEM) technique was used to study the morphology of samples, such as shape and lamellarity. Electron microscopy is the best methodology for the individual inspection of nanoparticles morphology. This technique is based on the irradiation of the samples with a particle beam of electrons and the capture of a magnified image. However, this technique presents several advantages, such as high resolution, but samples need to be processed before the analysis. For this reason, samples were cryogenised and the images were acquired by the technician of the Servei de Microscòpia of the Universitat Autonòma de Barcelona (UAB).

The images were taken using the JEOL JEM 2011 transmission electron microscope (JEOL LTD, Tokyo, Japan) at 200KV. First of all, two drops of samples were placed on 300 mesh copper grids coated with perforated polymer film, EMR Lacey Carbon (22-1MLC30-50; Micro To Nano; Netherlands) or Holey Carbon (22-1MLC30-50; Micro To Nano). The excess of sample was removed putting closer a filter paper. Then, samples were frozen in liquid ethane at the temperature just above the freezing point (-178.15 °C or 95K) by a vitrification system with a controlled environment using Leica, model EM GP (Leica Microsystems, Germany). The vitrified samples were placed into Gatan 626 cryo-transfer system, which maintain the sample cool (-196.15 °C 77K) in order to avoid sample alteration and crystals formation until the insertion into the JEOL JEM 2011 transmission electron microscope. Images were recorded using a Gatan Ultrascan US1000 CCD camera and analyzed with the Digital Micrograph 1.8 program. Representative images of samples were shown in this thesis.

3.2.11.3. Membrane components concentration by gravimetric analysis.

The membrane components concentration of QS or NS were measured by gravimetric analysis after freeze-drying. Lyophilization or freeze-drying, removes water from samples by freezing them and sublimating the ice directly from solid to gaseous state (steam) under a vacuum. This process consists of three steps: freezing, primary drying and secondary drying. During the freezing process, water from samples are turned into ice avoiding the ice crystals formation. The freezing was done reducing the temperature one degree per minute until arrive to - 55.15 °C (218K). The second step, in the primary drying or sublimation, the pressure reduction induces water sublimation and evaporation under the vacuum. Then, samples are solidified at low temperature. This step is performed at -80.15 °C (193K) and at 5 Pa for 5 days, in which more than 90% of water was eliminated. Finally, the secondary drying or desorption allows that water ionically attached is removed from samples by heating them until exceed the eutectic point. This step was carried out until achieve a temperature of 25 °C (298.15K) and a pressure of 1 Pa for 9 hours.

In this thesis, 1 mL of QS sample was lyophilized to remove the aqueous media, without interfering in the intramolecular water of samples, with the LyoQuest Logger (Telstar Life Science Solutions). Then lyophilized product, which corresponds mainly to the QS or NS membrane components, was weight using an XS analytical balance (Mettler Toledo, USA) and then was converted to a real concentration considering the volume of sample lyophilized. These experiments were performed at minimum per triplicate, so that the final yield of the samples (Table 14) was calculated dividing the real concentration with the theorical concentration and expressed as the mean yield of the process in percentage ± SD. The real concentration of membrane components was calculated assuming the final yield obtained after all processes of QS preparation or purification (Table 14).

Table 14. Yield and real concentrations of various QS systems after DELOS-SUSP preparation, diafiltration or concentration.

Systems	Molar ratio	Yield (%) [#]			Final yield (%)	Real membrane components concentrations (mg/mL) [‡]
		DELOS-SUSP or synthesis	Diafiltration	Concentration		
QS_0	1:0.75	78.2 ± 0.0	78.5 ± 0.1	-	61.4 ± 2.0	3.3 ± 0.15[a]
	1:1	84.3 ± 5.9	79.5 ± 5.5	98.5 ± 9.7	68.3 ± 3.75[a] 64.0 ± 6.0[b]	4.3 ± 0.34[a] 32.8 ± 4.5[b]
QS_1	1:1	97.9 ± 4.2[$]	62.1 ± 0.1	-	60.3 ± 2.0	3.4 ± 0.16[a]
	1:1.5	88.3 ± 0.0	49.1 ± 0.5	-	43.3 ± 1.1	2.0 ± 0.33[a]
	1:2	95.9 ± 1.6	46.3 ± 0.1	-	44.4 ± 0.6	2.4 ± 0.01[a]
	1:3	92.3 ± 3.15	35.7 ± 4.9	96.8 ± 4.3	34.3 ± 4.9[a] 32.1 ± 2.0[b]	1.8 ± 0.35[a] 16.1 ± 1.4[b]
QS_2	1:1	84.8 ± 3.0	55.2 ± 1.9	-	46.8 ± 2.0	2.7 ± 0.16[a]
QS_3	1:1	87.5 ± 2.0	60.9 ± 4.7	-	51.8 ± 2.8	3.1 ± 0.24[a]
QS_4	1:1	90.6 ± 1.1	47.8 ± 2.4	-	43.2 ± 1.9	2.8 ± 0.17[a]
$^{DiI(P)}QS^1$	1:1	99.6 ± 1.1	98.2 ± 1.8	-	97.5 ± 1.9	3.6 ± 0.17[a]
$^{DiI(8\mu M)}QS_4$	1:1	69.5 ± 2.1	39.5 ± 5.7	-	27.3 ± 3.1	1.9 ± 0.30[a]
$^{DiI(23\mu M)}QS_4$	1:1	63.7 ± 4.3	45.4 ± 4.9	-	28.1 ± 1.3	1.1 ± 0.11[a]
$^{DiI(70\mu M)}QS_4$	1:1	50.5 ± 1.1	37.9 ± 2.2	-	25.3 ± 1.0	1.8 ± 0.10[a]

[$] Nanovesicles done at 1:1 molar ratio of Chol:MKC are prepared by ultrasounds instead of DELOS-SUSP. [#] The yield was calculated by dividing the final mass of the membrane components, measured by gravimetric analysis of at least triplicate lyophilized samples, with the initial mass of membrane components loaded to the reactor for QS preparation (for DELOS-SUSP yield) or the initial mass of the last step done (for diafiltration and concentration yields). The final yield is the sum of the yields of each process done. [‡] The membrane components concentration (mg/ml) is the real concentration calculated assuming the loss of material after the processes steps done to prepare and purify QS (yield) in relation to the QS theorical concentration. [a] Real concentration of QS systems after preparation and diafiltration. [b] Real concentration of QS systems after preparation, diafiltration and concentration.

3.2.11.4. pH stability and buffering capacity

Stability of QS in terms of pH was characterized over time. The pH of QS samples was measured using the pHmeter of Hanna Instruments (Woonsocket, Rhode Island, EEUU) periodically. Temperature was kept at 25°C (298.15K) and samples were not modified or diluted along pH monitoring process. These measurements were done minimum per triplicate and the results were expressed as the average of at least three different samples ± standard deviation (SD) among samples.

pH titration curves evaluate the capacity of pH sensitive systems and the pH behavior of samples in slightly acidic or acidic conditions. DC-Chol, which is present in many QS-based nanovesicular structures of this thesis, may be protonated in slightly acidic or acidic pH (pKa ~ 7.8). In order to evaluate the different buffering capacity of QS free of DC-Chol and with DC-Chol, they were diluted at a final concentration of 1.8 mg/mL (total membrane components) in MilliQ treated water. The resulting QS were adjusted at pH 9 with NaOH 0.01M with the pHmeter. The titration curves were performed measuring the pH after each addition of 10 µL of HCl (0.01M) until the pH 3 was reached. At every point of pH the hydrodynamic diameter was measured in order to evaluate the stability of the sample after pH modification. Finally, pH titration curves were plotted as the mean of duplicate experiments ± the SEM of the experiments.

3.2.11.5. Fluorescent characterization by UV-Vis

Quatsomes labelled with DiI flurorophore were characterised by UV-Vis to determine the DiI concentration in QS membrane and the absorption spectra of ^{DiI}QS compared to DiI spectra in etOH.

DiI concentration in QS membrane

^{DiI}QS purified samples and DiI stock were diluted in ethanol 1:20 to ensure the full dissolution of QS and DiI. Then, 1 mL of each sample was placed in a quartz cell with 1 cm path length and the cuvette was introduced into the Varian Cary 500 UV-vis-NIR spectrophotometer. After the absorption spectra was acquired, the concentration of DiI in the samples was calculated using the Lambert-Beer Law and using the same protocol explained before for the determination of the concentration from DiI stock solution. Finally, ^{DiI}QS samples prepared at three different loadings, were called based on DiI concentrations, $^{DiI(8\ \mu M)}$QS, $^{DiI(23\ \mu M)}$QS and $^{DiI(70\ \mu M)}$QS.

DiI absorption spectrum after incorporation in QS membrane

^{DiI}QS purified samples were diluted in water (1:20) to avoid the QS membrane and the aggregates of DiI dissolution in etOH. On the other hand, DiI stock were diluted in ethanol (1:20) to ensure the DiI stock dissolution. Then, 1 mL of each sample was measured in a quartz cell using the Varian Cary 500 UV-vis-NIR spectrophotometer. After the absorption spectra was acquired, each spectrum was normalized with their peak of maximum absorption and using etOH as a blank control. The normalized spectra per each sample were represented and compared with the DiI spectra in etOH. These experiments were done in triplicate and a representative spectrum was shown.

3.2.12. QS-sRNA and MKC micelles complexes formation with miRNA

Complexes were generated by ionic interactions between the positive charges of QS or MKC micelles and the negative charges of sRNA. Several QS-sRNA complexes, with different loadings of sRNA per QS, were prepared by mixing an aqueous solution of sRNA with a constant sRNA concentration (2.5 µM), with various QS formulations with different membrane components concentrations. The protocol used for QS-sRNA complexes preparation is composed by only three steps. Previously, QS described in Table 14 were diluted in DEPC-treated water (ThermoFisher; #750024) 3.98 mg/mL for QS$_0$, 1.2 mg/mL for QS$_1$; 1.8 mg/mL for QS$_2$; 1.9 mg/mL for QS$_3$; 2.0 mg/mL, for QS$_4$; 2.0 mg/mL for DiI-QS$_1$ and 1.8 for DiI-QS$_4$. First, x µL of diluted QS were added into a sterile 1.5mL tubes depending on the desired amount of sRNA to be loadeded in QS (Table 15-Table 16). Next, 2.5 µL of sRNA were added over the QS solution to achieve a final concentration of 2.5 µM of sRNA. Finally, QS and sRNA mixture was diluted in PBS 1X (Fisher; #10462372). The QS-sRNA complexes were incubated for five minutes before being tested. The QS-sRNA complexes formulations, being sRNA miRNA or siRNA, were prepared at different sRNA loading in QS, and named QS-sRNA (I-VIII) (see Table 15-Table 16). The loading of sRNA in QS was calculated as the total mass ratio between sRNA and QS membrane components, using the relation in weight of $\frac{miRNA}{QS}$ or $\frac{siRNA}{QS}$ (Table 17-Table 18).

Table 15. Protocol for the preparation of QS$_0$-sRNA complexes at different loadings of sRNA in QS.

Loadings of QS$_0$–miRNA complexes	miRNA volume (µL)	QS$_0$ volume (µL)	PBS volume (µL)
QS$_0$-miRNA (I)	2.50	8.75	8,75
QS$_0$-miRNA (II)		6.56	10.94
QS$_0$-miRNA (III)		4.38	13.12
QS$_0$-miRNA (IV)		2.63	14.87
QS$_0$-miRNA (VI)		1.05	16.45

Table 16. Protocol for the preparation of QS$_{1\text{-}4}$-sRNA complexes the indicated loadings of sRNA in QS.

Loadings of QS$_{1\text{-}4}$–sRNA complexes	sRNA volume (µL)	QS$_{1\text{-}4}$ volume (µL)	PBS volume (µL)
QS-sRNA (I)	2.50	17.5	0.00
QS-sRNA (II)		13.13	4.38
QS-sRNA (III)		8.75	8.75
QS-sRNA (IV)		4.38	13.13
QS-sRNA (V)		2.63	14.87
QS-sRNA (VI)		1.75	15.75
QS-sRNA (VII)		1.17	16.33
QS-sRNA (VIII)		0.7	16.8

QS-sRNA complexes means that QS can be conjugated with miRNA or siRNA.

Table 17. Concentrations of the QS and miRNA solutions used for the preparation of QS nanoconjugates with different loading of miRNA.

Loading of Complexes QS-miRNA#	[miRNA] (µM)	[c] QS0 (mg/mL)	Mass ratio miRNA/QS1 (w/w·10^{-2})*	[c] QS_I (mg/mL)	Mass ratio miRNA/QS_1 (w/w·10^{-2})*	[c] QS_2 (mg/mL)	Mass ratio miRNA/QS_2 (w/w·10^{-2})*	[c] QS_3 (mg/mL)	Mass ratio miRNA/QS_3 (w/w·10^{-2})*	[c] QS_4 (mg/mL)	Mass ratio siRNA/QS_4 (w/w·10^{-2})*
QS-miRNA (I)	2.50	1.74	2.02	1.29	3.50	1.53	2.29	1.63	2.14	1.74	2.02
QS-miRNA (II)		1.30	2.70	0.96	4.67	1.15	3.05	1.22	2.86	1.30	2.70
QS-miRNA (III)		0.87	4.05	0.64	7.01	0.77	4.58	0.81	4.29	0.87	4.05
QS-miRNA (IV)		0.52	6.75	0.32	14.01	0.38	9.16	0.41	8.57	0.43	8.10
QS-miRNA(V)		0.31	11.21	0.19	23.35	0.23	15.26	0.24	14.29	0.26	13.50
QS-miRNA (VI)		0.21	16.87	0.13	35.03	0.15	22.89	0.16	21.43	0.17	20.24
QS-miRNA (VII)		0.14	25.31	0.09	52.40	0.10	34.24	0.11	32.05	0.12	30.28
QS-miRNA (VIII)		0.08	42.18	0.05	87.58	0.06	57.22	0.07	53.57	0.07	50.61

#The loading of QS-miRNA complexes describes the miRNA loading in QS indicated by their mass ratio (w/w·10^{-2}). *The mass ratio indicates the loading of miRNA into QS and was obtained dividing the mass of miRNA from QS. Hence, the concentration of QS was obtained assuming the yield obtained by gravimetrical mass analysis and the volume required to prepare the selected loading (X) for each QS-miRNA complex. The mass of the miRNA was calculated using the average molecular weight of a miRNA, which is 14100g/mol.

Table 18. Concentrations of the QS and siRNA solutions used for the preparation of QS nanoconjugates with different loading of siRNA.

Loading of Complexes QS-siRNA#	[siRNA] (µM)	[c] QS_I (mg/mL)	Mass ratio siRNA/QS_1 (w/w·10^{-2}) *	[c] QS_2 (mg/mL)	Mass ratio siRNA/QS_2 (w/w·10^{-2}) *	[c] QS_3 (mg/mL)	Mass ratio siRNA/QS_3 (w/w·10^{-2}) *	[c] QS_4 (mg/mL)	Mass ratio siRNA/QS_4 (w/w·10^{-2}) *
QS-siRNA (I)	2.50	1.29	3.30	1.53	2.16	1.63	2.02	1.74	1.91
QS-siRNA (II)		0.96	4.41	1.15	2.88	1.22	2.70	1.30	2.55
QS-siRNA (III)		0.64	6.61	0.77	4.32	0.81	4.04	0.87	3.82
QS-siRNA (IV)		0.32	13.22	0.38	8.64	0.41	8.09	0.43	7.64
QS-siRNA(V)		0.19	22.03	0.23	14.39	0.24	13.48	0.26	12.73
QS-siRNA (VI)		0.13	33.04	0.15	21.59	0.16	20.21	0.17	19.10
QS-siRNA (VII)		0.09	49.42	0.10	32.29	0.11	30.23	0.12	28.56
QS-siRNA (VIII)		0.05	82.61	0.06	53.98	0.07	50.53	0.07	47.74

#The loading of QS-siRNA complexes describes the siRNA loading in QS indicated by their mass ratio (w/w·10^{-2}). *The mass ratio indicates the loading of siRNA into QS and was obtained dividing the mass of siRNA from QS. Hence, the concentration of QS was obtained assuming the yield obtained by gravimetrical mass analysis and the volume required to prepare the selected loading (X) for each QS-siRNA complex. The mass of the siRNA was calculated using the average molecular weight of a siRNA, which is 13300g/mol.

Table 19. Concentrations and volumes of the MKC micelles and miRNA solutions used for the preparation of nanoconjugates of miRNA loaded in MKC micelles.

Loading of MKC micelles-miRNA complexes#	[miRNA] (µM)	miRNA volume (µL)	[c] MKC (mg/mL)	MKC volume (µL)	PBS volume (µL)	Mass ratio MKC-miRNA (w/w) *
Micelles MKC-miRNA (I)	2.50	2.50	0.06	2.63	14.87	11.42

#The loading of micelles MKC-miRNA complexes describes the miRNA loading in MKC micelles indicated by their mass ratio (w/w·10^{-2}). *The mass ratio indicates the loading of miRNA into MKC micelles and was obtained dividing the mass of miRNA from MKC micelles. The concentration of MKC micelles was calculated considering the ratio in charge with optimal efficiency over miRNA targets with QS_4-miRNA complexes. The mass of the miRNA was calculated using the average molecular weight of a miRIDIAN miRNA mimic, which is 14100g/mol.

For the conjugation of miRNA with MKC micelles, micelles of MKC in solution were incubated with miRNA to perform complexes through electrostatic interactions between the positive charge of the MKC surfactant and the negatives from miRNA. In this case, all the positive charge from micelles of MKC are considered for the miRNA conjugation because all the positive charges are accessible for the miRNA interaction. The micelles of MKC-miRNA (I) conjugates were prepared with the amounts indicated in Table 19. For the preparation of conjugates formed by micelles of MKC and miRNA (Table 19), 2.5 µL of miRNA (2.5 µM) were added above 2.6 µL of MKC micelles solution. Finally, PBS 1X was added to achieve the final volume of 20 µL of conjugates, like QS-sRNA complexes. After five minutes of micelles MKC and miRNA incubation the conjugates were formed.

3.2.13. Complexation efficiency of miRNA in QS

Electrophoresis on agarose gels permits the separation of nucleic acids based on their size. An electrical field induces the mobility of negatively charged molecules through the gel towards the positive electrode. DNA or RNA fragments are separated by their size in an inversely proportional manner between the distance travelled for nucleic acids and the logarithmic value of nucleic acids molecular weight. For this reason, shorter DNA or RNA fragments migrate faster than longer ones from the bottom (negatively charged electrode) to the down side (positively charged electrode) of the gel and their approximate length of nucleic acids can be determined comparing their mobility with the DNA ladder ones. Ethidium bromide (EtBr) is a DNA/RNA intercalating agent added to the agarose solution to visualize the nucleic acids when they are exposed to UV light. When EtBr is exposed into UV light, electrons of the aromatic ring of EtBr are activated and release energy (light) to return to their basal state. So that, the intensity of light emitted from nucleic acid is directly proportional to the amount of DNA or RNA.

QS-miRNA complexes were prepared following the procedure explained above. To load them on agarose gel, loading buffer composed by 0.08% of glycerol was added into the samples to increase the density of the sample. Then, the complexes were loaded on 2.5% agarose gels in Tris/Acetate/EDTA (TAE 1X) with 0.005% of Ethidium Bromide buffer and run at 120V for one hour. Electrophoretic gel images were acquired using Gel Doc XR + System (Biorad, Hercules, California, USA).

To release miRNA from QS-miRNA complexes, 0.25-1% of Sodium dodecyl sulfate (SDS) was added to the sample.

3.2.14. Cell Proliferation assays with QS-miRNA complexes

SK-N-BE(2) cells were seeded in 96-well plates at 18x10^3 cells/well (6 replicates/condition) and treated with QS (0.7µg/mL to 52µg/mL; Table 21) or with miR-Control-QS complexes. For complexes formation, 2.5 µM of miR-Control-Dy547 were conjugated with QS at various concentrations, achieving various loadings of miRNA in QS (I-VIII, Table 16-Table 17). Final miRNA concentration was 50nM. Twenty-four hours after QS treatment the experiments were stopped.

Table 20. QS and miRNA concentrations for cell viability assays.

QS-miRNA loading	[miRNA] (nM)	[c] QS_1 (µg/mL)	[c] QS_2 (µg/mL)	[c] QS_3 (µg/mL)	[c] QS_4 (µg/mL)
QS-miRNA (I)	50.0	25.73	30.61	32.52	34.76
QS-miRNA (II)		19.29	22.95	24.39	26.07
QS-miRNA (III)		12.86	15.30	16.26	17.38
QS-miRNA (IV)		6.43	6.12	8.13	8.69
QS-miRNA(V)		3.86	4.59	4.88	5.21
QS-miRNA (VI)		2.57	3.06	3.25	3.48
QS-miRNA (VII)		1.72	2.05	2.17	2.32
QS-miRNA (VIII)		1.03	1.22	1.30	1.39

To determine the functional effects of QS_4-sRNA (QS_4-miRNA or QS_4-siRNA) complexes on cell proliferation, SK-N-BE(2) cells were seeded in 96-well plates at 9x10^3 cells/well (6 replicates/condition) and reverse transfected with lipoplexes (previously explained in section 3.2.1) and with three different loadings of QS-miRNA (V, VI and VIII), which achieved a constant final miRNA concentration of 50nM. After o/n incubation the culture media was changed. Ninety-six hours post-transfection, cells were fixed with 1% of glutaraldehyde and stained with 0.5% crystal violet. Then, crystals were dissolved in 15% acetic acid and their absorbance were measured at 590 nm using an Epoch Microplate Spectrophotometer. The effect of QS or QS_4-sRNA complexes on cell viability was normalized to mock-control-non-transfected cells.

3.2.15. Internalization of QS-miRNA complexes in NB cells

For internalization experiments of QS-miRNA complexes in SK-N-BE(2) cells were seeded at 2 x 10^4 in 8-wells Ibidi- glass bottom chamber slides 24 hours before transfection. Next day, cells were transfected with the complexes prepared with QS conjugated with miR-Control labelled with Dy547 at the loading (V). After overnight (o/n) incubation cellular media was changed for IMDM supplemented with 10% FBS and antibiotics.

Confocal images were acquired using a Leica TCS SP5X microscope. Dy547 was excited using a 570-700 nm laser. The emitted signal was collected from 570 nm - 700nm. For lysosomal colocalization experiments, Lysotracker Green (#L7526; Thermo Fisher Scientific) was used and excited with 500-546 nm laser. These experiments were done in collaboration with the group of Dr. Lorenzo Albertazzi from Institute de Bioingenieria de Catalunya (IBEC) and Institute for Complex Molecular Systems (ICMS), also in the frame of the PhD thesis of Natalia Feiner.

3.2.16. QS_4-miRNA complexes stability in presence of serum

In order to evaluate the stability of QS_4-miRNA complexes in presence of serum, 20µL of QS_4-miRNA (V) complex was incubated with 10% of FBS for thirty minutes, one, two and four hours in a water bath at 37°C. Then, to visualize the integrity of miRNA, 0.25% of SDS was added to the samples and were run on 2.5% agarose gels.

3.2.17. RNAse A protection assays

To check the QS capacity to protect the miRNA from RNAse A compared to naked miRNA, both QS_4-miRNA (V) complexes and miRNA naked were treated with 25 µg/mL of RNAse A for thirty minutes, one, two and four hours in a water bath at 37°C. Then, 0.25% SDS was added to the samples to release the miRNA from the QS-miRNA complexes. Samples were finally resolved on 2.5% agarose gels.

3.2.18. FRET analysis

To evaluate the interaction between the miRNA and QS after complexes formation, Förster Resonance Energy Transfer (FRET) technique was used. FRET allows, through the excitation of one of two closer light sensitive molecules (e.g. fluorophores), the detection of proximity by the energy transfer from one molecule to another. When two fluorophores are located close to each other, the excitation of the donor transfers energy to the second fluorophore, called acceptor, which will emit fluorescence (Figure 15). For FRET to occur there are two main requirements. First one, the emission spectra of the donor and the absorption spectra of the acceptor must overlap; the second one, the two fluorophores must be close, ideally less than 10 nanometres (Figure 15).

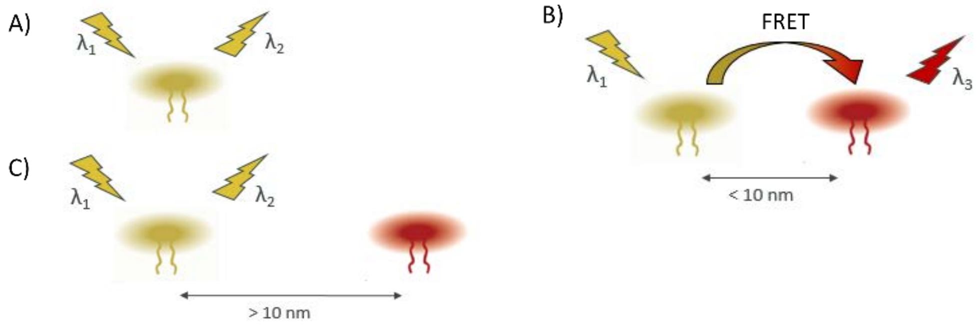

Figure 15. Schematic representation of FRET. A) Normal single fluorophore is excited with λ_1 and emits at λ_2. **B)** FRET phenomena occur and upon the excitation of the donor fluorophore with λ_1 energy is transferred and is the acceptor who emits at λ_3. **C)** The long separation between fluorophores (>10 nm) impedes the energy transfer and the emission emitted is the same as in case **A)** (λ_2).

The FRET efficiency between the two fluorophores, DiI in the QS membrane and Cy5 in the miRNA backbone, was evaluated by the fluorescent measurements of the emission spectra of QS-miRNA complexes using the microplate reader Infinite 200 PRO (Tecan, Switzerland). Complexes were diluted (1:10) in PBS, IMDM + 10% FBS or 10% of FBS and placed into a 96-well plate (3 replicates per condition). DiI and Cy5 were excited with a wavelength of 530 nm and 645 nm respectively and their spectra were recorded from 560 nm – 750 nm and 670 nm – 750 nm in static conditions. The overnight experiments were done also in static conditions, where the microplate reader was set to read the fluorescence at 37°C every 30 min for 18h. These experiments were done in duplicate and a representative spectrum was plotted. For FRET ratio graph, each system was represented as the mean ± SD.

The pharmacokinetics of QS-miRNA complexes internalization was evaluated using FRET and measured the detection of high or low FRET efficiency was evaluated by confocal imaging. If the miRNA remains conjugated with QS, the distance between the fluorophores will be short and the FRET efficiency will be high. On the other hand, when the miRNA is released the distance between the two fluorophores will increase and FRET will not occur. Cells were seeded in 8-wells Nunc Lab-Tek chamber slides 48h before the assay (Thermofisher, USA). Cells were incubated with complexes for 30 minutes and then the media was replaced to remove the non-internalized complexes. Confocal images were acquired using the LSM 800 microscope (Zeiss, Germany). Bright field images were obtained using a 488nm laser. DiI and Cy5 were excited using a 530 nm and 633 nm laser respectively and their signal collected from 550 nm – 620 nm and Cy5 from 640 nm – 750 nm respectively. DiI and Cy5 signals were acquired in two different channels and processed to remove the cross-talk signal. Images of complexes were processed to obtain the variation of the FRET ratio over time.

These experiments were done with technical triplicates in triplicate and were performed in collaboration with the group of Dr. Lorenzo Albertazzi from Institute de Bioingenieria de Catalunya (IBEC) and Institute for Complex Molecular Systems (ICMS), also in the frame of the PhD thesis of Natalia Feiner.

3.2.19. Statistical analysis

Unless otherwise stated, graphs represent the average of three independent experiments ± SEM. Statistical significance was determined by unpaired two-tailed Student's *t*-test (GraphPad Prism Software, USA). * means $p < 0.05$, ** means $p < 0.01$ and *** means $p < 0.001$.

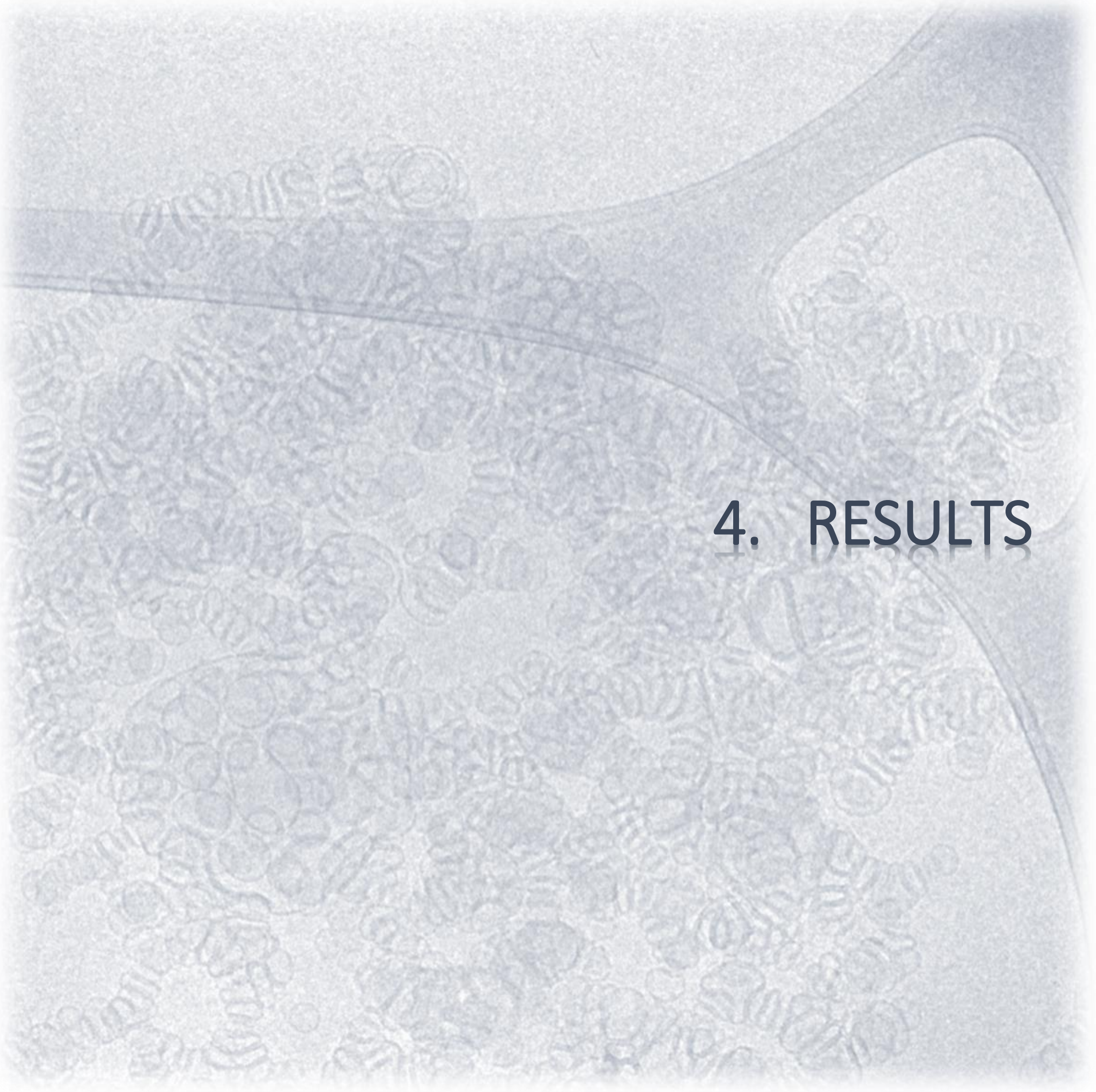

4. RESULTS

4. RESULTS

4.1. Tumour suppressor mir-323a-5p is a potential therapeutic tool for NB

With the aim to expand the druggable targets and discover an alternative treatment for high-risk NB patients, the therapeutic potential of miRNA restoration therapies has been evaluated.

4.1.1. Identification of miRNA with tumor-suppressive functions in NB by a functional high-throughput screening

In order to find miRNA with therapeutic potential in NB, a high-throughput screening of 2048 miRNA mimics was performed. The high-throughput screening was done using the largest library of miRNA mimics available, which allow the identification of miRNA with tumour-suppressive functions in NB. SK-N-BE(2) cells were transfected with individual miRNA mimics (Figure 16A). Previous published results of our laboratory demonstrated the miR-497-5p has tumour-suppressive effects in NB. Therefore, miR-497-5p was used as a positive control; miR-Controls (i.e., cel-miR-67 and cel-miR-239b) were used as negative controls[52]. Among 2048 tested miRNA, 52 of them, reduced ~50% the proliferation of the SK-N-BE(2) NB cell line (Z score < -2, adjusted p value < 0.05) (Figure 16B; Supplementary Tables 1-2 from Soriano et al.[157]).

Since it has been suggested that miRNA with similar functions cluster together[179], we examined the genomic distribution of miRNA whose overexpression produced the highest reduction on cell proliferation. Of note, 7 of the 52 miRNA (13.5%) are located in the same chromosomal locus 14q32, which means that are part of the same cluster (Figure 16C). It is reported that 14q32 locus presents a high miRNA density and is frequently lost or silenced in many tumours, such as NB[45].

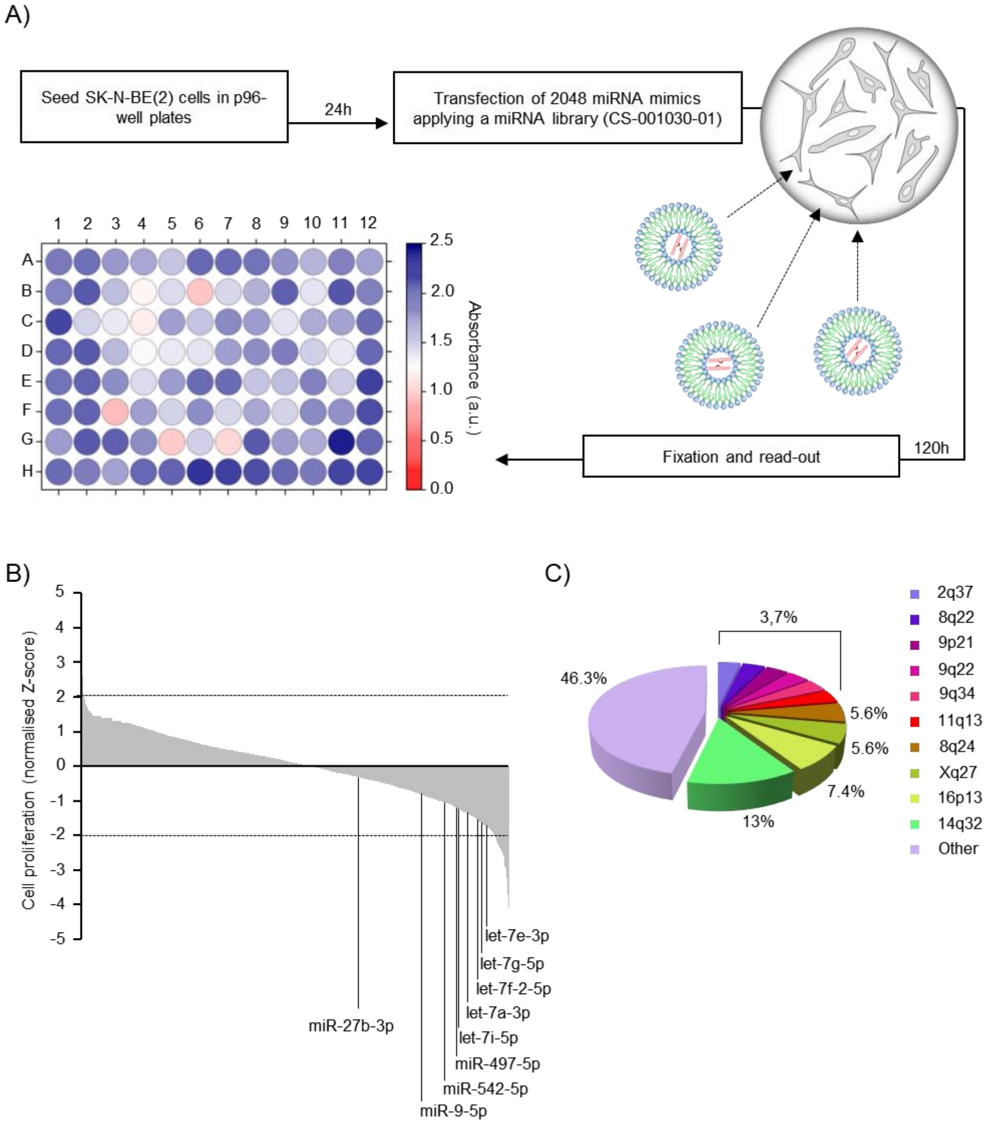

Figure 16. Functional high-throughput miRNA screening identified several tumor-suppressive miRNA. A) Screening design. **B)** Representative plot of the 2048 individual miRNA effects on cell proliferation. The percentage of growth inhibition was obtained by comparing the average of three independent miRNA mimics replicates with mock-transfected cells and standardized using the *Z* score transformation method. MiRNA previously reported as tumor-suppressive miRNA in NB are indicated. **C)** Pie chart representing the genomic distribution of miRNA that reduced cell proliferation ~ 50% (*Z* score < − 2).

4.1.2. Restoration of miRNA located at 14q32 reduces cell viability in NB cell lines

The tumour-suppressive effects of the seven miRNA (i.e., miR-380-5p, miR-665, miR-541-3p, miR-299-3p, miR-654-5p, miR-323a-5p and miR-342-5p) located at the 14q32 locus were evaluated in an extended panel of six NB cell lines. These cell lines presented genomic alterations, such as MYCN or non-MYCN amplification, which are associated with resistance to NB conventional therapies and poor patient outcome (Table 21).

Table 21. Neuroblastoma cell lines characteristics.

Cell lines	Stage	Age (months)	MYCN Status	P53 Status	ALK Status	Chemo-response*
CHLA-90	4	102	Not amplified	Non-functional	F1245V Mut[1]	Resistant
SH-SY5Y	4	48	Not amplified	Functional	F1174L Mut[1]	Sensitive
SK-N-AS	4	72	Not amplified	Non-functional	NA[2], wt[3]	Resistant
LA1-5s	4	36	Amplified	Non-functional	F1174L Mut[1]	Resistant
IMR-32	4	13	Amplified	Functional	PA[4], wt[3]	Sensitive
SK-N-BE(2)	4	24	Amplified	Non-functional	NA[2], wt[3]	Resistant

*DNA damaging agents (e.g. cisplatin, etoposide, etc). [1]Mut: Mutated; [2]NA: Not amplified; [3]wt: wild type; [4]PA: Partial Amplification.

The transient overexpression of the previous selected seven miRNA showed the capacity to reduce cell proliferation in multiple NB cell lines compared to mock- and miR-control-transfected cells. Among of them, miR-323a-5p was the one with the highest therapeutic potential for NB treatment (Figure 17).

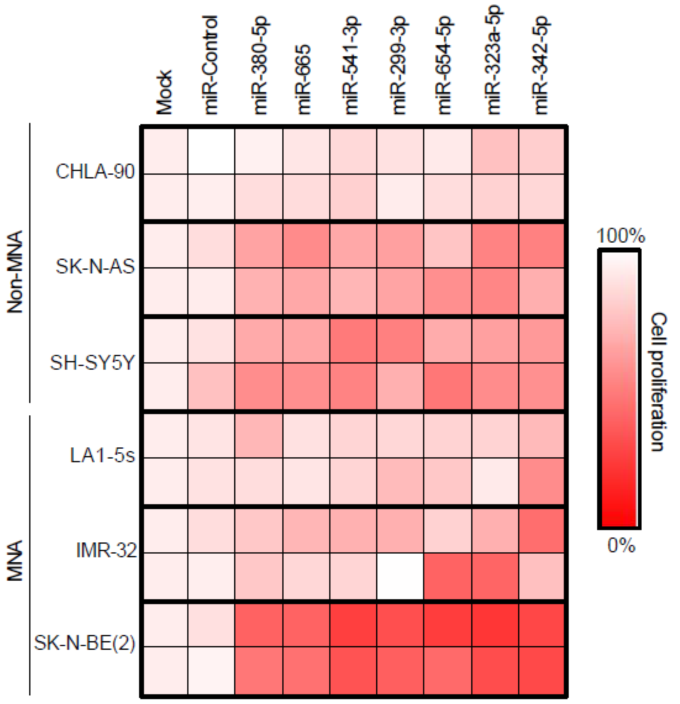

Figure 17. Overexpression of miRNA located at 14q32 reduced cell proliferation in multiple NB cell lines. Heat-map representing effects of the indicated miRNA on cell proliferation reduction in MYCN amplified (MNA) and MYCN non-amplified (non-MNA) cell lines. The overexpression effect of each miRNA on cell proliferation was compared to mock-transfected cells.

4.1.3. Ectopic expression of miR-323a-5p halts cell cycle progression and induces apoptosis in NB

To clarify whether the reduction in cell number upon miR-323a-5p overexpression was due to inhibition of cell proliferation and/or induction of cell death, cell cycle progression was analysed using flow cytometry. The overexpression of miR-323a-5p induced a modest increase in the subG1 peak and an increment in G0/G1-phase population accompanied by a reduction in the S and G2/M phases (Figure 18A-B). Next, we examined the chromatin status of miRNA transfected cells by Hoechst staining. MiR-323a-5p transfected cells showed a higher percentage of cells with condensed and fragmented chromatin staining, one of the typical hallmarks of apoptosis (Figure 18C).

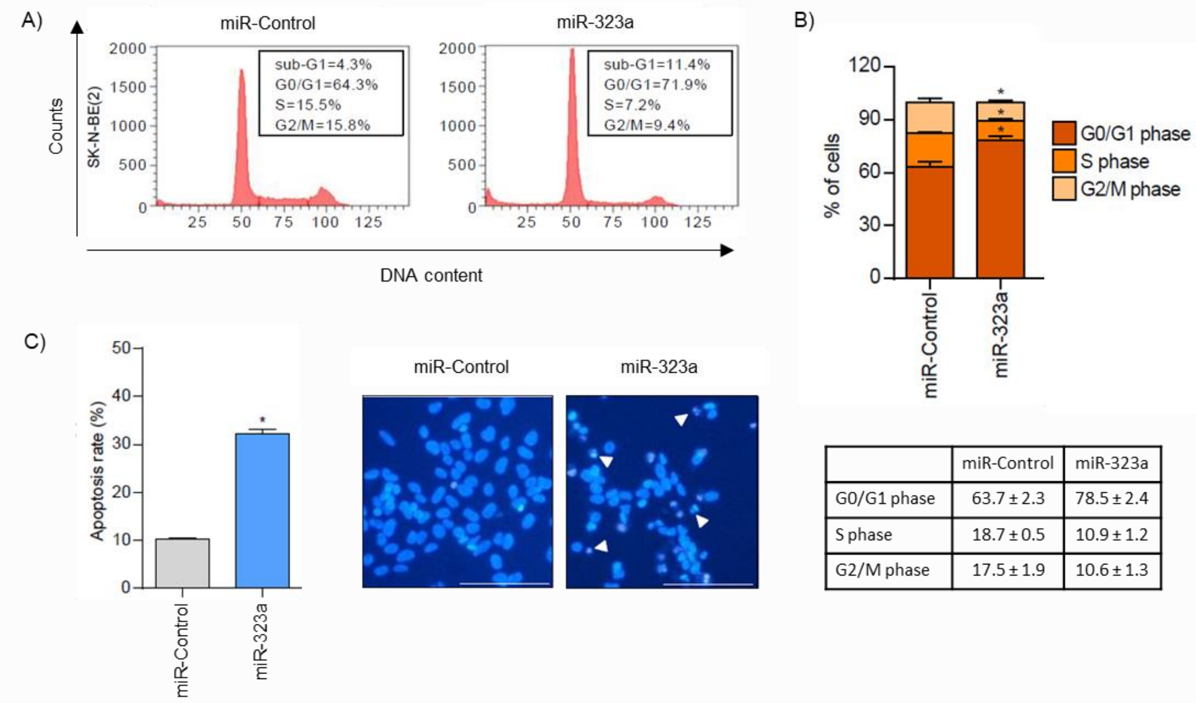

	miR-Control	miR-323a
G0/G1 phase	63.7 ± 2.3	78.5 ± 2.4
S phase	18.7 ± 0.5	10.9 ± 1.2
G2/M phase	17.5 ± 1.9	10.6 ± 1.3

Figure 18. MiR-323a-5p induces cell cycle arrest at G0/G1 phase and apoptosis in SK-N-BE(2) cells. A) Cell cycle low cytometry analysis of the indicated cell lines transfected with miR-control or miR-323a-5p at 25 nM for 96 h. One representative histogram of three independent experiments. **B)** Histograms representing the average percentage of living cell population from three independent experiments of SK-N-BE(2) cells in G0/G1, S, or G2/M phases. **C)** Analysis of chromatin fragmentation/condensation in SK-N-BE(2) transfected with 25 nM of miR-control or miR-323a-5p 96 h post-transfection. Images show a representative field of NB cells stained with Hoechst dye. White arrowheads point to cells with condensed and/or fragmented chromatin. *$p < 0.05$, two-tailed Student's t test.

Therefore, both cell cycle arrest and increased cell death might be contributing to the miR-323a-5p overexpression phenotype (Figure 19A). Concurring with these observations, a reduction in cyclins, D1, E1 and B1 was observed after miR-323a-5p overexpression at 72 h post-transfection and a consequent reduction in phospho-RB levels at later time points (Figure 19A).

Furthermore, upregulation of the cell cycle inhibitor p27 was also observed (Figure 19A). Furthermore, NB cells transfected with miR-323a-5p showed cleavage of the executor caspase-3 and one of its targets α-FODRIN, both indicative of apoptotic cell death (Figure 19B).

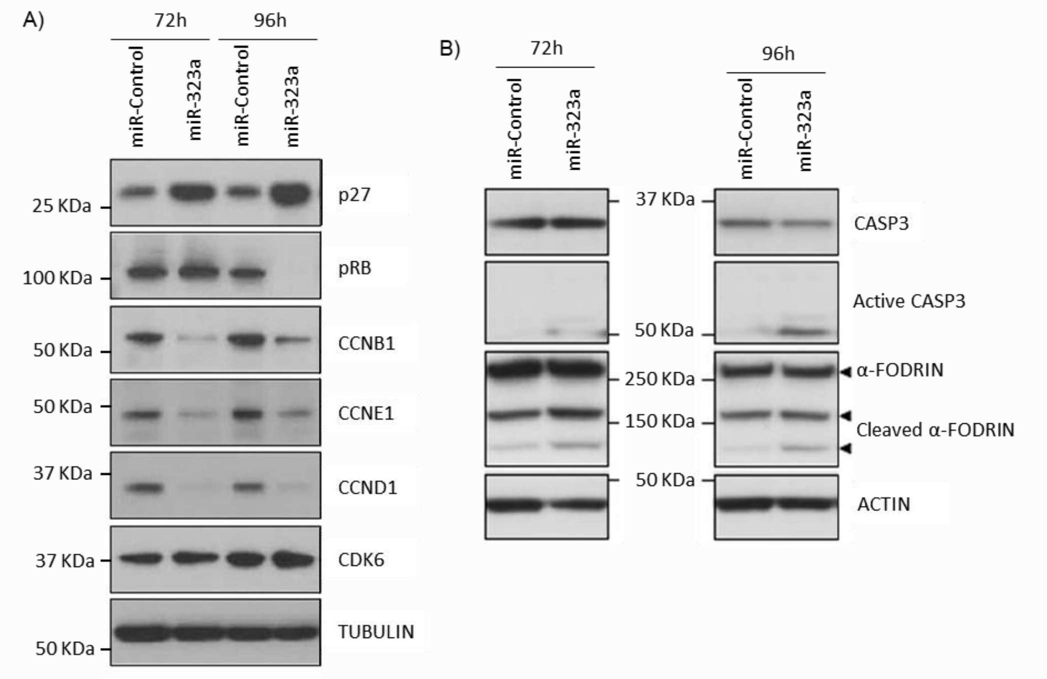
A)
72h
96h
miR-Control
miR-323a
miR-Control
miR-323a
25 KDa
p27
100 KDa
pRB
50 KDa
CCNB1
50 KDa
CCNE1
37 KDa
CCND1
37 KDa
CDK6
50 KDa
TUBULIN
B)
72h
96h
miR-Control
miR-323a
miR-Control
miR-323a
37 KDa
CASP3
Active CASP3
50 KDa
250 KDa
α-FODRIN
150 KDa
Cleaved α-FODRIN
50 KDa
ACTIN

Figure 19. MiR-323a-5p modify multiple target genes involved in cell cycle arrest at G0/G1 phase and apoptosis in SK-N-BE(2) cells. A-B) Western blot of the indicated cell cycle regulatory **(A)** and apoptosis-related proteins **(B)** in SK-N-BE(2) transfected with miR-Control or miR-323a-5p (25 nM) at 72 h and 96 h post-transfection.

4.1.4. MiR-323a-5p target cell cycle and survival genes

To find the downstream mediators of miR-323a-5p phenotypic effects in NB, a miRNA-target analysis was performed comparing five different platforms (Figure 20A). For miR-323a-5p, 905 potential targets were predicted by at least four independent algorithms (Supplementary Tables 4 from Soriano et al.[157]). According to the Kyoto Encyclopedia of Genes and Genomes (KEGG) pathway analysis[167], a significant number of these predicted targets were associated with cell cycle or commonly altered pathways in cancer (Figure 20B, p value < 0.05). These genes were selected for validation based on their expression association with NB outcome and/or previous reported functional role in cancer (Supplementary table 6 from Soriano et al.[157]).

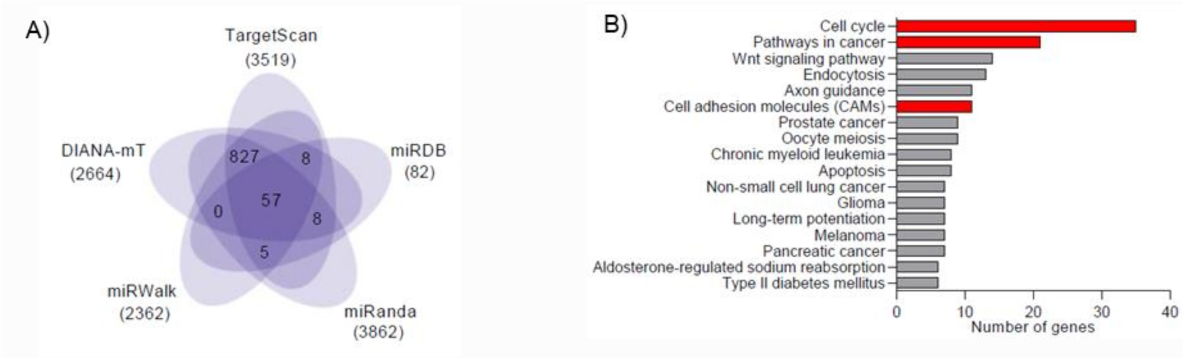

Figure 20. MiR-323a-5p modulate the expression of multiple cancer-related, cell cycle and cell adhesion genes. A) Venn diagram representing the overlap of predicted target genes among five miRNA-target prediction algorithms of miR-323a-5p. **B)** Representation of the functional annotation of predicted target genes of miR-323a-5p using KEGG pathways and Gene Ontology databases. Red bars indicate selected pathways to analyse potential miRNA targets.

Transient miRNA overexpression proved to consistently reduce the mRNA levels of several miR-323a-5p (i.e., *CHAF1A*, *KIF11*, *INCENP*, *CDC25A*, *CCND1*, *FADD* and *E2F2*) (Figure 21A). To confirm the reduction also in protein levels, Western blot was performed at 48 h and 72 h post-transfection of miR-323a-5p. CHAF1A, KIF11, INCENP, CDC25A, CCND1 and FADD protein levels decreased when SK-N-BE(2) cells were transfected with miR-323a-5p (Figure 21B).

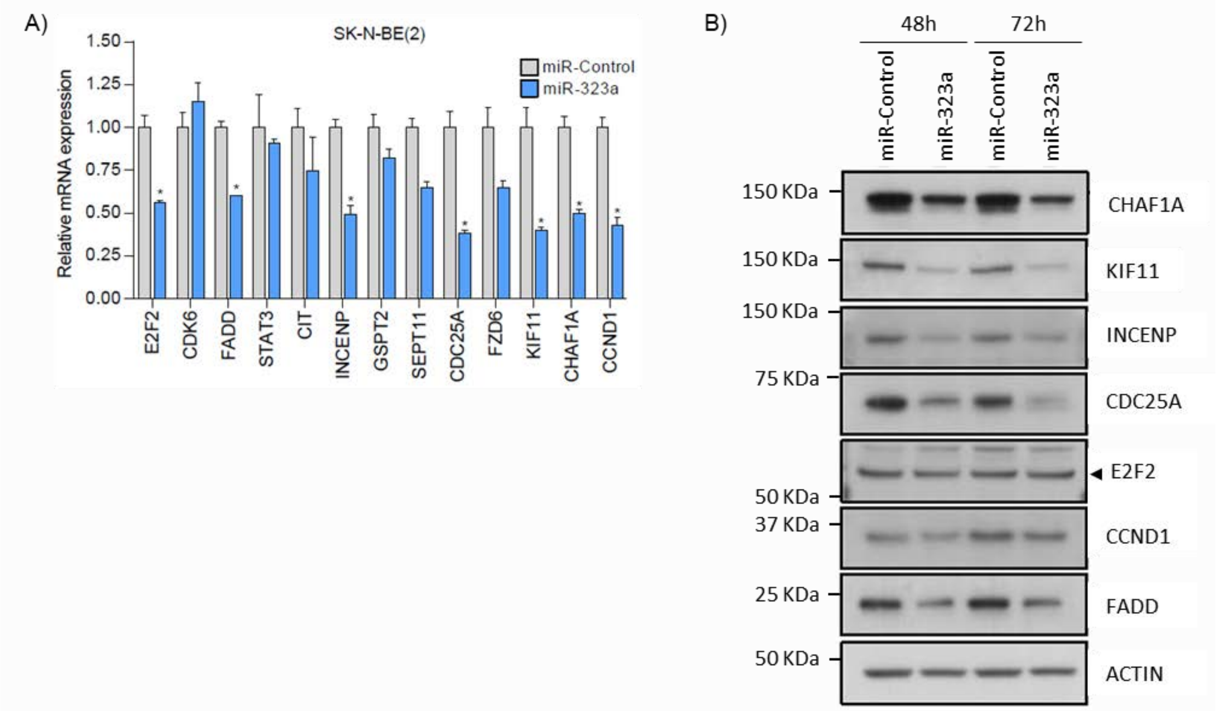

Figure 21. MiR-323a-5p modulate the expression of predicted miR-323a targets genes. A) mRNA relative expression levels of predicted miR-323a target genes in SK-N-BE(2) cells transfected with 25nM of miR-Control or miR-323a analysed by qPCR. **B)** Representative Western blot of predicted target genes in SK-N-BE(2) transfected with miR-Control or miR-323a-5p at 48h or 72 h post-transfection.

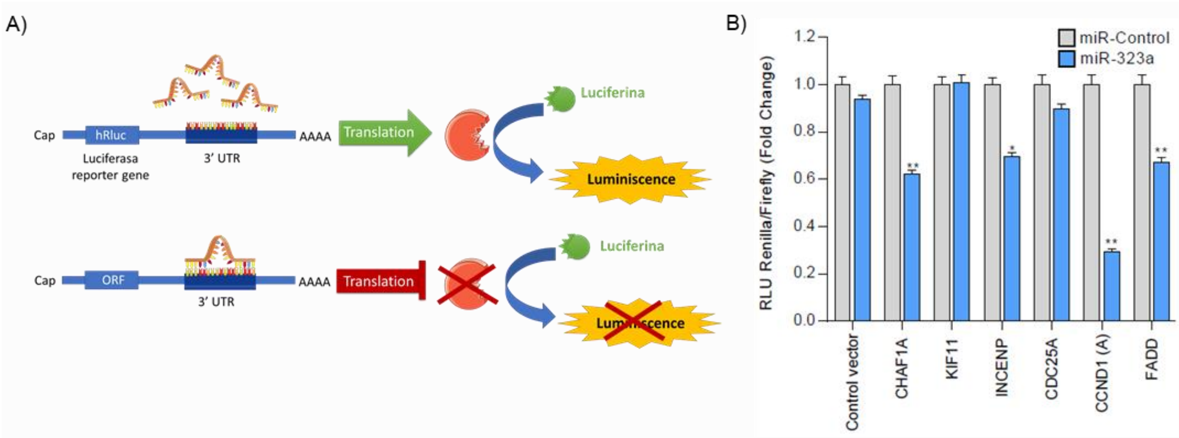

Figure 22. MiR-323a-5p modulate the expression of directed miR-323a targets genes. A) Representative scheme of the luciferase 3'UTR reporter assays in presence or or absence of miR-323a-5p. **B)** Luciferase 3'UTR reporter assays. Graph represents luciferase activity in HEK-293T cells co-transfected with 50 ng/well of the indicated reporter vectors and 25 nM of miR-control or miR-323a-5p. Data represented the average ± SEM of three independent experiments (n = 3 per experiment). $^*p < 0.05$, $^{**}p < 0.01$, $^{***}p < 0.001$.

To ascertain whether the potential targets were regulated directly by miR-323a-5p, we engineered luciferase-reporter vectors with the 3'UTR of genes bearing the putative miRNA-binding sites (Figure 9-Figure 22A). The reporter vectors were co-transfected with a miR-Control or miR-323a-5p and luciferase activity was quantified 24h after transfection. The overexpression of miR-323a-5p caused a reduction in luciferase activity in the CHAF1A, INCENP, CCND1 and FADD 3'UTR reporter vectors and no differences were observed for KIF11 and CDC25A, thereby indicating that these last two genes are not direct targets (Figure 22B).

4.1.5. CCND1, CHAF1A and INCENP silencing mostly reproduces miR-323a-5p overexpression effects

The contribution of each target to the miRNA overexpression phenotype was analysed by siRNA-mediated gene silencing. Silencing of CHAF1A, KIF11 and CCND1 showed a reduction in cell proliferation similar to that induced by miR-323a-5p, while INCENP and FADD silencing only produced a moderate effect (Figure 23A). Western blot analysis 72 h post-transfection confirmed siRNA efficacy (Figure 23B). Overall, CCND1 depletion mirrored the best miR-323a-5p overexpression, not only the general effects on cell proliferation, but also on the reduction in phospho-RB levels and p27 accumulation (Figure 23C). However, when apoptosis induction was analysed, CHAF1A and INCENP were the direct targets that better phenocopied the effects of miR-323a-5p overexpression (Figure 23D). These results suggest that the combination of CCND1, CHAF1A and INCENP inhibition is enough to reproduce the therapeutic effects of miR-323a-5p.

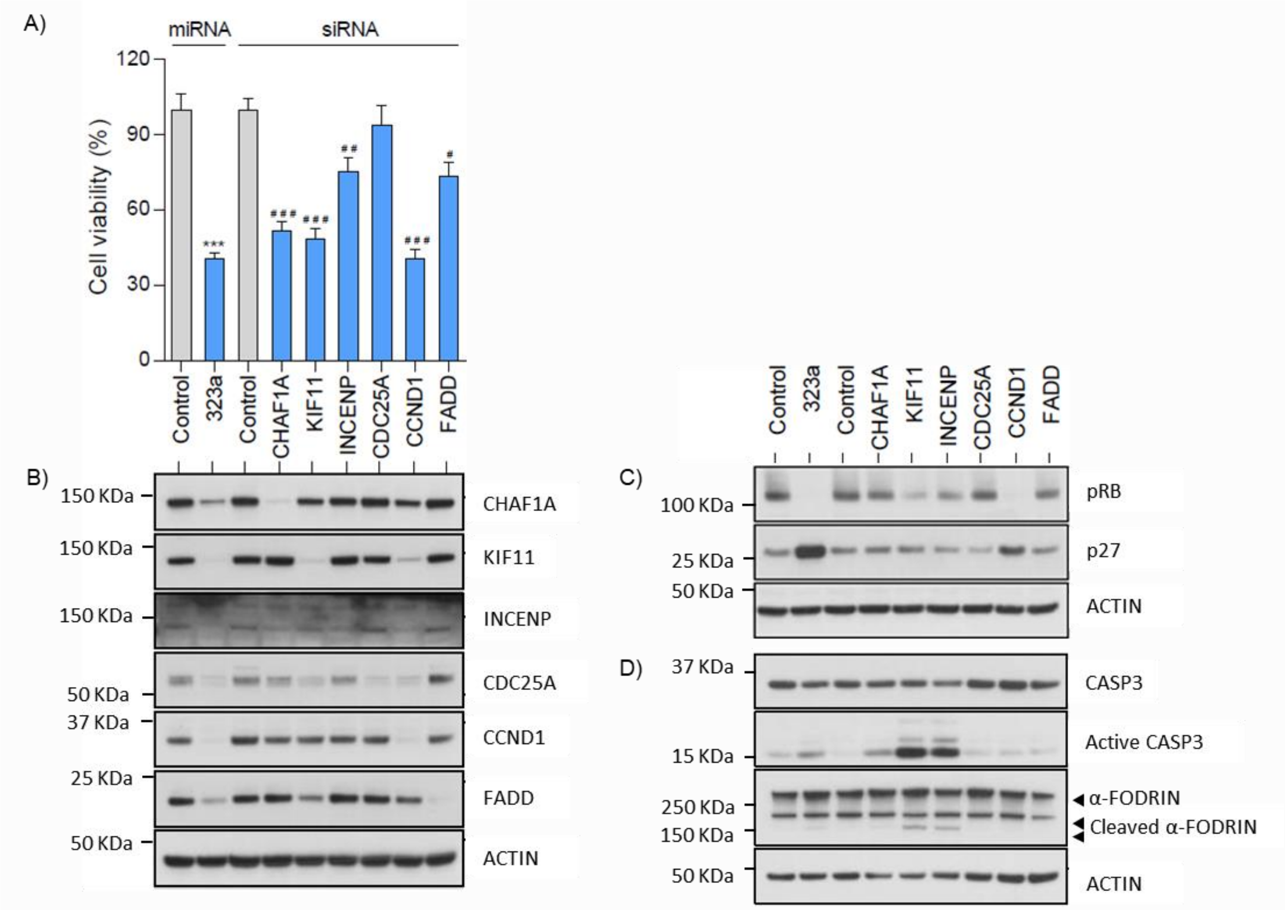

Figure 23. MiRNA target-knockdown partially reproduces the antitumoral effects of miR-323a-5p. A-B) Cell viability assay of SK-N-BE(2) transfected with 25 nM of miR-323a-5p or the indicated siRNA. Target protein knockdown was analysed by Western blot at 72 h post-transfection (lower panels). **C-D)** Expression of some representative cell cycle regulatory proteins **(C)** and apoptosis related-proteins **(D)** in SK-N-BE(2) transfected with miR-323a-5p or the indicated siRNA (25 nM) at 96 h post-transfection. Graph represents one of three independent experiments (n = 6 per experiment). Asterisk compares miR-323a-5p versus miR-Control and hash compares each siRNA versus control siRNA. * or #p < 0.05, ** or ##p < 0.01, *** or ###p < 0.001, two-tailed Student's t test.

Summary and perspectives:

In this chapter, several miRNA with tumour-suppressive functions have been identified. Among them, miR-323a-5p was one with the highest therapeutic potential in NB cell lines. However, the clinical administration of miRNA still presents several challenges owing to the short half-life, poor cellular penetration and rapid clearance. Our main goal is to solve some of these challenges with the conjugation of miRNAs with nanovesicles, which must translate our findings to patients benefit.

4.2. Quatsomes are good nanocarriers for the delivery of small RNAs

In order to use miRNA for clinical applications, their conjugation with a nanocarrier that is able to load, carry and release the miRNA is required. For this reason, the aim of this chapter is to develop a new Quatsome-based nanocarrier for sRNA delivery *in vitro* and *in vivo*.

New designed Quatsomes for miRNA transfection *in vitro*

4.2.1. Selection of the Quatsomes as small RNA nanocarriers

In bibliography is reported that cationic nanovesicles are efficient nanocarriers to load nucleic acids and to ensure their cellular uptake and their release into cytosol. Quatsomes (QS) are a new class of nanocarriers formed by the spontaneous self-assembly of quaternary ammonium surfactants (e.g. MKC or cetyltrimethylammonium bromide (CTAB)) and sterols (e.g. Cholesterol (Chol) and cholesterol derivatives, such as Chems) (Figure 24A-B). Previous results demonstrated that the self-assembly of Chol and CTAB molecules in aqueous medium forms closed bilayers. The positive polar head of the quaternary surfactant are approximately a half of these molecules in the inner and other half outside the bilayer. This conformation ensures a half of positive charges from the quaternary ammonium surfactant accessible outside the lipid membrane[171], which may entrap and load nucleic acids in their surface by electrostatic interactions (Figure 24C). One of the most commonly used surfactants for QS preparation is CTAB[171]. However, the presence of this molecule in our QS for clinical applications may not be suitable, since CTAB has been shown to have teratogenic effects in mice after intravenously administration[180,181]. In this thesis, different formulations of QS were prepared with the objective to use them to deliver small RNA *in vitro* and *in vivo*. To achieve the best formulation for sRNA delivery is necessary the preparation of a biocompatible nanocarrier for *in vivo* administration, capable to bind with sRNA[96].Therefore, in this thesis, the surfactant used for QS preparation was MKC, which is approved by FDA for other uses in animals and is part of another approved surfactant called Benzalkonium chloride (BAK) (EMA/352187/2012). MKC possess an amphiphilic character because is composed by a polar hydrophilic head and a long hydrophobic tail that in aqueous solution tend to associate by non-covalent interactions forming micelles[175]. This self-assembly capacity allows vesicle formation after interaction with sterols. Furthermore, MKC confers to vesicles a positive surface charge, that will allow the sRNA complexation through electrostatic interactions (Figure 24C).

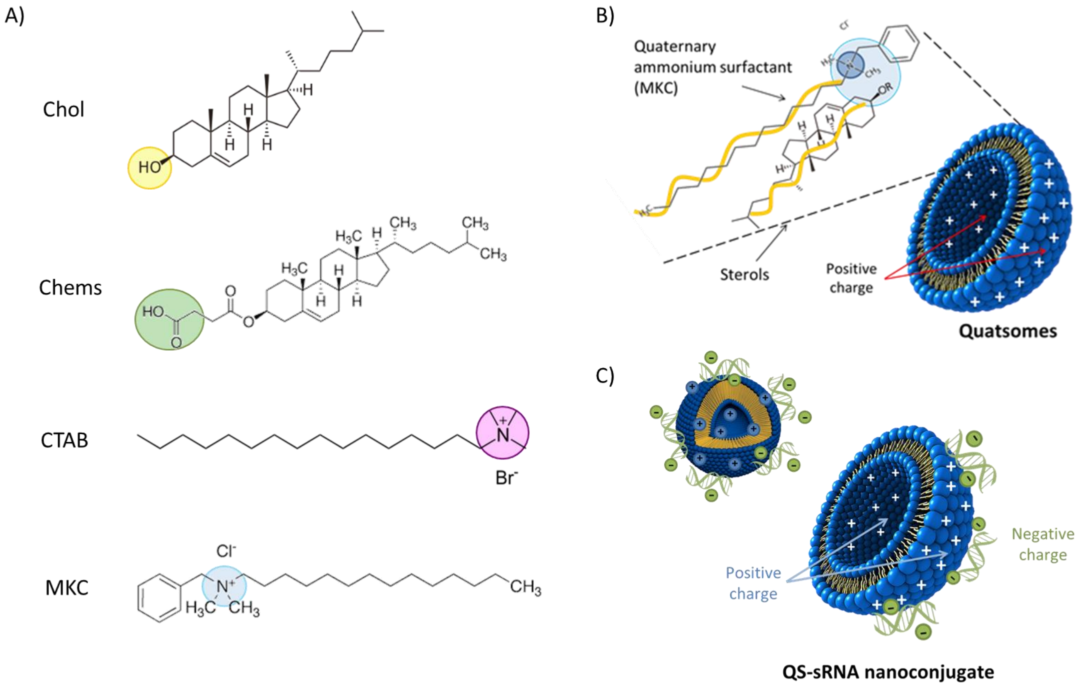

Figure 24. Representation of Quatsomes (QS) structure and their membrane components. A) Molecular structures of some surfactants and sterol derivatives, which could form QS nanovesicles. **B)** Schematic representation of QS formed by self-assembly of surfactants and sterols. **C)** Schematic representation of QS-miRNA complexes produced by electrostatic interactions between positive charges of the surfactant loacted outside QS membrane and the negative charge from miRNA backbone.

On the other hand, cholesterol, or their derivatives, were the sterols used for QS formation. Chol present a hydroxyl group in a hydrophobic structure, while Chems is a sterol derivative in which the hydroxyl group of the cholesterol has been esterified with succinic acid (Figure 24A). Chems molecular structure presents an ionizable anionic group that may be deprotonated in neutral or basic pH (pKa=5.8) and hydrated to adopt a lamellar membrane organization at acid pH[182]. The pH-sensitive cholesterol derivative, Chems, was used to neutralize part of the positive charge of MKC and to try to stablish weaker interactions with nucleic acids due to the electrostatic repulsion between negative charges from Chems and from nucleic acids, without compromising the sRNA complexation and ensuring the cargo release. The charge neutralization may prevent the high cellular toxicity observed in positively-charged nanocarriers[183]. Moreover, the negative charge adopted by Chems in neutral pH, might help to control sRNA release from QS membrane by electrostatic repulsion[182,183].

The methodology used for QS preparation was based on the compressed CO_2 technology, called DELOS-SUSP (US20150182590A1)[138]. After one week of stabilization, samples with translucent macroscopical appearance were physic-chemically characterised following the protocols described in the experimental section 63.

Nanovesicles particle size distribution was measured by DLS, nanovesicles morphology (unilamellar vesicles) and the presence of other colloidal structures was directly observed by cryo-TEM microscopy and membrane components concentration was determined by lyophilisation of the nanovesicular system and further gravimetric analysis. Then, samples with commonly physicochemical properties of small unilamellar vesicles (D_h< 100 nm and spherical and unilamellar morphology) were purified by diafiltration, in order to eliminate the ethanol and the non-incorporated surfactant and sterol molecules, and, if required, were concentrated by diafiltration, and characterised again (Figure 25).

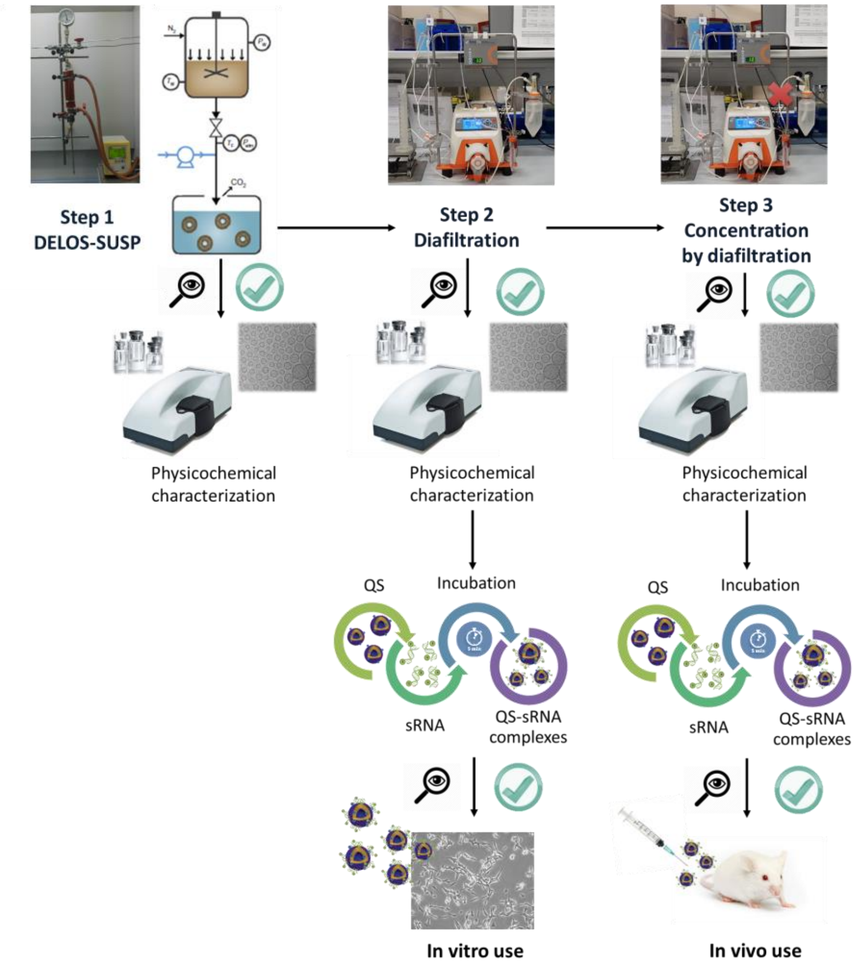
Step 1
DELOS-SUSP
Step 2
Diafiltration
Step 3
Concentration by diafiltration
Physicochemical characterization
Physicochemical characterization
Physicochemical characterization
QS
Incubation
sRNA
QS-sRNA complexes
QS
Incubation
sRNA
QS-sRNA complexes
In vitro use
In vivo use

Figure 25. Schematic representation of the steps done for QS samples preparation, diafiltration and concentration. Samples prepared in each step, 1st DELOS-SUSP production, 2nd diafiltration and 3rd concentration, were evaluated by their macroscopically appearance after one week of stabilization. If they did not precipitate, nanovesicles size distribution, morphology and membrane components concentration were characterized before their sRNA complexation and their *in vitro* or *in vivo* use.

In order to select the best formulation to deliver sRNA with longest stability over time, two systems of QS formulations were produced by DELOS-SUSP: Chol:MKC and Chems:MKC at 1:1 molar ratio between the sterol and the surfactant (Table 11). Two different strategies were followed to form nanovesicles by DELOS-SUSP methodology (see experimental part 3.2.10.1).

First, Chol was added in the organic phase and MKC in the aqueous solution. Alternatively, in a second strategy, both Chol and MKC were added in the organic phase. We observed that, following both strategies, stable QS based on Chol and MKC components could not be produced at 1:1 molar ratio, by DELOS-SUSP, since undesired precipitates, were always observed in the final colloidal dispersion (Figure 26A-B). To determine whether Chol:MKC (1:1) nanovesicles could be prepared using a different methodology, both components were diluted in an aqueous solution with 10% EtOH and, then, sonicated (Table 13). Ultrasounds allowed the formation of colloidal systems (Figure 26C) composed, as observed by cryo-TEM, by polydisperse nanostructures, in size (between 100 nm to more than 1 µm) and in shape, including oval, spherical and long spheres (Figure 26E). Nevertheless, when the ultrasounds were applied to a mixture of membrane components diluted separately, the Chol in the organic phase and the MKC in the aqueous solution, nanovesicles cannot be produced and samples precipitated (Figure 26D).

On the other hand, a colloidal stable solution was obtained after the preparation of Chems:MKC (QS_0) nanovesicles at 1:1 molar ratio by the DELOS-SUSP technology (Figure 26F; Table 11). Moreover, Chems:MKC nanovesicles at molar ratio 1:0.75 were prepared to compare physicochemical properties and stability over time with nanovesicles at molar ratio 1:1 (Figure 26G; Figure A1; Table 11). The morphology of Chems:MKC nanovesicles was analyzed by Cryo-TEM. Images showed that only small unilamellar vesicles (SUV) were formed, which indicates that QS_0 were formed with the Chems:MKC systems at molar ratios 1:0.75 and 1:1 (Figure 26H).

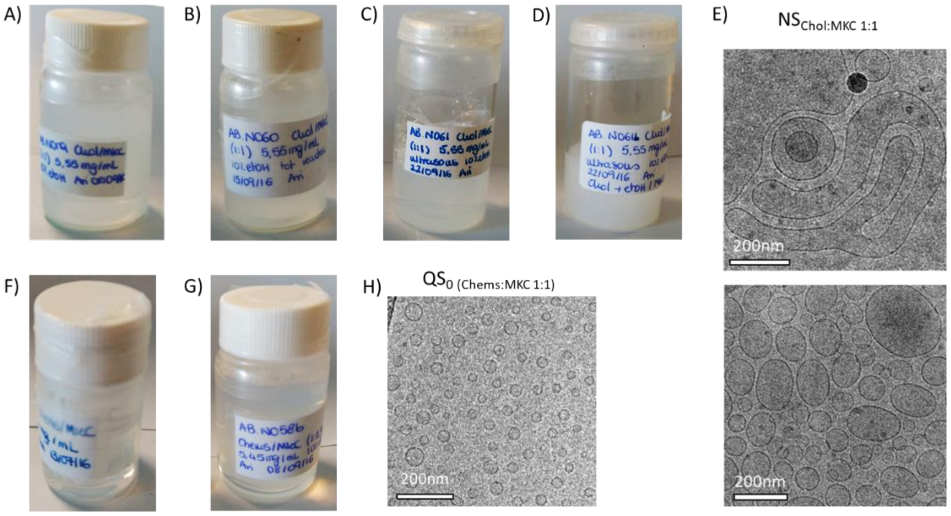

Figure 26. Representative images of vials showing the macroscopic appearance of Chol:MKC and Chems:MKC systems. Samples prepared using a 1:1 Chol:MKC molar ratio **(A-D),** by DELOS-SUSP technology **(A-B)** or by using ultrasounds **(C-D).** Representative cryo-TEM images of the nanostructures (NS) morphology prepared by sonication using a 1:1 Chol:MKC molar ratio **(E).** Samples prepared by DELOS-SUSP using a 1:1 Chems:MKC molar ratio **(F)** and a Chems:MKC 1:0.75 molar ratio **(G).** Representative cryo-TEM images of the morphology of QS_0 prepared by DELOS-SUSP using a a 1:1 Chems:MKC molar ratio **(H).**

After one week of stabilization at RT, QS_0 systems were purified by diafiltration (see experimental part 3.2.10.4) to remove the ethanol and the non-incorporated components such as sterols or surfactants. The QS_0 formulations using a 1:1 Chems:MKC molar ratio were prepared, at least three times to check the reproducibility among batches. QS_0 prepared by using the two different molar ratios were physicochemically characterised after one week of their preparation by DELOS-SUSP and their diafiltration. DLS measurements and cryo-TEM microscopy show that the colloidal samples QS_0 were composed by small nanovesicles (D_h ~ 50-60 nm) and measurement of Z-potential indicated, as expected, that the nanovesicle had a positive charge (ζ-potential ~ 50mV) (Figure 27A-B). Particle size distribution of QS_0 nanovesicles prepared by using the two different molar ratios of Chems:MKC is similar, but slightly polydisperse for the 1:0.75 ratio (Figure 27C). In the cryo-TEM images of Figure 27D could be observed that QS_0 samples prepared at both molar ratios of Chems:MKC are composed by spherical and unilamellar nanovesicles.

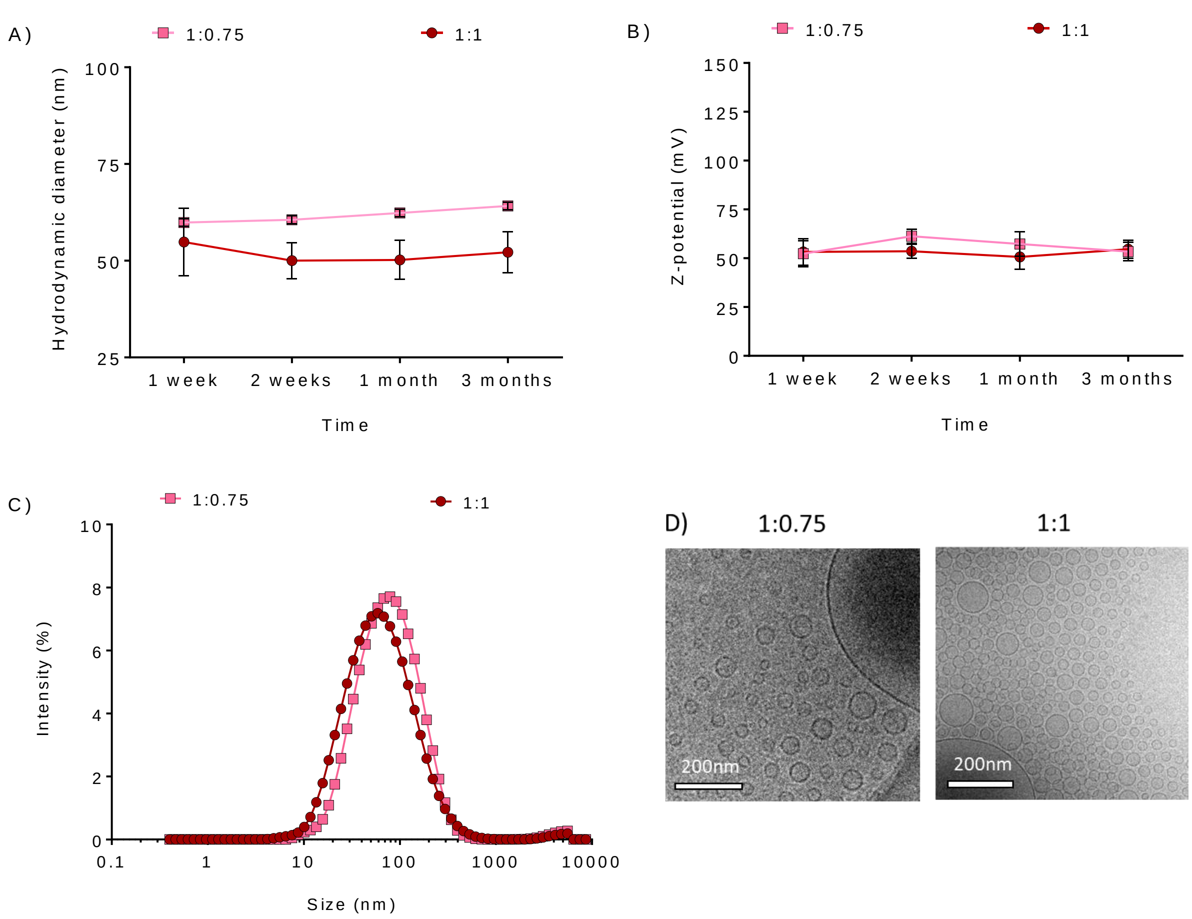

Figure 27. QS_0 systems produced at molar ratios 1:0.75 and 1:1 of Chems:MKC diafiltrated. (A-B) Evolution of the hydrodynamic diameter and Z-potential of QS_0 at different times after their preparation. Each point of the graphs represents the average of three different preparations ± SD. **C)** Particle size distribution measured by DLS of QS_0. Each curve is the average of at least two duplicate experiments. **D)** Representative cryo-TEM images of the morphology of QS_0.

Finally, the concentration of QS membrane components (surfactant plus sterol) in the QS_0 formulations was measured by lyophilizing known volumes of QS_0 and after weighting the dry solids obtained. From these measurements were also calculated the partial yields after each preparation process step and the final yield of QS preparation (sum of yields of each process) (see Table 14; Figure 28). To determine the final yield of QS_0 preparation (step 1; Figure 25) and purification (step 2; Figure 25), it was measured the loss of mass at each process preparation step of QS_0 and then both are considered (see section 3.2.11.3). In both preparations of QS_0, using the two different Chems:MKC molar ratios, it was observed a reduction in of membrane components weight of ~20% during the preparation of nanovesicles by DELOS-SUSP. This lost of material was slightly smaller when using the 1:1 Chems:MKC molar ratio (Figure 28).

On the other hand, after diafiltration the losses of material were similar (~20%), thereby the final yield of QS_0 were ~ 60-65%, which corresponded to a loss of ~35-40% of material (Figure 28). Considering all these characterizations, QS_0 prepared at 1:1 molar ratio was selected for further experiments owing to their unilamellar morphology, spherical shape, smaller size, smaller polydispersity, similar charge and better efficiency of preparation compared to QS_0 at 1:0.75 molar ratio.

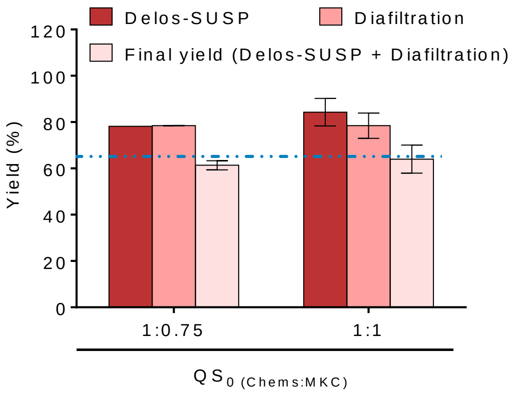

Figure 28. Yields of the preparation of QS_0 using initial molar ratios of Chems:MKC of 1:0.75 and 1:1. Graph columns represent the yield obtained after each process preparation step: after DELOS-SUSP preparation (step 1; Figure 25), after diafiltration (step 2; Figure 25). The column of the final yield represents the sum of the partial yields obtained after DELOS-SUSP and diafiltration, which indicates the yield of QS_0 obtainance. Each column in the graph represents the average of at least triplicate measurements ± SD.

Preliminary results of Chol:CTAB QS demonstrated that for QS bilayer performance a equimolar composition between sterol:surfactant, are required[171]. In consequence, in this thesis QS were prepared at this 1:1 molar ratio reproducing the previous standard QS conditions. However, considering that Chol:MKC nanovesicles at molar ratio 1:1 were impossible to be prepared, different molar ratios were tested. In particular, the same amount of Chol was used for all formulations, but increasing MKC amounts were used to prepare Chol:MKC QS by DELOS-SUSP.

The generation of QS based on Chol and MKC, named QS_1, was attempted using the initial molar ratios of 1:1.5, 1:2 and 1:3 (Table 11). In all cases, stable formulations were produced and it was not observed the formation of any precipitate after one week of stabilization (Figure 29).

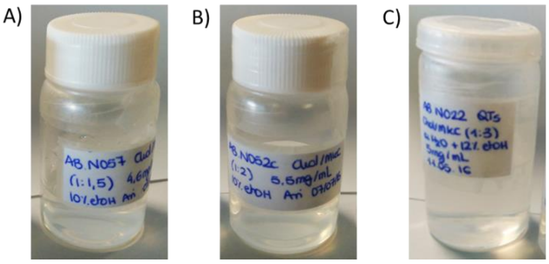

Figure 29. Macroscopic images of the vials containing Chol:MKC-based QS_1 produced by DELOS-SUSP. Representative images of samples of QS_1 produced by DELOS-sups using Chol:MKC molar ratios of 1:1.5 **(A),** 1:2 **(B)** and 1:3 **(C).**

After one week of stabilization, all these systems were diafiltrated and characterized by DLS, gravimetrical yield and cryo-TEM following the above-indicated protocols (section 3.2.11). Next, we compared QS_1 prepared at different molar ratios by DELOS-SUSP, with those prepared by sonication. Nanostructures prepared by sonication presented a larger hydrodynamic diameter (D_h > 80 nm) and polydispersity, compared with QS_1 prepared by DELOS-SUSP (Figure A2A and A2C). The surface charge density of these vesicles was higher for QS_1 prepared using molar ratios 1:2 and 1:3, probably due to the higher surfactant concentration in the membrane of QS_1 (Figure A2B). After one week of stabilization, purified samples were characterised by DLS and cryo-TEM. They presented a small size (D_h ~ 60-100 nm) and were less stable over time, especially those systems with molar ratio 1:1 and 1:1.5 (Figure 30A). On the contrary, the surface charge density was slightly reduced to ~ 70-80mV owing the loss of non-incorporated material (Figure 30B). Observing the particle size distributions of these samples, QS_1 produced by using initial molar ratio 1:3 seemed the most homogenous in size (Figure 30C). Cryo-TEM images confirmed that the nanostructures formed at molar ratio 1:1 were larger (> 100 nm) than QS_1 prepared by DELOS-SUSP at the molar ratios 1:2 and 1:3 (Figure 30D). Moreover, among QS_1, the one prepared at molar ratio 1:3 were the most homogeneous in size and shape, because by cryo-TEM the only spherical and unilamellar vesicles were observed.

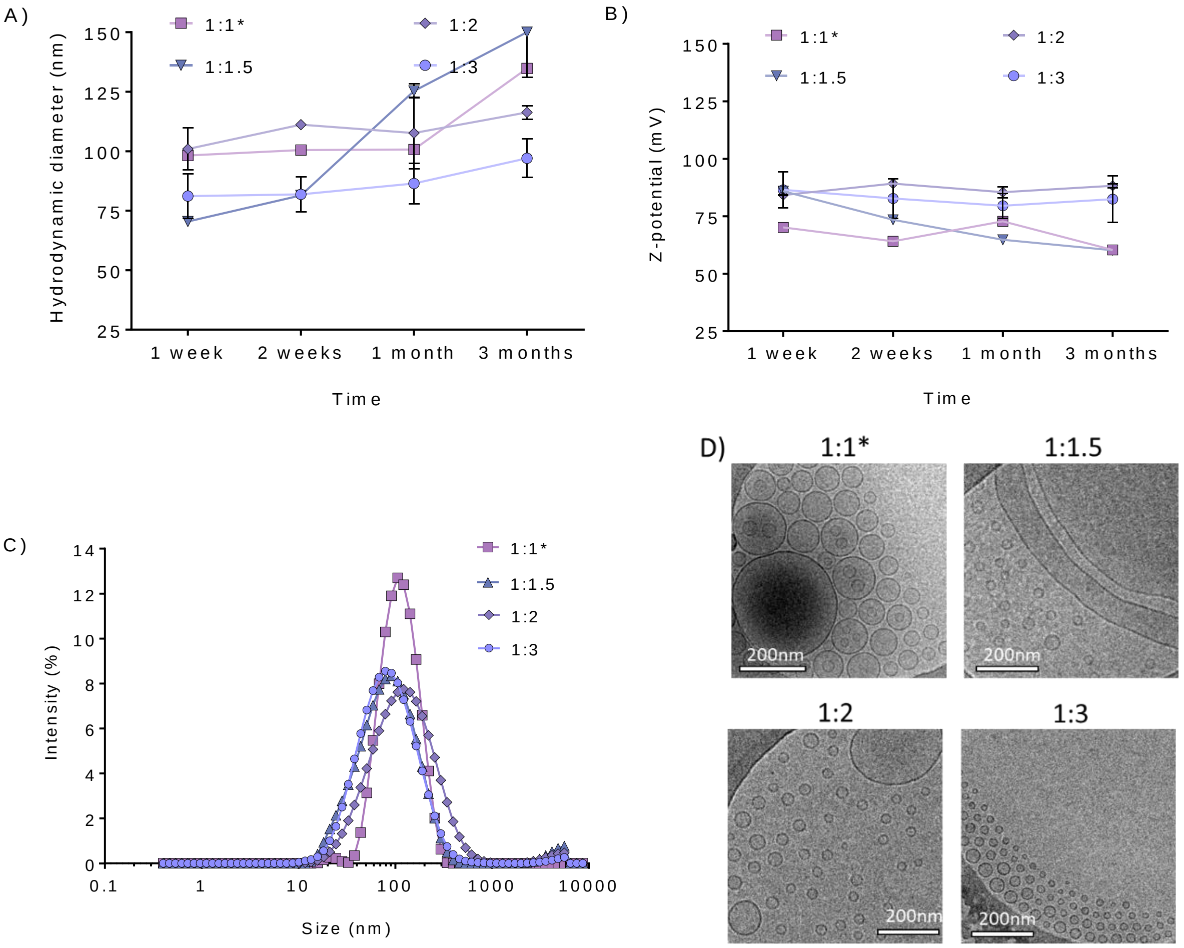

Figure 30.Comparison of the physicochemical properties of diafiltered QS_1, produced by DELOS-SUSP using initial molar ratios of Chol:MKC of 1:1.5, 1:2 and 1:3, and the nanostructures produced by sonication using a molar ratio of Chol:MKC of 1:1. Evolution of the hydrodynamic diameter over time **(A)** and Z-potential **(B).** Graph points represents the mean of triplicate samples ± SD. **C)** Particle size distributions measured by DLS after one week of QS_1 diafiltration. Each curve is the mean of at least three triplicate experiments. **D)** Representative cryo-TEM images of QS_1 nanovesicles. *Nanostructures composed by Chol:MKC at molar ratio 1:1 prepared by sonication, not by DELOS-SUSP.

Finally, the gravimetrical yield of these systems was analysed. The preparation yield of the different systems of QS_1 is nearly 95-100%, which means that there was not loss of material during vesicles preparation. On the contrary, during the diafiltration, there was a significant loss of material, reducing the yield to ~ 40-65% (Figure 31;Table 14). Lastly, the final yield was determined considering the yield after QS preparation by DELOS-SUSP or sonication and after diafiltration. These results indicated that the loses of material was increased in directly proportional manner with the MKC amounts used for QS_1 preparation. Thereby, despite QS_1 were prepared at higher molar ratios of sterol:surfactant due to the increasing amounts of MKC surfactant, the final amount of MKC surfactant incorporated into QS membrane was always the same.

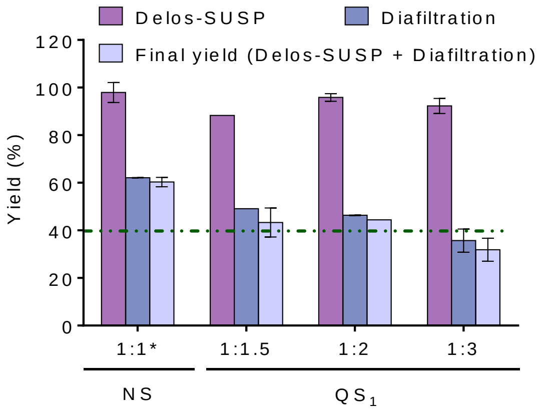

Figure 31. Comparison of the yields of each process and the final yield (DELOS-SUSP or sonication and diafiltration) developed for QS$_1$ systems at molar ratios 1:1.5, 1:2 and 1:3, between the sterol and the surfactant, and the nanostructures produced by sonication. Graph representing the yield of each process developed for the various QS$_1$ systems after preparation or purification and the sum of these partial yields, called final yield. Bars were the mean of at least triplicate measures ± SD. *Nanostructures composed by Chol:MKC at molar ratio 1:1 prepared by sonication, not by DELOS-SUSP. Results are reported at Table 14.

Considering the physicochemical properties of these QS, QS$_0$ composed by Chems:MKC at 1:1 molar ratio and QS$_1$ composed by Chol:MKC at 1:3 molar ratio, were selected for the following experiments.

Preparation of QS with appropriate physicochemical properties for clinical administration

A good nanocarrier for clinical administration requires the possibility to be produced at high concentrations or to be easily scaled-up. In this thesis, the desired miRNA concentration (2mg/kg) to inject in mice for the high-risk NB tumours treatment determines the concentration of QS required to deliver it. This is explained because QS-miRNA complexes are formed by electrostatic interactions, which depend on the relation between the negative charges of miRNA backbone (approximately forty per miRNA molecule) and only the half of the positive charges from MKC surfactant that located outside QS membrane. The MKC minimal concentration in QS was calculated to ensure the entrapment of all miRNA molecules and to test different loadings of miRNA into QS able to modify miRNA target genes. Considering that QS-miRNA complexes should be administrated intravenously, the injected volume in mice must be ~ 100 µL to do not compromise mice safety. Hence, the QS concentration to achieve was 8X for QS$_0$ or 10X for QS$_1$ the purified concentration obtained in these samples. Therefore, concentrated QS were obtained following two different strategies. The first one was based on the preparation of more concentrated QS directly by the DELOS-SUSP technology and the second one was to prepare less concentrated QS by DELOS-SUSP (Table 11), which were further concentrated by diafiltration (see experimental part 3.2.10.5). In the first approach, there were fixed parameters of DELOS-SUSP process that cannot be modified, such as the molar fraction of CO_2 in the reactor, the volume of EtOH and the temperature. On the other hand, three parameters might be variable, which are the volume of water and the concentration of each membrane components (sterol and surfactant). Therefore, QS_1 were prepared reducing the aqueous phase and increasing the concentration of membrane components without compromising the cholesterol or MKC solubility (< 32.5 mg/mL in etOH at 37°C or 50 mg/mL in water, respectively) and the critical micellar concentration of the MKC surfactant in water (> 2.2 mM). Taking into account these conditions, QS_1 nanovesicles were prepared in a range of final membrane components concentrations between 3.6 to 22.4 mg/mL. Highly-concentrated samples precipitated after one week of stabilisation (Figure 32A; vials on the left side of the image). QS_1 characterised by DLS demonstrated that nanovesicles of Chol:MKC at 1:3 molar ratio could not be prepared or measured at higher concentrations of 7.5 mg/mL, because samples were precipitated (Figure 32A) or presented too much polidispersity to be measured by DLS (e.g. QS_1 formed at 10 mg/mL, Figure 32B-C). Samples prepared at 10 mg/mL yielded three populations of vesicles with different hydrodynamic diameters around 50 nm, 150nm and larger than 1000nm. On the other hand, samples prepared with membrane components concentrations ranging from 3.6 to 7.5 mg/mL showed a vesicle population with a medium hydrodynamic diameter between ~ 40-100nm, which could be easily reproduced between batches and require to be concentrated by diafiltration to achieve the desired concentration (Figure 32C).

QS_1 with good macroscopical appearance were diafiltrated, following the procedure described in the materials and methods section 3.2.10.4, after one week of stabilization and then concentrated to reach the final desired concentration of membrane components (see section 3.2.10.5). Nanovesicle size distribution, measured by DLS analysis, did not show relevant variations in size, thereby suggesting that the physicochemical properties of QS are not altered during diafiltration or concentration processes (Figure 32D-F). Of note, concentrated samples presented, in addition to the D_h ~ 100 nm population, a smaller population (D_h ~ 20-30 nm), which may be originated owing to the membrane extrusion of QS vesicles after the application of high pressure produced during the concentration process (Figure 32F).

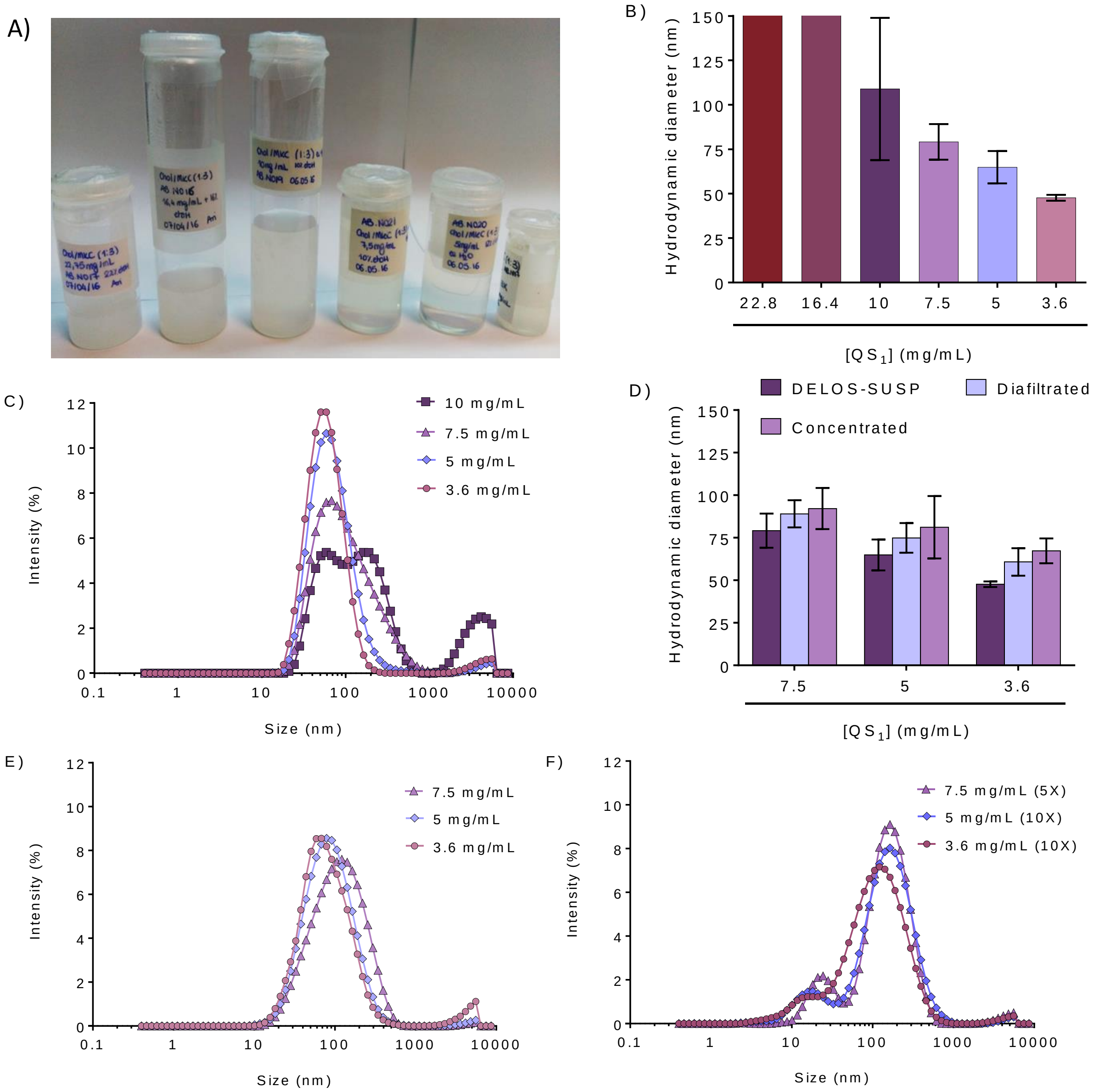

Figure 32. QS prepared at high concentrations presented different physicochemical properties and macroscopical appearance. A) Macroscopical appearance of vesicles composed by Chol:MKC at molar ratio 1:3 prepared by DELOS-SUSP. Samples prepared at higher concentrations than 10 mg/mL precipitated. **B)** Hydrodynamic diameter of QS$_1$ prepared at different concentrations. **C)** Particle size distributions measured by DLS of QS$_1$ prepared by DELOS-SUSP at different concentrations, from 3.6 to 10 mg/mL. **D)** Comparison among the hydrodynamic diameters of QS$_1$ prepared by DELOS-SUSP, diafiltrated and concentrated systems. **E-F)** Particle size distributions measured by DLS of QS$_1$ diafiltrated **(E)** and concentrated X times by diafiltration **(F)** from the systems prepared at indicated different initial concentrations. All graphs or curves represented the mean of triplicate samples ± SD.

In order to select for *in vitro* experiments the formulation with SUVs morphology, higher homogeneity and higher stability over time, the polydispersity and morphology of these samples was analysed (Figure 33A-D). QS$_1$ prepared using an initial 7.5mg/mL concentration of membrane components, presented higher polidispersity (Table A1 from Annex) and bigger vesicles size compared to samples prepared less concentrated (Figure 33A).

On the other hand, QS₁ prepared at 3.6 mg/mL required to be concentrated more than 10 times to achieve a similar final concentration than concentrated samples starting at 5 mg/mL (Figure 33B-C). Regarding the morphology, all QS₁ concentrated systems observed by cryo-TEM showed small unilamellar vesicles (SUV). QS₁ concentrated systems prepared at initial concentration of 7.5 mg/mL presented larger vesicles with hydrodynamic diameters more than 100 nm compared to QS₁ concentrated from 5 or 3.6 mg/mL, which were much smaller than 200 nm (Figure 33D).

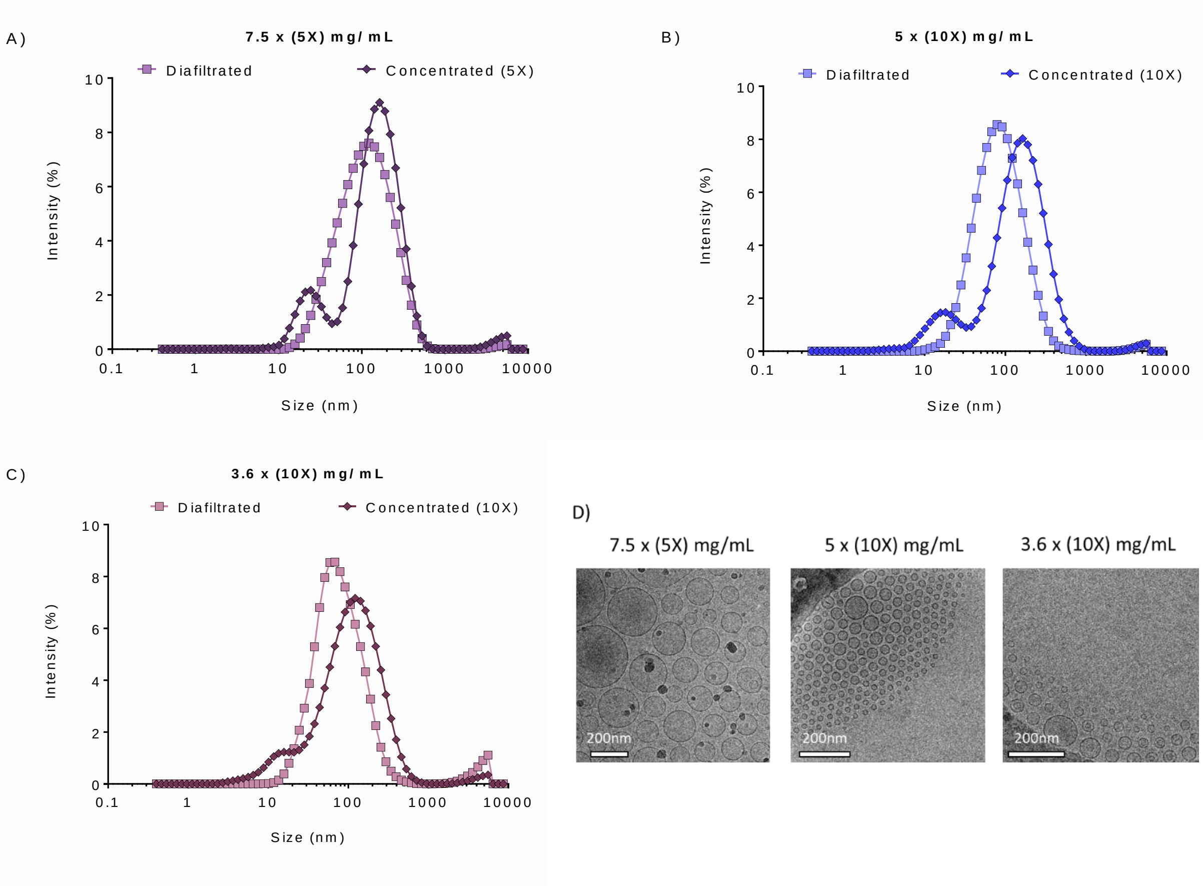

Figure 33. Comparison of the polidispersity and the morphology of QS₁ prepared at different starting concentrations (7.5, 5 and 3.6 mg/mL) and then concentrated by diafiltration (5X or 10X). A-C) Comparison of the particle size distributions measured by DLS after QS₁ diafiltration and concentration. Each curve are the mean of duplicate experiments. **D)** Representative cryo-TEM images of the different QS₁ concentrated systems demonstrated similar size and morphology than diafiltrated QS₁.

The hydrodynamic diameter and the Z-potential of the different QS₁ were also evaluated over time (Figure 34; Figure A3). On the diafiltrated and concentrated samples, a tendency in size increasing was observed after 1 month of purification (starting from D_h ~ 60-80nm and reaching D_h ~ 80-100nm) (Figure 34A and C). However, the three QS₁ prepared at different starting concentrations presented a similar behaviour. The Z-potential of purified and concentrated samples (Figure 34B and Figure 34D, respectively) were slightly lower than after DELOS-SUSP preparation (Figure A3B), owing to the loss of material during the diafiltration process but remained stable over time.

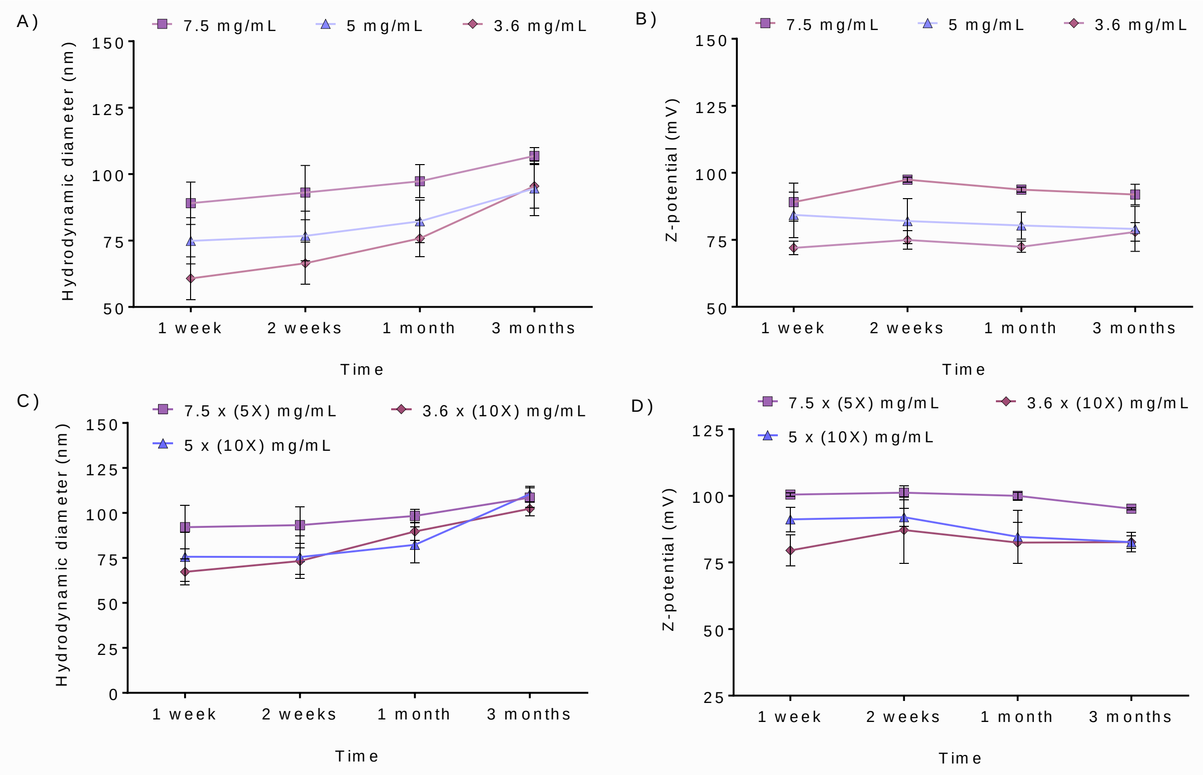

Figure 34. Physicochemical properties (hydrodynamic diameter and Z-potential) of QS$_1$ at diferent membrane components concentrations over time. Measurements were done after diafiltration **(A-B)** and after concentration **(C-D).** Graph represents the mean of at least triplicate samples ± SD.

Similar analyses were performed for QS$_0$, which are composed by the cholesterol derivative Chems, and the MKC surfactant. After diafiltration and concentration, samples maintained their size D$_h$ ~ 50-100nm, slightly increased in polydispersity after concentration and had a ζ-potential ~ 50mV of surface charge (Figure 35A-C). However, after concentration, QS$_0$ seemed larger (Figure 35A) and slightly polydisperse (Figure 35C; Table A2 from Annex) after DLS measurements, but by cryo-TEM images QS$_0$ were observed as SUVs with a similar spherical shape and small size (D$_h$ < 200nM, Figure 35D).

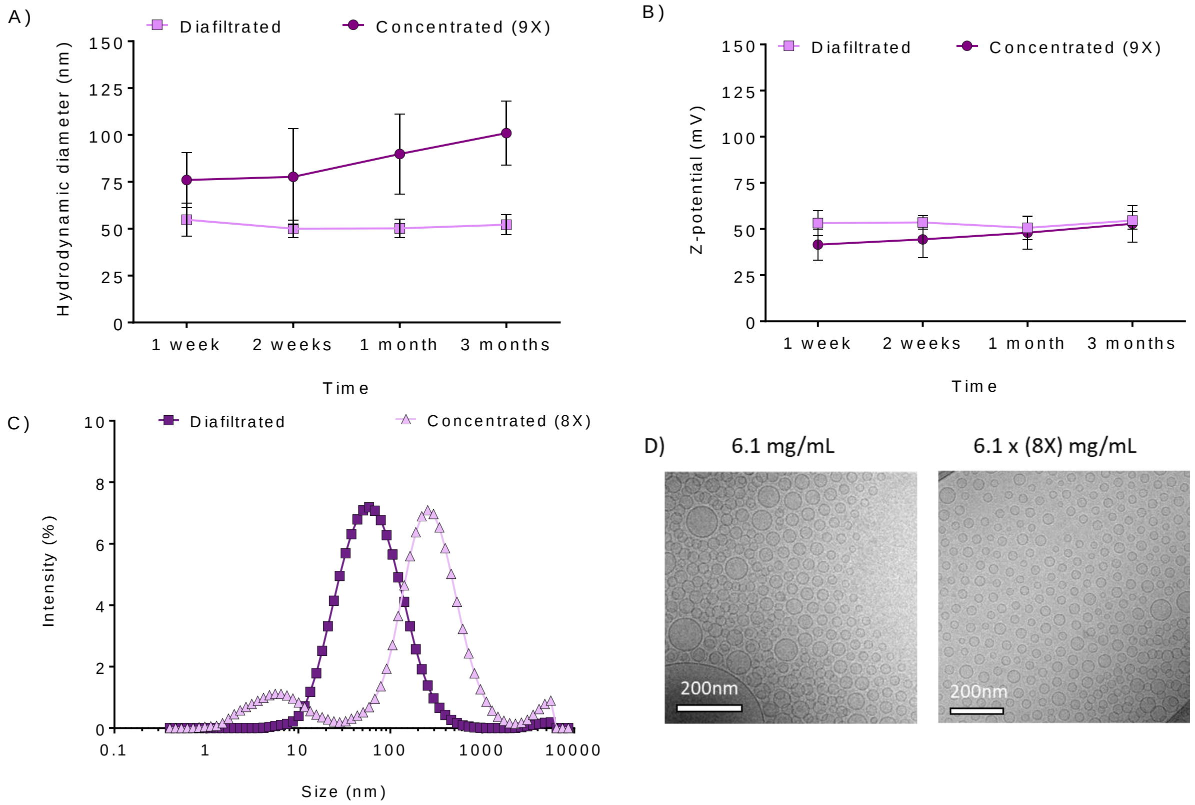

Figure 35. QS_0 physicochemical properties after purification and after concentration (8X) by diafiltration over time. Hydrodynamic diameter **(A)** and surface charge density (Z-potential) **(B)** of QS_0 determined by DLS over time. Graph represents the average of three preparations ±SD. **C)** Particle size distribution measured by DLS of QS_0. Each curve is the mean of at least three independent experiments. **D)** Representative images by cryo-TEM of the morphology of QS_0.

Quantification of QS concentration

As was explained before, for the administration *in vivo* of small RNA conjugated with QS, QS must be concentrated in order to load enough sRNA to be effective *in vivo* in the injected volumes (~100 µL). For QS and sRNA complexes formation is important to calculate the concentration of QS precisely. To determine the QS concentration, the lyophilization or freeze-drying method was used (Table 14). After DELOS-SUSP process, QS samples presented a similar theorical (6.1 mg/mL for QS_0 and 5 mg/mL for QS_1) and real concentration, which was 5.4 mg/mL for QS_0 and 4.6 mg/mL for QS_1. On the other hand, QS_0 and QS_1 did not present similar behaviour after diafiltration, because the concentration obtained is too much lower for QS_1 (1.8 mg/mL) than for QS_0 (4.3 mg/mL). However, both samples after concentration by diafiltration had few loses of material and the concentration was increased until 8X for QS_0 (~ 32.8 mg/mL) and 10X for QS_1 (~ 17 mg/mL). These high concentrated samples allow the conjugation of miRNA at the required concentration for *in vivo* studies.

For future experiments of this thesis QS_0 and QS_1, will be prepared at initial concentration of 6.1 and 5 mg/mL owing to the final concentration achieved and the maintenance of the analysed physicochemical properties.

4.2.2. QS are capable of complexing small RNA

For QS and sRNA conjugation, QS and sRNA were complexed by incubation through electrostatic interactions between the positive charges of QS surface and the negative charges of sRNA molecules. Only the positive charge located outside of QS membrane are functional for the sRNA complexation owing to the inaccessibility of the sRNA to interact with the inner positive charges of QS (Figure 36).

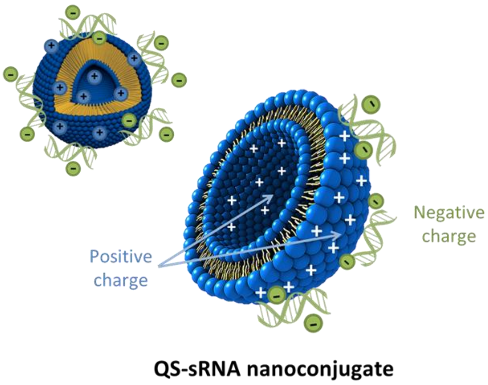

Figure 36. Schematic representation of QS-miRNA complexes produced by electrostatic interactions between positive charges of the MKC surfactant located outside the QS membrane and the negative charges from the miRNA backbone.

To study the complexation capacity of QS_0/QS_1, QS-miRNA complexes at different loadings of miRNA into QS (Table 15-Table 17) were run on agarose gels. The efficiency of complexation inversely correlates with the amount of free miRNA detected with ethidium bromide staining. Different amounts of free naked miRNA were loaded for reference. In electrophoretic gels, nucleic acids samples loaded on the top of the gel migrates to the down side of the gel. Differentially, nucleic acids entrapped in the surroundings of positively charged NP do not migrate and remained at the top of the gel. Thereby, the band detected at the bottom of the gel shows the miRNA that is not complexed with the QS. QS_0 did not have a fully complexation efficiency of the miRNA at any of the loadings tested (Figure 37A), even at loadings of low amount of miRNA per QS. On the other hand, QS_1 showed a higher complexation efficiency. At the lowest QS-miRNA loadings (i.e. I-IV) the miRNA is totally complexed with QS_1 as evidenced by the lack of free miRNA at the bottom of the gel (Figure 37B). Next, the QS-miRNA complexes were analysed by cryo-TEM. Both QS maintained the spherical shape but with multiple layers and aggregates (larger than 1 µm) (Figure 38).

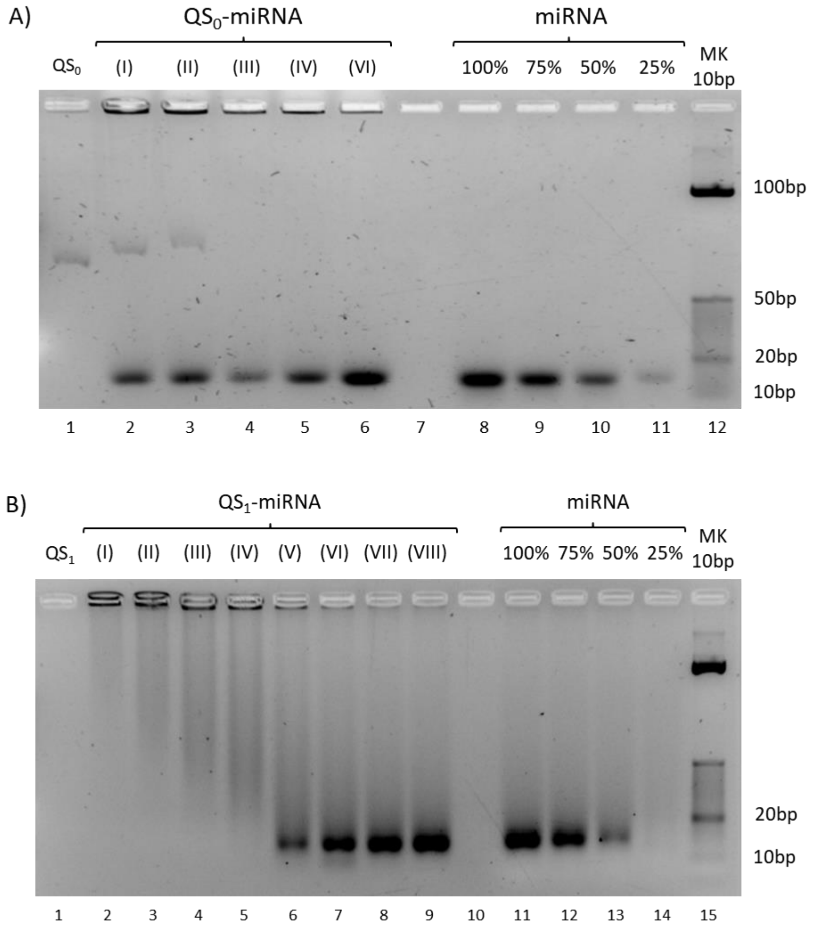

Figure 37. QS_1 has a higher miRNA complexation capacity than QS_0. A-B) Representative image of electrophoretic agarose gels showing the miRNA complexation efficiency with QS_0 **(A)** and QS_1 **(B)**. QS alone were loaded in lane 1. Different QS-miRNA loadings (i.e. from I to VIII) were loaded in lanes 2-6 **(A)** or 2-9 **(B)**. Free naked miRNA was used as a reference (lane 8-11 **(A)** or lane 11-14 **(B)**). All QS-miRNA complexes are described in Table 15-Table 17.

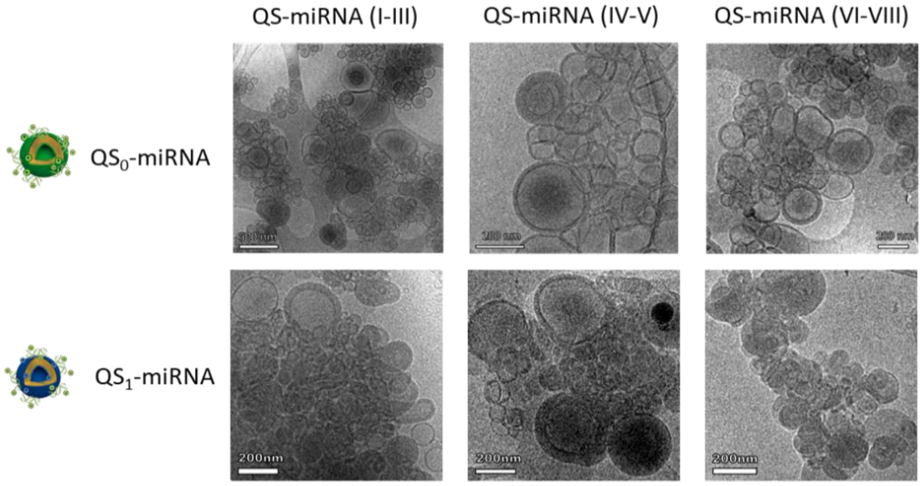
QS-miRNA (I-III)
QS-miRNA (IV-V)
QS-miRNA (VI-VIII)
QS0-miRNA
QS1-miRNA
200nm
200nm
200nm
200nm
200nm
200nm

Figure 38. QS_{0-1}-miRNA complexes presented similar morphology. High resolution representative cryo-TEM images of QS_{0-1}-miRNA complexes at various loadings of miRNA into QS. From left to right, the amount of miRNA loaded per QS increases. Scale bar, 200nm. All QS-miRNA complexes are described in Table 15-Table 17.

For functional experiments, the ratios of QS-miRNA complexes with the higher complexation efficiency (i.e. QS_0-miRNA (III-IV) and QS_1-miRNA (III-V)) were selected.

4.2.3. miR-497-5p is efficiently transfected by QS_0-miR-497-5p and QS_1-miR-497-5p complexes

In a functional screening developed previously in our laboratory, several miRNA with tumour suppressor functions were tested in chemoresistant NB cell lines. Among these miRNA, miR-497 was the most effective reducing the NB cells proliferation by inducing apoptosis in MYCN-amplified cell lines. Moreover, the conditional expression of miR-497 in NB xenografts reduced tumour growth and inhibited vascular permeabilization by targeting multiple genes related to DNA damage response, cell cycle, survival and angiogenesis[52]. Considering that miR-497 is a promising candidate for NB therapy, the conjugation of miR-497 with QS nanocarrier may achieve their clinical administration.

In order to evaluate the transfection capacity, QS_0 and QS_1 were complexed with miR-Control or with miR-497-5p and then incubated with SK-N-BE(2) NB cells. Forty-eighth hours post-transfection, cells were harvested and miR-497-5p expression levels were analysed by real-time qPCR. As a positive control, miR-497-5p was also transfected using Lipofectamine 2000®, a commonly-used liposome-based transfection reagent. Similar to Lipofectamine 2000®, QS-miR-497-5p conjugates increased the miR-497-5p expression levels ~ 10^3-10^4-fold change compared with miR-Control (Figure 39). Of note, QS_0 was equally efficient in transfecting the miRNA despite not displaying full miRNA complexation.

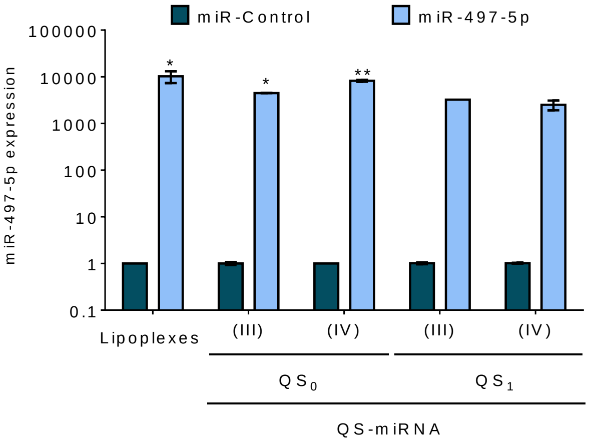

Figure 39. $QS_{0/1}$-miR-497-5p complexes transfect miR-497-5p in NB cells. MiR-497-5p expression levels in SK-NBE(2) cells transfected with lipoplexes or $QS_{0\text{-}1}$-miR-497-5p compared to $QS_{0/1}$-miR-Control nanoconjugates, measured by qPCR. All QS-miRNA complexes are described in Table 15-Table 17. Graph represents the mean of three independent experiments ± SEM. P<0.05*, p<0.01**.

4.2.4. QS$_{0-1}$-miR-497-5p complexes do not modify the expression of miR-497 direct targets

The next step was to evaluate the functional effects of QS$_{0-1}$-miR-497 transfection in SK-N-BE(2) cells. Among miR-497 targets, multiple cell cycle regulators such as CHEK1[52], WEE1[184] or proteins involved in apoptosis such as BCL2[185], have been described. When miR-497-5p expression levels were restored in NB cells, the phosphorylation of CHEK1 and WEE1 is reduced and CDC25A is inhibited. All these processes avoid the cell cycle progression and reduced the cellular division. On the other hand, miR-497-5p may reduce the NB cellular proliferation by the inhibition of BCL-2 (Figure 40).

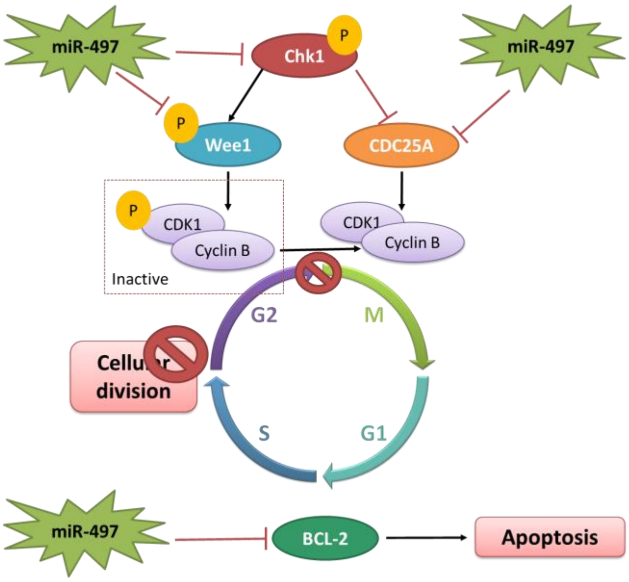

Figure 40. Schematic illustration of miR-497-5p targets functions in cancer cells when miR-497-5p is overexpressed.

Therefore, we proceed to analyse the levels of some of the above-mentioned targets, such as WEE1, CHEK1 or BCL-2. While the transfection of miR-497-5p with lipoplexes reduced the levels of WEE1, CHEK1, and BCL-2 at mRNA (Figure 41A-B) and protein level (Figure 41D-E), the transfection of QS$_{0-1}$-miR-497-5p (IV) complexes did not.

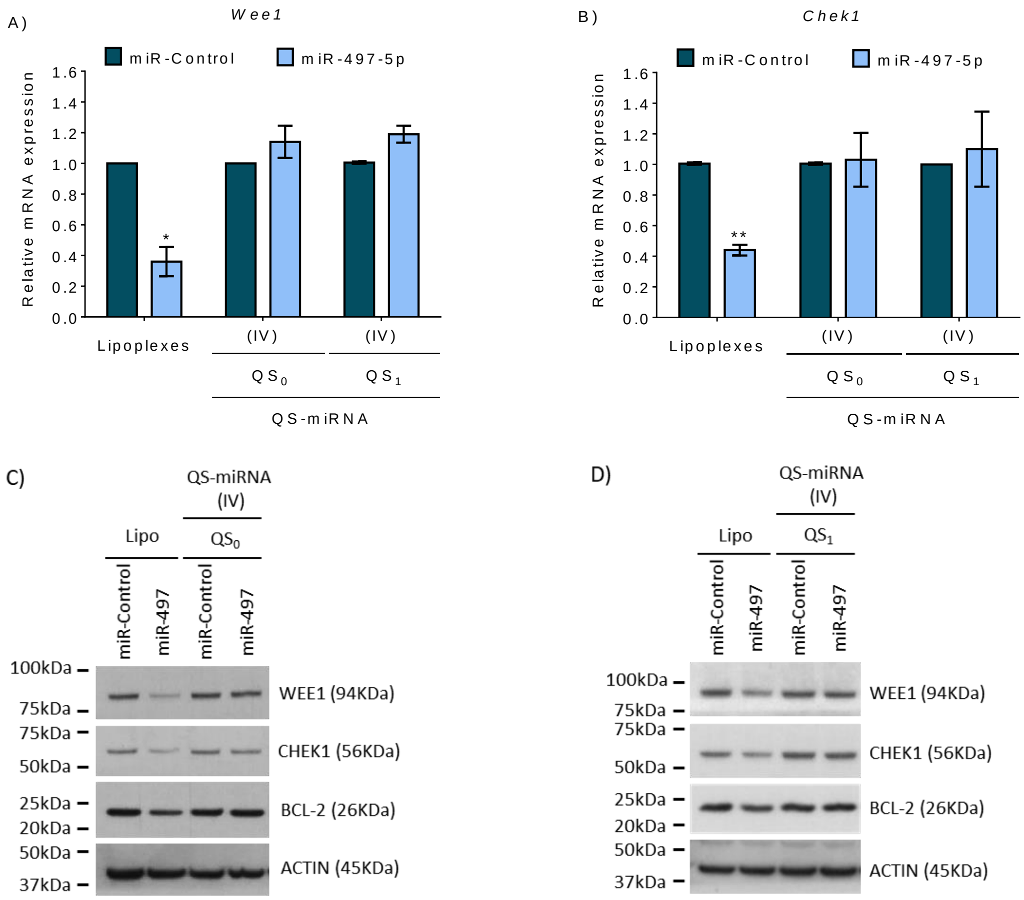

Figure 41. QS-miR-497-5p complexes did not modify miR-497-5p targets expression. A-B) *WEE1* **(A)** and *CHEK1* **(B)** mRNA expression measured by qPCR after miR-497-5p transfection compared to miR-Control-transfected cells for 48h. Graph represents the mean of three independent experiments ± SEM. $P<0.05$*, $p<0.01$**. **C-D)** Representative Western blot of the indicated proteins after transfection of miR-Control or miR-497-5p (50nM) with QS_{0-1} in SK-N-BE(2) cells for 48 hours. All QS-miRNA complexes are described in Table 15-Table 17.

Summary and perspectives:

In this section, different QS systems were prepared and characterized before and after concentration. Moreover, the miRNA complexation efficiency of these QS was evaluated as well as the miRNA internalization and functionality of these QS-miRNA complexes when transfected into NB cell lines. In particular:

- Stable colloidal nanovesicles composed by Chems:MKC and Chol:MKC formed QS, called QS_0 and QS_1 respectively, when were prepared at various molar ratios, except for 1:1 Chol:MKC molar ratio.
- The preparation of QS_{0-1} at the concentrations required for *in vivo* administration was not possible directly using the DELOS-SUSP technology, because the samples precipitated during the stabilization time. However, QS can be concentrated by diafiltration.
- Concentrated QS_{0-1} maintain good physicochemical properties in terms of size (~ 100-150nm) and polydispersity (0.25-0.60) over time.
- The study of QS morphology using Cryo-TEM demonstrated that concentrated QS are small unilamellar vesicles with spherical shape and smaller size than 200 nm. Moreover, the QS-miRNA complexes formed multilayers generated by the interactions among miRNA with different vesicles.
- The miRNA complexation capacity of QS may be evaluated using electrophoretic agarose gels. QS_0 had less miRNA complexation capacity than QS_1.
- Both, QS_0 and QS_1 were capable of transfecting miRNA in SK-N-BE(2) cells. However, miRNA was not functional.

In summary, these results demonstrate that despite the good physicochemical properties of QS and the capacity of transfection, the complexes cannot release functional miRNA inside the cells. Therefore, a new composition of QS should be tested.

4.2.5. Synthesis and physicochemical characterization of QS with different pH sensitive behaviour

With the aim of developing a new nanocarrier for small RNA (i.e. miRNA) delivery *in vitro* and *in vivo*, four QS formulations were engineered comprising two sterols, cholesterol (Chol) and DC-cholesterol (DC-Chol), at different molar ratios, and the surfactant Miristalkonium chloride (MKC) (Figure 42A). Specifically, Chol presents a hydroxyl group in a hydrophobic chain, while DC-Chol presents an amide with a tertiary amine in the end of the hydrophobic chain. The tertiary amine in DC-Chol confers ionizable pH-sensitive behaviour on this molecule since it may be protonated in acidic pH. This self-assembly capacity of MKC, together with sterol interaction, enables the formation of vesicles. Furthermore, the complexation of negatively-charged molecules, such as miRNA or siRNA, with these new nanovesicles occurs through electrostatic interactions with positively-charged quaternary ammonium of MKC or with the protonated tertiary amine of DC-Chol.

Thus, QS_1 composed by Chol:MKC at molar ratio 1:3, which are based on 0% of DC-Chol versus total sterols, was used as the negative control formulation. QS_1 was selected as the standard formulation because high miRNA complexation and internalization was observed after QS_1 conjugation, which not occurred with QS_0. Therefore, three new QS were prepared at ratio 1:1 between MKC moles and the total sterols moles (Chol plus DC-Chol) tuning the ratio of DC-Chol sterol composition versus total sterols composition. The resulting QS formulation had approximately a ratio of 10, 50 and 100% of DC-Chol versus the total sterols, which were called QS_2, QS_3 and QS_4, respectively (Figure 42B). The protocol used for QS preparation was detailed in Table 11 and explained in section 3.2.10.1.

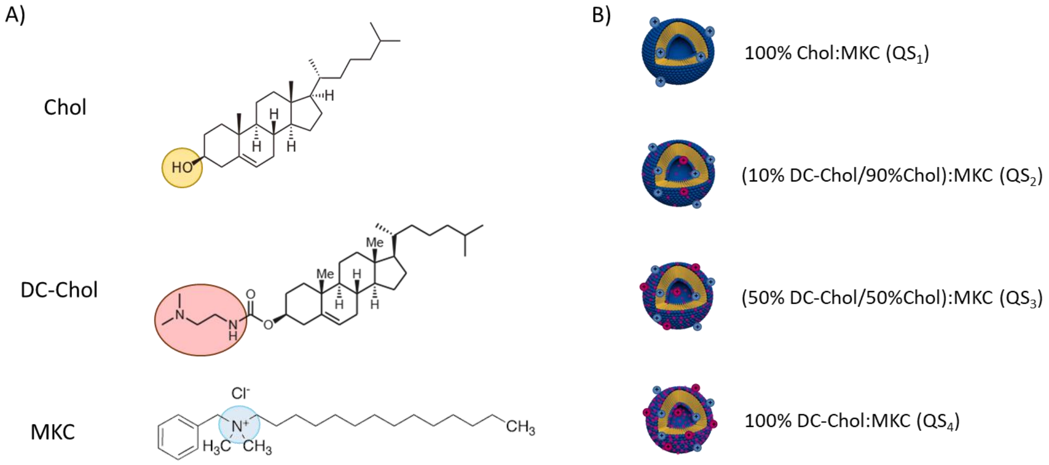

Figure 42. Membrane components used for the preparation of various QS systems (A) and schematic representation of the various compositions of QS prepared (B).

After one week of stabilization, QS formulations were purified by diafiltration to remove ethanol and the non-incorporated membrane components. The resulting QS systems (QS$_1$, QS$_2$, QS$_3$ and QS$_4$) were physicochemically characterised to study their functional use as a nanocarrier for miRNA delivery.

Physicochemical properties of DC-cholesterol nanovesicles composing QS$_{1\text{-}4}$ formulations

The physicochemical properties of colloidal samples QS$_{1\text{-}4}$ were evaluated over time by dynamic light scattering (DLS) and pHmeter. All formulations have a small size (D$_h$ between 50-100nm; Figure 43A and Figure A4A), with a low polydispersity index (PDI, 0.15-0.3 except QS$_2$; Figure 43C and Table A3), positive charge (ζ-potential between 80-100mV; Figure 43B and Figure A4B) and slightly acidic-neutral pH (pH ~6-7) (Figure 43). However, analysing in deep the polydispersity of these nanovesicles, QS$_2$ differed from the others because had a high polidisperisty index (PDI ~ 0.40; Table A3) and two populations were observed by DLS, one around 50 nm and another higher than 100 nm after QS$_2$ preparation (Figure A4C). The other formulations after DELOS-SUSP preparation presented only one population around D$_h$ ~ 50 nm for QS$_{3\text{-}4}$ (PDI ~ 0.15-0.20) and D$_h$ ~ 100 nm for QS$_1$ (PDI ~ 0.24), which slightly increased after purification (Figure A4C and Table A3). Furthermore, the QS stability measurements demonstrated a long-term colloidal stability in terms of size, charge and pH until six months, especially for QS$_{3\text{-}4}$ which did not significantly increase their size after 6 months (Figure 43).

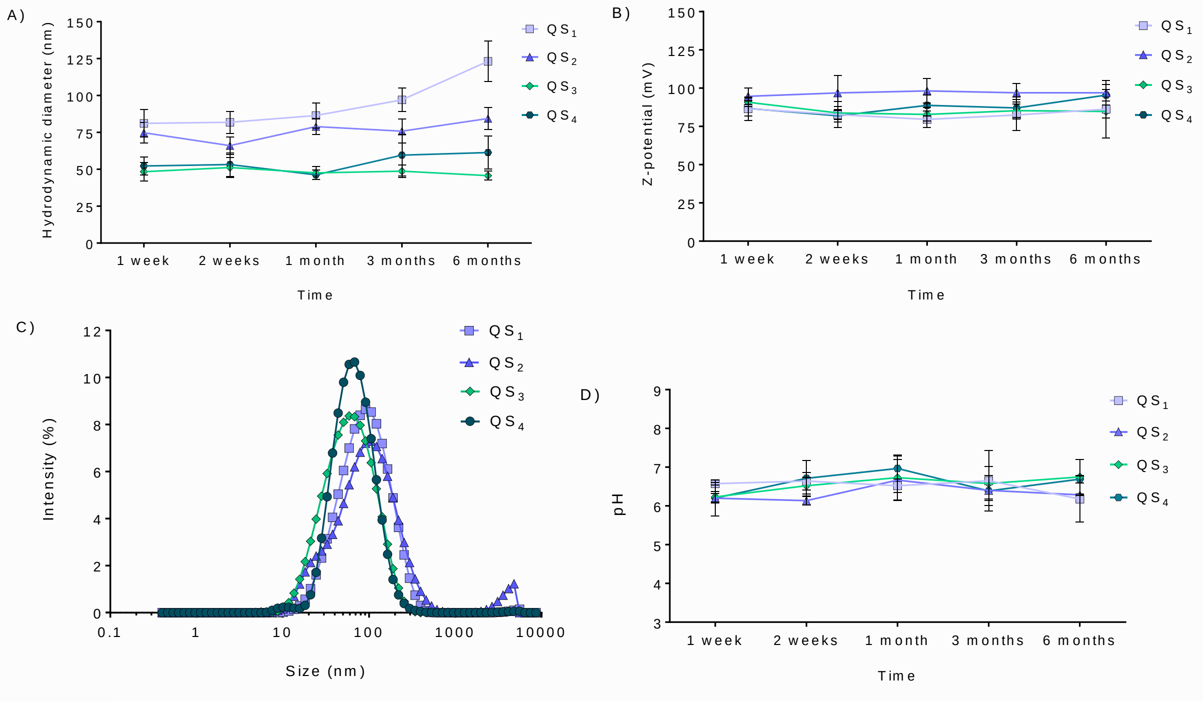

Figure 43. QS presented good physicochemical properties over time, such as small size, positive charge and slightly acidic-neutral pH after purification by diafiltration. A-B) Hydrodynamic diameter **(A)** and surface charge density (Z-potential) stability **(B)** of the indicated QS$_{1\text{-}4}$ systems determined through DLS technique over time. Each line represents the mean ± SD from the three independent samples. **C)** Particle size distribution of QS$_{1\text{-}4}$. Each curve are the mean of at least triplicate experiments. **D)** pH stability of the QS$_{1\text{-}4}$ systems over time. Error determined by the standard deviation of at least duplicate samples.

Furthermore, the final concentration of QS systems was determined by lyophilization, as was detailed in the Section 3.2.11.3 of materials and methods. As was explained before, QS_1 presented a high loss of material during the diafiltration process (~ 70%), leading to a final concentration of QS_1 ~ 1.8 mg/mL. On the other hand, $QS_{2\text{-}4}$ presented a similar yield after DELOS-SUSP compared to QS_1, which is almost ~ 85-90%. However, likewise happened with QS_1, during the diafiltration process there were a high loss of material to nearly ~ 45-50%, which implied a final yield of the $QS_{2\text{-}4}$ of nearly 43-51%. Thereby, the final concentration of these samples were 2.7, 3.1 and 2.8 mg/mL for QS_2, QS_3 and QS_4, respectively (Figure 44; Table 14).

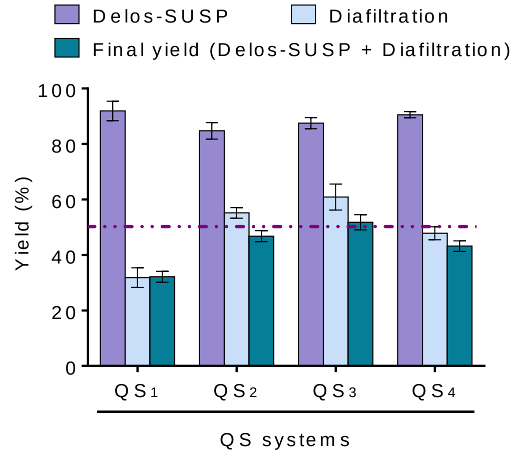

Figure 44. $QS_{2\text{-}4}$, composed by Dc-Chol, had a higher yield than QS_1 after their purification. Graph representing the yield of each process developed for QS preparation and purification. Bars were the mean of at least triplicate measures ± SD.

On the other hand, high-resolution cryogenic transmission electron microscopy (cryo-TEM) showed that all $QS_{1\text{-}4}$ formulations were homogeneous, unilamellar and had a spherical shape (Figure 45).

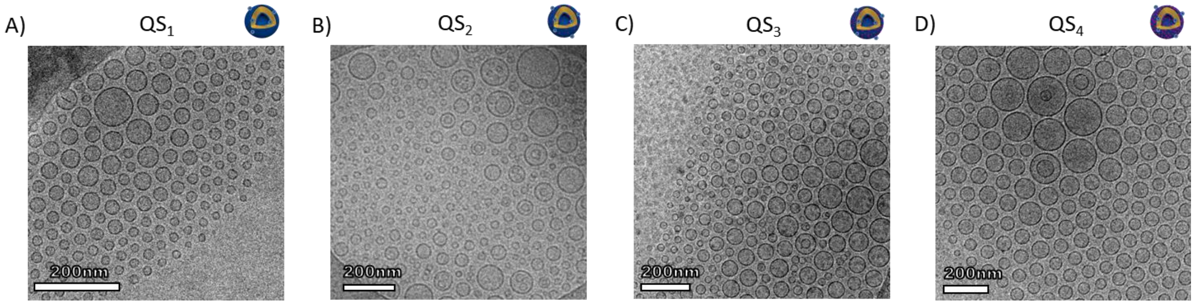

Figure 45. All $QS_{1\text{-}4}$ prepared are SUVs and presented spherical morphology. High resolution Cryo-TEM images of QS, varying the sterols composition, **(A)** QS_1, **(B)** QS_2, **(C)** QS_3 and **(D)** QS_4 after one week of diafiltration. Scale bar, 200nm.

pH sensitive behaviour of QS_{1-4} formulations comprising DC-Cholesterol

In order to determine the influence of QS formation in the protonation capacity of tertiary amines from the pH sensitive DC-Chol sterol, the buffering capacity of the different QS_{1-4} formulations in response to a gradient of HCl was measured. Water and QS_1, prepared without DC-Chol in their QS membrane, had no pH buffering effect and pH decreased after HCl addition. On the other hand, the QS systems with increasing DC-Chol concentrations, QS_{2-4}, presented a progressive maintenance on the pH after HCl addition. Hence, the Figure 46 confirmed that QS_{2-4}, entrapped the protons of HCl in the tertiary amine group of DC-Chol and impeded a pH reduction in a concentration-dependent manner (Figure 46). As it was expected, a higher progression on buffering capacity was correlated with the systems with higher DC-Chol ratio in their formulations. So QS_3, which has an intermediate ratio of DC-Chol, has less buffering capacity than QS_4 and higher than QS_2. Thus, we conclude that DC-Chol incorporated in QS_{2-4} preserves their pH sensitive properties after QS formation. This property may facilitate sRNA release within the cytosol owing to deprotonation of the pH-sensitive amine of DC-Chol[186,187].

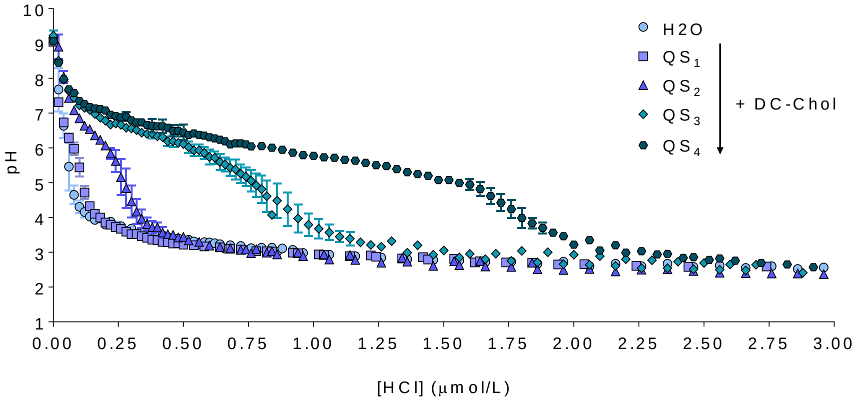

Figure 46. QS prepared with the sterol DC-Chol maintain the pH sensitive behavior after QS formation. Buffering capacity of QS_{1-4} with different % of the pH sensitive sterol DC-Chol. The graph shows pH variations with an acidic HCl concentration from 0 µM to 3 µM. Mean ± SEM is plotted from the duplicate experiments done.

We engineered QS of different lipid compositions with homogeneous small size, spherical shape and pH sensitive properties that may facilitate the sRNA cellular uptake and cargo release.

4.2.6. High efficiency of QS-miRNA complexes formation

The complexation of negatively-charged molecules, such as miRNA or siRNA, with QS can occur through electrostatic interactions with the positively-charged quaternary ammonium of MKC or with the protonated tertiary amine of DC-Chol.

Therefore, to demonstrate the formation of QS-miRNA complexes the mature form of miR-323a-5p was mixed with the different QS formulations for 5 min in PBS. Eight QS-miRNA complexes were prepared at constant miRNA concentration with increasing QS concentrations (Table 16 and Table 17). Detailed protocol of the QS-miRNA complexes formation was explained before (section 3.2.12).

Morphology observed by cryo-TEM

After $QS_{1\text{-}4}$-miRNA complexes formation, the morphological differences at three different loadings of miRNA in QS were characterized (Figure 47). When DC-Chol sterol composition was low or absent ($QS_{1\text{-}2}$), nanoparticles maintained their vesicular structure but with multilayers of miRNA embedded in the QS membranes. On the other hand, complexes with higher amounts of DC-Chol ($QS_{3\text{-}4}$) presented a bunch structure, consisting of different vesicles bound through the negative charges of microRNA.

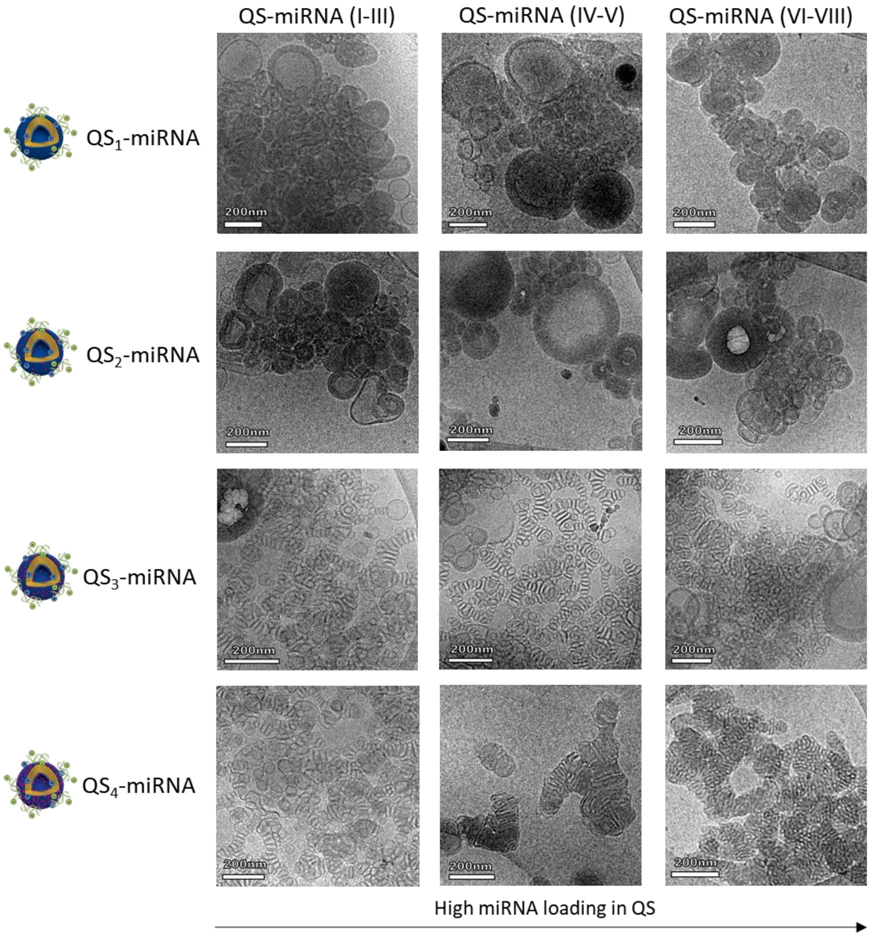

Figure 47. QS-miRNA complexes present different morphology and lamellarity. High resolution representative Cryo-TEM images of QS-miRNA complexes at various loadings of miRNA into QS. From left to right the miRNA loading in QS increases, which means less mass ratio miRNA/QS on left panel and higher mass ratio on right. Scale bar, 200nm. All QS-miRNA complexes are described in Table 16-Table 17.

Analysing in deep QS-miRNA complexes, we observed that $QS_{1\text{-}3}$-miRNA did not have a change on complexes morphology depending on the miRNA loading in QS surface. However, QS_4-miRNA complexes presented morphological differences when the content of miRNA in QS was increased. At low miRNA content in QS, called low loading of miRNA in QS, i.e. QS-miRNA (I-III), QS predominantly aggregated in brain chains and free QS, which indicated an excessive concentration of QS (Figure 47). Nevertheless, in QS_4 when the amount of miRNA is increased, e.g. QS_4-miRNA (IV-V), QS membranes become more flexible and highly compacted fingerprint structures are observed (Figure 47). Finally, an excessive amount of nucleic acids destabilizes QS membranes, inducing the rupture of vesicles and formation of large aggregates (e.g. QS_4-miRNA (VI-VIII), Figure 47)[188].

High efficiency of QS-miRNA complexes formation by agarose gels

To further investigate the differences in complexation capacity of the various $QS_{1\text{-}4}$ types, we performed an agarose gel with the loadings of QS-miRNA described in Table 16-Table 17.

As was explained before, the efficiency of complexation inversely correlates with the amount of free miRNA detected with ethidium bromide staining. Among all tested formulations, QS_4 was the most efficient in binding miRNA at a lower QS concentration (Figure 48). QS_1, however, was the formulation with the lowest miRNA-binding capacity. The correlation observed between the amount of DC-Chol and miRNA binding efficiency in $QS_{2\text{-}4}$ suggests that DC-Chol is a critical component for optimal QS-miRNA complexation.

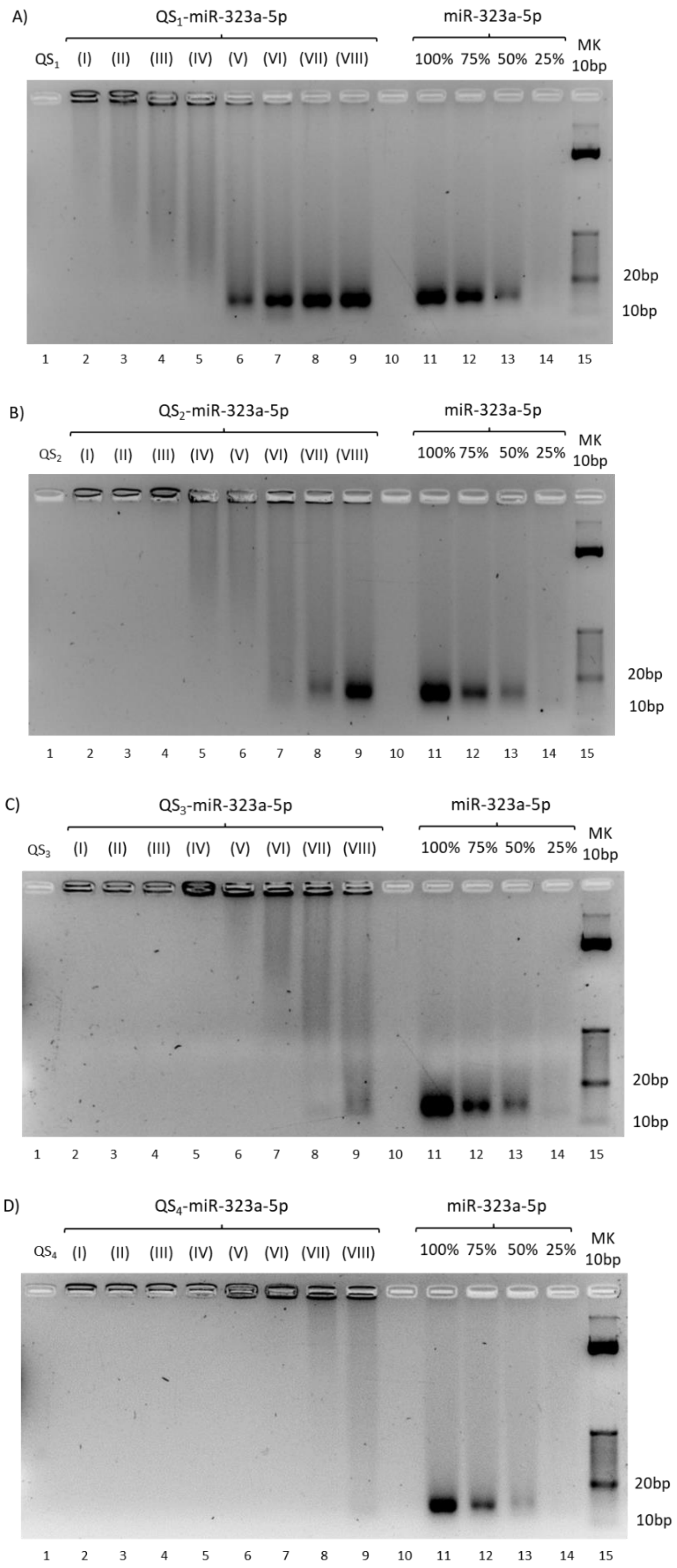
A)
QS$_1$-miR-323a-5p
miR-323a-5p
QS$_1$ (I) (II) (III) (IV) (V) (VI) (VII) (VIII)
100% 75% 50% 25%
MK 10bp
20bp
10bp
1 2 3 4 5 6 7 8 9 10 11 12 13 14 15
B)
QS$_2$-miR-323a-5p
miR-323a-5p
QS$_2$ (I) (II) (III) (IV) (V) (VI) (VII) (VIII)
100% 75% 50% 25%
MK 10bp
20bp
10bp
1 2 3 4 5 6 7 8 9 10 11 12 13 14 15
C)
QS$_3$-miR-323a-5p
miR-323a-5p
QS$_3$ (I) (II) (III) (IV) (V) (VI) (VII) (VIII)
100% 75% 50% 25%
MK 10bp
20bp
10bp
1 2 3 4 5 6 7 8 9 10 11 12 13 14 15
D)
QS$_4$-miR-323a-5p
miR-323a-5p
QS$_4$ (I) (II) (III) (IV) (V) (VI) (VII) (VIII)
100% 75% 50% 25%
MK 10bp
20bp
10bp
1 2 3 4 5 6 7 8 9 10 11 12 13 14 15

Figure 48. High miRNA complexation efficiency of Quatsomes (QS) prepared with DC-Chol derivative sterol. A-D) Representative gel electrophoresis showing the miRNA complexation efficiency with QS$_1$ **(A),** QS$_2$ **(B),** QS$_3$ **(C)** and QS$_4$ **(D)** diluted in PBS. QS free are loaded in lane 1 and the various loadings of QS-miRNA (I-VIII) are loaded in lanes 2-9 **(A-D).** Standard calibration of miRNA naked as a negative control (lane 11-14 **(A-D)).** These experiments were done in triplicate. All QS-miRNA complexes are described in Table 16-Table 17.

Finally, to study if the complexation between miRNA and QS is a reversible process and not impede the miRNA release, an agarose gel was done using the negatively charged surfactant SDS as competing molecule for the binding with positively charged QS$_{1-4}$. After the addition of SDS, into previously formed QS-miRNA complexes, all QS$_{1-4}$ were able to release the miRNA (Figure 49).

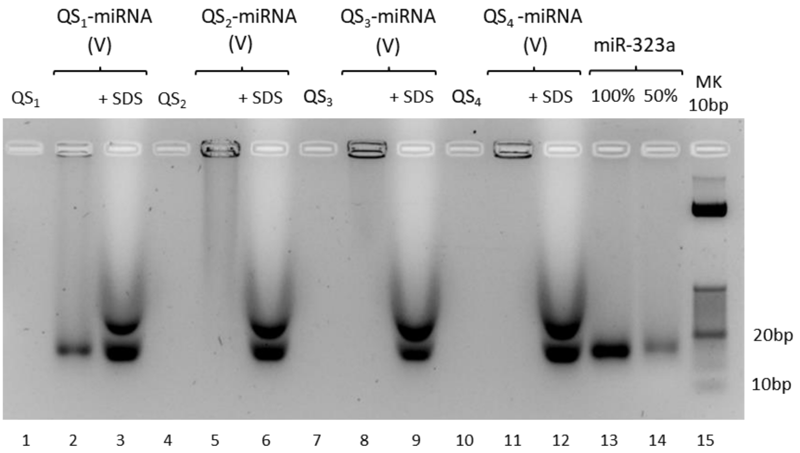

Figure 49. miRNA is released from QS$_{1-4}$, after previous complexation, through SDS treatment. Representative gel electrophoresis of miRNA release after SDS addition in QS$_{1-4}$-miRNA complexes. QS$_{1-4}$ free, as a negative control (lane 1,4,7 and 10), the QS$_{1-4}$-miRNA complexes at loading (V) (lane 2-3, 5-6, 8-9 and 11-12) and miRNA naked, as a positive control (lane 13-14), were loaded in the gel. SDS 1% was added after complexes formation in the indicated wells (lane 3, 6, 9 and 12). These experiments were done in duplicate. All QS-miRNA complexes are described in Table 16-Table 17.

Overall, we consider that the optimal QS-miRNA formulations for further experiments are the indicated loadings of miRNA in QS, such as QS$_1$-miRNA (I-IV), QS$_2$-miRNA (I-VI), QS$_3$-miRNA (I-VII) and QS$_4$-miRNA (I-VIII) because a fully miRNA complexation was observed.

4.2.7. QS$_{1-4}$-miRNA complexes not impair cell viability

To determine the potential toxicity of QS$_{1-4}$-miRNA complexes, all QS$_{1-4}$ formulations indicated in Table 16-Table 17 were loaded with a control miRNA, i.e. cel-miR-67 labelled with Dy547, which does not target human sequences. This control miRNA was previously shown to do not impair cellular viability *in vitro*[52,157]. Cell proliferation experiments were evaluated after 24h of incubation with increasing concentrations of QS$_{1-4}$ alone or QS$_{1-4}$-miR-Control complexes (Table 20; Figure 50A-B, respectively). All formulations had a similar impact on cell viability, with IC$_{50}$ ranging from 7 to 11 µg/mL for QS$_{1-4}$ alone and from 8 to 13 µg/mL for QS$_{1-4}$-miR-Control. IC$_{50}$ for QS$_{1-4}$-miRNA complexes were higher than for QS$_{1-4}$ alone, probably due to the neutralization of the positive charge of QS by miRNA. Of note, formulations with optimal miRNA binding (i.e QS$_{1-4}$-miRNA (IV, V or VI)) can be safely used for miRNA delivery to target cells.

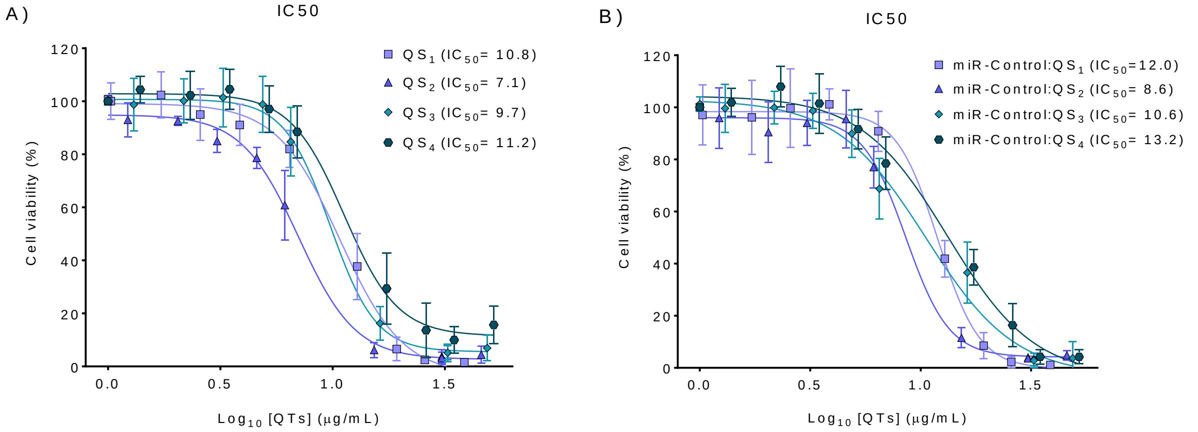

Figure 50. High cellular viability of SK-N-BE(2) cells after QS_{1-4} treatment at different concentrations (Table 20) or after QS_{1-4}-miR-Control complexes transfection at various loadings QS_{1-4}-miRNA (I-VIII). IC_{50} determined in proliferation studies after QS_{1-4} treatment (A) or QS_{1-4}-miR-control transfection (B). Mean ± SEM is plotted from the triplicate experiments done. All QS-miRNA complexes are described in Table 16, Table 17 and Table 20.

4.2.8. QS-miRNA formulations efficiently internalized into SK-N-BE(2) cells

In collaboration with the group of Dr. Lorenzo Albertazzi from Institute for Bioengineering of Catalunya (IBEC) and Institute for Complex Molecular Systems (ICMS), we analysed the internalization of QS-miRNA complexes into SK-N-BE(2) cell line by confocal imaging. Cells were incubated with complexes formed with QS_{1-4} and miRNA control labelled with Dy547 to follow the internalization of the complex using confocal microscopy. Figure 51A demonstrated that all 4 types of QS-miRNA complexes can internalize into cells while free miRNA cannot penetrate the cells. However, QS_{1-2}-miRNA complexes internalized but with less fluorescent intensity compared to QS_{3-4}-miRNA complexes. In order to decipher if QS-miRNA complexes internalized using an endocytic pathway that ends up in lysosomes, the colocalization of miRNA transfected with QS in lysosomes was determined by confocal images. In Figure 51B was demonstrated that QS_{1-2}-miRNA complexes colocalize with lysosomes (orange dots with white arrows) in some cases.

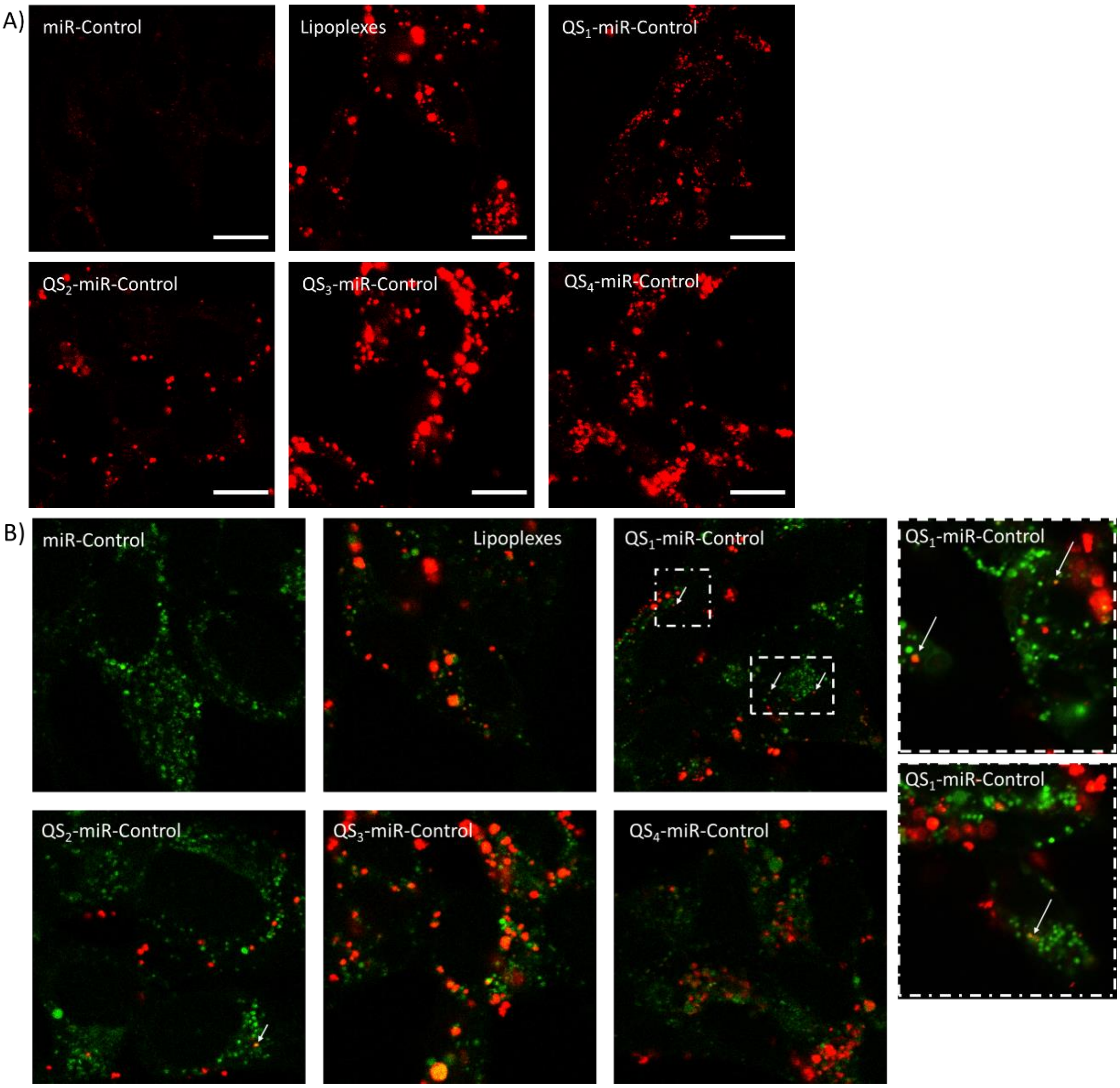
A)
miR-Control
Lipoplexes
QS$_1$-miR-Control
QS$_2$-miR-Control
QS$_3$-miR-Control
QS$_4$-miR-Control
B)
miR-Control
Lipoplexes
QS$_1$-miR-Control
QS$_1$-miR-Control
QS$_1$-miR-Control
QS$_2$-miR-Control
QS$_3$-miR-Control
QS$_4$-miR-Control

Figure 51. QS-miRNA complexes are efficiently internalized in NB cells but only few QS$_1$-miRNA complexes colocalize with lysosomes after 24 h post-transfection. A) Representative confocal images of NB cells treated with miRNA naked, lipoplexes and QS-miRNA (V) complexes. miR-Control was labelled with Dy547. **B)** Confocal images of NB cells treated with miRNA naked, lipoplexes and QS-miRNA (V) complexes while lysosomes were stained using Lysotracker Green. Scale bar, 200nm. QS-miRNA complexes are described in Table 16-Table 17.

Indeed, to prove the favoured release of miRNA in complexes formed with QS$_4$ we studied the localization of miRNA at more than 24 hours (Figure 52-Figure 53). However, Figure 52A demonstrated that after 48h there was still miRNA internalised inside NB cells in all the conditions, except miRNA naked, but few complexes of QS$_1$-miRNA were already colocalizing with lysosomes (Figure 52B).

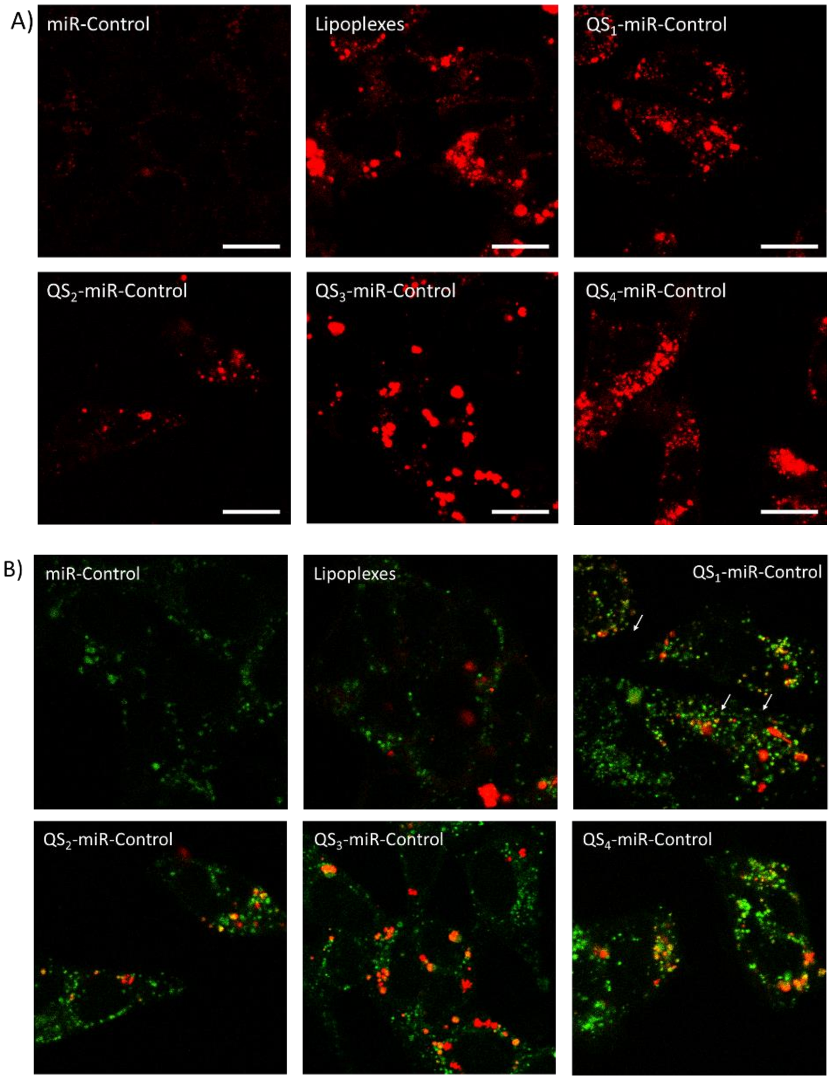
A)
miR-Control
Lipoplexes
QS1-miR-Control
QS2-miR-Control
QS3-miR-Control
QS4-miR-Control
B)
miR-Control
Lipoplexes
QS1-miR-Control
QS2-miR-Control
QS3-miR-Control
QS4-miR-Control

Figure 52. QS-miRNA complexes remain into NB cells cytosol after 48 h post-transfection. A) Representative confocal images of NB cells treated with miRNA naked, lipoplexes and QS-miRNA (V) complexes. miR-Control was labelled with Dy547. **B)** Confocal images of NB cells treated with miRNA naked, lipoplexes and QS-miRNA (V) complexes while lysosomes were stained using Lysotracker Green. Scale bar, 200nm. All QS-miRNA complexes are described in Table 16-Table 17.

After 72 hours post-transfection of QS-miR-Control labelled with Dy547 complexes, high accumulation of the nucleic acids in the cytoplasm was observed when the cells were treated with complexes formed with QS_4 compared to the amount of miRNA accumulated inside the cells after being transfected with QS_1 (Figure 53A). In both cases a high amount of miRNA can be observed inside cells forming complexes, however, only in QS_4 case were detected miRNA molecules not forming part of these clusters with high a clear distribution in the cytoplasm. Furthermore, at this time miRNA did not colocalize with lysosomes in any case (Figure 53B).

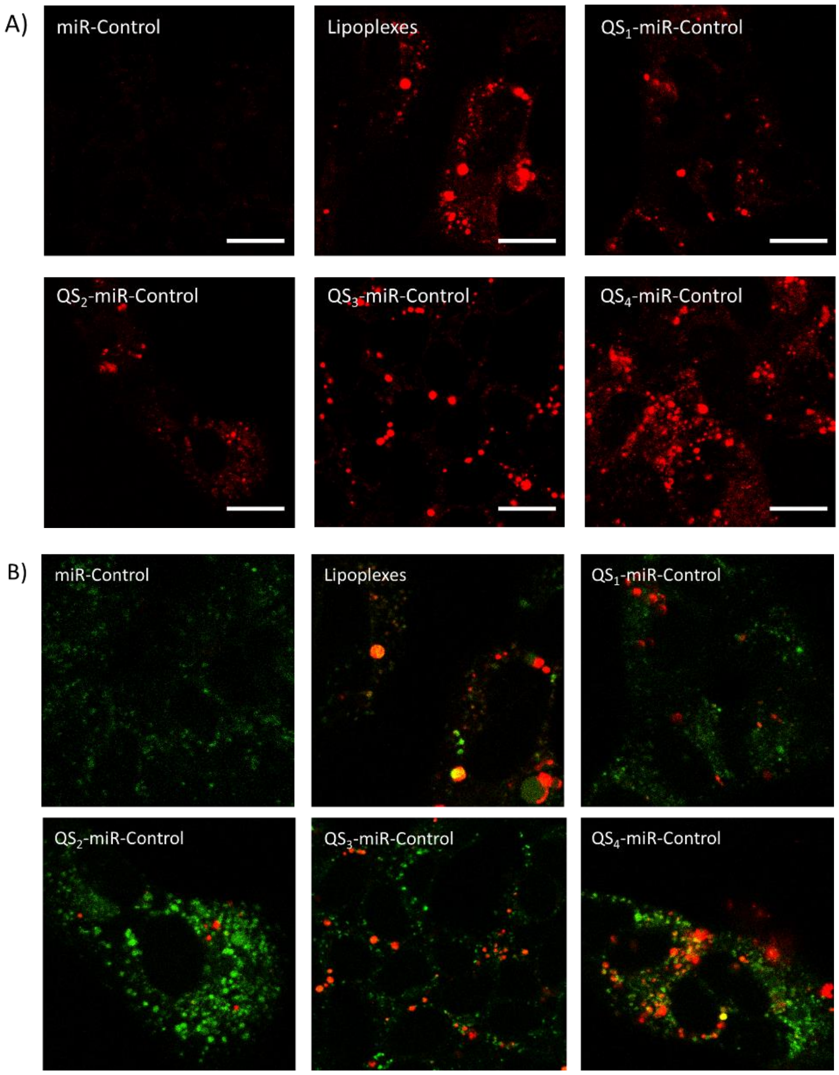
A)
miR-Control
Lipoplexes
QS_1-miR-Control
QS_2-miR-Control
QS_3-miR-Control
QS_4-miR-Control
B)
miR-Control
Lipoplexes
QS_1-miR-Control
QS_2-miR-Control
QS_3-miR-Control
QS_4-miR-Control

Figure 53. miRNA transfected with QS_4 are in the NB cells cytosol after 72 h post-transfection. A) Representative confocal images of NB cells treated with miRNA naked, lipoplexes and QS-miRNA (V) complexes. miR-Control was labelled with Dy547. **B)** Confocal images of NB cells treated with miRNA naked, lipoplexes and QS-miRNA complexes with lysosomes stained using Lysotracker Green. Scale bar, 200nm.

For further studies, miR-323a-5p was selected owing to its tumour-suppressive potential in NB. Low miR-323a-5p expression was shown to be associated with shorter progression-free survival in NB patients and miR-323a-5p restoration reduced NB growth *in vitro* and *in vivo*[157].

4.2.9. QS-miR-323a-5p are efficiently transfected and raise intracellular levels of miR-323a-5p

Next, miR-323a-5p expression levels were determined in SK-N-BE(2) cells 48 hours post-transfection by real-time qPCR. While naked miR-323a-5p was unable to enter into the cells, a ~ 10^3-fold change was observed for miR-323a-5p after transfection with the indicated QS-miR-323a-5p formulations compared with QS-miR-Control transfected cells (Figure 54).

Moreover, the miR-323a-5p expression levels of QS-miRNA complexes were compared with lipoplexes formed by the positive transfection reagent, Lipofectamine 2000®, and miR-323a-5p. These results demonstrated a similar fold change with both transfection systems. Of note, the complexation of miR-323a-5p only with the positively-charged surfactant MKC forming micelles, was unable to raise the intracellular miRNA levels (Figure 54).

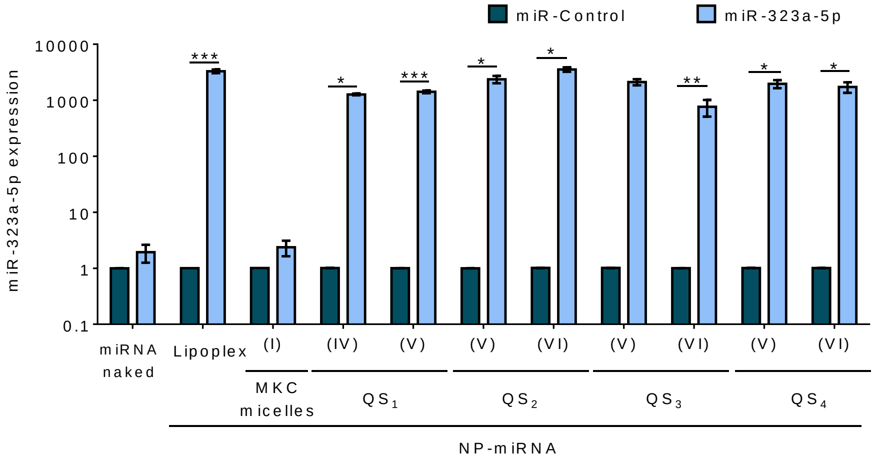

Figure 54. miR-323a-5p transfected with various QS formulations and lipoplexes increase intracellular miR-323a-5p expression levels. High miR-323a-5p expression levels in SK-NBE(2) cells transfected with naked miR-323a-5p, lipoplexes formed by Lipofectamine 2000® and miR-323a-5p, nanoconjugates of MKC micelles and miR-323a-5p or QS_{1-4}-miR-323a-5p complexes compared to miR-Control naked or miR-Control transfected with each transfection system, measured by qPCR. Graph represents the mean ± SEM of three independent experiments. P<0.05*, p<0.01**, p<0.001***. All QS-miRNA complexes are described in Table 16-Table 17.

4.2.10. Only QS_4-miR-323a-5p modulates miR-323a-5p target expression

Mir-323a-5p tumour-suppressive effects are mediated, at least in part, by the modulation of cell cycle related gens such as cyclin D1 (CCND1) and chromatin assembly factor 1 subunit A (CHAF1A)[157]. Therefore, we proceed to analyse the levels of such miR-323a-5p target genes after the treatment with the different QS formulations for 48h at mRNA and protein levels. Despite the similar transfection efficacy described above for all QS formulations, different outcomes were observed. Lipoplexes was also used as a positive control to evaluate the miR-323a-5p target genes modification at mRNA and protein level. As was expected, lipoplexes reduced *CCND1* and *CHAF1A* mRNA and protein levels after 48h post-transfection. Neither naked miR-323a-5p, MKC-miR-323a-5p micelles or QS_{1-2}-miR-323a-5p complexes produced variations either in CCND1 nor CHAF1A 48h at the mRNA (Figure 55) or protein levels (Figure 56). QS_3-miR-323a-5p only modified *CHAF1A* and *CCND1* minimally with QS_3-miR-323a-5p (VI) complexes. However, QS_4-miR-323a-5p complexes were able to efficiently downregulate CHAF1A and CCND1 at mRNA and protein level with comparable effects to Lipofectamine 2000 transfection reagent (Figure 55 and Figure 56).

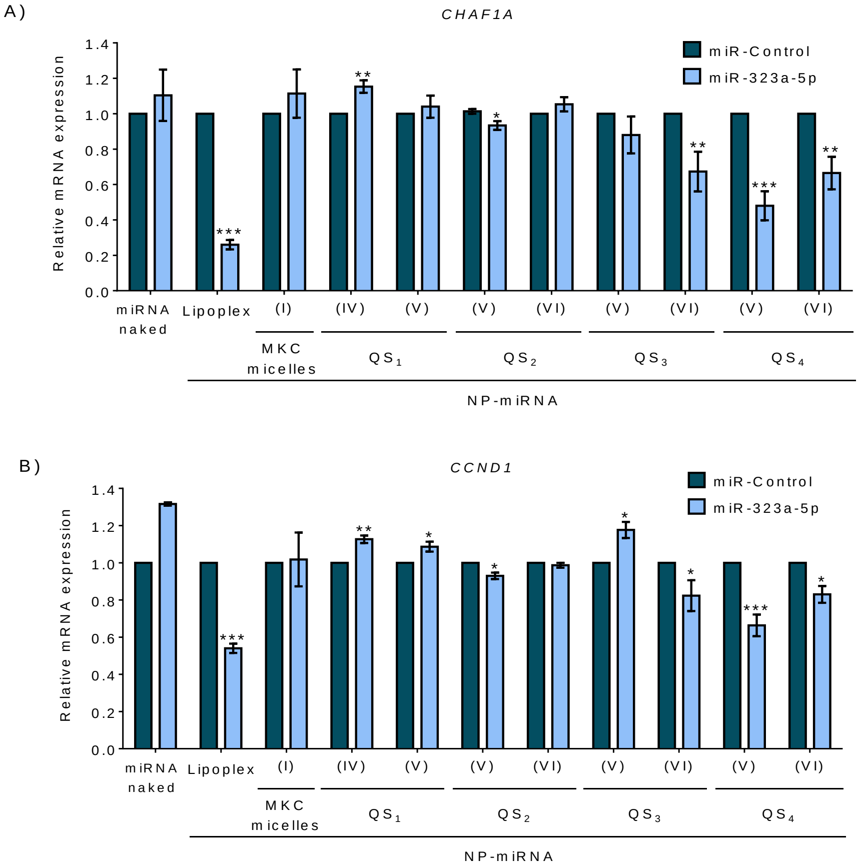

Figure 55. Inducible expression of QS-miR-323a-5p complexes, modify miR-323a-5p targets expression at mRNA after QS$_4$-miR-323a transfection in chemoresistant NB cells (SK-N-BE(2)), as well as lipoplexes. A-B) MiR-323a targets expression levels, **(A)** CHAF1A and **(B)** CCND1, measured by qPCR after miR-323a-5p versus miR-Control (50 nM) reverse transfection using naked miRNA, lipoplexes, micelles of MKC or complexes with QS$_{1-4}$ in SK-N-BE(2) cells at 48h. Graph represents the mean ± SEM of three independent experiments. P<0.05*, p<0.01**, p<0.001***. P<0.05*, p<0.01 **, p<0.001. All QS-miRNA complexes are described in Table 16-Table 17.

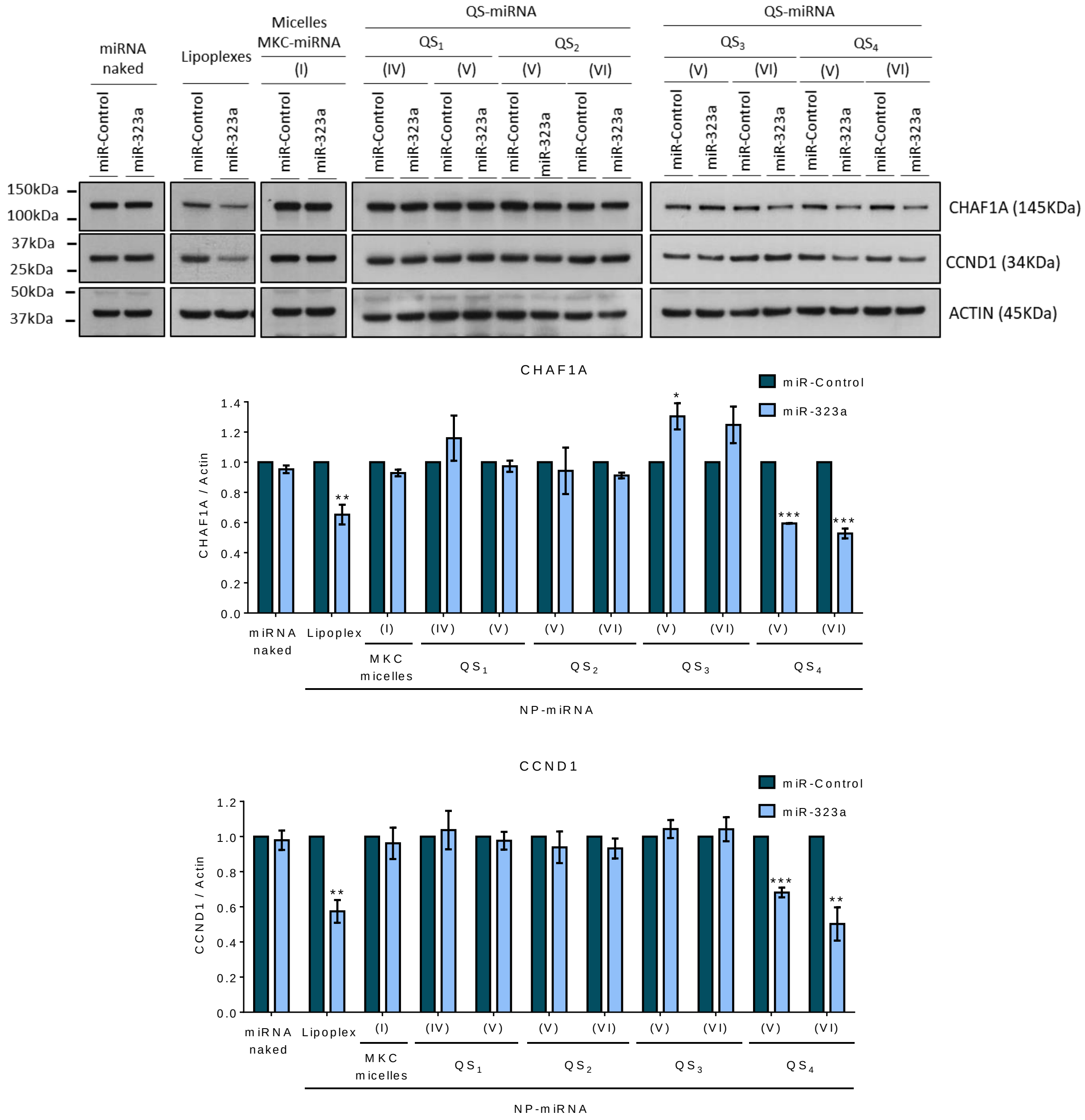

Figure 56. Inducible expression of QS-miR-323a-5p complexes, modify miR-323a-5p targets expression at protein level after QS_4-miR-323a transfection in chemoresistant NB cells (SK-N-BE(2)), as well as lipoplexes. Representative Western blot of the indicated proteins after transfection of miR-Control or miR-323a-5p (50nM) using naked miRNA, lipoplexes, micelles of MKC or complexes with $QS_{1\text{-}4}$ in SK-N-BE(2) cells at 48 hours. Histograms represent the quantification of band intensity signal mean ± SEM from three independent experiments. P<0.05*, p<0.01 **, p<0.001. All QS-miRNA complexes are described in Table 16-Table 17.

Taking into account these results, we chose QS_4 to study in depth a range of loadings of QS_4-miRNA useful for miR-323a-5p delivery and to evaluate the functional consequences of the treatment with these complexes. First, we evaluate again the miR-323a expression levels and miR-323a targets modification after 48 hours post-transfection with a higher range of loadings (V, VI and VIII) of QS_4-miR-323a-5p complexes in SK-N-BE(2) (Figure 57).

By RT-qPCR, we observed a significant increase in miRNA levels expression (~ 10^3-fold change) after miR-323a-5p transfection, compared to miR-Control transfected cells, at all QS_4-miRNA loadings used, even at the highest loading of miRNA in QS_4 (Figure 57A). However, analysing their miR-323a targets modification we observed that only QS_4-miRNA (V-VI) complexes reduced CHAF1A and CCND1 target genes at mRNA and protein level (Figure 57B-D). Thus, QS_4-miRNA (VIII) complexes can increase miR-323a expression but cannot modify significantly miR-323a targets expression (Figure 57A-D). In consequence, we assume that the range of loadings among (IV-VI) of QS_4-miRNA complexes is useful for miR-323a targets modification without compromising cellular viability.

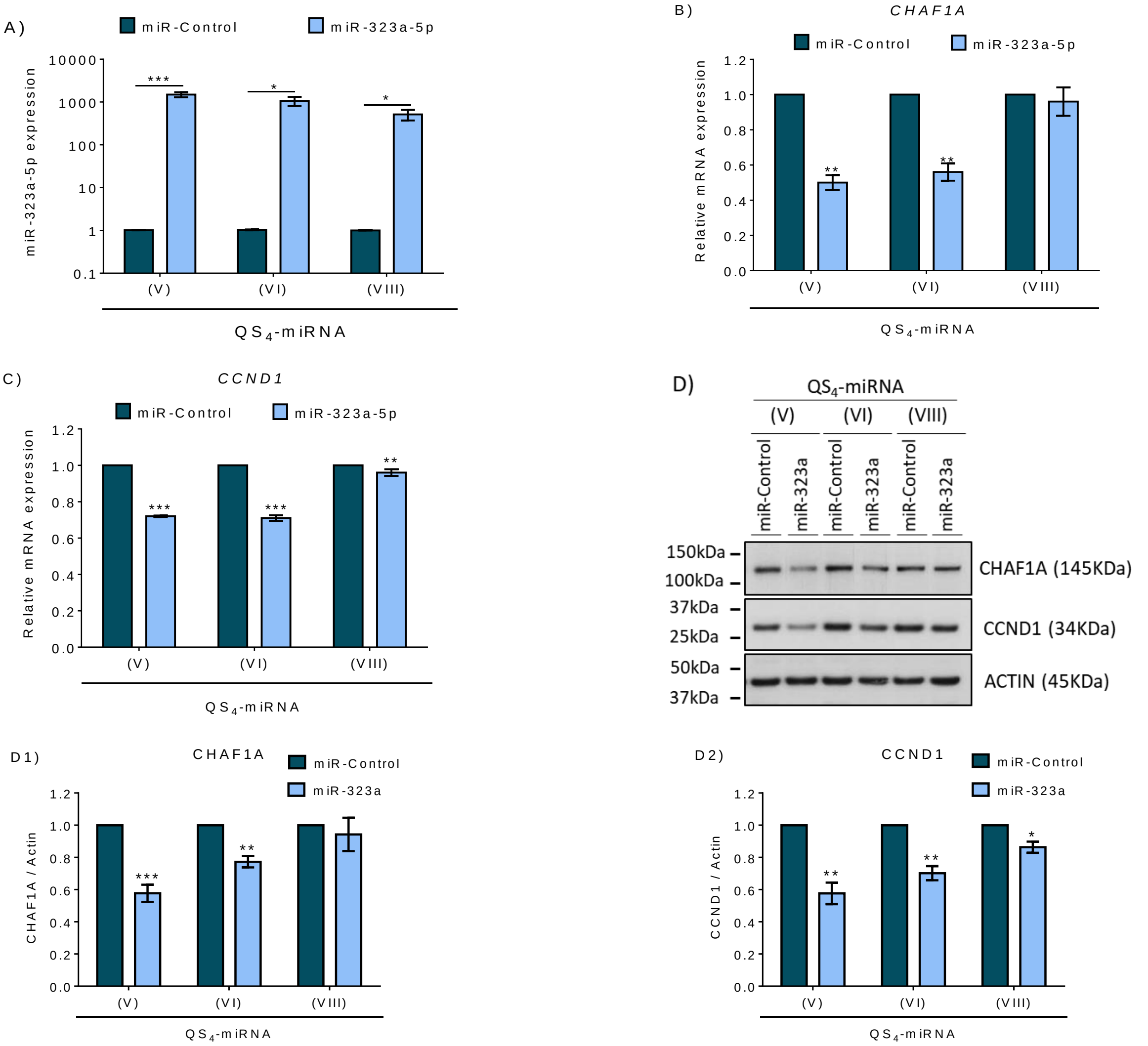

Figure 57. Inducible expression of QS_4-miR-323a-5p complexes increase miR-323a-5p expression levels in SK-N-BE(2) cells and modify direct miR-323a-5p targets expression at mRNA and protein level. A) miR-323a levels expression in SK-N-BE(2) cells transfected with QS_4 at three loadings (V, VI and VIII) measured by qPCR. B-C) qPCR of miR-323a-5p target genes, **(B)** *CHAF1A* and **(C)** CCND1, after 48 hours of SK-N-BE(2) cells transfection with QS_4-miRNA, using miR-Control or miR-323a-5p (50nM). **D)** Representative Western blot of the indicated proteins after 48 h of SK-N-BE(2) cells transfection at different loadings of QS_4-miRNA, using miR-Control or miR-323a-5p (50nM). Histograms of the quantification of band intensity signal of (**D1**) CHAF1A and (**D2**) CCND1 versus actin. Graphs represent the mean ± SEM of three independent experiments. $P<0.05$*, $p<0.01$**, $p<0.001$***. All QS-miRNA complexes are described in Table 16-Table 17.

Next, the functional consequences of QS$_4$-miR-323a-5p treatment were explored. In basal conditions, CCND1 interacts with CDK4 and CDK6, thereby activating the complex and inducing the phosphorylation of RB, which becomes activated and allows cell cycle progression (Figure 58A)[189,190]. If CCND1 levels fall, RB phosphorylation is reduced and cell cycle progression is halted. Therefore, cell cycle inhibitor p27 is increased (Figure 58B)[157,191].

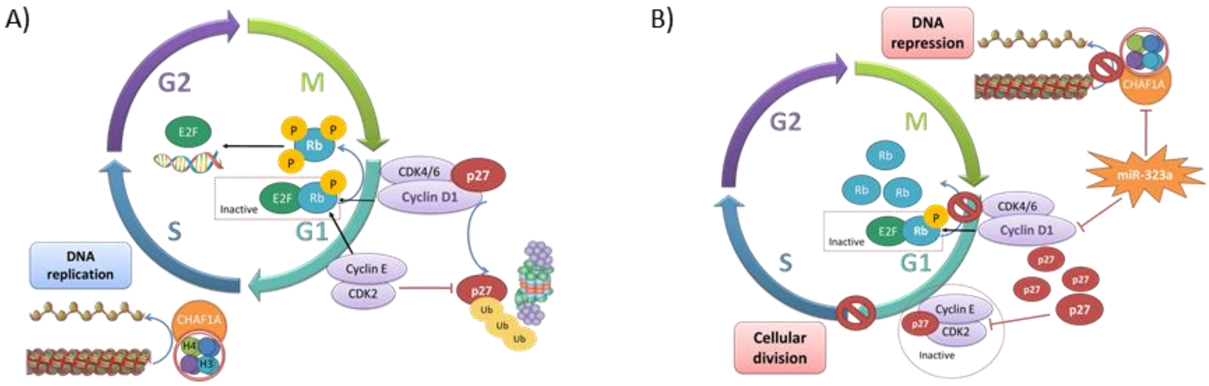
A)
G2
M
S
G1
E2F
Rb
P
Inactive
CDK4/6
Cyclin D1
p27
Cyclin E
CDK2
Ub
DNA replication
CHAF1A
H4
H3
B)
DNA repression
CHAF1A
miR-323a
G2
M
S
G1
Rb
E2F
P
Inactive
CDK4/6
Cyclin D1
p27
Cyclin E
CDK2
Cellular division

Figure 58. Schematic illustration of miR-323a-5p targets functions in cancer cells where miR-323a-5p is downregulated (A) and with restored levels (B).

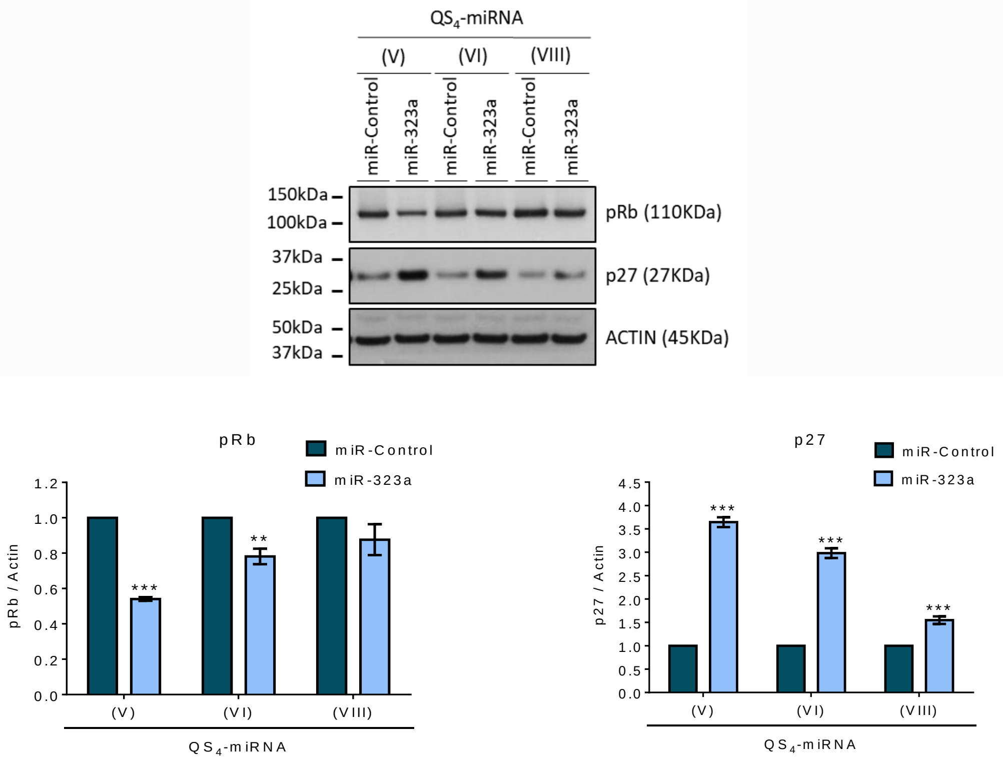

Figure 59. Inducible expression of QS$_4$-miR-323a-5p complexes modify indirect miR-323a-5p targets expression at protein level. Representative Western blot of the indicated proteins after 72 hours of SK-N-BE(2) transfection at different loadings of QS$_4$-miRNA, using miR-Control or miR-323a-5p (50nM). Histograms represent the quantification of band intensity signal mean ± SEM from three independent experiments. $p<0.01$ **, $p<0.001$ ***. All QS-miRNA complexes are described in Table 16-Table 17.

When NB cells were incubated in presence of QS_4-miR-323a-5p for 72h, the levels of phospho-Rb were lowered, particularly in the case of QS_4-miR-323a-5p (V) and (VI). As a result, accumulation of the p27 protein was observed (Figure 59). As expected, miR-323a-5p naked (Figure 60A) or conjugated to MKC micelles (Figure 60B) did not impact on RB phosphorylation or p27 accumulation.

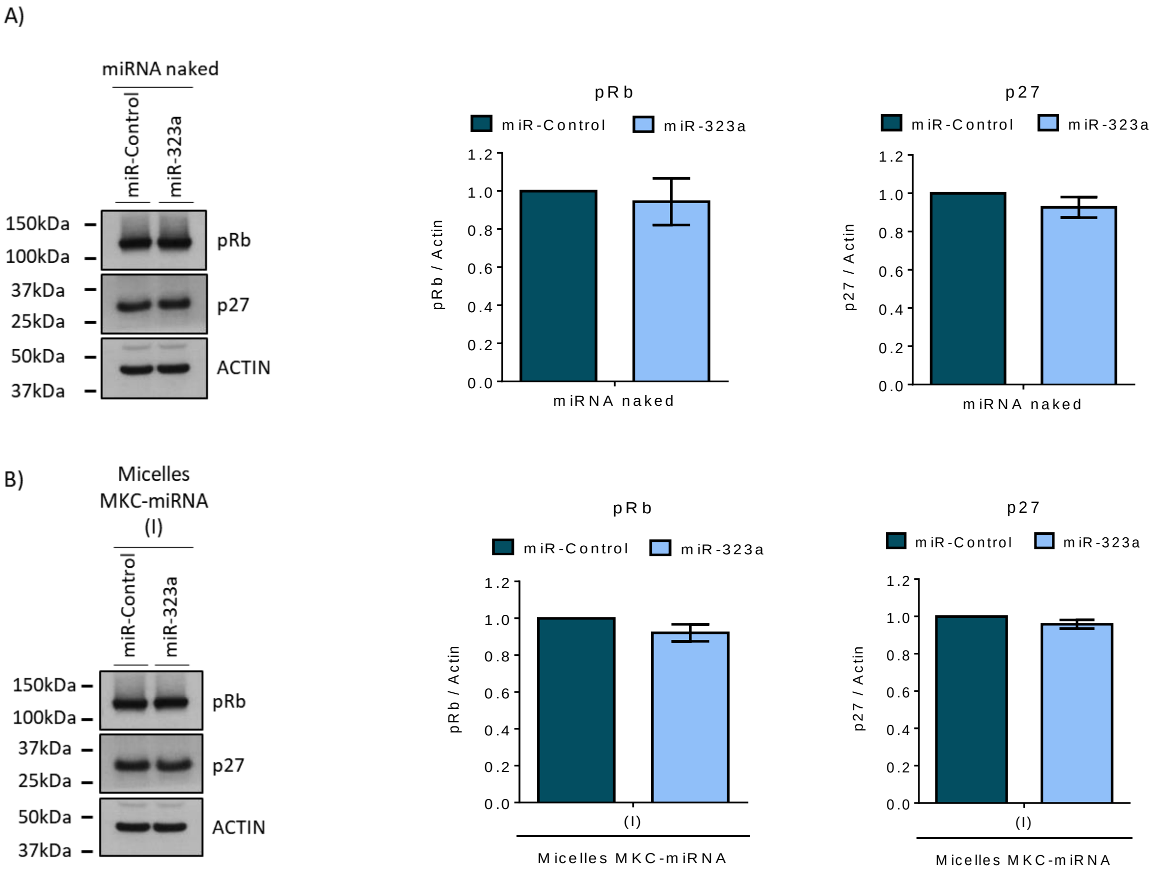

Figure 60. miR-323a-5p transfection with naked miRNA or complexed with MKC micelles did not modify the indirect miR-323a-5p targets expression at protein level in SK-N-BE(2) cells. A-B) Representative Western blot of the indicated proteins after 72h post-transfection of miR-Control or miR-323a-5p (50nM) with miRNA naked **(A)** or micelles of MKC-miRNA at loading (I) **(B)** in SK-N-BE(2) cells. All MKC micelles nanoconjugates with miRNA are described in Table 19. Histograms represent the quantification of band intensity signal mean ± SEM from three independent experiments.

After that, QS_4-miR-323a-5p complexes were transfected in SK-N-BE(2) in order to determine the effects of miR-323a-5p overexpression in cell viability. Concurring with the molecular observations, cell proliferation was also reduced. Only QS_4-miR-323a-5p (V) and (VI) formulations impacted significantly on the proliferation of NB cells (Figure 61).

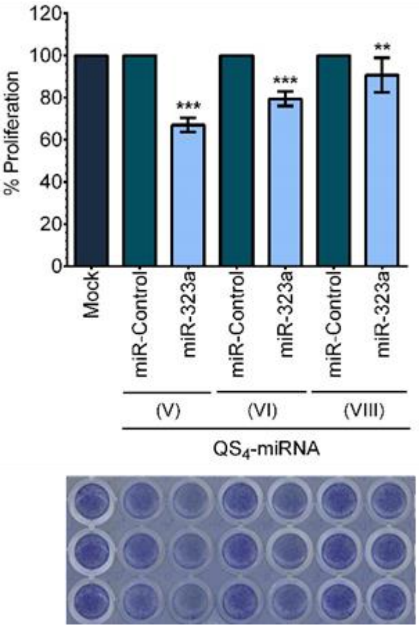

Figure 61. Inducible expression of QS4-miR-323a-5p complexes reduce SK-N-BE(2) cellular proliferation. Proliferation experiment at 96h of SK-N-BE(2) cells reverse transfected with QS4-miRNA, using in miR-323a-5p versus miR-Control (50nM).

4.2.11. QS4 is also a suitable delivery system for sRNA delivery

In an attempt to ascertain whether QS4 might be a suitable delivery system for other small RNA, we proceed to complex QS4 with a siRNA control (siCT) or with siRNA against CCND1 (siCCND1) and use them to transfect SK-N-BE(2) cells. Forty-eight hours post-transfection, QS4-siCCND1 was able to reduce *CCND1* mRNA (Figure 62) and protein levels (Figure 63A) while CCND1 levels remain unaltered when QS4-siCT was present. Similarly, QS4-siCCND1 complexes blocked RB phosphorylation, induced p27 accumulation (Figure 63B) and reduced NB cell proliferation (Figure 63C).

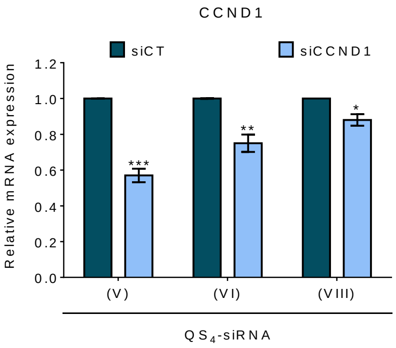

Figure 62. Inducible expression of QS4-siCCND1 complexes modify direct siCCND1 targets expression at mRNA level. qPCR of siCCND1 target gene after 48 hours post-transfection of siCT or siCCND1 (50nM) with QS4, at different loadings of siRNA in QS4, in SK-N-BE(2) cells. Graph represents the mean ± SEM from three independent experiments. P<0.05*, p<0.01 **, p<0.001 ***. QS-miRNA complexes are described in Table 16-Table 18.

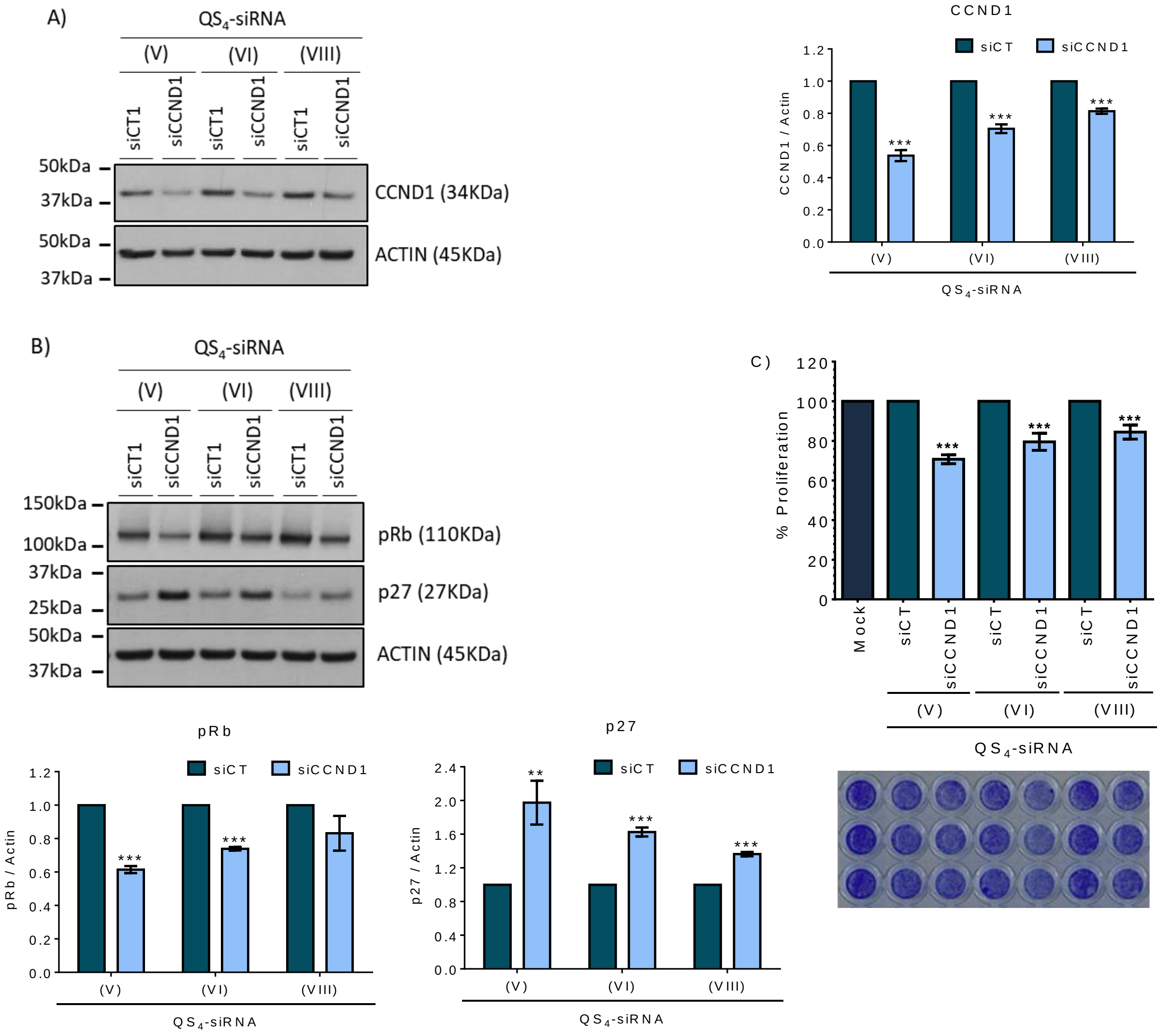

Figure 63. Inducible expression of QS4-siCCND1 complexes modify direct and indirect siCCND1 targets expression at protein level and reduce SK-N-BE(2) cells proliferation. A-B) Representative Western blot of the indicated proteins after 48 **(A)** or **(B)** 72 hours of SK-N-BE(2) transfection at different loadings of QS4-siRNA, using in siRNA Control (siCT) or siCCND1 (50nM). Histograms represent the quantification of band intensity signal mean ± SEM from three independent experiments. P<0.05*, p<0.01 **, p<0.001 ***. **C)** Proliferation experiment at 96h of SK-N-BE(2) cells reverse transfected with QS4-siRNA, using siCCND1 versus siCT (50 nM). All QS-miRNA complexes are described in Table 16-Table 18.

4.2.12. QS_4-miRNA complexes are stable in biological fluids and protect miRNA from RNAses

QS_4-miRNA complexes are stable after FBS incubation

To delve into the behaviour of the QS_4-miRNA complexes after *in vivo* administration, the stability of QS_4-miR-323a-5p complexes was studied with the addition of 10% foetal bovine serum (FBS) for thirty minutes, one, two and four hours. The presence of serum for the indicated times did not alter the binding of miR-323a-5p to QS_4, which suggested that serum components do not interfere with or alter the stability of QS_4-miRNA complexes, thereby preventing miRNA release by interactions with serum proteins. (Figure 64). Only the presence of SDS can release miRNA from the complexes. Therefore, we conclude that QS_4-miR-323a-5p complexes are stable in serum, which may ensure their stability until they reach the target cells, thus avoiding the premature release of miRNA in the bloodstream.

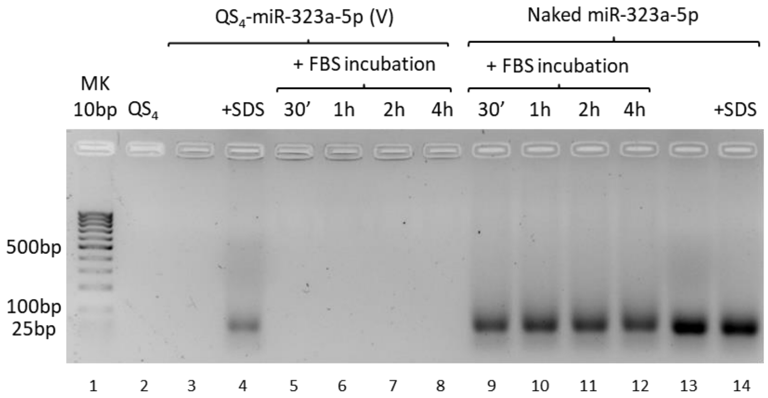

Figure 64. QS_4-miRNA complexes are stable in serum. Gel electrophoresis of QS_4-miRNA after FBS incubation. Empty QS_4 refers to plain QS. SDS (0.25%) is added as a reference for full miRNA separation from QS. The complex QS-miRNA (V) is described in Table 16-Table 17.

QS_4 protects miRNA from RNAse-mediated degradation

Many studies have shown that naked miRNA has a short half-life after *in vivo* administration owing to nucleases degradation[192-194]. Therefore, we proceed to analyze whether the complexation of miRNA with QS_4 could prevent the action of nucleases. QS_4-miR-323a-5p complexes were incubated with supra-physiological concentrations of RNAse A (i.e. 25µg/ml), a ribonuclease capable of degrading naked small RNAs in thirty minutes[144]. After the indicated times QS_4-miR-323a-5p complexes, were incubated with SDS at 0.025% to release the miRNA fraction. Naked miR-323a-5p was clearly cleaved after thirty minutes of RNAse A incubation, as shown the evident mobility shift of the miRNA in the agarose gel (Figure 65, lanes 9-12). However, miRNA released from QS_4-miR-323a-5p complexes (Figure 65, lanes 5-8) presented the same size as untreated naked miR-323a-5p (Figure 65, lanes 13-14) or from complexes without RNAse A incubation (Figure 65, lane 4).

Thus, QS_4 protects miR-323a-5p from RNAses degradation several hours, which may increase the miRNA half-life in the *in vivo* circulation.

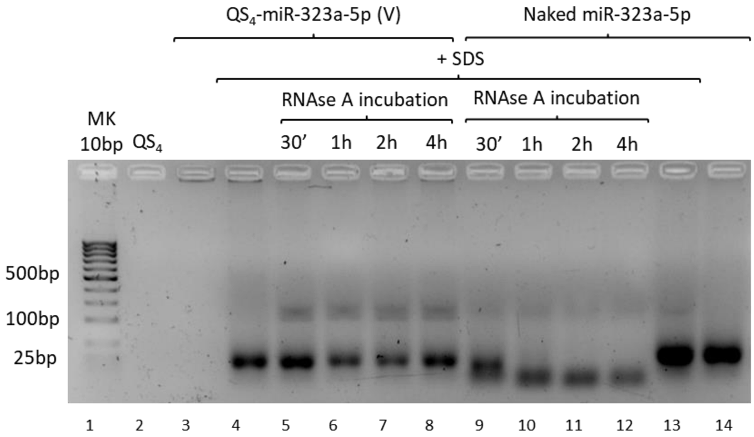
QS₄-miR-323a-5p (V)
Naked miR-323a-5p
+ SDS
RNAse A incubation
RNAse A incubation
MK 10bp
QS₄
30'
1h
2h
4h
30'
1h
2h
4h
500bp
100bp
25bp
1
2
3
4
5
6
7
8
9
10
11
12
13
14

Figure 65. QS_4 protects miRNA from nuclease degradation. Gel electrophoresis of QS_4-miRNA complexes incubated with RNAse A. QS_4 refers to empty QS. SDS (0.25%)-mediated miRNA decomplexation from performed QS_4-miRNA complexes after RNAse A treatment. The complex QS_4-miRNA (V) is described in Table 16-Table 17.

Summary and perspectives:

New QS, containing ionizable tertiary amines on their surface, for sRNA complexation and transport were designed, synthetized and characterized. The suitability of these QS to be used as nanocarriers for the intracellular delivery and functional miRNA targets modification, was evaluated using NB cell lines. In particular:

- A novel class of stable positively charged QS were synthesized with pH-sensitive properties and good physicochemical properties in terms of size (D_h< 100nm) and polydispersity (PDI < 0.3).
- The study of QS morphology using Cryo-TEM demonstrated that QS_{2-4} are small unilamellar vesicles with spherical shape.
- QS_{2-4} form complexes with miRNAs by electrostatic interactions. The QS_2-miRNA complexes have multilayer structures, while QS_{3-4}-miRNA complexes form grape like structures generated by the interactions among miRNA and QS_{3-4}.
- The capacity of QS to load miRNA was directly proportional to the content of DC-Chol in the QS membrane (QS_4> QS_3> QS_2).
- QS_4-miRNA complexes were stable in physiological fluids.
- QS_4 protected miRNA from RNAse-mediated degradation.
- QS_{2-4} were capable of transfecting miRNA in SK-N-BE(2) cells and internalize them.
- QS_{1-2}-miRNA complexes were partially degraded in lysosomes, while QS_{3-4}-miRNA complexes seems to be released in the cytosol.
- QS_4-miRNA complexes reduced significantly miR-323a direct and undirect target genes.
- QS_4-miRNA complexes reduced SK-N-BE(2) cellular proliferation.
- QS_4 transfected siRNA, modified their targets genes and reduced NB cell proliferation.

In summary, QS_4, composed of MKC and DC-Chol, is an efficient nanoformulation for the intracellular delivery and the induction of phenotypic and molecular effects of conjugated tumour-suppressive miRNAs or siRNAs in NB.

4.3. Cellular dynamics of QS_4-miRNA demonstrated miRNA release from QS_4

With the aim to understand the different outcome of miR-323a-5p transfection with the different QS systems, the behaviour of QS-miRNA complexes inside the cells was studied. In particular, the miRNA release from QS_1 and QS_4 was analyzed due to their different membrane composition, pH-responsiveness and functional efficacy over miR-323a-5p target genes.

4.3.1. QS labelling for *in vitro* and *in vivo* tracking

In order to track the conformational changes of QS-miRNA complexes during and after their cellular internalization, fluorescent QS-miRNA complexes were prepared using miRNA and QS labelled with two different fluorophores. These fluorophores, the first one the donor and another one the acceptor, could experience transfer of energy by FRET phenomena, at the appropriate distance. The conformational changes of QS-miRNA complexes can be monitored by FRET technology (see section 3.2.18), which could give information about the level of interaction between QS and miRNA as a function of the FRET intensity. When QS and miRNA are forming a complex, they are near enough to transmit energy from the donor fluorophore to the acceptor which, in turn will emit light at a further wavelength. However, when miRNA is released from the complex, there is no transference of energy from the donor to the acceptor fluorophore and FRET is not observed.

Previous results of Nanomol group reported that QS may be functionalized with several fluorophores, especially with fluorescent cyanines such as DiI, DiD and DiR. Molecular dynamics analysis of those QS demonstrated that the fluorophores were incorporated in QS surface, mainly by the high hydrophobicity of fluorescent cyanines[176,195]. Moreover, these QS maintained their good physicochemical and fluorescent properties in terms of size upon two months at 4°C[176,195]. Thus, to achieve a high FRET efficiency the fluorophores selected must have a high overlapping area between the emission of the donor fluorophore and the absorption or excitation of the acceptor fluorophore. Among all possible fluorophores combinations, as it is shown in Figure 66, the selection of DiI for the QS labelling and the Cy5 for miRNA was the most feasible option to have a good overlap between their spectrum and, in consequence, optimum FRET efficiency.

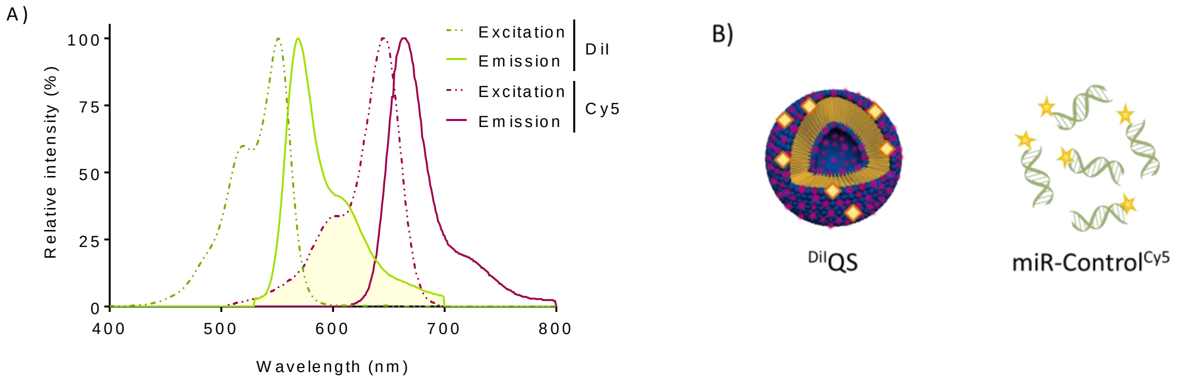

Figure 66. Excitation and emission spectra of DiI (green) and Cy5 (magenta) fluorophores. A) Excitation spectrum is represented in dotted lines and emission spectrum with solid lines. The overlapping area is represented in light yellow. **B)** Schematic representation of the QS labelled with DiI, called ^{DiI}QS, and the miR-Control labelled with Cy5, named miR-Control^{Cy5}.

QS labelled with DiI were prepared by DELOS-SUSP technology following the previously described methodologies (see 3.2.10.1). Particularly, the DiI fluorophore was added in the reactor together with the QS membrane components previously dissolved in EtOH (Table 12). The DiI incorporated in QS membrane was expressed as a DiI loading calculated as the moles of DiI divided by the moles of QS membrane components, including DiI[1]. Previous work of Nanomol group used loading of DiI in QS was in the range of $0.5 \cdot 10^{-3}$ to $10 \cdot 10^{-3}$. Undesirably, QS$_1$ prepared in water with 10% of etOH at three different DiI loadings precipitated after one week of stabilization (Table 12). Previous results of Nanomol group demonstrated that QS$_1$ labelled with 70 µM of DiI can be prepared at 1:1 molar ratio of Chol:MKC in PBS with 10% of etOH, instead of water (*Vargas-Nadal et al., thesis manuscript under preparation*). Hereafter these nanovesicles were called ^{DiI}QS$_1$.

At the same time, three ^{DiI}QS$_4$, containing DC-Chol and MKC, were prepared maintaining constant the membrane components and increasing the amount of DiI during samples preparation by DELOS-SUSP (Table 12). After one week of stabilization, ^{DiI}QS$_4$ were purified by diafiltration. Then, the DiI loading in the QS membrane were calculated from the known concentrations of membrane components of QS$_4$ (Table 14) and the concentrations of DiI measured by UV-Vis using the Lambert-Beer law (Table 22). Hereafter, in this thesis, samples of ^{DiI}QS$_4$ samples are called $^{DiI(x\,\mu M)}$QS$_4$, being x the concentration of the indicated systems (8 µM, 23 µM and 70 µM).

Table 22. Chemical description of the ^{DiI}QS samples used for monitoring cellular dynamics of QS-miRNA complexes.

Sample code	[QS]$^{\#}$ (mg/mL)	[DiI] in sample (µM)	DiI loading in QS (·10^{-3} mol DiI/mol membrane components)
$^{DiI}QS_1^{*}$	2.0	71.0 ± 0.2	3.3 ± 0.2
$^{DiI(8\ \mu M)}QS_4$	1.9	8.0 ± 0.1	1.9 ± 0.1
$^{DiI(23\ \mu M)}QS_4$	1.1	23.0 ± 0.2	5.5 ± 0.3
$^{DiI(70\ \mu M)}QS_4$	1.8	70.0 ± 0.3	16.8 ± 0.4

Final real concentration of QS$^{\#}$ and DiI and loading of DiI in QS calculated by gravimetrical yield and UV-Vis using lambert-Beer Law and (1), respectively. Values were represented as the mean of three independent experiments ± SD.$^{*DiI}QS_1$ prepared in *Vargas et al. thesis manuscript under preparation*.

On the other hand, to discover whether the QS composition permits the miRNA release selectively and explains the different outcome over miR-323a molecular targets, FRET analysis was done with $^{DiI}QS_4$ in comparison to $^{DiI}QS_1$.

^{DiI}QS have the same physico-chemical properties of unlabelled QS

$^{DiI}QS_1$ demonstrated similar physicochemical properties compared to plain QS_1 and were stable in terms of size (D_h ~ 100-120 nm), ζ-potential (~ 30-50mV) and polydispersity (PDI ~ 0.1-0.2) upon two months after their purification (*Vargas-Nadal et al., thesis manuscript under preparation*).

On the other hand, $^{DiI}QS_4$ formed, as well as plain QS_4, colloidal nanovesicles with a nanometric average size (D_h comprised between ~ 50-75 nm) but presented less surface charge density, which decreases gradually in $^{DiI}QS_4$ with the increase of DiI concentration (Figure 67A). However, all $^{DiI}QS_4$ maintained the required positive charge for miRNA complexation. Particle size distribution of $^{DiI}QS_4$ samples was composed by a unique population of vesicles, smaller than 100 nm, with small polydispersity (PDI ~ 0.15-0.25) like plain QS_4 (Figure 67B). Besides, $^{DiI}QS_4$ maintained the nanometric size, as well as a high positive charge after their storage at 4°C over time (Figure 67C-D). Although the loading of DiI has an impact in QS, the overall physicochemical characteristics of $^{DiI}QS_4$ are similar to plain QS_4. None of the three $^{DiI}QS_4$ samples were unstable because no sign of precipitation could be observed. To confirm the formation of SUVs like in plain QS_4, high-resolution cryogenic transmission electron microscopy (cryo-TEM) showed that all $^{DiI}QS_4$ formulations were homogeneous, unilamellar and spherical after diafiltration (Figure 67E).

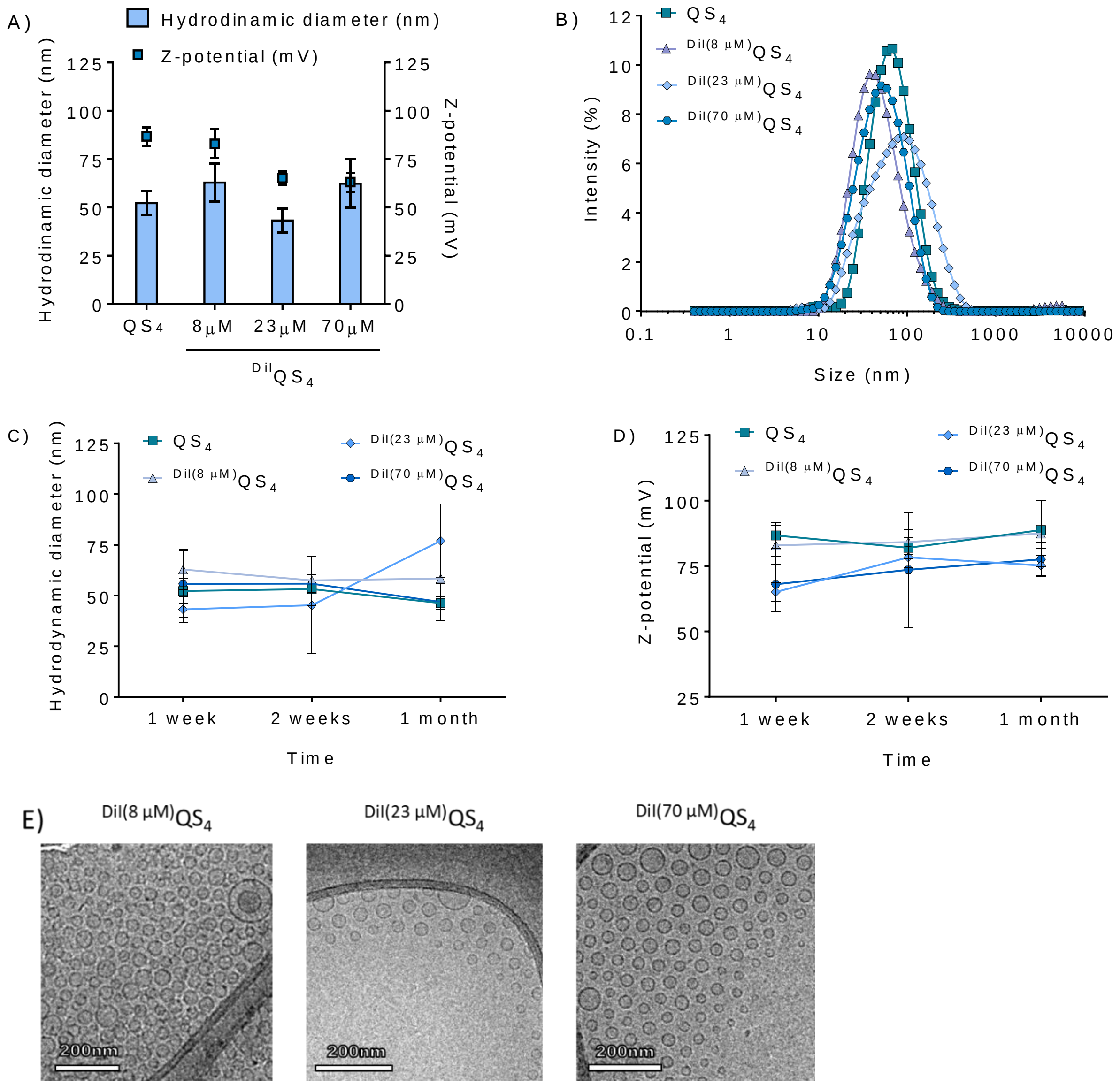

Figure 67. Physicochemical properties of the indicated QS₄ labelled with DiI fluorophore, at different dye concentrations (8, 23 and 70 µM), are similar for non-labelled QS₄ after diafiltration. A-B) Hydrodynamic diameter and surface charge density **(B)** of QS₄ labelled with DiI at three different concentrations (8, 23 and 70 µM) measured by DLS technique. **C)** Particle size distribution of ^{DiI}QS₄ at three concentrations of DiI, compared to non-labelled QS₄, measured by DLS technique. Particle size **(C)** and Z-potential **(D)** stability over time of ^{DiI}QS₄ at three concentrations of DiI, compared to non-labelled QS₄, measured by DLS technique**. E)** High resolution Cryo-TEM images of ^{DiI}QS₄ at the increasing DiI concentration 8, 23 and 70 µM. Scale bar, 200nm.

Finally, the final concentration of ^{DiI}QS$_1$ and ^{DiI}QS$_4$ systems was determined by lyophilization (see Table 14). Hence, the final concentration of ^{DiI}QS$_1$ at 70 µM was 3.4 mg/mL, while the final concentration of ^{DiI}QS$_4$ at 8, 23 and 70 µM was 1.9, 1.1 and 1.8 mg/mL, respectively (Table 14).

Optical properties of $^{DiI}QS_4$

The absorption spectra of $^{DiI}QS_4$ showed how an increase of DiI in QS_4 membrane resulted in a higher absorbance of the sample (Figure 68A). Also, the fact that DiI loaded QS_4 had the same absorbance that the free DiI monomer in ethanol (at the same concentration) indicates that most likely DiI behaves like a free dissolved monomer in ethanol, when it is dissolved in the QS membrane.

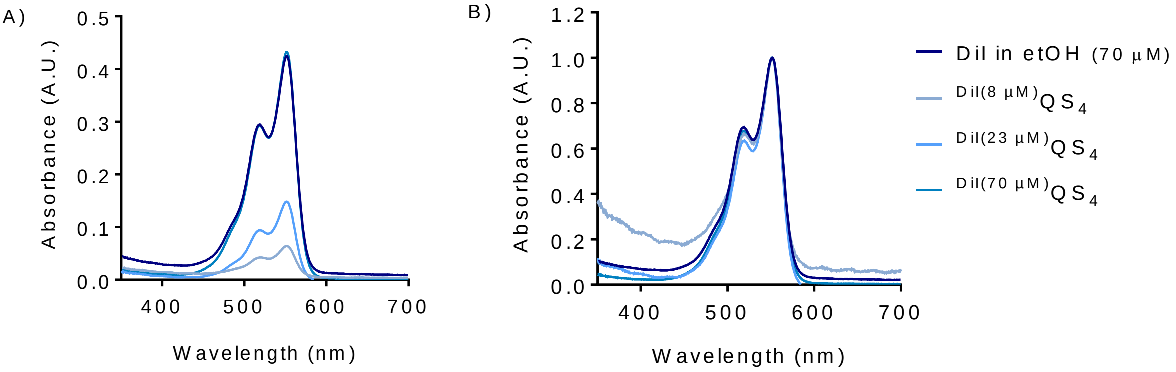

Figure 68. Optical properties of $^{DiI}QS_4$ at different DiI loadings, in comparison to DiI optical properties in ethanol. Absorption spectra **(A)** and normalized absorption spectra **(B)** of QS_4 labelled with DiI and monomeric DiI in ethanol (70 µM). The normalized spectra were obtained dividing each spectrum by the value of maximum absorbance. Graph represents the mean of duplicate measures.

The comparison between the DiI absorption spectra, when it is dissolved in the QS membrane and when its dissolved in etOH, gives information about the degree of aggregation of DiI when it is dissolved in QS membrane. To fully ensure that the DiI was not aggregated in QS_4 surface, the absorbance spectra were normalised by their peak of maximum absorption. In the normalized spectra (Figure 68B), no major shift on the spectra of $^{DiI}QS_4$ was observed compared to the spectra of free DiI dissolved in ethanol and the ratio between the two spectral peaks was also the same. This means that there was no sign of J- nor H- aggregates of DiI in the QS_4 membrane. Thus, DiI maintained the fluorescent characteristics after their integration in QS_4, which means that the labelling of QS with DiI has the required characteristics for the further FRET measurements.

4.3.2. ^{DiI}QS present similar complexation efficiency than plain QS

^{DiI}QS-miRNA complexes were prepared by incubation of miR-Control (Cy5) with the different ^{DiI}QS formulations in PBS, using the detailed protocol explained before (see section 3.2.12).

Morphology of $^{DiI}QS_4$-miRNA complexes

Cryo-TEM images of $^{DiI}QS_4$-miRNA complexes were acquired to compare their morphology to plain QS_4 (Figure 69). Despite complexes prepared with $^{DiI}QS_4$-miRNA at 8 and 23 µM of DiI seemed bigger, all systems were similar with bunch structures.

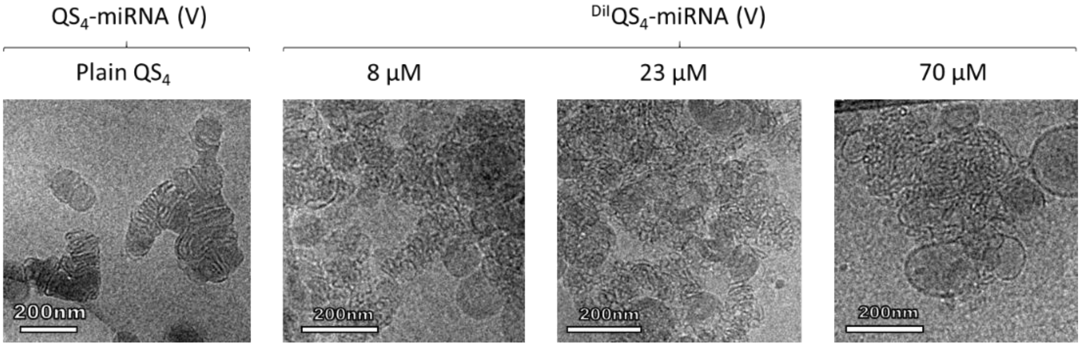

Figure 69. $^{DiI}QS_4$-miRNA complexes presented similar morphology and lamellarity despite being labelled with DiI at different concentration in QS_4 surface. High resolution representative Cryo-TEM images of loading (V) of $^{DiI}QS_4$-miRNA complexes at different DiI concentrations compared with plain QS_4. From left to right the QS_4 labelling with DiI increases. Scale bar, 200nm.

High complexation efficiency of ^{DiI}QS-miRNA complexes

To check the miRNA complexation efficiency of ^{DiI}QS, ^{DiI}QS-miRNA complexes at eight different loadings (I-VIII) of miRNA attached to QS (see Table 16-Table 17) were loaded in agarose gels. As was explained before, the complexation efficiency was determined by an inverse correlation with the signal of the naked miRNA.

Plain QS_1 and $^{DiI(70\ \mu M)}QS_1$ conjugated with miR-Control (Cy5) presented a fully miRNA complexation even if at high loadings of miRNA in QS (i.e. VI) (Figure 70). Hence, incorporation of DiI in QS membrane did not interfere in the miRNA complexation with QS.

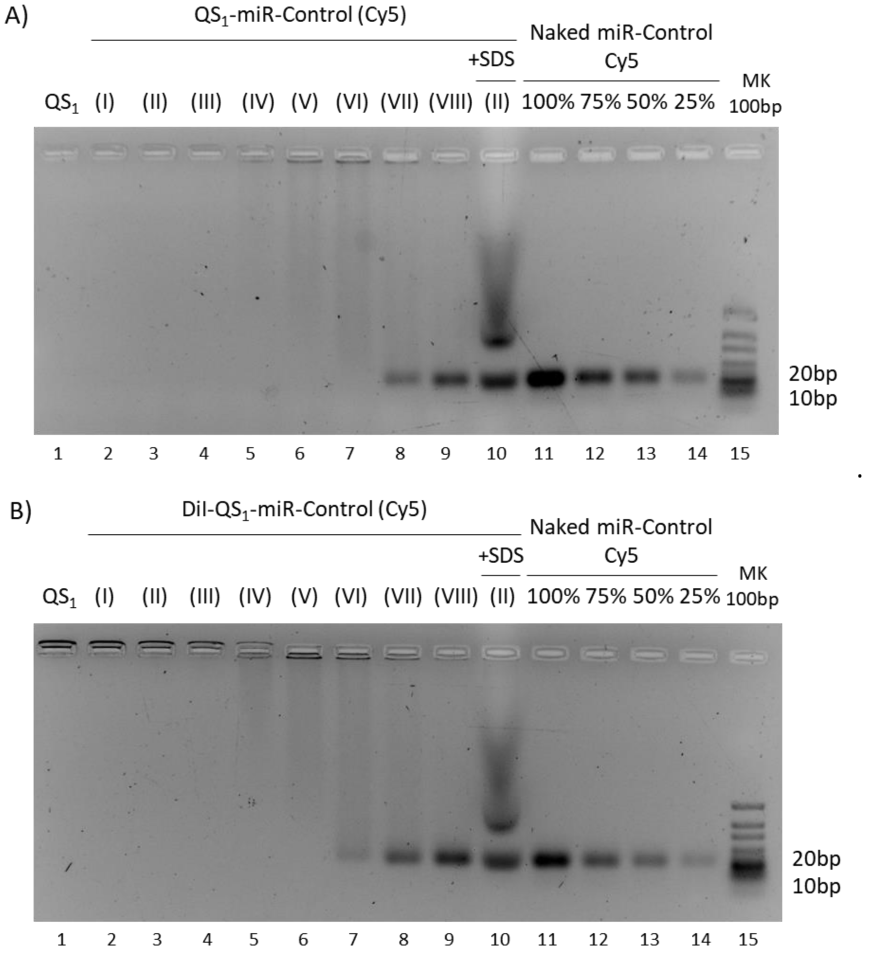
A)
QS1-miR-Control (Cy5)
Naked miR-Control
Cy5
+SDS
MK
100bp
QS1 (I) (II) (III) (IV) (V) (VI) (VII) (VIII) (II) 100% 75% 50% 25%
20bp
10bp
1 2 3 4 5 6 7 8 9 10 11 12 13 14 15
B)
DiI-QS1-miR-Control (Cy5)
Naked miR-Control
Cy5
+SDS
MK
100bp
QS1 (I) (II) (III) (IV) (V) (VI) (VII) (VIII) (II) 100% 75% 50% 25%
20bp
10bp
1 2 3 4 5 6 7 8 9 10 11 12 13 14 15

Figure 70. High miRNA complexation efficiency of DiI labelled or non-labelled Quatsomes (QS_1) prepared in PBS. A-B) Representative gel electrophoresis showing the miRNA complexation efficiency with non-labelled QS_1 **(A)** or with DiI labelled QS_1 **(B)** diluted in PBS. QS free were loaded in lane 1 and the various loadings of QS-miRNA (I-VIII) were loaded in lanes 2-10. Complexes were treated with SDS and loaded in lane 10. Standard calibration of miRNA naked was loaded as a negative control in lanes 11-14. These experiments were done in duplicate. All QS-miRNA complexes are described in Table 16-Table 17.

On the other hand, $^{DiI}QS_4$-miRNA complexation was also studied in comparison with plain QS_4-miRNA. In this case, $^{DiI}QS_4$-miRNA labelled with DiI concentration of 8 µM presented the same complexation efficiency as plain QS_4, at lowest loading QS-miRNA (VIII) (Figure 71A). Whereas, $^{DiI}QS_4$-miRNA prepared at DiI concentration of 23 and 70 µM had already a fully miRNA complexation at loading QS-miRNA (VIII) (Figure 71B). Thus, the addition of DiI in QS_4 surface did not decrease the QS_4 capacity to complex miRNA.

Moreover, after SDS treatment free miRNA was observed in the bottom of the gel due to the miRNA release from QS (Figure 70A-B, lane 10; Figure 71A-B, lanes 6 and 12).

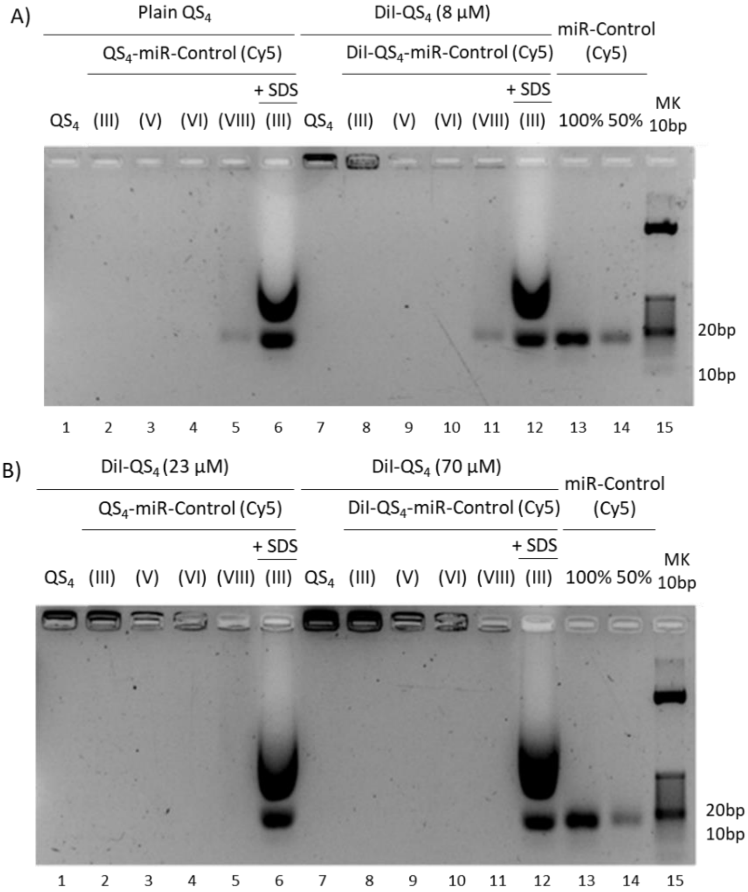
A)
Plain QS4
DiI-QS4 (8 µM)
QS4-miR-Control (Cy5)
DiI-QS4-miR-Control (Cy5)
miR-Control (Cy5)
+ SDS
+ SDS
QS4 (III) (V) (VI) (VIII) (III) QS4 (III) (V) (VI) (VIII) (III) 100% 50%
MK 10bp
20bp
10bp
1 2 3 4 5 6 7 8 9 10 11 12 13 14 15
B)
DiI-QS4 (23 µM)
DiI-QS4 (70 µM)
QS4-miR-Control (Cy5)
DiI-QS4-miR-Control (Cy5)
miR-Control (Cy5)
+ SDS
+ SDS
QS4 (III) (V) (VI) (VIII) (III) QS4 (III) (V) (VI) (VIII) (III) 100% 50%
MK 10bp
20bp
10bp
1 2 3 4 5 6 7 8 9 10 11 12 13 14 15

Figure 71. High miRNA complexation efficiency of DiI labelled QS4 compared to plain QS4. A-B) Representative gel electrophoresis showing the miRNA complexation efficiency with DiI labelled or non-labelled QS4 diluted in PBS. QS free were loaded in lane 1 and 7 and the various loadings of QS-miRNA (III-VIII) were loaded in lanes 2-6 or 8-12. Complexes were treated with SDS and loaded in lane 6 or 12. Standard calibration of miRNA naked was loaded in lanes 13-14. All QS-miRNA complexes are described in Table 16-Table 17.

4.3.3. Fluorescent QS4-miRNA complexes demonstrated FRET efficiency

In collaboration with the group of Dr. Lorenzo Albertazzi from Institute de Bioingenieria de Catalunya (IBEC) and Institute for Complex Molecular Systems (TU/e), we determined if DiI incorporated in QS4 surface is enough close (distance < 10 nm) to perform FRET with the Cy5 fluorophore added in the miRNA backbone after QS-miRNA complexes formation. First, the emission spectra of DiI loaded in QS4 was analysed to determine the maximum excitation of DiI (Figure 72A). At ʎ= 530nm DiI had the peak of excitation and a good emission peak was observed. Lower excitation wavelengths resulted in lower emission intensity, while higher wavelengths overlapped with the DiI excitation peak. DiI emission spectra was identical to was reported in literature, showing no sign of fluorophore aggregation. QS4 loaded with a higher amount of DiI showed, as expected, a higher emission intensity (Figure 72A and Figure 68).

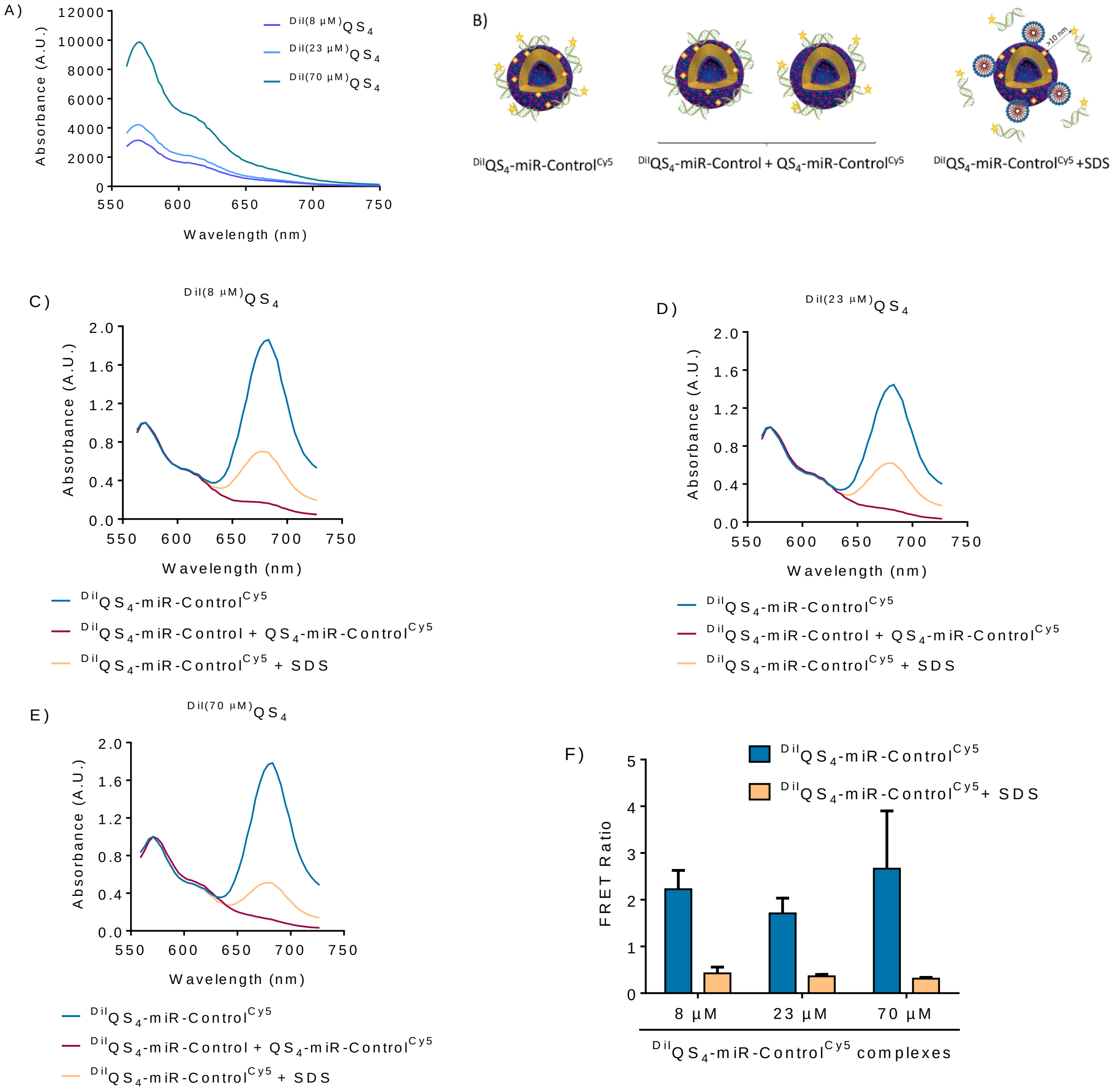

Figure 72. Complexes of miRNA labelled with Cy5 and QS$_4$ labelled with DiI at three different concentrations (8 µM, 23 µM and 70 µM) produce FRET. A) Emission spectrum of QS labelled with DiI excited at λ = 530nm. **B)** Schematic representation of the ^{DiI}QS$_4$-miR-Control^{Cy5} system, in which occur FRET (on the left), the ^{DiI}QS$_4$-miR-Control plus QS$_4$-miR-Control^{Cy5} system (in the middle) and the ^{DiI}QS$_4$-miR-Control^{Cy5} system treated with SDS (on the right). In the ^{DiI}QS$_4$-miR-Control^{Cy5} system, QS$_4$ and miRNA were labelled with DiI (rhombus symbol) and Cy5 (star symbol), respectively. **C-E)** Emission spectra of complexes prepared with Cy5 labelled miRNA and QS$_4$ loaded with DiI. The ^{DiI}QS$_4$-miR-Control^{Cy5} system (blue) corresponds to the complexes with both miR-Control labelled with Cy5 and QS$_4$-DiI. The magenta spectra correspond to the addition of the spectra of ^{DiI}QS$_4$-miR-Control (non-labelled miRNA) plus the spectra of QS$_4$-miR-Control^{Cy5} (non-labelled QS). After SDS addition the spectra of ^{DiI}QS$_4$-miR-Control^{Cy5} system was observed. **F)** Graph of the FRET ratio obtained from emission spectrum of ^{DiI}QS$_4$-miR-Control^{Cy5} complexes with or without SDS addition. The values are represented as the mean ± SD from duplicate experiments.

A schematic representation of the systems studied is shown in Figure 72B. The $^{DiI}QS_4$-miR-Control^{Cy5} system was formed by the conjugation of $^{DiI}QS_4$ with the miR-Control labelled with Cy5, while the control system was obtained from the sum of the emission spectra by the complexes prepared with the $^{DiI}QS_4$ with non-labelled miR-Control and the plain QS_4 with the labelled miR-Control^{Cy5}. The emission spectra of Cy5-labelled miRNA and DiI-labelled QS_4 was recorded upon excitation at λ_{exc} = 530 nm. The FRET efficiency of the $^{DiI}QS_4$-miR-Control^{Cy5} was evaluated for the DiI loaded QS_4 at three different concentrations of DiI (8, 23 and 70 µM). Finally, the $^{DiI}QS_4$-miR-Control^{Cy5} system was treated with SDS to unbind the miRNA from the QS_4 surface and to observe the reduction in the FRET ratio due to the increased distance between the labelled miRNA and $^{DiI}QS_4$ after their separation (Figure 72B-E). All the emission spectra were normalized with respect to the maximum intensity of the donor (DiI) to monitor the variation in relative intensity of the acceptor (Cy5). Upon excitation, complexes labelled with both fluorophores, called $^{DiI}QS_4$-miR-Control^{Cy5} system, presented a first peak at 570 nm, due to the excitation of DiI and a second one at 683 nm, which corresponded to the FRET emission of Cy5. This second peak was not appreciated in the control systems, because there were not complexes loaded simultaneously with both fluorophores. These results showed that when the complexes were formed with both, Cy5 labelled miRNA and $^{DiI}QS_4$, the fluorophores were close enough to transfer the energy from the donor (DiI) to the acceptor fluorphore (Cy5), which emitted fluorescence. Whereas, after SDS addition the second peak was reduced due to the miRNA release from QS_4 surface and, consequently, the FRET ratio efficiency was reduced (Figure 72B-E).

Among the QS_4 with increasing concentrations of DiI, the one with the highest concentration of DiI ($^{DiI(70\ \mu M)}QS_4$) was selected as the optimum to observe *in vitro* miRNA release. So, further experiments were done with QS prepared at 70µM of DiI, $^{DiI(70\ \mu M)}QS_1$ or $^{DiI(70\ \mu M)}QS_4$.

4.3.4. miRNA is released from QS_4 after transfection

MiRNA release from QS_4 surface was studied by FRET using live cell confocal imaging. The $^{DiI}QS_4$-miR-Control^{Cy5} system was compared with the $^{DiI}QS_4$-miR-Control plus QS_4-miR-Control^{Cy5} systems (Figure 72B). At time zero and after 30 minutes, the FRET ratio of $^{DiI}QS_4$-miR-Control^{Cy5} was high (mean ~ 3), owing to the large percentage of green dots (high FRET efficiency) versus magenta (low FRET efficiency) (Figure 73A-B). These results suggest that there is no release of miRNA prior the cellular internalization of the QS-miRNA complexes during their incubation with NB cells in IMDM supplemented with 10% FBS.

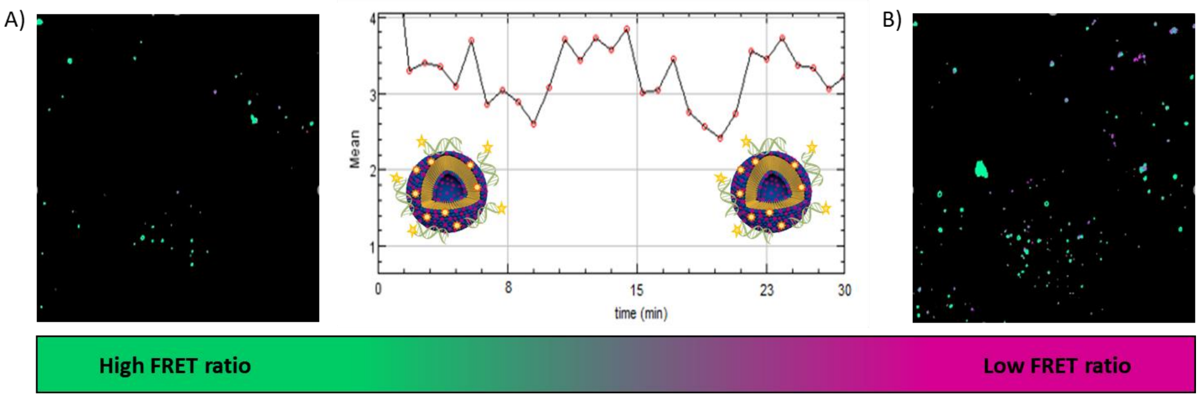

Figure 73. QS_4-miRNA complexes remain stable prior to cell transfection. Images at time zero **(A)** and after 30 min of incubation **(B)** of $^{DiI}QS_4$-miR-Control^{Cy5} complexes. When miRNA molecules are attached to QS the system presents high FRET efficiency (represented in green). Meanwhile, when miRNA molecules are not attached to QS the system presents low FRET efficiency (represented in magenta).

After 30 minutes of complexes incubation in SK-N-BE(2) cells, cell media was replaced to remove the non-internalized complexes and follow the miRNA release after cell transfection. Right after complex formation, the FRET ratio is high because the miRNA is attached to the QS_4 membrane (Figure 74A and C). At longer incubation times, the FRET ratio gradually decreases, which means that miRNA is released from the QS_4 surface after o/n transfection (Figure 74B and C).

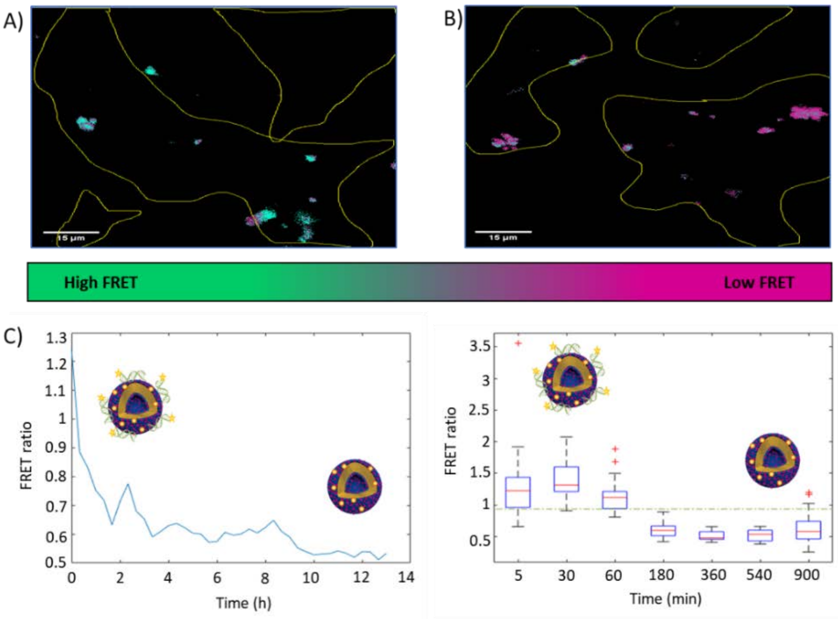

Figure 74. QS_4-miRNA complexes are separated after overnight transfection in SK-N-BE(2) cells. Images at time zero **(A)** and fourteen hours post-transfection **(B)** of $^{DiI}QS_4$-miR-Control^{Cy5} complexes. When miRNA molecules are attached to QS the system presents high FRET efficiency (represented in green). However, when miRNA molecules are separated from QS, FRET efficiency is lost (represented in magenta). **C)** Graphs of the FRET ratio of $^{DiI}QS_4$-miR-Control^{Cy5} complexes over time.

In order to determine if the miRNA release from QS$_4$ caused the different effects observed in targets modification after QS-miRNA complexes transfection, the FRET ratio of ^{DiI}QS$_1$-miR-Control^{Cy5} complexes was checked. Figure 75 shows that before (Figure 75A) and after overnight incubation (Figure 75) FRET ratio of ^{DiI}QS$_1$-miR-Control^{Cy5} complexes remained stable and the miRNA was not released from QS$_1$.

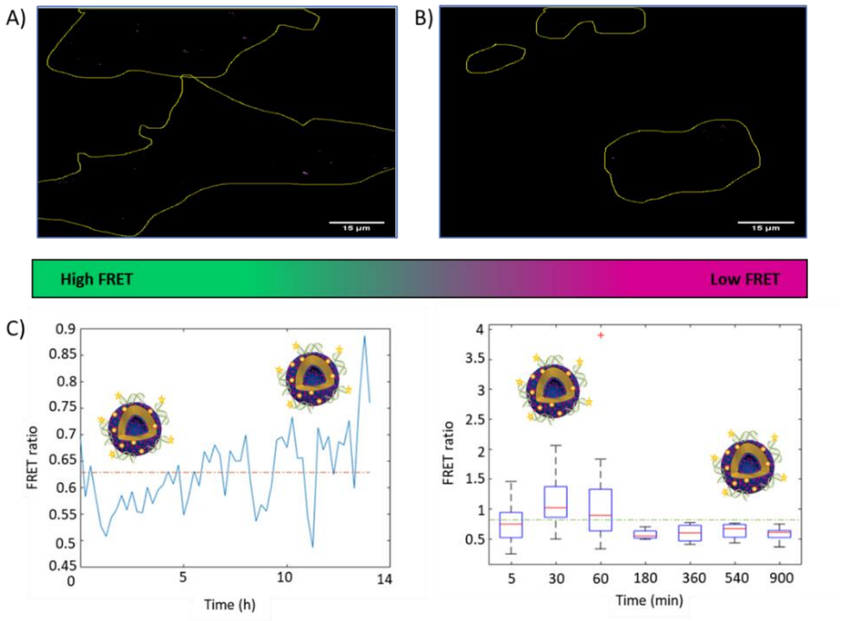

Figure 75. QS$_1$-miRNA complexes remain attached after overnight transfection in SK-N-BE(2) cells. Images at time zero **(A)** and fourteen hours post-transfection **(B)** of ^{DiI}QS$_1$-miR-Control^{Cy5} complexes. When miRNA molecules are attached to QS$_1$ the system presents high FRET efficiency (represented in green). However, when miRNA molecules are de-attached from QS, FRET efficiency is lost (represented in magenta). **C)** Graphs of the FRET ratio of ^{DiI}QS$_1$-miR-Control^{Cy5} complexes over time.

Lastly, QS$_4$-miRNA complexes that do FRET could be used to understand and predict the behaviour of their components inside the cells, in physiological solutions (e.g. serum, bloodstream) and their biodistribution and accumulation after *in vivo* administration.

Summary and perspectives:

In this section, it is described the preparation of QS-miRNA complexes showing FRET, in order to study their cellular internalization and understand their biological properties. In particular:

- QS_4, composed of DC-Chol and MKC, were labelled with DiI and maintained the excellent physicochemical properties of plain QS_4.
- $^{DiI}QS_4$ had a similar miRNA complexation capacity than QS_4; and the morphology of the labelled $^{DiI}QS_4$ and $^{DiI}QS_4$-miRNA^{Cy5} complexes were also similar to those non-fluorescent ones.
- $^{DiI}QS_4$ were able to maintain attached the Cy5-miRNA in complexes before their internalization and release the miRNA in the cytoplasm after overnight of transfection. On the contrary, $^{DiI}QS_1$, composed of Cholesterol and MKC, did not release the miRNA after cellular internalization.

In summary, $^{DiI}QS_4$ is an efficient nanovesicle for the intracellular delivery of sRNA because allow the miRNA release from QS_4 surface in order to express its functionality.

5. DISCUSSION

5. DISCUSSION

5.1. The present and the future of RNA-based therapies

In the last ten years, researchers and clinicians have made several efforts to develop novel treatments for cancer. However, most of the studies are focused on treatments for adult cancers (~ 30%) or that could be effective for both, adult and children (~ 50%). Only 13% of the orphan medicines currently in development are specific for children patients. One of these few examples is a new biological medicine called Qarziba®, which, was commercialized in 2017 to treat high-risk neuroblastoma tumours. Although Qarziba's efficacy was not considered optimal and its dose is limited owing to immunogenicity, its benefits were considered higher than risks and Qarziba was authorised for NB treatment. Among childhood cancers, NB is the third most prevalent. Despite NB patients with low and intermediate risk are cured in high rates, more than 60% of patients with high-risk NB tumours are not cured[34,40]. Thereby, the poor outcome of high-risk NB tumours and the lack of an effective treatment due to the resistance of these patients to conventional therapies generate an unmet clinical need. Moreover, the aggressive and intensive standard treatments cause severe and long-lasting side effects in these patients. For these reasons, it is important to discover new therapies to solve the clinical needs of high-risk NB patients and to improve their quality of life.

On the other hand, owing to the multiple mechanisms implicated in high-risk NB resistance to conventional therapies, it is unlikely that treatments addressed to a single target will be enough to treat NB tumours successfully. Therefore, the identification of new targets able to regulate multiple cellular processes may improve the treatment response and minimize the risk of resistance[52]. Currently approved medicines are directed to target druggable proteins that interact with less than 700 gene products, meaning that only 0.05% of the human-genome is druggable. On the contrary, directly targeting mRNA proteins difficult to target or undruggable could be modulated. Furthermore, approximately 70% of the human genome is transcribed into non-coding RNA[2]. Hence the use of RNA-based therapies, to modulate coding and non-coding RNA, will expand the number of druggable targets[1]. One the most conventionally-used methodologies to target RNA is the use of small RNA molecules, such as miRNA or siRNA. Moreover, the use of RNA molecules to modify gene expression without altering the host DNA sequence, will end up in fewer and non-permanent side-effects. From the therapeutic point of view, miRNA are one of the most studied RNA molecules. MicroRNA are small non-coding RNAs (~ 20nt) which interact with target mRNAs inducing translation repression or mRNA degradation. Mounting evidence show miRNA to be deregulated and functionally contributing to the development and progression of different human diseases such as cancers, including NB[14,196].

Different approaches for miRNA-based therapies must be applied depending on whether the target miRNAs are upregulated (behaving as oncogenes) or downregulated (behaving as tumour suppressors)[197]. While upregulated miRNAs could be inhibited using antimiRs, miRNA with tumour suppressor functions should be restored using miRNA mimics[47]. In advanced NB, an overall reduction in miRNA was observed, mainly due to alterations in the miRNA processing machinery[198]. Therefore, restoration of miRNA, with tumour suppressor functions represents an attractive novel therapeutic approach for this type of tumour (reviewed in [40]).

On the other hand, the radio- or chemoresistance observed in paediatric solid tumours is the main reason for treatment failure and relapse in NB patients. Thereby, miRNA ability to simultaneously modulate multiple target genes involved in tumorigenic processes simultaneously, render miRNA to be suitable candidates to be used as a miRNA restoration therapy for improving the clinical response of NB patients with chemoresistance[199]. Despite, multiple pharmaceutical companies had already included miRNA in their developmental drug pipelines (e.g., miR-34[128,155], miR-16[200], miR-122[201]) and some of them entered in clinical trials, they have not reached the market yet or fail in phase I or II of clinical trials (Table 3). Of note, none of these studies target the paediatric population. Therefore, the promotion of new programs for paediatric tumours using miRNA replacement therapies could provide a therapeutic opportunity for high-risk NB patients.

5.2. Finding tumor-suppressive miRNAs in NB

Chen and Stallings demonstrated that many miRNA loci are differentially expressed in different genomic subtypes of NB. It was further noted that a large number of miRNA are downregulated in MYCN amplified NB tumours, which was also correlated to NB progression, aggressive NB phenotype and poor outcome in patients[41,198]. Thereby, miRNA restoration therapies may improve the opportunities to treat NB patients with chemoresistance, due to a single miRNA can inhibit multiple targets involved in tumorigenic processes[157]. Hence, the first step of this thesis was the identification of a tumour-suppressive miRNA with the highest therapeutic potential in NB. The high-throughput functional screening performed allowed us to identify miRNA with tumour suppressor functions in NB. Of the 2048 miRNA tested, we identified 52 that significantly reduced cell proliferation with a Z-score lower than − 2 (~ 50% of cell proliferation). Concurring with previous reports, multiple tumour-suppressive miRNA, such as members of the let-7 miRNA tumour-suppressive family (e.g., let-7i-5p, let-7a-3p, let-7f-2-5p, let-7g-5p or let-7e-3p[202,203]), were also identified in our screening, thereby validating our approach to identifying tumour-suppressive miRNA.

Notably, 7 of the 52 miRNA (13.5% of the total) that showed to reduce cell proliferation ~ 50% are encoded in the 14q32 genomic region. This region is frequently altered in cancer and particularly in NB[45], which raises the possibility that this region contains tumour-suppressor genes. All 7 miRNA identified in our screening showed the capacity to reduce cell proliferation in multiple NB cell lines *in vitro*, being miR-323a-5p the one with highest therapeutic potential.

MiR-323a-5p is located in the 14q32 locus, region frequently altered in cancers, including NB. 14q32 region is epigenetically lost in NB, with the subsequent reduction of several miRNA with tumour suppressor functions, such as miR-323a-5p[45]. However, miR-323 functions seem to depend on the tumour tissue, because in glioma cells higher expression of miR-323a-5p was correlated with increased glioma progression[204] while in NB[157,205] and bladder cancer[206] have tumour suppressor functions. Despite miR-323 is implicated in prostate cancer progression, differentiation of normal B cells[207], bladder cancer[206] and medulloblastoma[207], among other cancers[208], the mature form of miR-323a-5p has been less studied than miR-323a-3p. Zeka et al., demonstrated that miR-323a-3p expression was associated with metastatic stage four NB[209]. Bray and their colleagues demonstrated that MYCN amplification significantly affected the miRNA expression in NB tumours and, in consequence, the dysregulation of miRNA may predict clinical outcome of NB patients[210]. In order to correlate the miR-323a-5p expression levels with the clinical parameters and outcome in NB patients, a large cohort of NB tissue samples was analysed. These results showed that low expression levels of miR-323a-5p were observed in NB tumours with MYCN genomic amplification (Figure 76A) and were correlated to short overall patient survival (Figure 76B)[211]. Hence, the restoration of miR-323a-5p expression levels may be a potential therapeutic alternative tool to conventional therapies against high-risk NB.

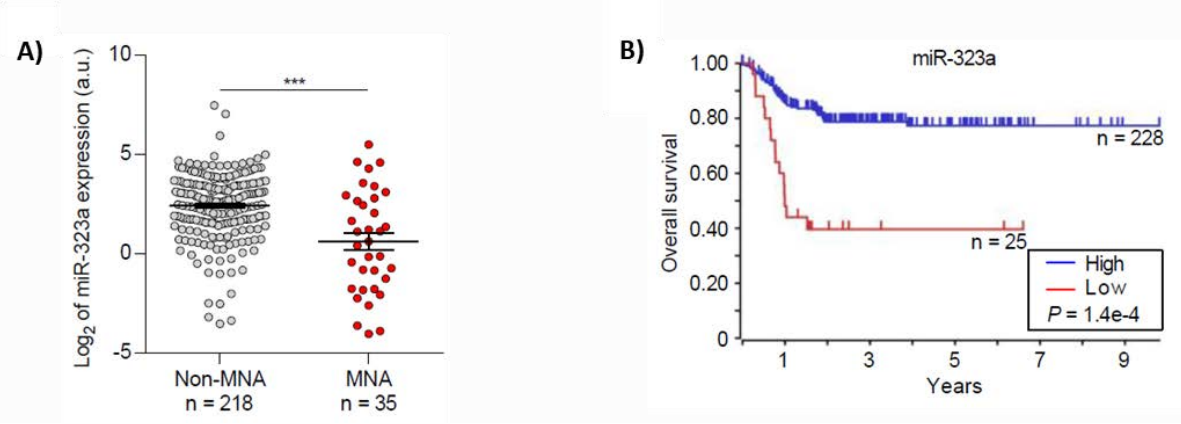

Figure 76. MiR-323a-5p expression levels correlated with clinical parameters. A) Relative expression ($\log_2$) of miR-323a in MNA and non-MNA NB tumors. **B)** Overall survival Kaplan–Meier plot of the indicated miRNA expression in human NB tissues.

Here, we demonstrated that the ectopic expression of miR-323a-5p suppressed cell growth through the direct modulation of several cell cycle-associated genes such as CCND1, CHAF1A, INCENP and FADD and caused a G1 cell cycle arrest followed by induction of apoptosis. The silencing of the miR-323a-5p direct targets CHAF1A, INCENP and CCND1 were those that more closely recapitulate the phenotypic effects of miR-323a-5p overexpression. CCND1 is a well-established oncogene frequently overexpressed and associated with poor outcome in different types of tumours including NB[212]. CCND1 interacts with CDK4 and CDK6 and the activation of this complex phosphorylates RB and other transcription factors which promote cell cycle progression[189]. To date, the best approach to targeting CCND1 is using CDK4/6 inhibitors such as palbociclib, ribociclib and abemaciclib. Although the best-known functions of CCND1 are related to cell cycle control, CCND1 has CDK-independent functions. For example, CCND1 regulates cell differentiation by binding to several transcription factors such as the estrogen receptor α and the androgen receptor (reviewed in [213]). Therefore, a direct inhibition of CCND1 could be therapeutically more effective than CDK4/6 inhibition.

Another of the newly identified relevant miR-323a-5p target is CHAF1A, a chromatin modifier protein recently involved in maintaining the undifferentiated state of highly aggressive NB[214].

The silencing of INCENP phenocopied the apoptosis induction of miR-323a-5p overexpression. INCENP (inner centromere protein) is a component of the chromosomal passenger complex (CPC), a complex that regulates mitosis. INCENP is a scaffolding subunit for the CPC and activates Aurora B kinase[215]. Similar to CHAF1A, high levels of INCENP in primary NB tumours are associated with poor prognosis (Supplementary Table 6 from Soriano *et al.,*[157]). Thus, in addition to halting cell cycle progression, miR-323a-5p could also be relevant for NB therapy through repressing the expression of genes that block the differentiation and induced apoptosis in NB cells.

Considering these results, miR-323a-5p restoration might present high potential therapeutic as an alternative treatment for high-risk NB patients with resistance to conventional therapies.

5.3. Clinical delivery of microRNAs

To use miRNAs as a medicinal product, there are numerous challenges that need to be solved. For example, naked miRNA, which are hydrophilic and poly-anionic biomolecules, have low cellular penetration[95], may activate the immune response[216] and have short half-life in blood leading to a rapid clearance[95,216]. In order to improve the miRNA cellular internalization and efficacy over modulating the expression of miRNA target genes, the application of nanomedicine field can help to solve these difficulties. Hence, the miRNA conjugation with a nanocarrier is a promising strategy for the implementation of the miRNA therapies into the clinics.

To date, a large number of nanocarriers have been developed and engineered to improve drug delivery, increase their efficacy and reduce side-effects. Despite a wide range of nanocarriers based on organic, inorganic, lipid, polymers or glycan compounds have been employed to load and carry chemotherapeutic agents, few of them reach the clinical trials when they load small RNA (sRNA) molecules. Among the clinical trials that include the use of sRNA, most of them have been conducted using siRNA. Nanocarriers for nucleic acids delivery are usually composed of lipids, phospholipids and/or polymers[95,135,216]. Although, several of them have reached Phase II of clinical trials, few of them have achieved Phase III or have reached the market. One of them is Eteplirsen (Exondys 51®) is a non-conjugated phosphorodiamidate morpholino antisense oligonucleotide approved by FDA to treat Duchenne muscular dystrophy patients. However, the small amounts of dystrophin expression restored by Exondys treatment induced modest effects[217]. Another example is Patisiran (Onpattro®), which is a double-stranded siRNA encapsulated in a lipid nanoparticle for the treatment of the polyneuropathy of hATTR (NCT01960348)[218]. It is not unexpected that Patisiran have a highly efficient delivery of siRNA to their target tissue, because liver is the primary organ where drugs accumulate after their intravenous infusion[121]. Differentially to siRNA, miRNA used as RNAi therapeutics only have reached Phase II. One of the most advanced molecules was MRX34, miR-34 lipoplexes with Smarticles (NCT02862145), which arrived at phase II, but it was withdrawn due to the immune adverse effects observed[132,155]. Another example is Miravirsen®, which is composed by the LNA antimir-122 and is directed to treat chronic hepatitis C patients. Like happens with Patisiran®, Miravirsen® targets liver cells, thus favoured its efficacy (NCT01200420)[219]. Considering all ongoing clinical trials, liposomes are the most used NP for the development of nanomedicines based on nucleic acids. Although they present good performance, they present some unsolved drawbacks. Among them the most important ones are short colloidal stability, difficulties in their scale-up at industrial level[138] and, in several cases, immune adverse effects *in vivo* have shown, which can be caused by proinflammatory cytokines, liver damage indicated by elevated transaminases, leukopenia or trombocytopenia[220]. For this reason, the selection of a suitable nanocarrier to solve these pitfalls is essential.

5.4. Quatsomes as a nanomedical-delivery platform

Among the wide range of nanomaterials currently available, the demand of improved nanotechnology platforms for sRNA delivery require the development of a new nanocarrier for sRNA clinical administration. In the last years, Nanomol group from the Institute of Material Science of Barcelona (ICMAB) has developed Quatsomes (QS), a new class of lipid non-liposomal nanovesicles[138]. QS are composed by sterols, such as Cholesterol or β-sitosterol, and quaternary ammonium surfactants, such as CTAB and myristyl trimethyl ammonium bromide (MTAB). Ferrer-Tasies et al., demonstrated that QS based on the self-assembly of Chol and CTAB in aqueous solution can form stable unilamellar nanovesicles[171]. Meanwhile, both components separately in aqueous solution formed CTAB micelles or crystals of Chol. Cabrera et al. demonstrated that QS and QS-bioactive conjugates could be prepared by a single-step and green methodology, named DELOS-SUSP, based on the use of compressed CO_2, which has a high batch-to-batch consistency and shows reproducibility upon scaling-up[172]. Moreover, the preparation of QS by DELOS-SUSP allow QS membrane components to self-organise into exceptional homogeneous vesicles with nanometric size (D_h ~ 100nm), small polydispersity (PDI ~ 0.25) and unilamellar spherical shape. Compared to liposomes, QS demonstrated a long-term colloidal stability (for several years), high vesicle-to-vesicle homogeneity and their morphology do not change upon rising temperature (up at least 70°C) or dilution[171]. According to these properties, QS are promising colloidal nanoparticles to improve the stability and the efficacy of therapeutically active biomolecules and for the development of new medicines, based on nanotechnology[172]. Regarding the fact that QS are positively, due to the presence of quaternary ammonium surfactants in their membranes, like CTAB, they can easily transport negatively charged molecules through electrostatic interactions. QS can be also easily functionalized with targeting ligands, through their covalent attachment to the membrane components of QS. For example, RGD peptides can be conjugated to QS to promote QS cell internalization thanks to the interaction of RGD peptides with extracellular membrane proteins or integrins[221].

Furthermore, to increase the blood circulation time of bioactives QS can be functionalised with a stealth polymer such as PEG[222]. This modification can avoid protein corona formation and the clearance of QS complexes by the mononuclear phagocyte system (MPS) (patent nº WO2014/001509)[172]. PEGylated QS present also a nanometric size (D_h< 100 nm), high homogeneity and positive charge (ζ-potential > 30 mV), which ensure their high stability under storage conditions over time and low cellular toxicity[172].

Finally, QS can be efficiently functionalised, by electrostatic or lipophilic interactions, with different families of fluorophores, such as carbocianines[176], diketopyrrolopyrroles[223] or fluorenyl derivates[195], which convert them in promising probes for bio-imaging and theragnostic applications.

5.4.1. QS as a nanocarriers for protein-based medicinal products

QS have already been used for the development of a new nanomedicine candidate for the topical treatment of complex wounds, such as diabetic foot ulcers (patent nº WO2014/019555). In this case, epidermal growth factor (EGF) is integrated into QS without considerable size increase (D_h ~ 100-150nm), maintaining unilamellarity, stability over time and high entrapment efficiencies (~ 99%). In rat models, QS-EGF were capable to stimulate wound healing process, epithelial migration and fibro-angiogenic response[224]. Phase I/II clinical trial for the topical treatment of chronic venous ulcers are currently under design in the frame of Nanonafres RIS3CAT project. In addition to tissue reparation properties, EGF-QS nanoconjugates have antimicrobial activity that kill microorganisms, such as gram-positive and some gram-negative bacteria and fungus, and thus, can prevent nosocomial infections in the diabetic foot patients[225].

5.4.2. QS as potential nanocarriers for small RNAs

Despite liposomes are the most frequently used class of drug delivery nanoparticles, their translation from the bench to the market is still challenging[123], mainly due to their frequent colloidal instability and difficulties in their scaling-up.

Quatsomes, like liposomes are also vesicular structures, composed by a closed bilayer formed by the molecular assembling of amphiphilic molecules, but on the contrary to liposomes they have a high colloidal stability. Considering the high colloidal stability of QS and the positive charge of their surface, the application of QS as a nanocarrier to deliver nucleic acids seems promising. In this thesis, a new type of QS has been engineered for the intracellular transport of sRNA, such as microRNA or siRNA, through electrostatic interactions with the negative charges of the sRNA backbone. In the frame of this thesis, all the sRNA-QS conjugates were prepared by incubation. By using this preparation procedure, and as it is schematically represented in Figure 24C, only the QS positive charges of the outer bilayer can interact with the negative charges of the sRNA, since the charges of the QS inner bilayer are inaccessible.

Selection of QS membrane components

In order that QS can be used for the clinical intravenous delivery of sRNA, their chemical components of QS must be biocompatible *in vitro* and *in vivo*. Even though QS composed by Chol and CTAB membrane components can be used for topical applications[171], the intravenous administration of CTAB is not authorized. It was reported that CTAB was embryotoxic and teratogenic after intraperitoneal injection[180] and may cause animal death at low intravenous administration doses, such as lethal dose of 12mg/kg in mice and 15mg/kg in rats [226]. Taking into account these considerations, in the present thesis MKC, was used instead of CTAB, for the preparation of QS. Like CTAB, MKC is a non-lipid cationic quaternary ammonium surfactant that forms micelles in water above its critical micellar concentration and could form QS by their self-assembly with sterol like molecules (Figure 77). Moreover, MKC was approved by regulatory agencies for other uses in animals (UNII 0W255OL75T) and is part of Benzalkonium chloride (BAK), which is also approved (EMA/352187/2012). Furthermore, the mice lethal dose of 50%, LD_{50}, after intravenous administration of MKC was 18mg/kg, which is much higher than the required for QS *in vivo* administration[180].

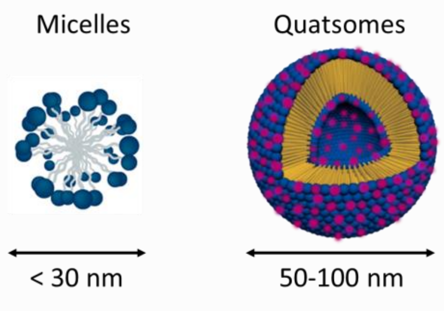

Figure 77. Schematic representation of the different sizes of MKC surfactant micelles compared to Quatsomes (QS).

Regarding sterol like, it is reported that Chol and their derivates, such as Chems or DC-Chol, have been approved by regulatory agencies (like FDA or EMA) or were not toxic *in vivo* or in clinical trials (UNII 97C5T2UQ7J; NCT00009841). Even though cationic lipids with quaternary amines were the most common lipids used in nucleic acids delivery systems, lipids with tertiary amines have been considered fundamental to deliver sRNA into the cytosol. Quaternary amines form stronger electrostatic interactions with negatively charged oligonucleotides, such as sRNA, than tertiary amines[227,228]. Some examples of liposomes used for sRNA delivery are composed by permanent cationic lipids with quaternary amines, like DOTAP[229]; in combination with protonable lipids, for example 1,2-dioleoyl-3-dimethylammonium-propane (DODAP)[230], 1,2-dilinoleyloxy3-dimethylaminopropane (D-Lin-DMA)[230,231]; or DC-Chol[229], with pH responsive properties, which allow the sRNA release in the cytosol by endosomal escape[229-231].

All QS synthetized in this thesis are composed by the cationic quaternary ammonium surfactant MKC but by different sterols, such as Chol, Chems and DC-Chol (in Figure 24 and Figure 42 are depicted the molecular structures of these three molecules). All QS synthesized, using the different sterol derivatives and different molar ratios between the sterols and MKC surfactant, showed good physicochemical properties in terms of size, size distribution, zeta potential, shape and lamellarity to be used as nanocarriers for the intravenous delivery of sRNA. Considering the fact that QS_1 composed by Chol:MKC remained stable over time when were prepared at initial Chol:MKC molar ratios of 1:1.5, 1:2 and 1:3 molar ratios of sterol:surfactant but could not be prepared at initial molar ratio 1:1 by DELOS-SUSP, as well as is possible for other QS formulations, means that for QS_1 formation was required more surfactant amount than sterols to form nanovesicles. However, after QS_1 purification the non-incorporated material in QS membrane, like MKC or Chol molecules dispersed on QS media, was eliminated achieving an approximately relative membrane components concentration nearly to the obtained by 1:1 nanovesicles. To discern the exactly amount of each membrane component removed after diafiltration in QS_1 prepared at different molar ratios, HPLC technique could be used to quantify samples composition. Now, HPLC protocol has been already optimized to study our QS composition prepared in this thesis, but results are not processed yet.

QS physicochemical properties impact on cellular uptake and viability

Physicochemical properties of the nanovesicles impacts on their cellular uptake and cargo delivery. Foroozandeh and Aziz reported that the size of the NP dictates the internalization pathways. Several studies showed that NP of D_h ~ 50 nm have the optimum size to be more efficiently internalized[232]. On the contrary, smaller NP (D_h ~ 15-30 nm) or larger NP (D_h~ 100-250 nm) are less efficiently up taken[232]. QS have an optimal size to be efficiently internalised (QS size are D_h ~ 50-100nm). However, after miRNA complexation, QS properties are modified due to agglomeration or aggregation, due to their interaction with miRNA, which may affect the cellular internalization pathway. For this reason, in this thesis the internalization studies were done after miRNA complexes formation.

Another critical parameter to study is the surface charge of NP. Positive-charged NP, like QS, enhance their uptake because after their interaction with the negatively charged proteins from cellular membrane they can modify the fluidity of the cellular membrane[96,233,234]. However, excessive positively-charged NP may disrupt the integrity of cellular membrane and lead to cellular toxicity and, in consequence, cell death[232]. Interestingly, neutral NP enter with low efficiencies compared to negatively charged NP, because these last ones leads to a membrane gelation or micropinocytosis formation to internalise[232,235]. Although all plain QS have high positive charge (ζ-potential ~ 50-

100mV), the final surface charge of the QS-miRNA complexes were not measured. However, the similar Z-potential of plain QS_{1-4} (ζ-potential ~ 80-100mV) may indicate that, after miRNA incubation, QS-miRNA complexes presented similar surface charge which, in consequence, could explain the high transfection efficiencies observed with QS_{1-4}-miRNA complexes. On the contrary, miRNA incubation with QS_0, which have lower surface charge (~ 50mV), may produce complexes nearly to neutrality or with slightly negative charge that impede the complete miRNA binding to QS_0. Nevertheless, the miRNA expression levels increased similarly to other QS-miRNA complexes after transfection due to the high miRNA concentration transfected.

A third parameter that may have an impact on the cellular uptake is the homogeneity and shape of the NP. QS are homogeneous in their spherical shape; however, it was reported that nanoparticles with this form could be susceptible of degradation before or after their internalization by phagocytosis (D_h ~250 nm – 3 µm)[113,232,236]. Moreover, it was observed that elongated NP, like rod-shaped or sharp shaped NP, were easily adhered and taken to cells because presented higher surface area to interact with the cell surface compared to spherical NP. While ellipsoidal NP had a lower cellular uptake[237].

In addition to shape, NP entry into the cell depends also on their particle rigidity, which is inversely proportional to phagosomes formation or opsonization and, in consequence, to their cellular entry. Longer and saturated alkyl chains of lipids reduce the lipid membrane fluidity and, in consequence, reduce the lipid membrane fusion[238]. For this reason, QS with large contents of Chol or their derivatives have a liquid like membrane bilayer[239], which facilitate their cellular uptake[130,240]. It is reported that helper lipids, such as Chol and Dc-Chol, are used with cationic lipids in order to decrease lipoplexes toxicity, stabilise lipid membranes and simultaneously increase transfection efficiencies[240]. These effects are accomplished because these molecules improve the membrane fluidity and may change the NP membrane conformation from an inverted hexagonal (H_{II}) phase to lamellar phases[241], which serve as an intermediate structure for membrane fusion and cargo release[242]. Moreover, after sRNA conjugation, QS demonstrated their high deformability through the changes observed in their morphology which could be an advantage to facilitate their internalization using the opsonization or phagocytosis pathways or the lipid fusion with cellular membrane[113,130].

Furthermore, NP hydrophobicity can determine their interaction with the cellular membrane. While hydrophobic NP created inclusions that directly diffuse across the membrane, hydrophilic NP were wrapped and absorbed onto the cellular membrane[232]. It was reported that liposomes formed with DOTAP and Chol or DC-Chol and DOPE are flexible and their aggregation with DNA or polymers sandwiched the lipid vesicles to form multilamellar and highly compacted vesicles, called fingerprints structures[238,243]. However, our results demonstrated that DC-Chol sterol seems to be involved in the different conformation adopted among QS-miRNA complexes, changing the multilayers formed with QS_{0-2} for brain-chain structures obtained by the bounding of miRNA and QS_{3-4}, one with others. These results may be explained by the different complexation capacity among QS, as was observed in Figure 47 QS_{0-2} induced the formation of multilayers composed by miRNA embedded in various QS membranes. On the other hand, QS_{3-4} required more miRNA amounts to deform QS membranes and form high compacted structures, like fingerprints[243]. To confirm this hypothesis, the morphology of the QS-miRNA complexes depending on the loading of miRNA per QS was analysed. QS_{3-4} presented similar structures like were the observed previously by Kennedy and their colleagues in the self-assembly of cationic phospholipids and nucleic acids[188]. Specifically, at low loadings of miRNA in QS_4, a brain-shaped chains and free QS were observed. These structures were observed when nucleic acids are added to a positive charged vesicle solution and the amount of nucleic acids to be complexed on the vesicle surface is limiting. Hence, the same nucleic acids bind to different vesicles leading to the sandwiching of vesicles[188]. When the amount of miRNA is increased, intermediate QS_4-miRNA loadings, highly compacted fingerprint structures were observed probably because vesicles tend to stack up by the bonding of two vesicles through the nucleic acids. Finally, an excessive amount of miRNA destabilizes QS membranes, inducing the rupture of vesicles and formation of large aggregates of QS_4-miRNA complexes, like was observed by Kennedy and their colleagues[188]. Meanwhile, the increase of miRNA amount in complexes formed with QS_{0-3} did not modify significantly complexes morphology.

QS complexation efficiency with sRNA

In this thesis has been demonstrated the importance of QS composition and morphology to allow the efficient conjugation of negatively charged hydrophilic molecules, such as sRNA, in QS surface by electrostatic interactions.

Among all QS tested formulations, QS_0, composed by Chems sterol (pka = 5.8), had the least miRNA binding capacity. However, it was reported that in pH sensitive liposomes, Chems was considered an excellent stabilizer of vesicles membranes that alters the fluidity of cell membranes allowing the efficient cargo release. Besides, Hafez and their colleagues observed that liposomes formed with Chems and DOPE only could be prepared at neutral or slightly alkaline pH adopting a lamellar organisation but not at acidic pH, in which Chems was unstable[182]. Meanwhile, QS_0 was prepared at acidic pH (pH ~ 2.5-3 and increased until pH ~ 4.5-5 after purification) without compromising their colloidal stability. Moreover, when QS are incubated with miRNA, maybe the deprotonated form of Chems, produce a repulsive effect between the negative charges from Chems and those from miRNA backbone, explaining the low conjugation of miRNA in QS_0. This hypothesis may be corroborated considering that QS_0 had a less positive charge (ζ-potential ~ 50mV) compared to other QS (ζ-potential ~ 80-100mV). However, to determine if the low miRNA complexation efficiency with QS_0 depends on the deprotonation of Chems at high pH, QS_0-miRNA complexes were prepared using other buffers, such as Depc-treated water (pH ~ 5), HEPES (pH = 7) and IMDM medium (pH = 7), instead of PBS (pH = 7). Figure 78 shows that the complexation efficiency of QS_0 was not improved, when the buffer used in complexes formation is changed.

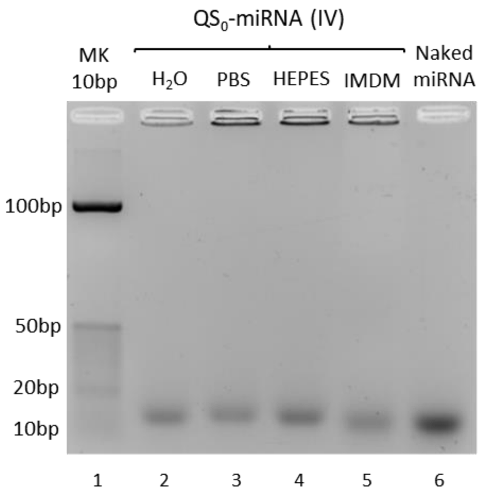

Figure 78. miRNA complexation efficiency of QS_0 using different buffers in complexes formation. Representative image of electrophoretic agarose gel showing the miRNA complexation efficiency with QS_0 at loading (IV) with Depc treated water (H_2O), PBS, HEPES and IMDM medium (lane 2-5). Free naked miRNA was used as a reference (lane 6).

It was expected that complexes formed at acidic conditions (using Depc water) presented more miRNA unbound than complexes formed at alkaline conditions (using PBS, HEPES or IMDM), because the pH ~ 5 of Depc treated water might facilitate the anionic Chems form and the electrostatic repulsion between miRNA and Chems should increase the miRNA release. However, this did not happen because probably the small amount of buffer added to QS_0 and miRNA was not able to modify the pH of the complexes. The principal limitation of these experiments was the pH determination of the small volumes (20 µL) used for complexes formation that impeded us to study in deep the pH of the complexes preformed. Hence, we can conclude that the incorporation of negative charged molecules, such as Chems, into QS membrane did not facilitate the miRNA release inside cells even impeded the miRNA conjugation with QS_0 during their incubation.

Differentially to QS_0, QS_1, composed of MKC and Cholesterol, can attach all the miRNA molecules in their surface through interactions between the positive charges from the quaternary amines of MKC and the negative ones from miRNA backbone. The permanent positive charge of the quaternary amine of MKC, which is not a switchable molecule able to be protonated or deprotonated, is the only involved in the miRNA conjugation with QS_1 (Figure 79). By the contrary, QS_2, QS_3 and QS_4 contain MKC and DC-Cholesterol, which has a tertiary amine, that might be protonated or deprotonated depending on the pH. Thereby, in QS_{2-4}, miRNA molecules can interact by electrostatic interactions with the permanent positive charge from MKC and, also, with the protonable positive charge of the tertiary amine of DC-Chol in acidic pH (Figure 79). In consequence, the increasing concentrations of DC-Chol (0% QS_1 <10% QS_2< 50% QS_3< 100% QS_4) in QS_{2-4} membrane induced a proportional higher miRNA complexation capacity to the DC-Chol amount (QS_1< QS_2< QS_3< QS_4). Titration curves (Figure 46) confirmed the different buffering capacity of QS_1-QS_4 depending on the concentration of DC-cholesterol on their membranes (0% of sterols molecules in QS_1 are DC-Chol and 100% of sterols molecules in QS_4 are DC-chol). At pH ~ 5-6 the tertiary amines of DC-Chol units are protonated and can interact with the negative charges of miRNA, increasing the miRNA loading capacity in QS membranes.

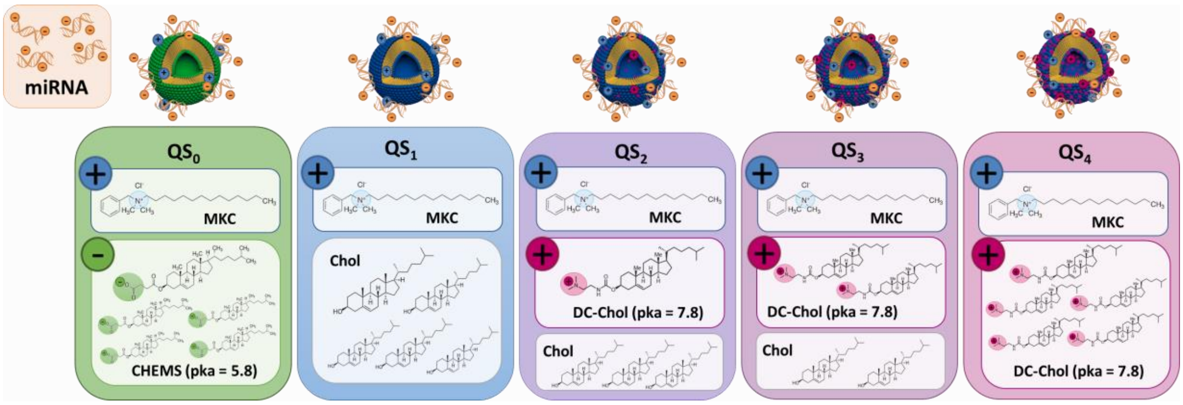

Figure 79. Schematic representation of the charges involved in the QS-miRNA complexation process by electrostatic interactions. In QS_0 and QS_1 the miRNA is entrapped in the QS membrane only by the positive charge of MKC. While in QS_{2-4} the miRNA interacts with the permanent positive charge of MKC and with the pH sensitive positive charge of DC-Chol.

The good complexation efficiency is in concordance to what was observed with cationic liposomes composed by DOTAP, DOPE or DC-Chol, which had a yield of miRNA encapsulation of 80-95%. However, it is surprisingly that QS_0 presented positive surface charge but does not have a fully miRNA complexation at any loading tested. This could be due to the steric impairment produced by the anionic form of Chems that avoids the miRNA interaction with some free positive charges of MKC in QS_0 (Figure 79). Similarly to QS_0, other nanoparticles, like lipid nanocapsules or calcium phosphate particles, had a lower miRNA encapsulation yield (~ 40-60%)[144].

QS and QS-miRNA complexes are biocompatible

Another important challenge for nanomedicines is their biocompatibility. Multiple parameters influence the toxicity, such as the nature of the cationic lipids, the surface charge, the cell type or the cell density[229]. Our results have demonstrated that QS-miRNA complexes had higher biocompatibility compared with QS alone, due to the neutralization or reduction of the positive charge of QS after miRNA binding. Despite a high positive or negative charge of NP is required to ensure high internalization efficiencies, charged NP are more toxic than neutral NP. Specifically, positively charged NP or hydrophilic NP with zwitterionic head-groups of the phospholipids may interact electrostatically with the negatively charged glycocalyx on the cellular membrane and enhance cellular toxicity due to transient cellular membrane deformations or rupture[233]. Moreover, positively charged NP have a faster internalization rates compared to negatively charged NP[232]. In general, charged NP are more cytotoxic than neutral forms, like happens with PAMAM dendrimers in which the neutralization of amino groups correlated to a decreased toxicity[244]. Furthermore, cell type has different sensitivity to NP in terms of toxicity. For example, in non-phagocytic cells such as SH-SY5Y or A549 cell lines, positively-charged NP internalize better and may induce toxic effects after their electrostatic interaction, while phagocytic cells, e.g. macrophages or THP-1 cells, preferentially interact with negatively charged NP and their toxicity is higher[245]. Hence, it is expected that in NB cells, non-phagocytic cells, the neutralization of QS positive charge reduces the cellular toxicity. Despite plain QS and QS-miRNA complexes present a safe range of concentrations in which QS do not impair cell viability and high transfection efficiencies are observed, higher QS concentrations than IC_{50} (7 to 11 µg/mL for QS_{1-4} or 8 to 13 µg/mL for QS_{1-4}-miR-Control) cell viability is compromised due to unspecific toxicity. Finally, the technique used to measure cellular toxicity must be selected carefully because false-positive or –negative may be observed due to interference of NP with the fixation or staining substrate or due to DNA damage or sublethal cellular alterations. In our case, the crystal violet is an indirect measure of cellular toxicity, because reflex the remaining number of cells. Therefore, to ensure a safe range of QS concentrations another technique could be used, like lactate dehydrogenase (LDH) leakage or 3-(4,5-dimethylthiazol-2-yl)-2,5-diphenyltetrazolium bromide (MTT) assays[246].

Study of QS-miRNA mechanism of cellular uptake

QS-miRNA complexes internalization in NB cells

It is well-known that naked sRNAs cross the cell membranes with difficulties. In general, they may enter through passive diffusion, but their hydrophilicity and their negative charges make the process poorly efficient[247]. However, when sRNAs are conjugated with nanocarriers, especially those positively charged, they rapidly internalise into cells[248]. Concurring with previous results, our experiments (Figure 54) demonstrated that naked miRNA did not enter in NB cells while when the miRNA is complexed to QS and Lipofectamine 2000® a huge increase in the miRNA expression levels was observed after transfection. Surprisingly, MKC micelles alone did not help to internalise miRNA. In order to discern why QS allowed the internalization of miRNA, but MKC micelles did not, some possibilities are explored. We discard that the QS buffering capacity are required for QS internalization, because only QS_{2-4} present this property. Considering that MKC micelles and QS were conjugated with miRNA at the same ratio in charge between the positive and negative charges from the complex, but only when miRNA is complexed with QS can internalise inside the cells, we suppose that MKC micelles structure could interfere in miRNA internalization. Omedes and their colleagues demonstrated that the incorporation of nucleic acids, e.g. siRNA, in preformed polymeric micelles increased the CMC required to form micelles[249]. Hence, after miRNA addition into MKC preformed micelles, MKC micelles might suffer an increase of their CMC that destabilize them. In this case, the miRNA molecules could be conjugated only with separately MKC surfactant molecules, instead of being entrapped into MKC micelles surface, which could not be able to internalize. Furthermore, this hypothesis might be corroborated because siRNA internalization was observed in HEK293T embryonic kidney cells after their transfection with cationic polymeric micelles, like PDMAEMA[250], in which the unloaded micellar CMC was ~ 300 nM but increased until 1.7 µM after siRNA loading. The higher CMC of MKC micelles compared to the CMC of polymeric micelles may difficult the micelles formation after miRNA addition and facilitate their destruction[249].

Possible internalization pathways used of QS-miRNA complexes

Most of nanocarriers usually tend to internalise using endocytic pathways where they encounter pitfalls related to their lysosomal degradation and inability of cargo release in the appropriate cellular compartment.[251]. For this reason, several efforts have been made to avoid the endosomal degradation of the cargo. One of such examples is the one reported by Gujrati et al. The authors demonstrated that siRNA encapsulated in cationic lipid nanocarrier (1-aminoethyl)iminobis[N-(oleicylcysteinyl-1-amino-ethyl)propionamide]) (ECO) internalised in U87 glioblastoma cells and induce an effective gene silencing due to the siRNA delivery. ECO/siRNA conjugates readily escaped from late endosomes using a pH-dependent membrane disruption prior the cytosol cargo release. In the cytosol siRNA were efficiently released by the glutathione-mediated reduction[252]. Hence, the rational design of sRNA nanocarriers is critical for intracellular siRNA delivery and the cargo release.

Our **confocal images** (Figure 51-Figure 53), performed at the laboratory of Dr. L Albertazzi from IBEC and ICMS, confirmed that QS-miRNA complexes enter inside the NB cells and arrive to the cytosol; however, we have not been able to unveil their internalization pathway. In the nanomedicine field, the internalization pathway of NP is a determining factor to ensure their biodistribution and cargo release. Several studies reported that the composition and structure of NP are important parameters that determine the cellular internalization. For example, particle size determined that small particles entered by passive diffusion, NP with D_h ~ 50-120 nm tend to internalize using endocytosis while NP with $D_h > 1$ µm tend to use the macropinocytic pathway or phagocytosis in phagocytic cells[253]. Another mechanism usually employed by liposomes is the membrane fusion, which is an independent energy pathway produced by the fusion of lipid membranes of NP with the cellular membrane (Figure 80)[254].

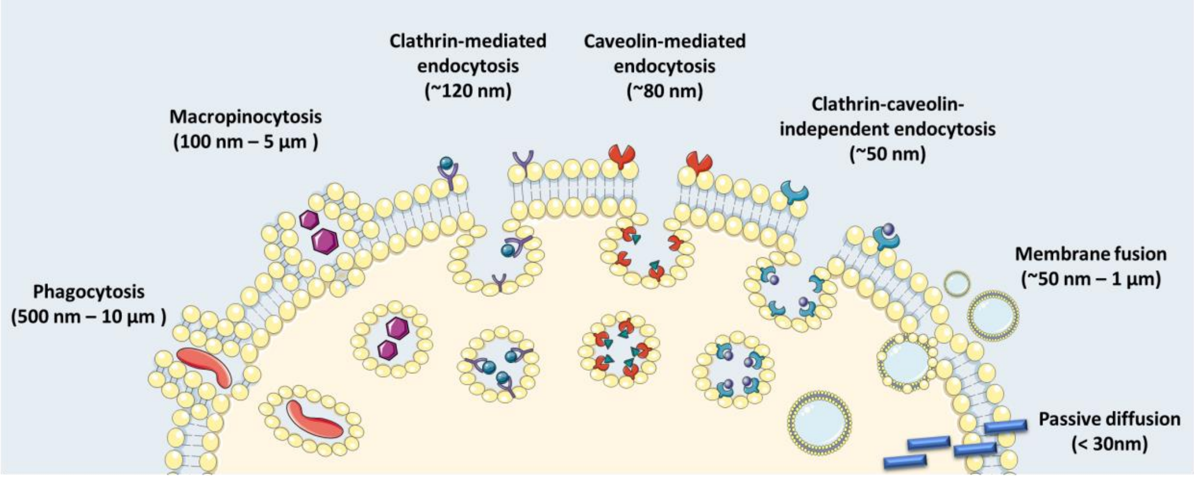
Clathrin-mediated endocytosis (~120 nm)
Caveolin-mediated endocytosis (~80 nm)
Macropinocytosis (100 nm – 5 µm)
Clathrin-caveolin-independent endocytosis (~50 nm)
Membrane fusion (~50 nm – 1 µm)
Phagocytosis (500 nm – 10 µm)
Passive diffusion (< 30nm)

Figure 80. Principal internalization pathways used for nanocarriers in mammalian cells. Adapted from Hillaireau & Couvreur[236].

Another important parameter involved in NP internalization is the hydrophobic chains of lipids. The decreased chain length or increased chain branching (or unsaturation) presented higher transfection efficiencies due to high membrane fluidity and fusogenicity[253,255]. Particle shape influence also to internalization capacity, but no conclusive opinions was generated on the internalization kinetics[253,256]. Besides surface properties of NP are fundamental to decipher their internalization pathway used, because there are proteins, like clathrin or caveolin, or cholesterol molecules that conduce in a protein/sterol-dependent internalization manner[253]. Nevertheless, NP internalization depends on several parameters, the most studied and well-known is the NP surface charge.

Generally, NP and specifically positively or negatively charged nanocarriers tend to internalize using endocytic pathways, that absorb extracellular molecules by invagination of the plasma membrane and form intracellular vesicles[245,247,252]. However, neutral NP internalize using the caveolae-mediated pathway, which differentially to clathrin mediated endocytosis do not end up into lysosomes (Figure 81). Cationic liposomes, polymeric NP (e.g. chitosan or poly(lactic-co-glycolic acid)) and silica-based NP internalised through the endocytic pathways which ends up in lysosomes. Hence, these materials and their content are digested at the lysosomal acidic pH (pH ~ 4.5-5) by hydrolytic enzymes from lysosomal lumen. To improve the NP arrival into cytosol, many strategies have been designed to promote the endosomal escape of NP before their fusion with lysosomes[144,252].

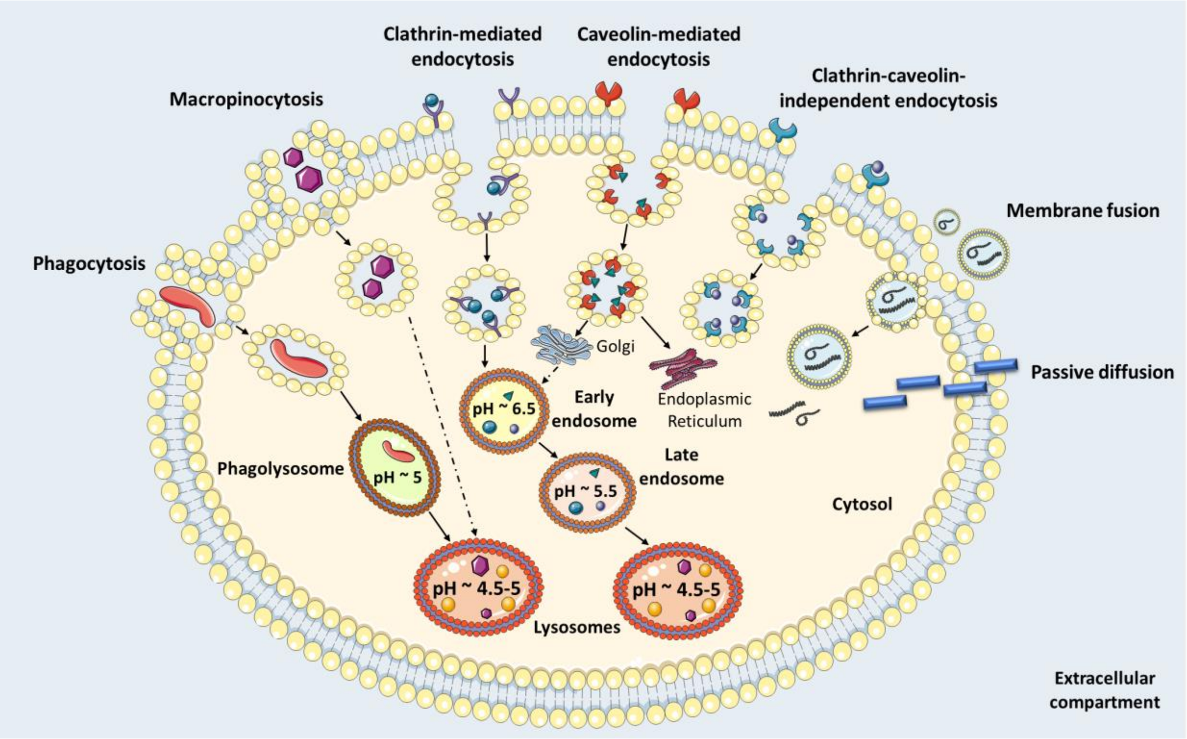
Clathrin-mediated endocytosis
Caveolin-mediated endocytosis
Clathrin-caveolin-independent endocytosis
Macropinocytosis
Membrane fusion
Phagocytosis
Golgi
pH ~ 6.5
Early endosome
Endoplasmic Reticulum
Passive diffusion
Late endosome
pH ~ 5.5
Phagolysosome
pH ~ 5
Cytosol
pH ~ 4.5-5
pH ~ 4.5-5
Lysosomes
Extracellular compartment

Figure 81. Intracellular trafficking of nanoparticles using the principal internalization pathways. Adapted from Hillaireau & Couvreur[236].

Therefore, the escape from the endosomes is essential for the NP efficient cargo release in the desired cellular compartment. Three mechanisms were reported to facilitate the endosomal escape: 1) the "proton sponge effect" or pH-buffering effect; 2) the "flip-flop" mechanism; and 3) the endosomal membrane fusion or destabilization mechanism.

1) Cationic polymers (like poly(ethyleneimen) (PEI)) or lipids are the most common NP that used the "proton sponge effect"[145]. The most known endosomolytic pH-buffering agent is chloroquine, which can avoid the fusion of endosomes with lysosomes.

Recently the **pH buffering capacity** of NP with titratable secondary and tertiary amines (like polylysine, polyamidoamine or PAMAM dendrimers) are highly studied[257,258]. These polymers or lipids usually contain a protonable secondary and or tertiary amine group with pKa ~ 5-7, that can be protonated at endosomal pH (~ 5.5-6.5)[259]. Briefly, upon endolysosomal acidification, the amines from pH sensitive molecules become protonated by the protons from endosomes, avoiding the endosomal pH decrease and promoting the influx of more protons from cytosol. Concomitantly, counterions are up taken inside the endosomes. At the same time, in order to compensate and maintain the osmotic concentration and pressure inside the endosomes, water is introduced causing endosomes swelling and, finally, their rupture. Consequently, the entrapped molecules inside endosomes are released into the cytoplasm[255,258].

2) The **"flip-flop" mechanism** has been observed for cationic lipoplexes to avoid the lysosomal degradation. When lipoplexes contact with anionic lipids from the cell membrane, they tend to form a monolayer and induce the fusion of endosomes with the lipids of the nanocarrier membrane. This binding induces a flip-flop of the negatively-charged phospholipids from the cytoplasmic to the inner face of the endosomes that neutralize the charges and destabilize the endosomal lamellar membrane. Thereby, local perturbations or pores on the endosomal membranes release the cargo from NP and from the endosomes[245,258]. This mechanism has been observed generally in NP with quaternary amine groups, like DOTMA or DOTAP[146].

3) Finally, the nanocarrier **fusion with the endosomal membrane** can result in the cargo release into the cytosol[260]. This process happens usually with cationic liposomes composed by fusogenic helper lipids (e.g. DOPE) that enhances endosomal fusion and escape, by undergoing a conformational change upon acidification and promoting a non-lamellar lipid phase change[146]. It was reported that lipoplexes of DNA with liposomes composed by DC-Chol sterol and DOPE helper lipid internalize using endocytosis and escape from endosomal compartments by endosomal membrane destabilization. In this case, DOPE can promote the lamellar-to-hexagonal phase transition of membranes at low pH, which is a crucial step to induce the membrane perturbation and/or destabilization to release the DNA. One example of an elegant strategy to discern the NP internalization and cargo release mechanism, was the one reported by Cardarelli et al. In this work, the authors conjugated DOPE-DC-Chol, DC-Chol-DOPC or DOTAP-DOPC liposomes with DNA and transfected into Chinese hamster ovary (CHO) living cells. Combining pharmacological and confocal imaging approaches showed that both lipoplexes internalize by a cholesterol-dependent macropinocytosis, instead of by clathrin- or caveolin-dependent endocytosis. Moreover, co-localization experiments with fluorescent lypoplexes and a lysosomal marker, revealed that DOTAP-DOPC/DNA and DC-Chol-DOPC/DNA lipoplexes are largely

degraded in the lysosomes, while DC-Chol-DOPE/DNA systems can efficiently escape from endosomal compartments[261].Following with this experiments, Pozzi et al., demonstrated that the endosomal escape of DC-Chol-DOPE/DNA lipoplexes was produced by membrane desestabilization due to DOPE fusogenic properties, not by DC-Chol properties[242]. Another interesting example were the liposomes formed by Chems and DOPE, which at neutral pH, Chems act as stabilizer and allow to maintain DOPE bilayer structure. Meanwhile, at lower pH, Chems is protonated and cause the destabilization of the liposomal bilayer and, in consequence the liposomal content is released. Although this system presented an efficient delivery *in vitro*, *in vivo* their efficacy was questionable due to lack of stability in presence of serum[236].

Considering the previously reports of several NP that are degraded inside the lysosomes and the lack of functional effects of miRNA transfected with QS_{0-1}, the designed series of pH-sensitive QS_{2-4} composed by DC-Chol sterol might facilitate the endosomal escape of QS_{3-4}-miRNA complexes, before their arrival into lysosomes. Confocal imaging (Figure 51) showed that all QS-miRNA complexes were visualized with a punctuated pattern that may indicate the complexes internalization by endocytosis[262,263]. However, mostly of them did not co-localize with lysosomes. Therefore, they are probably internalizing by another pathway, such as caveolae-mediated endocytosis, which is cholesterol-dependent pathway that may go through endoplasmic reticulum to cytosol or via Golgi following the endosomal pathway (Figure 81). It is reported that caveolin proteins directly bind to membranes with cholesterol, which may activate the endocytosis of the complex inducing actin reorganization and dynamin recruitment from the cytosol to stimulate membrane invagination and vesicle budding without ending up in the lysosomal compartment[253]. Despite this pathway may explain the non-lysosomal co-localization of QS-miRNA complexes after their internalization, the uptaken particles tend to be smaller than our QS-miRNA complexes[253]. For this reason, we guess that QS-miRNA complexes are entering inside the cells using mostly **macropinocytosis** to internalize the big complexes (D_h ~ 1 µm) and **caveolin-dependent endocytosis** or **membrane fusion** as alternative routes for some cases (D_h ~ 120 nm). Macropinocytosis, as well as caveolin-endocytosis, may end up in lysosomes or their cargo may escape during endosomal maturation when are following a cholesterol-dependent manner[261]. On the other hand, in some cases the membrane fusion pathway allows the NP cargo release in the cytosol directly after internalization due the similarities between the NP membrane and cellular membrane. Moreover, our hypothesis is in concordance to what Pozzi and their colleagues observed. DC-Chol/Chol/DNA lipoplexes internalized using a cholesterol-dependent macropinocytosis without colocalization with lysosomes. These results may suggest that an early release of the lipoplexes was produced after their internalization owing to a change of the membrane conformation and pores formation during the membrane fusion process by cholesterol[264].

Previous studies with plain QS_1 demonstrated the different localization compared to QS-miRNA complexes, which is not surprisingly due to the changes observed in terms of size, morphology and the neutralization of the positive charge of QS after miRNA complexation. Ardizzone et al., demonstrated that plain QS_1 labelled with DiC_{18} co-localize with lysosomes in cancer cell lines, such as HCT116 and COS-7 cells, after 8 h of $^{DiC18}QS_1$ incubation, but not with mitochondria organelles[195].

The understanding of the internalization and cargo release may even be more complex. Lu and their colleagues demonstrated that siRNA lipoplexes can enter using one internalization pathway, but the pathway does not ensure the siRNA release to the cytosol and their functional delivery. They reported that more than 95% of siRNA lipoplexes, formed with the cationic lipid DharmaFECT1 complexed with a siRNA, enter into cells through endocytosis; however, when the authors used inhibitors of the endocytic pathways (e.g. chlorpromazine, cytochalasin D, dynamin K44A; Figure 82) the functionality of the released siRNA was not impaired. These results mean that the lipoplexes may internalize through different and simultaneously mechanisms. They may be internalized by endocytosis but siRNA will be only released through direct fusion between the siRNA lipoplexes and the plasma membrane in a cholesterol dependent manner[265].

To confirm which pathway QS-miRNA complexes are using, two experimental strategies might be used. The first one is related to the co-localization of NP with specific endocytic markers or cellular compartments and the second one is based on the exclusion of specific endocytosis mechanisms by inhibitors or by cell mutants. Following the first strategy, confocal images demonstrated that only few $QS_{1\text{-}2}$-miRNA complexes co-localize with lysosomes, while any of $QS_{3\text{-}4}$-miRNA complexes did not co-localize with the lysosomal marker Lysotracker Green. However, to decipher the exact localization of QS-miRNA complexes requires more efforts using other cell compartment trackers or sensors, such as Mitotracker for mitochondria. Alternatively, NB cells could be transfected with constructs that express a specific protein from the organelle to label in fusion with a fluorescent protein, such as Green Fluorescent Protein (GFP). For example, Cell-Light Early Endosomes GFP, include a Rab5a protein with a GFP that label early endosomes. The advantage of such approach is to perform the imaging with live cells, but the disadvantage is that these markers sometimes are not selective of specific localization or that could be localized differentially in different cell types. Another technique to study the localization of QS is by immunocytochemistry using antibodies against proteins that are located at specific organelles. However, this approach usually requires the use of fixation protocols, which could alter the structure or localization of our particles[256]. Other techniques that could be used to visualize NP in different structures are electron microscopy and atomic force microscopy (AFM).

However, these techniques cannot provide detailed information on the lamellarity and internal structure of vesicles and samples can suffer perturbation on vesicle size and shape due to the vacuum conditions or the NP absorption during their fixation[266].

The second strategy, which could be used to investigate the internalization pathway used for QS-miRNA complexes is the blocking of the entry pathways using inhibitors (Figure 82) or cell mutants. This can be achieved using various pharmacologic inhibitors of endocytosis[267]. For example, hypertonic sucrose, potassium depletion or Chlorpromazine are chemical inhibitors of clathrin-mediated endocytosis[268]; Filipin, genistein and Nystatin to inhibit caveolae endocytosis[251,261,268]; Amiloride and Rottlerin to block macropinocytosis[269] and methyl-β-cyclodextrin to inhibit the cholesterol dependent pathways[261]. However, this approach presents several drawbacks to interpret the results obtained, because inhibitors are rarely specific or selective and often disturb multiple pathways and induce compensatory mechanisms to uptake NP when another route is blocked[256].

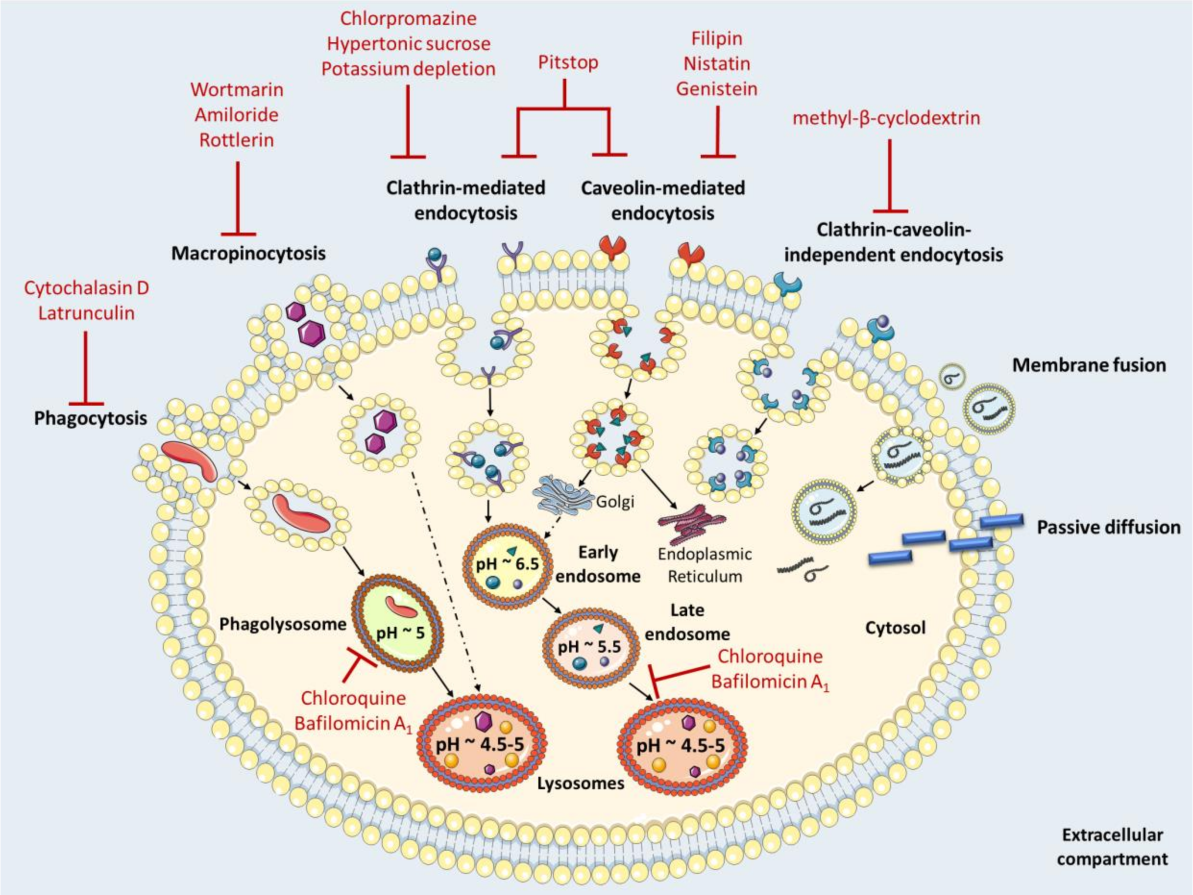
Chlorpromazine
Hypertonic sucrose
Potassium depletion
Pitstop
Filipin
Nistatin
Genistein
Wortmarin
Amiloride
Rottlerin
methyl-β-cyclodextrin
Clathrin-mediated endocytosis
Caveolin-mediated endocytosis
Macropinocytosis
Clathrin-caveolin-independent endocytosis
Cytochalasin D
Latrunculin
Phagocytosis
Membrane fusion
Golgi
Passive diffusion
Early endosome
pH ~ 6.5
Endoplasmic Reticulum
Late endosome
pH ~ 5.5
Phagolysosome
pH ~ 5
Cytosol
Chloroquine
Bafilomicin A1
Chloroquine
Bafilomicin A1
pH ~ 4.5-5
pH ~ 4.5-5
Lysosomes
Extracellular compartment

Figure 82. Intracellular trafficking followed by the principal cellular uptake pathways and the pharmacological inhibitors to block the internalization or endosomes maturation to lysosomes. Adapted from Zhang et al.[269], Russell et al.[270], Mauthe et al.[271], and Wolfram et al.,[272].

Alternatively, knockdown of specific proteins related to internalization pathways by siRNA or using dominant negative forms, could also shed light on the NP internalization mechanisms. In summary, to have a better understanding of the internalization pathways used for QS-miRNA complexes, multiple approaches need to be contemplated.

Tuning QS for cargo release

Another of the major barriers that NP designed for drug delivery encountered is the lack of sRNA functional effects due to difficulties in the cargo release from nanocarriers. Several techniques can be used to measure the release of sRNA from nanocarriers, among them the most commonly used are the competition assays with anionic molecules, like heparin or SDS, through electrophoretic agarose gels. For example, PEI-siRNA complexes or cationic lipid-based NP, called ECO, conjugated with siRNA demonstrated that electrostatic interactions with large polyanions, like heparin, separated the siRNA from NP surface[252,273]. Nevertheless, other studies reported that sRNA separation from NP needed higher competitive electrostatic forces, like SDS[273]. Barlett et al. demonstrated ^{64}Cu-DOTA-siRNA nanoconjugates released the siRNA after 1% of SDS addition[274]. In our case, the miRNA was released of all preformed QS-miRNA complexes by electrostatic competition with SDS, which may indicate the release of miRNA from QS under strong electrostatic interactions (Figure 49). It is reported that electrostatic interactions performed with tertiary amines, from DC-Chol molecules, are weaker than those done with quaternary amines, from the MKC surfactant[275]. Hence, the miRNA binding from QS surface is a reversible process independently of their binding molecule, MKC or DC-Chol. Although to separate the miRNA from MKC are required high electrostatic forces to release the miRNA. It is also known that in the cellular environment there are electrolytes, such as potassium, magnesium and phosphates, and proteoglycans or negatively charged proteins (dextran, sulfate or heparin) which may break the weak interactions of miRNA with tertiary amines, like may happen with QS_{2-4}, or may induce the miRNA release by membrane destabilization, like happened with cationic liposomes[275]. Jang and their colleagues demonstrated that electrostatic interactions with large polyanions, such as heparin or sulphated glycosaminoglycans, separated the siRNA from PEI-siRNA complexes, reducing the siRNA delivery efficiency inside the cells[273]. Raja and their colleagues also demonstrated that heparin can separate siRNA loaded from chitosan NP, but after these complexes incubation with serum components, like FBS, only some siRNA had been unbound from NP and interacted with FBS[276]. Hence, this phenomenon might be a double-edge sword, since it may increase the cargo release from NP inside the cells or also during the time in circulation, thereby resulting in lower amounts of miRNA delivered.

Our $QS_{2\text{-}4}$-miRNA complexes are quite stable in presence of FBS (Figure 64), thereby suggesting that the QS structure is protecting miRNA from interactions with biomolecules that could form weak interactions with tertiary amines from QS and trigger an undesired release of the miRNA.

Considering that the release of miRNA from QS_4 has been confirmed, the miRNA bound to the protonable amine of DC-Chol may be related to pH variations. The experiments conducted in collaboration with Dr. Albertazzi from IBEC and ICMS (see section 4.3.4) using FRET technique showed that QS and miRNA remain attached before and after cellular internalization in the case of QS_1, free of DC-Chol. However, miRNA is released from QS_4, composed of DC-Chol and MKC, inside NB cells. Hence, these results could explain why in the case of QS_1-miRNA conjugates, where no miRNA release was observed (Figure 75), it was not neither observed targets modification nor functional effects after transfection. On the contrary, the release of miRNA observed by FRET, after QS_4-miRNA complexes internalization, could explain why after QS_4 transfection the miRNA modified its target genes and induced its functional effects (Figure 74).

Lastly, Persi et al., reported that tumoral cells have alkaline intracellular pH (pH > 7.4 compared with pH ~ 7.2 in healthy tissues) and acidic extracellular pH (pH ~ 6.7 – 7.1 compared with pH ~ 7.3 – 7.4)[277].The alkalization of the cytosolic compartment creates a perfect environment to maintain the cancer cell proliferation rates and metastatic progression[278], because the high energy needed obligate cancer cells to produce adenosine 5'-triphosphate (ATP) using the called Warburg effect or "aerobic glycolysis"[279]. Taking advantage of this condition, our hypothesis is that the protonated tertiary amines of DC-cholesterol, present in QS_4 and not in QS_1, lose their proton and their positive character once they enter in the cytosol of the cancer cells, which is more basic than extracellular media (Figure 83). The decrease of the positive character of the QS_4 surface, due to the deprotonation of DC-cholesterol, could explain the release of the miRNA from QS_4-miRNA complexes, due to a decrease of the electrostatic interaction that keeps them compact.

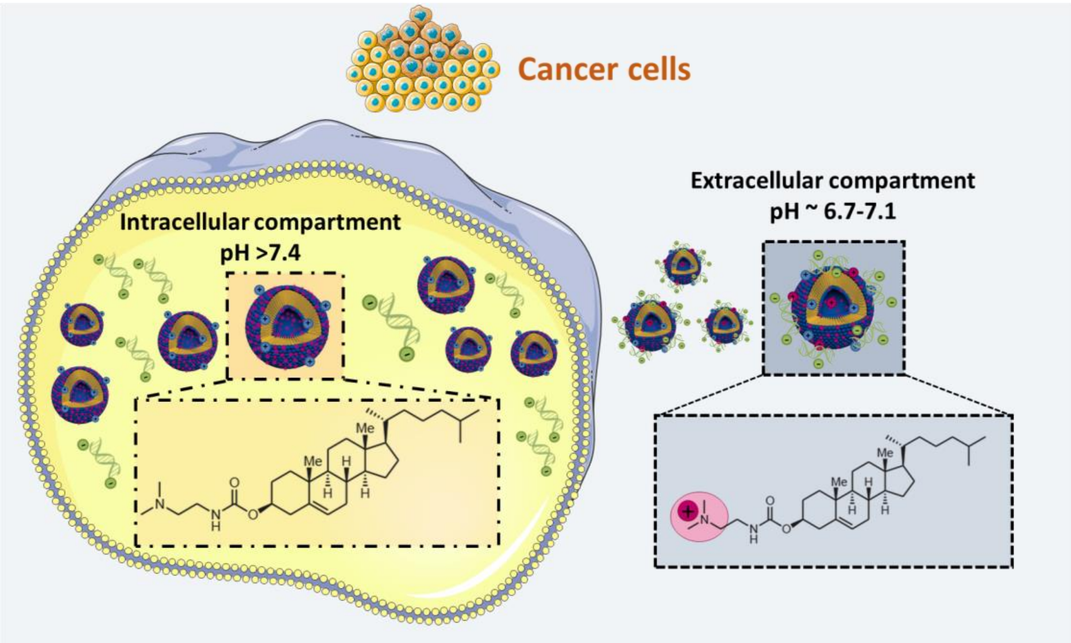
Cancer cells
Intracellular compartment
pH >7.4
Extracellular compartment
pH ~ 6.7-7.1
Me
Me
H
H
H
N
N
H
O
O

Figure 83. Hypothesis of the pH dependent mechanism employed by QS_4 to release the miRNA into cytosol after deprotonation of DC-Chol tertiary amine.

On the contrary, the positive charge of QS_1 surface is not sensitive to pH variations, since quaternary amines of MKC could not be protonated or deprotonated. For that reason, pH variations from extracellular to intracellular media, could not induce in that case the release of miRNA from miRNA-QS_1 complexes (Figure 84).

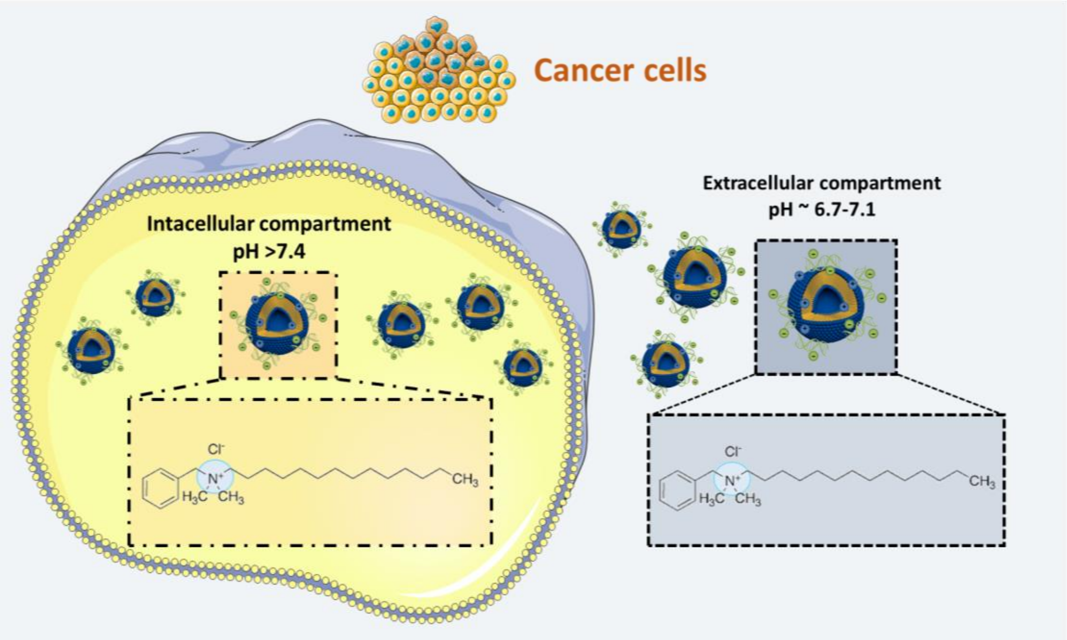
Cancer cells
Intacellular compartment
pH >7.4
Extracellular compartment
pH ~ 6.7-7.1
Cl⁻
N⁺
H₃C CH₃
CH₃

Figure 84. Hypothesis of the reason why QS_1 did not release the miRNA in the cytosol. The non-pH dependent permanent positive charge of QS_1 do not change by pH variations from extracellular to intracellular cancer cells environment.

5.4.3. Road into clinics of QS nanocarrier

Scaling-up QS production

Despite Quatsomes, in particular QS_4, are promising nanocarriers for sRNA deliver *in vitro*, their applicability *in vivo* must be tested before reaching the clinical phases. The overspread of a nanocarrier to reach the market depends on their availability to be prepared at industrial scale. Here, we demonstrated that QS could be produced at the required concentration and with the required quantities, for an *in vivo* use and clinical application, without chemical or structural modifications, by using a scalable technology, such as diafiltration. Generally, conventional preparation methods allow to produce NP at the laboratory scale, but they usually fail when their production is scaled-up to the industrial level. Therefore, complex processes, time and chemical-consuming purifications are usually required to produce them at industrial scale, which increases costs and slow down the production chain because harsh conditions are applied. Despite the interest in nanomedicine field has raised in recent years, NP used in preclinical studies are generally prepared in small batches and their scale-up for large quantity in a pharmaceutical grade is not possible. One of the factors involved in the difficulties of scale-up are that nanocarriers must be prepared by a consistent and highly reproducible method[280]. Thereby, platforms for the preparation of complex or laborious NP have limited their clinical use due to problems of manufacturing them into pharmaceutically grade on a large-scale. Processing nanocarriers with compressed-fluid technologies, allow the preparation of Quatsomes with an easy scale-up, maintaining their sterility, their high homogeneity among nanovesicles, their high control of materials and their reproducibility among batches using a simple one-pot green technology. Whereas basic nanomedicines have been successfully developed, the more complex systems still present challenges to overcome. Specifically, these problems are related to poor quality control, scalability complexities, incomplete purification, high costs of material or manufacturing process, low production yield, not reproducibility batch-to-batch, consistency and stability upon storage[281]. For these reasons, a low number of NP conjugated with bioactives are used in clinical trials despite most of them are effective *in vivo*[138].

On the contrary, the production of QS, developed in this thesis, at industrial scale is not a challenge, because batches produced at laboratory scale are able to be concentrated by diafiltration. Also the DELOS-SUSP method allow the preparation of high homogeneous liposomal and non-liposomal lipid nanovesicles at industrial scale using a liter scale plant or a continuous process, instead the mililiter scale plant used in this thesis[172]. In addition, DELOS-SUSP is a compressed-fluid based technology, which use mild conditions and green solvents, and has been shown to be cost-viable.

Moreover, QS are prepared in a one-step phase with controlled size distribution, uniform shape and high colloidal stability at laboratory or industrial scale[138,172], as was observed after QS samples physicochemical characterization by DLS and cryo-TEM techniques.

QS suitability to deliver other sRNAs

Quatsomes QS_4, composed of MKC and DC-Chol, were able to have a high entrapment efficiency of miRNA, high cellular uptake of QS_4-miRNA complexes and induce the modification of miRNA targets genes due to the miRNA release into cytosol. Functional effects observed with QS_4-siCCND1 complexes demonstrated that QS_4 is a potential nanomaterial platform to deliver different types of small RNA, including miRNA and siRNA. However, the reduction in cellular proliferation was not so effective after QS_4-siCCND1 because siRNA are specific for one target, while miRNA can modify multiple target genes in the same or in different pathways[132].

Integrity of QS-miRNA complexes in biological fluids

For an efficient *in vivo* sRNA delivery, nanocarriers must overcome intracellular and extracellular challenges still unsolved in many cases. The major **extracellular obstacles** observed are the **poor systemic stability**, the **rapid clearance**, the **immunogenicity** and the **lack of efficient** and **specific delivery** into target tissues. After systemic administration of naked sRNA, sRNAs remain in the bloodstream a couple of minutes, due to their short half-life. After NP-sRNA conjugation, their half-life can be improved to several hours, but, in some cases, nucleases from bloodstream can degrade rapidly the oligonucleotides even if they are conjugated with nanocarriers[91]. For this reason, we tested the QS_4 capability to protect miRNA from nucleases such as RNAse A (see section 3.2.17). Although miRNA molecules are not incorporated inside QS_4 and still may be in contact with the external environment, incubation of QS_4-miRNA complexes with RNAse A showed that QS_4 protected miRNA from degradation (Figure 65), which means that miRNA conjugation with QS_4 may increase the miRNA half-life *in vivo*. Compared to other miRNA-based nanoformulations such as dendrimers or liposomes[192,193], QS_4 may protect miRNA despite miRNA are conjugated outside the QS membrane and our challenging experimental conditions (i.e. RNAse concentration).

Another concerning issue in nanomedicine field is the formation of the **protein corona** outside the nanoconjugates. When NP enters in the bloodstream, interstitial fluid or extracellular membrane, proteins present in the media rapidly are absorbed onto NP surface altering the NP size, stability and surface properties that may alter the physiological response, the cellular uptake, biodistribution and toxicity. Moreover, among all proteins involved in protein corona formation, the binding of NP with opsonins can trigger into NP recognition and clearance by the mononuclear phagocyte system (MPS)[282]. As a consequence to MPS activation, NP are filtered and destroyed from bloodstream but also, they may activate the innate immune response (complement proteins and/or macrophages), which can have toxic side-effects *in vivo*[144]. The plasma proteins binding over NP surface depends also on NP composition, fact that impacts in NP internalization and biocompatibility. It is reported that lipid nanovesicles rich in cholesterol, like the ones developed in the present thesis had less protein binding than cholesterol-free liposomes due to their increased rigidity in their lipid bilayer[283]. Also, lipids derived from steroid structure, like cholesterol and DC-Chol, stabilize lipid bilayers which confers to NP a high biocompatibility with biological membrane[229,284]. In relation to this, our preliminary data (Figure 64) of the QS-miRNA complexes stability in presence of FBS proteins, demonstrated that complexes remained stable and miRNA were not released after four hours post-incubation at physiological temperature (~ 37°C). These results mean that electrostatic interactions produced between proteins and QS_4, do not destabilize the QS_4-sRNA complexes but do not discard the possibility of protein corona formation. In order to know which proteins binds to QS_4-miRNA complexes, which density, conformation, thickness, affinity and dynamics have these complexes after protein corona formation, several techniques can be used. For example, high-throughput characterization, UV-Vis, liquid chromatography mass spectrometry, spectrofluorometry or nuclear magnetic resonance have been used to know the serum proteins that interact with NP [285-287].

Biodistribution of QS-miRNA complexes

In addition to the time that nanoconjugates remain in blood circulation to be uptaken by tissues, they may encounter other pitfalls, such as the **first pass hepatic metabolism** and **renal excretion**. Likewise, it happens for conventional drugs, the most common organs involved in the metabolism and excretion of sRNA are the liver and kidney, respectively (Figure 85).

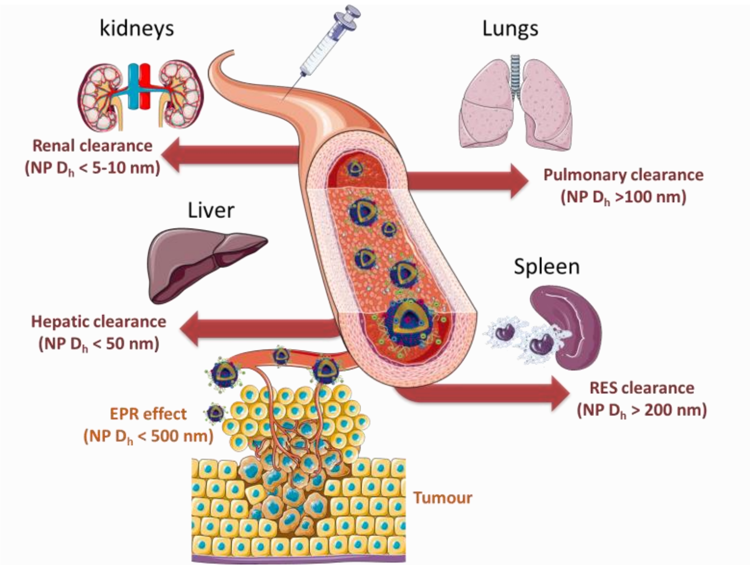

Figure 85. Principal extracellular barriers of administered NP for drug delivery and their excretion routes before reaching the tumour. Adapted from Ernsting *et al.,*[283].

All NP, excreted via the biliary system, are metabolized in the first pass hepatic metabolism from hepatocytes. This process is more complex than renal clearance, because use the reticuloendothelial system (RES). The RES system is formed by phagocytic Kupffer cells of liver and spleen macrophages that usually eliminate the oligonucleotides and other unwanted substances from the bloodstream. Despite hepatocytes play an important role in liver clearance via bile through endocytosis and enzymatic breakdown, their phagocytic capacity is lower compared to kupffer cells[258,288]. As was explained before, some NP can be uptaken by phagocytosis, introducing the NP inside the phagosomes, which are then integrated into lysosomes and degraded by nucleases[282].

On the other hand, sRNA may be accumulated in the kidney where are rapidly cleared from the body via renal clearance. Filtration of particles through the glomerular filtration is highly dependent on NP size (Figure 85)[282,288]. Currently, it is accepted that nanoparticle-based nanomedicines with a D_h ~ 50-200 nm presented the optimal size to deliver sRNA from nanocarriers[113] because they can avoid the first pass hepatic metabolism (observed in particles <50 nm) and the renal clearance (observed in smaller particles D_h < 5-10 nm or 50KD[96]) and RES clearance (observed in bigger particles D_h >200 nm)[283]. Although QS presented a nanometric size (D_h ~ 50-100 nm) after their purification, the complexes formation with sRNA modify their size and morphology, which makes it difficult to predict the expected sRNA biodistribution and the circulation time after their conjugation. In addition to size, surface charge is important in the renal clearance depending on the potential interactions between charged molecules and serum proteins or proteins from the glomerular capillary wall. Previous reports demonstrated that filtration is higher for cationic NP, than for neutral NP and negatively charged NP[288].

Furthermore, the NP charge may influence as well as on renal clearance, on stability, protein aggregation, and RES uptake *in vivo.* Negatively charged plasma proteins from the bloodstream may be bound to positively charged NP, therefore enhancing the RES clearance prior to uptake into target tissues and rendering it ineffective[96,289].

In this thesis, surface charge of QS-miRNA complexes could not be measured by ζ-potential because they were prepared in small volumes. For this reason, it is impossible to predict the possible protein corona formed around QS-miRNA complexes, the RES clearance and their metabolism or excretion after *in vivo* administration. However, the ζ-potential measurements of QS-miRNA complexes may not be representative of the charge density of QS because it may be altered in contact with physiological media or serum.

Previous studies reported that PEG addition in NP surface may prevent particle size increase and particle aggregation with proteins present in serum. Consequently, pegylated NP have a prolonged half-life and less renal or liver clearance[289]. Moreover, proteins aggregated to NP surface may promote opsonization and rapid renal clearance via uptake by Kupfer cells in the liver. One example was observed by Martina and their colleagues, which reported that NP pegylation protect siRNA from phagocytes recognition and immune system activation[290]. Thereby, the conjugation of PEG molecules on QS surface is an ongoing strategy in our laboratory but was not tested within the present thesis because the length of the PEG chain needs to be optimized for each individual delivery system to have the desired effect on stabilization and protection from degradation or immune system activation[96].

Another physicochemical parameter involved in NP biodistribution and resilience time is the NP shape. It is reported that the spherical particle shape enhanced circulation time and reduced phagocytosis[283]. Moreover, spherical particles tend to accumulate and be adhered to endothelial cells enhancing site-specific delivery[282]. Despite the fact, Decuzzi and colleagues demonstrated that geometry of nanoparticles contributes to biodistribution, internalization opsonization and adhesion strength into cells, the different morphologies observed after sRNA complexation to QS_{0-4} difficult the prediction of the QS-miRNA complexes behaviour after *in vivo* administration[291].

Specific tumour targeting of QS nanocarrier

Despite the disadvantages observed on biodistribution and protein corona formation after intravenously administration of nanomedicines for the systemic transport into tumours, it is well known that NP preferentially tend to accumulate in tumours using the increased tumour microvasculature. This process is called **enhanced permeability and retention (EPR) effect**, which enhanced the permeability of the tumour microenvironment and enable NP to enter into the tumour interstitial space, while lymphatic drainage causes retention of these NP inside this tissue[282]. Numerous lipoplexes formed by siRNA and liposomes demonstrated this tumoral targeting. For example, ATF5 siRNA-loaded CaP-rHDL NP was incubated with apolipoprotein E3 (ApoE3) to ensure their active targeting through their selective binding to low-density lipoprotein receptor (LDLR) and low-density lipoprotein receptor-related protein 1 (LRP1) that are expressed in the blood brain barrier, blood–brain tumour barrier (BBTB) and glioblastoma cells[292].

Considering our results, if QS_4, with high DC-Chol content, might reach the NB tumours after intravenous administration, the DC-Chol molecules of QS formulation may allow the miRNA release from QS and, consequentially, miRNA may induce their functional effects. During QS-miRNA complexes formation, a slightly acidic pH could promote that DC-Chol is protonated, thereby increasing miRNA complexation efficiency. Thus, at intratumoural physiologic pH ($pH > 7.4$), DC-Chol could be partially deprotonated, thereby lessening the attraction between DC-Chol and miRNA, resulting in miRNA release[187,277].

Although the passive targeting favours the accumulation of nanomedicines in tumoral sites, this strategy presents several limitations. EPR effect allows the extravasation through endothelium inflammation that do not lead to an exclusive cancerous cell targeting. Besides, the efficacy of the passive targeted nanomedicines using EPR effect depends on the angiogenesis, tumour type, maturity and host environment. In consequence, the **active targeting** of NP using markers, peptides, ligands or antibodies may improve the nanomedicines accumulation and internalization in the desired tumour site[282,293,294]. Several NP demonstrated that an active targeting increases the nanoconjugates arrival to targeted tissues, their internalization, their efficacy and their low side-effects due to unspecific arrival to other tissues[295,296]. An example is the integration of RGD peptides in micelles, chitosan NP or in liposomes, which led to improved targeting efficacy in breast and ovarian cancer models[144].

In our case, despite NB are highly irrigated and haemorrhagic tumours, to improve the arrival of QS_4-miR- 323a-5p complexes into NB tumours our QS_4 could be functionalized with anti-GD2 peptides or anti-GD2 antibodies. Ganliosides are surface glycolipids highly overexpressed in NB tumours[297-299].

Despite antibodies are the most used type of targeting specific cell receptors, they are highly immunogenic and quite big to introduce it in QS membrane, as well as expensive[299,300].

However, the active targeting also has limitations based on tumour heterogenicity, high immunogenicity and receptor overexpression in tumours. Sometimes the expression percentage of a specific receptor is insufficient to lead a successful NP tumour arrival[294,295]. Thereby, a combination of various active targeting strategies can be used[295].

Finally, if nanocarriers conjugated with sRNA are capable to cross the endothelial cells into the interstitial space of the tumour, they must be delivered into the cytoplasm and the intracellular barriers previously mentioned before, e.g. lysosomal degradation, become crucial. Although the impact of NP physicochemical properties on biodistribution and accumulation in target site is important, modifications only on one of these parameters do not impact in their efficacy to deliver sRNA because tumour heterogeneity is also highly relevant. Hence, the prediction of the biodistribution and the efficacy in knocking-down miR-323a-5p targets in mice need to be determined experimentally.

6. CONCLUSIONS

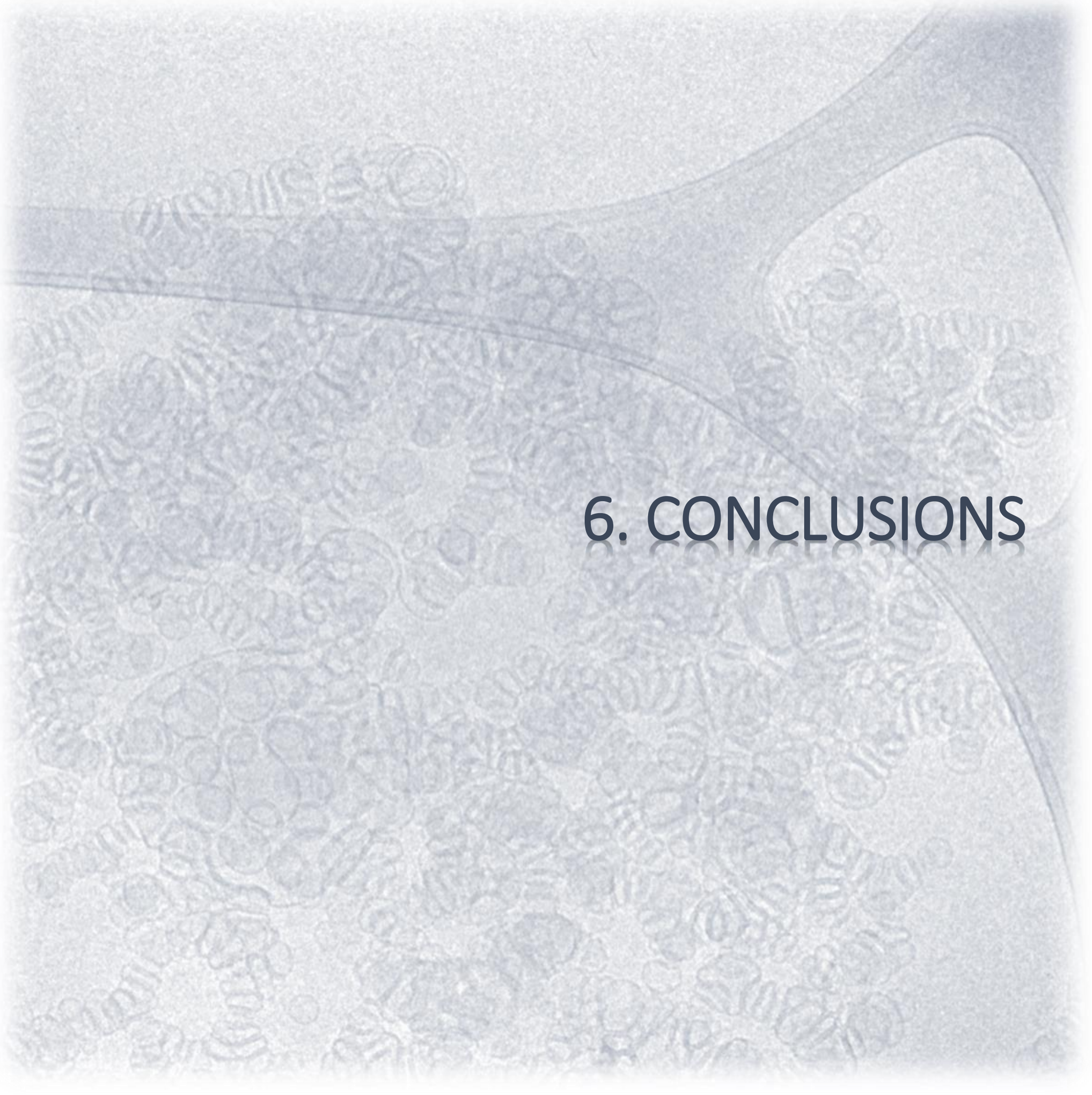

6. CONCLUSIONS

First: The restoration of the tumour suppressive miR-323a-5p could be the basis for a new epigenetic therapy to treat high-risk neuroblastoma.

Second: Quatsomes are novel lipid-based non-liposomal nanoparticles with outstanding physicochemical properties in terms of size, surface charge and morphology, to be used as a nanocarrier for small RNA, such as miRNA or siRNA.

Third: The new class of pH sensitive Quatsomes, engineered in this thesis, have a similar nanometric size, unilamellar spherical shape and positive charge, and are able to conjugate sRNA.

Fourth: The miRNA complexation capacity of Quatsomes depends on the membrane components used to form their membranes.

Ffith: The presence of DC-Cholesterol in Quatsomes membranes favours the loading of sRNA in this new type of non-liposomal nanovesicles.

Sixth: All Quatsomes formulations, tested in the present thesis, lead to high miRNA transfection efficiencies in SK-N-BE(2) cells, but have different outcomes in their functional effects.

Seventh: QS_4-miRNA complexes are stable in physiologic fluids and protected miRNA from nucleases degradation.

Eighth: Quatsomes are suitable nanocarriers for the *in vivo* administration of sRNA, since they allow the preparation of pharmaceutical formulations with the desired sRNA clinical concentrations.

Ninth: Only Quatsomes QS_4, containing DC-Cholesterol as sterol unit in the membrane, can release the miRNA intracellularly and, in consequence, induce miR-323a-5p target genes modification and phenotypic functional effects on cell proliferation.

Tenth: Quatsomes QS_4 is an efficient nanocarrier for the intracellular delivery of siRNAs and their targets modification.

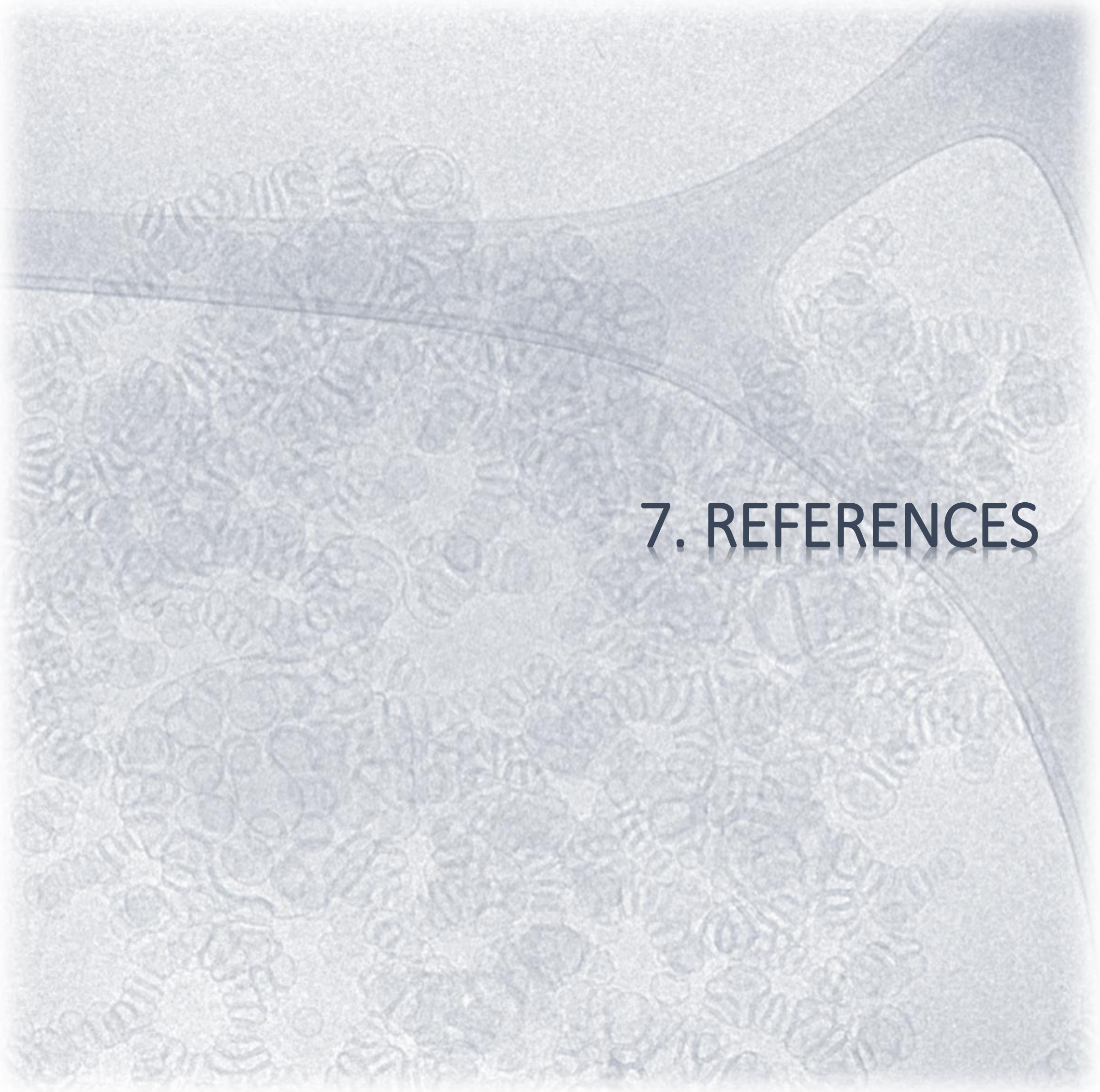

7. REFERENCES

7. REFERENCES

1 Esteller, M. Non-coding RNAs in human disease. *Nat Rev Genet* **12**, 861-874, doi:10.1038/nrg3074 (2011).

2 Warner, K. D., Hajdin, C. E. & Weeks, K. M. Principles for targeting RNA with drug-like small molecules. *Nat Rev Drug Discov* **17**, 547-558, doi:10.1038/nrd.2018.93 (2018).

3 Matsui, M. & Corey, D. R. Non-coding RNAs as drug targets. *Nat Rev Drug Discov* **16**, 167-179, doi:10.1038/nrd.2016.117 (2017).

4 Dahariya, S. *et al.* Long non-coding RNA: Classification, biogenesis and functions in blood cells. *Mol Immunol* **112**, 82-92, doi:10.1016/j.molimm.2019.04.011 (2019).

5 Wittrup, A. & Lieberman, J. Knocking down disease: a progress report on siRNA therapeutics. *Nat Rev Genet* **16**, 543-552, doi:10.1038/nrg3978 (2015).

6 Lam, J. K., Chow, M. Y., Zhang, Y. & Leung, S. W. siRNA Versus miRNA as Therapeutics for Gene Silencing. *Mol Ther Nucleic Acids* **4**, e252, doi:10.1038/mtna.2015.23 (2015).

7 Kole, R., Krainer, A. R. & Altman, S. RNA therapeutics: beyond RNA interference and antisense oligonucleotides. *Nat Rev Drug Discov* **11**, 125-140, doi:10.1038/nrd3625 (2012).

8 He, L. & Hannon, G. J. MicroRNAs: small RNAs with a big role in gene regulation. *Nat Rev Genet* **5**, 522-531, doi:10.1038/nrg1379 (2004).

9 Hombach, S. & Kretz, M. Non-coding RNAs: Classification, Biology and Functioning. *Adv Exp Med Biol* **937**, 3-17, doi:10.1007/978-3-319-42059-2_1 (2016).

10 Huntzinger, E. & Izaurralde, E. Gene silencing by microRNAs: contributions of translational repression and mRNA decay. *Nat Rev Genet* **12**, 99-110, doi:10.1038/nrg2936 (2011).

11 Place, R. F., Li, L. C., Pookot, D., Noonan, E. J. & Dahiya, R. MicroRNA-373 induces expression of genes with complementary promoter sequences. *Proc Natl Acad Sci U S A* **105**, 1608-1613, doi:10.1073/pnas.0707594105 (2008).

12 Eiring, A. M. *et al.* miR-328 functions as an RNA decoy to modulate hnRNP E2 regulation of mRNA translation in leukemic blasts. *Cell* **140**, 652-665, doi:10.1016/j.cell.2010.01.007 (2010).

13 Ha, M. & Kim, V. N. Regulation of microRNA biogenesis. *Nat Rev Mol Cell Biol* **15**, 509-524, doi:10.1038/nrm3838 (2014).

14 Soriano, A. *et al.* microRNAs as pharmacological targets in cancer. *Pharmacol Res* **75**, 3-14, doi:10.1016/j.phrs.2013.03.006 (2013).

15 Lin, S. & Gregory, R. I. MicroRNA biogenesis pathways in cancer. *Nat Rev Cancer* **15**, 321-333, doi:10.1038/nrc3932 (2015).

16 Melo, S. A. & Esteller, M. Dysregulation of microRNAs in cancer: playing with fire. *FEBS Lett* **585**, 2087-2099, doi:10.1016/j.febslet.2010.08.009 (2011).

17 Li, Z. & Rana, T. M. Therapeutic targeting of microRNAs: current status and future challenges. *Nat Rev Drug Discov* **13**, 622-638, doi:10.1038/nrd4359 (2014).

18 Treiber, T., Treiber, N. & Meister, G. Regulation of microRNA biogenesis and its crosstalk with other cellular pathways. *Nat Rev Mol Cell Biol* **20**, 5-20, doi:10.1038/s41580-018-0059-1 (2019).

19 Wahid, F., Shehzad, A., Khan, T. & Kim, Y. Y. MicroRNAs: synthesis, mechanism, function, and recent clinical trials. *Biochim Biophys Acta* **1803**, 1231-1243, doi:10.1016/j.bbamcr.2010.06.013 (2010).

20 de Carvalho, I. N., de Freitas, R. M. & Vargas, F. R. Translating microRNAs into biomarkers: What is new for pediatric cancer? *Med Oncol* **33**, 49, doi:10.1007/s12032-016-0766-4 (2016).

21 Pasquinelli, A. E. *et al.* Conservation of the sequence and temporal expression of let-7 heterochronic regulatory RNA. *Nature* **408**, 86-89, doi:10.1038/35040556 (2000).

22 Feng, X., Wang, Z., Fillmore, R. & Xi, Y. MiR-200, a new star miRNA in human cancer. *Cancer Lett* **344**, 166-173, doi:10.1016/j.canlet.2013.11.004 (2014).

23 Vidigal, J. A. & Ventura, A. The biological functions of miRNAs: lessons from in vivo studies. *Trends Cell Biol* **25**, 137-147, doi:10.1016/j.tcb.2014.11.004 (2015).

24 Olive, V., Minella, A. C. & He, L. Outside the coding genome, mammalian microRNAs confer structural and functional complexity. *Sci Signal* **8**, re2, doi:10.1126/scisignal.2005813 (2015).

25 Reinhart, B. J. *et al.* The 21-nucleotide let-7 RNA regulates developmental timing in Caenorhabditis elegans. *Nature* **403**, 901-906, doi:10.1038/35002607 (2000).

26 Cordova-Rivas, S. *et al.* 5p and 3p Strands of miR-34 Family Members Have Differential Effects in Cell Proliferation, Migration, and Invasion in Cervical Cancer Cells. *Int J Mol Sci* **20**, doi:10.3390/ijms20030545 (2019).

27 Concepcion, C. P., Bonetti, C. & Ventura, A. The microRNA-17-92 family of microRNA clusters in development and disease. *Cancer J* **18**, 262-267, doi:10.1097/PPO.0b013e318258b60a (2012).

28 Kim, J. S. *et al.* MiR-34a and miR-34b/c have distinct effects on the suppression of lung adenocarcinomas. *Exp Mol Med* **51**, 9, doi:10.1038/s12276-018-0203-1 (2019).

29 Griffiths-Jones, S., Grocock, R. J., van Dongen, S., Bateman, A. & Enright, A. J. miRBase: microRNA sequences, targets and gene nomenclature. *Nucleic Acids Res* **34**, D140-144, doi:10.1093/nar/gkj112 (2006).

30 Rupaimoole, R., Calin, G. A., Lopez-Berestein, G. & Sood, A. K. miRNA Deregulation in Cancer Cells and the Tumor Microenvironment. *Cancer Discov* **6**, 235-246, doi:10.1158/2159-8290.CD-15-0893 (2016).

31 Calin, G. A. *et al.* A MicroRNA signature associated with prognosis and progression in chronic lymphocytic leukemia. *N Engl J Med* **353**, 1793-1801, doi:10.1056/NEJMoa050995 (2005).

32 Lopez-Serra, P. & Esteller, M. DNA methylation-associated silencing of tumor-suppressor microRNAs in cancer. *Oncogene* **31**, 1609-1622, doi:10.1038/onc.2011.354 (2012).

33 Spector, L. G., Pankratz, N. & Marcotte, E. L. Genetic and nongenetic risk factors for childhood cancer. *Pediatr Clin North Am* **62**, 11-25, doi:10.1016/j.pcl.2014.09.013 (2015).

34 Saletta, F., Seng, M. S. & Lau, L. M. Advances in paediatric cancer treatment. *Transl Pediatr* **3**, 156-182, doi:10.3978/j.issn.2224-4336.2014.02.01 (2014).

35 Adamson, P. C. Improving the outcome for children with cancer: Development of targeted new agents. *CA Cancer J Clin* **65**, 212-220, doi:10.3322/caac.21273 (2015).

36 Matthay, K. K. *et al.* Neuroblastoma. *Nat Rev Dis Primers* **2**, 16078, doi:10.1038/nrdp.2016.78 (2016).

37 Irwin, M. S. & Park, J. R. Neuroblastoma: paradigm for precision medicine. *Pediatr Clin North Am* **62**, 225-256, doi:10.1016/j.pcl.2014.09.015 (2015).

38 Leichter, A. L., Sullivan, M. J., Eccles, M. R. & Chatterjee, A. MicroRNA expression patterns and signalling pathways in the development and progression of childhood solid tumours. *Mol Cancer* **16**, 15, doi:10.1186/s12943-017-0584-0 (2017).

39 Newman, E. A. *et al.* Update on neuroblastoma. *J Pediatr Surg* **54**, 383-389, doi:10.1016/j.jpedsurg.2018.09.004 (2019).

40 Boloix, A. *et al.* [Novel micro RNA-based therapies for the treatment of neuroblastoma]. *An Pediatr (Barc)* **85**, 109 e101-109 e106, doi:10.1016/j.anpedi.2015.07.016 (2016).

41 Chen, Y. & Stallings, R. L. Differential patterns of microRNA expression in neuroblastoma are correlated with prognosis, differentiation, and apoptosis. *Cancer Res* **67**, 976-983, doi:10.1158/0008-5472.CAN-06-3667 (2007).

42 Stallings, R. L., Foley, N. H., Bryan, K., Buckley, P. G. & Bray, I. Therapeutic targeting of miRNAs in neuroblastoma. *Expert Opin Ther Targets* **14**, 951-962, doi:10.1517/14728222.2010.510136 (2010).

43 Dzieran, J. *et al.* MYCN-amplified neuroblastoma maintains an aggressive and undifferentiated phenotype by deregulation of estrogen and NGF signaling. *Proc Natl Acad Sci U S A* **115**, E1229-E1238, doi:10.1073/pnas.1710901115 (2018).

44 Thompson, P. M. *et al.* Loss of heterozygosity for chromosome 14q in neuroblastoma. *Med Pediatr Oncol* **36**, 28-31, doi:10.1002/1096-911X(20010101)36:1<28::AID-MPO1008>3.0.CO;2-0 (2001).

45 Hoshi, M. *et al.* Detailed deletion mapping of chromosome band 14q32 in human neuroblastoma defines a 1.1-Mb region of common allelic loss. *Br J Cancer* **82**, 1801-1807, doi:10.1054/bjoc.2000.1108 (2000).

46 Gattolliat, C. H. *et al.* Expression of miR-487b and miR-410 encoded by 14q32.31 locus is a prognostic marker in neuroblastoma. *Br J Cancer* **105**, 1352-1361, doi:10.1038/bjc.2011.388 (2011).

47 Rupaimoole, R. & Slack, F. J. MicroRNA therapeutics: towards a new era for the management of cancer and other diseases. *Nat Rev Drug Discov* **16**, 203-222, doi:10.1038/nrd.2016.246 (2017).

48 Mestdagh, P. *et al.* The miR-17-92 microRNA cluster regulates multiple components of the TGF-beta pathway in neuroblastoma. *Mol Cell* **40**, 762-773, doi:10.1016/j.molcel.2010.11.038 (2010).

49 Swarbrick, A. *et al.* miR-380-5p represses p53 to control cellular survival and is associated with poor outcome in MYCN-amplified neuroblastoma. *Nat Med* **16**, 1134-1140, doi:10.1038/nm.2227 (2010).

50 Buechner, J. *et al.* Tumour-suppressor microRNAs let-7 and mir-101 target the proto-oncogene MYCN and inhibit cell proliferation in MYCN-amplified neuroblastoma. *Br J Cancer* **105**, 296-303, doi:10.1038/bjc.2011.220 (2011).

51 Tivnan, A. *et al.* MicroRNA-34a is a potent tumor suppressor molecule in vivo in neuroblastoma. *BMC Cancer* **11**, 33, doi:10.1186/1471-2407-11-33 (2011).

52 Soriano, A. *et al.* MicroRNA-497 impairs the growth of chemoresistant neuroblastoma cells by targeting cell cycle, survival and vascular permeability genes. *Oncotarget* **7**, 9271-9287, doi:10.18632/oncotarget.7005 (2016).

53 Fontana, L. *et al.* Antagomir-17-5p abolishes the growth of therapy-resistant neuroblastoma through p21 and BIM. *PLoS One* **3**, e2236, doi:10.1371/journal.pone.0002236 (2008).

54 Ragusa, M. *et al.* MIR152, MIR200B, and MIR338, human positional and functional neuroblastoma candidates, are involved in neuroblast differentiation and apoptosis. *J Mol Med (Berl)* **88**, 1041-1053, doi:10.1007/s00109-010-0643-0 (2010).

55 Liu, X. *et al.* MiR-181a/b induce the growth, invasion, and metastasis of neuroblastoma cells through targeting ABI1. *Mol Carcinog* **57**, 1237-1250, doi:10.1002/mc.22839 (2018).

56 Li, M. M. *et al.* Long noncoding RNA KCNQ1OT1 promotes apoptosis in neuroblastoma cells by regulating miR-296-5p/Bax axis. *FEBS J*, doi:10.1111/febs.15047 (2019).

57 Xu, X. *et al.* LincRNA-p21 Inhibits Cell Viability and Promotes Cell Apoptosis in Parkinson's Disease through Activating alpha-Synuclein Expression. *Biomed Res Int* **2018**, 8181374, doi:10.1155/2018/8181374 (2018).

58 Shohet, J. M. *et al.* A genome-wide search for promoters that respond to increased MYCN reveals both new oncogenic and tumor suppressor microRNAs associated with aggressive neuroblastoma. *Cancer Res* **71**, 3841-3851, doi:10.1158/0008-5472.CAN-10-4391 (2011).

59 Qu, H. *et al.* miRNA-558 promotes tumorigenesis and aggressiveness of neuroblastoma cells through activating the transcription of heparanase. *Hum Mol Genet* **24**, 2539-2551, doi:10.1093/hmg/ddv018 (2015).

60 Qu, H. *et al.* microRNA-558 facilitates the expression of hypoxia-inducible factor 2 alpha through binding to 5'-untranslated region in neuroblastoma. *Oncotarget* **7**, 40657-40673, doi:10.18632/oncotarget.9813 (2016).

61 Molenaar, J. J. *et al.* LIN28B induces neuroblastoma and enhances MYCN levels via let-7 suppression. *Nat Genet* **44**, 1199-1206, doi:10.1038/ng.2436 (2012).
62 Laneve, P. *et al.* The interplay between microRNAs and the neurotrophin receptor tropomyosin-related kinase C controls proliferation of human neuroblastoma cells. *Proc Natl Acad Sci U S A* **104**, 7957-7962, doi:10.1073/pnas.0700071104 (2007).
63 Zhang, H. *et al.* microRNA-9 targets matrix metalloproteinase 14 to inhibit invasion, metastasis, and angiogenesis of neuroblastoma cells. *Mol Cancer Ther* **11**, 1454-1466, doi:10.1158/1535-7163.MCT-12-0001 (2012).
64 Lee, J. J., Drakaki, A., Iliopoulos, D. & Struhl, K. MiR-27b targets PPARgamma to inhibit growth, tumor progression and the inflammatory response in neuroblastoma cells. *Oncogene* **31**, 3818-3825, doi:10.1038/onc.2011.543 (2012).
65 Welch, C., Chen, Y. & Stallings, R. L. MicroRNA-34a functions as a potential tumor suppressor by inducing apoptosis in neuroblastoma cells. *Oncogene* **26**, 5017-5022, doi:10.1038/sj.onc.1210293 (2007).
66 Cole, K. A. *et al.* A functional screen identifies miR-34a as a candidate neuroblastoma tumor suppressor gene. *Mol Cancer Res* **6**, 735-742, doi:10.1158/1541-7786.MCR-07-2102 (2008).
67 Wei, J. S. *et al.* The MYCN oncogene is a direct target of miR-34a. *Oncogene* **27**, 5204-5213, doi:10.1038/onc.2008.154 (2008).
68 Tivnan, A. *et al.* Inhibition of neuroblastoma tumor growth by targeted delivery of microRNA-34a using anti-disialoganglioside GD2 coated nanoparticles. *PLoS One* **7**, e38129, doi:10.1371/journal.pone.0038129 (2012).
69 Chakrabarti, M., Banik, N. L. & Ray, S. K. miR-138 overexpression is more powerful than hTERT knockdown to potentiate apigenin for apoptosis in neuroblastoma in vitro and in vivo. *Exp Cell Res* **319**, 1575-1585, doi:10.1016/j.yexcr.2013.02.025 (2013).
70 Wang, Z., Lei, H. & Sun, Q. MicroRNA-141 and its associated gene FUS modulate proliferation, migration and cisplatin chemosensitivity in neuroblastoma cell lines. *Oncol Rep* **35**, 2943-2951, doi:10.3892/or.2016.4640 (2016).
71 Zhang, H. *et al.* MicroRNA-145 inhibits the growth, invasion, metastasis and angiogenesis of neuroblastoma cells through targeting hypoxia-inducible factor 2 alpha. *Oncogene* **33**, 387-397, doi:10.1038/onc.2012.574 (2014).
72 Lodrini, M. *et al.* MYCN and HDAC2 cooperate to repress miR-183 signaling in neuroblastoma. *Nucleic Acids Res* **41**, 6018-6033, doi:10.1093/nar/gkt346 (2013).
73 Foley, N. H. *et al.* MicroRNA-184 inhibits neuroblastoma cell survival through targeting the serine/threonine kinase AKT2. *Mol Cancer* **9**, 83, doi:10.1186/1476-4598-9-83 (2010).
74 Tivnan, A., Foley, N. H., Tracey, L., Davidoff, A. M. & Stallings, R. L. MicroRNA-184-mediated inhibition of tumour growth in an orthotopic murine model of neuroblastoma. *Anticancer Res* **30**, 4391-4395 (2010).
75 Gao, S. L. *et al.* miR-200a inhibits tumor proliferation by targeting AP-2gamma in neuroblastoma cells. *Asian Pac J Cancer Prev* **15**, 4671-4676, doi:10.7314/apjcp.2014.15.11.4671 (2014).
76 Ooi, C. Y. *et al.* Network Modeling of microRNA-mRNA Interactions in Neuroblastoma Tumorigenesis Identifies miR-204 as a Direct Inhibitor of MYCN. *Cancer Res* **78**, 3122-3134, doi:10.1158/0008-5472.CAN-17-3034 (2018).
77 Chen, S. *et al.* miR-205 Inhibits Neuroblastoma Growth by Targeting cAMP-Responsive Element-Binding Protein 1. *Oncol Res* **26**, 445-455, doi:10.3727/096504017X14974834436195 (2018).
78 Qiao, J. *et al.* miR-335 and miR-363 regulation of neuroblastoma tumorigenesis and metastasis. *Surgery* **154**, 226-233, doi:10.1016/j.surg.2013.04.005 (2013).
79 Xiang, X. *et al.* miRNA-337-3p suppresses neuroblastoma progression by repressing the transcription of matrix metalloproteinase 14. *Oncotarget* **6**, 22452-22466, doi:10.18632/oncotarget.4311 (2015).

80 Wu, K. *et al.* miR-362-5p inhibits proliferation and migration of neuroblastoma cells by targeting phosphatidylinositol 3-kinase-C2beta. *FEBS Lett* **589**, 1911-1919, doi:10.1016/j.febslet.2015.05.056 (2015).

81 Boyineni, J. *et al.* SPARC overexpression combined with radiation retards angiogenesis by suppressing VEGF-A via miR410 in human neuroblastoma cells. *Int J Oncol* **49**, 1394-1406, doi:10.3892/ijo.2016.3646 (2016).

82 Althoff, K. *et al.* miR-542-3p exerts tumor suppressive functions in neuroblastoma by downregulating Survivin. *Int J Cancer* **136**, 1308-1320, doi:10.1002/ijc.29091 (2015).

83 Bray, I. *et al.* MicroRNA-542-5p as a novel tumor suppressor in neuroblastoma. *Cancer Lett* **303**, 56-64, doi:10.1016/j.canlet.2011.01.016 (2011).

84 Xiang, X. *et al.* miRNA-584-5p exerts tumor suppressive functions in human neuroblastoma through repressing transcription of matrix metalloproteinase 14. *Biochim Biophys Acta* **1852**, 1743-1754, doi:10.1016/j.bbadis.2015.06.002 (2015).

85 Verissimo, C. S., Molenaar, J. J., Fitzsimons, C. P. & Vreugdenhil, E. Neuroblastoma therapy: what is in the pipeline? *Endocr Relat Cancer* **18**, R213-231, doi:10.1530/ERC-11-0251 (2011).

86 Gambari, R., Brognara, E., Spandidos, D. A. & Fabbri, E. Targeting oncomiRNAs and mimicking tumor suppressor miRNAs: Nuew trends in the development of miRNA therapeutic strategies in oncology (Review). *Int J Oncol* **49**, 5-32, doi:10.3892/ijo.2016.3503 (2016).

87 Simonson, B. & Das, S. MicroRNA Therapeutics: the Next Magic Bullet? *Mini Rev Med Chem* **15**, 467-474 (2015).

88 Pereira, D. M., Rodrigues, P. M., Borralho, P. M. & Rodrigues, C. M. Delivering the promise of miRNA cancer therapeutics. *Drug Discov Today* **18**, 282-289, doi:10.1016/j.drudis.2012.10.002 (2013).

89 Miele, E. *et al.* Nanoparticle-based delivery of small interfering RNA: challenges for cancer therapy. *Int J Nanomedicine* **7**, 3637-3657, doi:10.2147/IJN.S23696 (2012).

90 Fernandez-Pineiro, I., Badiola, I. & Sanchez, A. Nanocarriers for microRNA delivery in cancer medicine. *Biotechnol Adv* **35**, 350-360, doi:10.1016/j.biotechadv.2017.03.002 (2017).

91 Ganju, A. *et al.* miRNA nanotherapeutics for cancer. *Drug Discov Today* **22**, 424-432, doi:10.1016/j.drudis.2016.10.014 (2017).

92 Chen, Y., Gao, D. Y. & Huang, L. In vivo delivery of miRNAs for cancer therapy: challenges and strategies. *Adv Drug Deliv Rev* **81**, 128-141, doi:10.1016/j.addr.2014.05.009 (2015).

93 Rosenblum, D., Joshi, N., Tao, W., Karp, J. M. & Peer, D. Progress and challenges towards targeted delivery of cancer therapeutics. *Nat Commun* **9**, 1410, doi:10.1038/s41467-018-03705-y (2018).

94 Ben-Shushan, D. *et al.* Overcoming obstacles in microRNA delivery towards improved cancer therapy. *Drug Deliv Transl Res* **4**, 38-49, doi:10.1007/s13346-013-0160-0 (2014).

95 Barata, P., Sood, A. K. & Hong, D. S. RNA-targeted therapeutics in cancer clinical trials: Current status and future directions. *Cancer Treat Rev* **50**, 35-47, doi:10.1016/j.ctrv.2016.08.004 (2016).

96 Whitehead, K. A., Langer, R. & Anderson, D. G. Knocking down barriers: advances in siRNA delivery. *Nat Rev Drug Discov* **8**, 129-138, doi:10.1038/nrd2742 (2009).

97 Yin, H. *et al.* Non-viral vectors for gene-based therapy. *Nat Rev Genet* **15**, 541-555, doi:10.1038/nrg3763 (2014).

98 Kota, J. *et al.* Therapeutic microRNA delivery suppresses tumorigenesis in a murine liver cancer model. *Cell* **137**, 1005-1017, doi:10.1016/j.cell.2009.04.021 (2009).

99 Shim, M. S. & Kwon, Y. J. Efficient and targeted delivery of siRNA in vivo. *FEBS J* **277**, 4814-4827, doi:10.1111/j.1742-4658.2010.07904.x (2010).

100 Wicki, A., Witzigmann, D., Balasubramanian, V. & Huwyler, J. Nanomedicine in cancer therapy: challenges, opportunities, and clinical applications. *J Control Release* **200**, 138-157, doi:10.1016/j.jconrel.2014.12.030 (2015).

101 Zhang, Y., Wang, Z. & Gemeinhart, R. A. Progress in microRNA delivery. *J Control Release* **172**, 962-974, doi:10.1016/j.jconrel.2013.09.015 (2013).

102 Petros, R. A. & DeSimone, J. M. Strategies in the design of nanoparticles for therapeutic applications. *Nat Rev Drug Discov* **9**, 615-627, doi:10.1038/nrd2591 (2010).

103 Peer, D. *et al.* Nanocarriers as an emerging platform for cancer therapy. *Nat Nanotechnol* **2**, 751-760, doi:10.1038/nnano.2007.387 (2007).

104 Young, S. W., Stenzel, M. & Yang, J. L. Nanoparticle-siRNA: A potential cancer therapy? *Crit Rev Oncol Hematol* **98**, 159-169, doi:10.1016/j.critrevonc.2015.10.015 (2016).

105 Gu, Z., Biswas, A., Zhao, M. & Tang, Y. Tailoring nanocarriers for intracellular protein delivery. *Chem Soc Rev* **40**, 3638-3655, doi:10.1039/c0cs00227e (2011).

106 Coutinho, C. & Somoza, A. MicroRNA sensors based on gold nanoparticles. *Anal Bioanal Chem* **411**, 1807-1824, doi:10.1007/s00216-018-1450-7 (2019).

107 Bayda, S. *et al.* Inorganic Nanoparticles for Cancer Therapy: A Transition from Lab to Clinic. *Curr Med Chem* **25**, 4269-4303, doi:10.2174/0929867325666171229141156 (2018).

108 Rout, G. K. *et al.* Current advances in nanocarriers for biomedical research and their applications. *Artif Cells Nanomed Biotechnol* **46**, 1053-1062, doi:10.1080/21691401.2018.1478843 (2018).

109 Deng, X. *et al.* Hyaluronic acid-chitosan nanoparticles for co-delivery of MiR-34a and doxorubicin in therapy against triple negative breast cancer. *Biomaterials* **35**, 4333-4344, doi:10.1016/j.biomaterials.2014.02.006 (2014).

110 Sonawane, N. D., Szoka, F. C., Jr. & Verkman, A. S. Chloride accumulation and swelling in endosomes enhances DNA transfer by polyamine-DNA polyplexes. *J Biol Chem* **278**, 44826-44831, doi:10.1074/jbc.M308643200 (2003).

111 Xu, D. *et al.* miR-22 represses cancer progression by inducing cellular senescence. *J Cell Biol* **193**, 409-424, doi:10.1083/jcb.201010100 (2011).

112 Rafael, D. *et al.* AKT2 siRNA delivery with amphiphilic-based polymeric micelles show efficacy against cancer stem cells. *Drug Deliv* **25**, 961-972, doi:10.1080/10717544.2018.1461276 (2018).

113 Aslan, B., Ozpolat, B., Sood, A. K. & Lopez-Berestein, G. Nanotechnology in cancer therapy. *J Drug Target* **21**, 904-913, doi:10.3109/1061186X.2013.837469 (2013).

114 Ma, X., Xiong, Y. & Lee, L. T. O. Application of Nanoparticles for Targeting G Protein-Coupled Receptors. *Int J Mol Sci* **19**, doi:10.3390/ijms19072006 (2018).

115 Anajafi, T. & Mallik, S. Polymersome-based drug-delivery strategies for cancer therapeutics. *Ther Deliv* **6**, 521-534, doi:10.4155/tde.14.125 (2015).

116 Rideau, E., Dimova, R., Schwille, P., Wurm, F. R. & Landfester, K. Liposomes and polymersomes: a comparative review towards cell mimicking. *Chem Soc Rev* **47**, 8572-8610, doi:10.1039/c8cs00162f (2018).

117 Gallon, E. *et al.* Triblock Copolymer Nanovesicles for pH-Responsive Targeted Delivery and Controlled Release of siRNA to Cancer Cells. *Biomacromolecules* **16**, 1924-1937, doi:10.1021/acs.biomac.5b00286 (2015).

118 Torchilin, V. P. Lipid-core micelles for targeted drug delivery. *Curr Drug Deliv* **2**, 319-327 (2005).

119 Wilner, S. E., Sparks, S. E., Cowburn, D., Girvin, M. E. & Levy, M. Controlling lipid micelle stability using oligonucleotide headgroups. *J Am Chem Soc* **137**, 2171-2174, doi:10.1021/ja512012m (2015).

120 Torchilin, V. P. Recent advances with liposomes as pharmaceutical carriers. *Nat Rev Drug Discov* **4**, 145-160, doi:10.1038/nrd1632 (2005).

121 Hoy, S. M. Patisiran: First Global Approval. *Drugs* **78**, 1625-1631, doi:10.1007/s40265-018-0983-6 (2018).

122 Kanasty, R., Dorkin, J. R., Vegas, A. & Anderson, D. Delivery materials for siRNA therapeutics. *Nat Mater* **12**, 967-977, doi:10.1038/nmat3765 (2013).

123 Bozzuto, G. & Molinari, A. Liposomes as nanomedical devices. *Int J Nanomedicine* **10**, 975-999, doi:10.2147/IJN.S68861 (2015).

124 Campani, V., Salzano, G., Lusa, S. & De Rosa, G. Lipid Nanovectors to Deliver RNA Oligonucleotides in Cancer. *Nanomaterials (Basel)* **6**, doi:10.3390/nano6070131 (2016).

125 Wang, T., Larcher, L. M., Ma, L. & Veedu, R. N. Systematic Screening of Commonly Used Commercial Transfection Reagents towards Efficient Transfection of Single-Stranded Oligonucleotides. *Molecules* **23**, doi:10.3390/molecules23102564 (2018).

126 Wu, Y. *et al.* Therapeutic Delivery of MicroRNA-29b by Cationic Lipoplexes for Lung Cancer. *Mol Ther Nucleic Acids* **2**, e84, doi:10.1038/mtna.2013.14 (2013).

127 Trang, P. *et al.* Systemic delivery of tumor suppressor microRNA mimics using a neutral lipid emulsion inhibits lung tumors in mice. *Mol Ther* **19**, 1116-1122, doi:10.1038/mt.2011.48 (2011).

128 Daige, C. L. *et al.* Systemic delivery of a miR34a mimic as a potential therapeutic for liver cancer. *Mol Cancer Ther* **13**, 2352-2360, doi:10.1158/1535-7163.MCT-14-0209 (2014).

129 Tolcher, A. W. *et al.* A phase 1 study of the BCL2-targeted deoxyribonucleic acid inhibitor (DNAi) PNT2258 in patients with advanced solid tumors. *Cancer Chemother Pharmacol* **73**, 363-371, doi:10.1007/s00280-013-2361-0 (2014).

130 Cheng, X. & Lee, R. J. The role of helper lipids in lipid nanoparticles (LNPs) designed for oligonucleotide delivery. *Adv Drug Deliv Rev* **99**, 129-137, doi:10.1016/j.addr.2016.01.022 (2016).

131 Daige, C. P., L.; Wiggins, J.; Nelligan-Davis, T.; Enzler, D.; Vadnagara, K.; Brown, D.; . MRX34, a liposomal miR-34 mimic and potential first-in-class microRNA therapeutic: activity in animal models of liver cancer. *Journal of Clinical Oncology* **34**, doi:10.1200/JCO.2016.34.15_suppl.e14076 (2017).

132 Chakraborty, C., Sharma, A. R., Sharma, G., Doss, C. G. P. & Lee, S. S. Therapeutic miRNA and siRNA: Moving from Bench to Clinic as Next Generation Medicine. *Mol Ther Nucleic Acids* **8**, 132-143, doi:10.1016/j.omtn.2017.06.005 (2017).

133 Balazs, D. A. & Godbey, W. Liposomes for use in gene delivery. *J Drug Deliv* **2011**, 326497, doi:10.1155/2011/326497 (2011).

134 Zimmermann, T. S. *et al.* RNAi-mediated gene silencing in non-human primates. *Nature* **441**, 111-114, doi:10.1038/nature04688 (2006).

135 Xue, H. Y., Guo, P., Wen, W. C. & Wong, H. L. Lipid-Based Nanocarriers for RNA Delivery. *Curr Pharm Des* **21**, 3140-3147, doi:10.2174/1381612821666150531164540 (2015).

136 Titze-de-Almeida, R., David, C. & Titze-de-Almeida, S. S. The Race of 10 Synthetic RNAi-Based Drugs to the Pharmaceutical Market. *Pharm Res* **34**, 1339-1363, doi:10.1007/s11095-017-2134-2 (2017).

137 Chen, Y., Zhu, X., Zhang, X., Liu, B. & Huang, L. Nanoparticles modified with tumor-targeting scFv deliver siRNA and miRNA for cancer therapy. *Mol Ther* **18**, 1650-1656, doi:10.1038/mt.2010.136 (2010).

138 Grimaldi, N. *et al.* Lipid-based nanovesicles for nanomedicine. *Chem Soc Rev* **45**, 6520-6545, doi:10.1039/c6cs00409a (2016).

139 Grijalvo, S. *et al.* Cationic Niosomes as Non-Viral Vehicles for Nucleic Acids: Challenges and Opportunities in Gene Delivery. *Pharmaceutics* **11**, doi:10.3390/pharmaceutics11020050 (2019).

140 Babu, A., Munshi, A. & Ramesh, R. Combinatorial therapeutic approaches with RNAi and anticancer drugs using nanodrug delivery systems. *Drug Dev Ind Pharm* **43**, 1391-1401, doi:10.1080/03639045.2017.1313861 (2017).

141 Yang, C. *et al.* Theranostic Niosomes for Efficient siRNA/MicroRNA Delivery and Activatable Near-Infrared Fluorescent Tracking of Stem Cells. *ACS Appl Mater Interfaces* **10**, 19494-19503, doi:10.1021/acsami.8b05513 (2018).

142 Chaudhary, V., Jangra, S. & Yadav, N. R. Nanotechnology based approaches for detection and delivery of microRNA in healthcare and crop protection. *J Nanobiotechnology* **16**, 40, doi:10.1186/s12951-018-0368-8 (2018).

143 Decuzzi, P., Pasqualini, R., Arap, W. & Ferrari, M. Intravascular delivery of particulate systems: does geometry really matter? *Pharm Res* **26**, 235-243, doi:10.1007/s11095-008-9697-x (2009).

144 Resnier, P., Montier, T., Mathieu, V., Benoit, J. P. & Passirani, C. A review of the current status of siRNA nanomedicines in the treatment of cancer. *Biomaterials* **34**, 6429-6443, doi:10.1016/j.biomaterials.2013.04.060 (2013).

145 Benjaminsen, R. V., Mattebjerg, M. A., Henriksen, J. R., Moghimi, S. M. & Andresen, T. L. The possible "proton sponge " effect of polyethylenimine (PEI) does not include change in lysosomal pH. *Mol Ther* **21**, 149-157, doi:10.1038/mt.2012.185 (2013).

146 Martens, T. F. R., K.; Demeester, J.; De Smedt, S.C. & Braeckmans, K. Intracellular delivery of nanomaterials: how to catch endosomal escape in the act. . *Nano Today* **9**, 344-364, doi:10.1016/j.nantod.2014.04.011 (2014).

147 Limcumpao, J. A., Horimoto, T., Xuan, X., Takahashi, E. & Mikami, T. Immunological relationship between feline herpesvirus type 1 (FHV-1) and canine herpesvirus (CHV) as revealed by polyvalent and monoclonal antibodies. *Arch Virol* **111**, 165-176, doi:10.1007/bf01311051 (1990).

148 Choi, Y. H. & Han, H. K. Nanomedicines: current status and future perspectives in aspect of drug delivery and pharmacokinetics. *J Pharm Investig* **48**, 43-60, doi:10.1007/s40005-017-0370-4 (2018).

149 Hanna, J., Hossain, G. S. & Kocerha, J. The Potential for microRNA Therapeutics and Clinical Research. *Front Genet* **10**, 478, doi:10.3389/fgene.2019.00478 (2019).

150 van der Ree, M. H. *et al.* Safety, tolerability, and antiviral effect of RG-101 in patients with chronic hepatitis C: a phase 1B, double-blind, randomised controlled trial. *Lancet* **389**, 709-717, doi:10.1016/S0140-6736(16)31715-9 (2017).

151 Hydbring, P. & Badalian-Very, G. Clinical applications of microRNAs. *F1000Res* **2**, 136, doi:10.12688/f1000research.2-136.v3 (2013).

152 Gallant-Behm, C. L. *et al.* A MicroRNA-29 Mimic (Remlarsen) Represses Extracellular Matrix Expression and Fibroplasia in the Skin. *J Invest Dermatol* **139**, 1073-1081, doi:10.1016/j.jid.2018.11.007 (2019).

153 Zeisel, M. B. & Baumert, T. F. Clinical development of hepatitis C virus host-targeting agents. *Lancet* **389**, 674-675, doi:10.1016/S0140-6736(17)30043-0 (2017).

154 Bouchie, A. First microRNA mimic enters clinic. *Nat Biotechnol* **31**, 577, doi:10.1038/nbt0713-577 (2013).

155 Beg, M. S. *et al.* Phase I study of MRX34, a liposomal miR-34a mimic, administered twice weekly in patients with advanced solid tumors. *Invest New Drugs* **35**, 180-188, doi:10.1007/s10637-016-0407-y (2017).

156 van Zandwijk, N. *et al.* Safety and activity of microRNA-loaded minicells in patients with recurrent malignant pleural mesothelioma: a first-in-man, phase 1, open-label, dose-escalation study. *Lancet Oncol* **18**, 1386-1396, doi:10.1016/S1470-2045(17)30621-6 (2017).

157 Soriano, A. *et al.* Functional high-throughput screening reveals miR-323a-5p and miR-342-5p as new tumor-suppressive microRNA for neuroblastoma. *Cell Mol Life Sci* **76**, 2231-2243, doi:10.1007/s00018-019-03041-4 (2019).

158 Mestdagh, P. *et al.* MYCN/c-MYC-induced microRNAs repress coding gene networks associated with poor outcome in MYCN/c-MYC-activated tumors. *Oncogene* **29**, 1394-1404, doi:10.1038/onc.2009.429 (2010).

159 Schneider, C. A., Rasband, W. S. & Eliceiri, K. W. NIH Image to ImageJ: 25 years of image analysis. *Nat Methods* **9**, 671-675 (2012).

160 Blangy, A. *et al.* Phosphorylation by p34cdc2 regulates spindle association of human Eg5, a kinesin-related motor essential for bipolar spindle formation in vivo. *Cell* **83**, 1159-1169, doi:10.1016/0092-8674(95)90142-6 (1995).

161 Honda, R., Korner, R. & Nigg, E. A. Exploring the functional interactions between Aurora B, INCENP, and survivin in mitosis. *Mol Biol Cell* **14**, 3325-3341, doi:10.1091/mbc.e02-11-0769 (2003).

162 Ni, D., Xu, P. & Gallagher, S. Immunoblotting and Immunodetection. *Curr Protoc Protein Sci* **88**, 10 10 11-10 10 37, doi:10.1002/cpps.32 (2017).

163 Vlachos, I. S. *et al.* DIANA-miRPath v3.0: deciphering microRNA function with experimental support. *Nucleic Acids Res* **43**, W460-466, doi:10.1093/nar/gkv403 (2015).

164 Betel, D., Koppal, A., Agius, P., Sander, C. & Leslie, C. Comprehensive modeling of microRNA targets predicts functional non-conserved and non-canonical sites. *Genome Biol* **11**, R90, doi:10.1186/gb-2010-11-8-r90 (2010).

165 Agarwal, V., Bell, G. W., Nam, J. W. & Bartel, D. P. Predicting effective microRNA target sites in mammalian mRNAs. *Elife* **4**, doi:10.7554/eLife.05005 (2015).

166 Ashburner, M. *et al.* Gene ontology: tool for the unification of biology. The Gene Ontology Consortium. *Nat Genet* **25**, 25-29, doi:10.1038/75556 (2000).

167 Kanehisa, M. & Goto, S. KEGG: kyoto encyclopedia of genes and genomes. *Nucleic Acids Res* **28**, 27-30, doi:10.1093/nar/28.1.27 (2000).

168 Kocak, H. *et al.* Hox-C9 activates the intrinsic pathway of apoptosis and is associated with spontaneous regression in neuroblastoma. *Cell Death Dis* **4**, e586, doi:10.1038/cddis.2013.84 (2013).

169 Su, Z. *et al.* An investigation of biomarkers derived from legacy microarray data for their utility in the RNA-seq era. *Genome Biol* **15**, 523, doi:10.1186/s13059-014-0523-y (2014).

170 Livak, K. J. & Schmittgen, T. D. Analysis of relative gene expression data using real-time quantitative PCR and the 2(-Delta Delta C(T)) Method. *Methods* **25**, 402-408, doi:10.1006/meth.2001.1262 (2001).

171 Ferrer-Tasies, L. *et al.* Quatsomes: vesicles formed by self-assembly of sterols and quaternary ammonium surfactants. *Langmuir* **29**, 6519-6528, doi:10.1021/la4003803 (2013).

172 Cabrera, I. *et al.* Multifunctional nanovesicle-bioactive conjugates prepared by a one-step scalable method using CO2-expanded solvents. *Nano Lett* **13**, 3766-3774, doi:10.1021/nl4017072 (2013).

173 Temelli, F., Córdoba, A.; Elizondo, E.; Cano-Sarabia, M.; Veciana, J. & Ventosa, N. Phase behavior of phytosterols and cholesterol in carbon dioxide-expanded ethanol. *The Journal of Supercritical Fluids* **63**, 59-68, doi:10.1016/j.supflu.2011.12.012s (2012).

174 Cano-Sarabia, M. *et al.* Preparation of uniform rich cholesterol unilamellar nanovesicles using CO2-expanded solvents. *Langmuir* **24**, 2433-2437, doi:10.1021/la7032109 (2008).

175 Elizondo, E. *et al.* in *Prog Mol Biol Transl Sci* Vol. 104 1-52 (2011).

176 Ardizzone, A. *et al.* Nanostructuring Lipophilic Dyes in Water Using Stable Vesicles, Quatsomes, as Scaffolds and Their Use as Probes for Bioimaging. *Small* **14**, e1703851, doi:10.1002/smll.201703851 (2018).

177 Ardizzone, A., autor; Veciana i Miró, Jaume, dir.; Ventosa, Nora, ISBN 9788449070945. <https://ddd.uab.cat/record/180082> [Consulta: 10 setembre 2019]. *New fluorescent nanovesicles, by self-assembly of organic fluorophores, sterols and surfactants, as probes for bioimaging.* Doctorado de Ciencia de Materiales thesis, Universitat Autònoma de Barcelona, (2017).

178 Heurtault, B., Saulnier, P., Pech, B., Proust, J. E. & Benoit, J. P. Physico-chemical stability of colloidal lipid particles. *Biomaterials* **24**, 4283-4300, doi:10.1016/s0142-9612(03)00331-4 (2003).

179 Wang, Y., Luo, J., Zhang, H. & Lu, J. microRNAs in the Same Clusters Evolve to Coordinately Regulate Functionally Related Genes. *Mol Biol Evol* **33**, 2232-2247, doi:10.1093/molbev/msw089 (2016).

180 Final Report on the Safety Assessment of Cetrimonium Chloride, Cetrimonium Bromide, and Steartrimonium Chloride. *International Journal of Toxicology* **16**, 195-220, doi:10.1080/109158197227152 (1997).

181 Isomaa, B. & Ekman, K. Embryotoxic and teratogenic effects of CTAB, a cationic surfactant, in the mouse. *Food Cosmet Toxicol* **13**, 331-334 (1975).

182 Hafez, I. M. & Cullis, P. R. Cholesteryl hemisuccinate exhibits pH sensitive polymorphic phase behavior. *Biochim Biophys Acta* **1463**, 107-114, doi:10.1016/s0005-2736(99)00186-8 (2000).

183 Adami, R. C. *et al.* An amino acid-based amphoteric liposomal delivery system for systemic administration of siRNA. *Mol Ther* **19**, 1141-1151, doi:10.1038/mt.2011.56 (2011).

184 Creevey, L. *et al.* MicroRNA-497 increases apoptosis in MYCN amplified neuroblastoma cells by targeting the key cell cycle regulator WEE1. *Mol Cancer* **12**, 23, doi:10.1186/1476-4598-12-23 (2013).

185 Zhu, W. *et al.* miR-497 modulates multidrug resistance of human cancer cell lines by targeting BCL2. *Med Oncol* **29**, 384-391, doi:10.1007/s12032-010-9797-4 (2012).

186 Zhang, X., Lin, Y. & Gillies, R. J. Tumor pH and its measurement. *J Nucl Med* **51**, 1167-1170, doi:10.2967/jnumed.109.068981 (2010).

187 Robey, I. F. *et al.* Bicarbonate increases tumor pH and inhibits spontaneous metastases. *Cancer Res* **69**, 2260-2268, doi:10.1158/0008-5472.CAN-07-5575 (2009).

188 Kennedy, M. T., Pozharski, E. V., Rakhmanova, V. A. & MacDonald, R. C. Factors governing the assembly of cationic phospholipid-DNA complexes. *Biophys J* **78**, 1620-1633, doi:10.1016/S0006-3495(00)76714-2 (2000).

189 Lukas, J. *et al.* DNA tumor virus oncoproteins and retinoblastoma gene mutations share the ability to relieve the cell's requirement for cyclin D1 function in G1. *J Cell Biol* **125**, 625-638, doi:10.1083/jcb.125.3.625 (1994).

190 Goel, S., DeCristo, M. J., McAllister, S. S. & Zhao, J. J. CDK4/6 Inhibition in Cancer: Beyond Cell Cycle Arrest. *Trends Cell Biol* **28**, 911-925, doi:10.1016/j.tcb.2018.07.002 (2018).

191 Hydbring, P., Castell, A. & Larsson, L. G. MYC Modulation around the CDK2/p27/SKP2 Axis. *Genes (Basel)* **8**, doi:10.3390/genes8070174 (2017).

192 Pandi, P. *et al.* Dendrimer as a new potential carrier for topical delivery of siRNA: A comparative study of dendriplex vs. lipoplex for delivery of TNF-alpha siRNA. *Int J Pharm* **550**, 240-250, doi:10.1016/j.ijpharm.2018.08.024 (2018).

193 Zhang, L. *et al.* Cytosolic co-delivery of miRNA-34a and docetaxel with core-shell nanocarriers via caveolae-mediated pathway for the treatment of metastatic breast cancer. *Sci Rep* **7**, 46186, doi:10.1038/srep46186 (2017).

194 Koberle, V. *et al.* Differential stability of cell-free circulating microRNAs: implications for their utilization as biomarkers. *PLoS One* **8**, e75184, doi:10.1371/journal.pone.0075184 (2013).

195 Liu, X. *et al.* Fluorenyl-Loaded Quatsome Nanostructured Fluorescent Probes. *ACS Omega* **2**, 4112-4122, doi:10.1021/acsomega.7b00779 (2017).

196 Lee, Y. S. & Dutta, A. MicroRNAs in cancer. *Annu Rev Pathol* **4**, 199-227, doi:10.1146/annurev.pathol.4.110807.092222 (2009).

197 Mei, H., Lin, Z. Y. & Tong, Q. S. The roles of microRNAs in neuroblastoma. *World J Pediatr* **10**, 10-16, doi:10.1007/s12519-014-0448-2 (2014).

198 Stallings, R. L. MicroRNA involvement in the pathogenesis of neuroblastoma: potential for microRNA mediated therapeutics. *Curr Pharm Des* **15**, 456-462, doi:10.2174/138161209787315837 (2009).

199 Galardi, A. *et al.* MicroRNAs in Neuroblastoma: Biomarkers with Therapeutic Potential. *Curr Med Chem* **25**, 584-600, doi:10.2174/0929867324666171003120335 (2018).

200 Reid, G. K., S. C.; Pavlakis, N.; Brahmbhatt, H.; MacDiarmid, J.; Clarke, S.; Boyer, M.; & van Zandwijk N. Clinical development of TargomiRs, a miRNA mimic-based treatment for patients with recurrent thoracic cancer. *Future Medicine* **8**, 1079-1085, doi:10.2217/epi-2016-0035 (2016).

201 Thakral, S. & Ghoshal, K. miR-122 is a unique molecule with great potential in diagnosis, prognosis of liver disease, and therapy both as miRNA mimic and antimir. *Curr Gene Ther* **15**, 142-150 (2015).

202 Powers, J. T. *et al.* Multiple mechanisms disrupt the let-7 microRNA family in neuroblastoma. *Nature* **535**, 246-251, doi:10.1038/nature18632 (2016).

203 Beckers, A. *et al.* MYCN-targeting miRNAs are predominantly downregulated during MYCNdriven neuroblastoma tumor formation. *Oncotarget* **6**, 5204-5216, doi:10.18632/oncotarget.2477 (2015).

204 Lian, H. W., Zhou, Y., Jian, Z. H. & Liu, R. Z. MiR-323-5p acts as a tumor suppressor by targeting the insulin-like growth factor 1 receptor in human glioma cells. *Asian Pac J Cancer Prev* **15**, 10181-10185, doi:10.7314/apjcp.2014.15.23.10181 (2014).

205 Hsu, C. L. *et al.* Unveiling MYCN regulatory networks in neuroblastoma via integrative analysis of heterogeneous genomics data. *Oncotarget* **7**, 36293-36310, doi:10.18632/oncotarget.9202 (2016).

206 Qiu, J., Zeng, F. R., Fang, Y., Li, J. & Xiao, S. Y. Increased miR-323a induces bladder cancer cell apoptosis by suppressing c-Met. *Kaohsiung J Med Sci*, doi:10.1002/kjm2.12091 (2019).

207 Malpeli, G. *et al.* Identification of microRNAs implicated in the late differentiation stages of normal B cells suggests a central role for miRNA targets ZEB1 and TP53. *Oncotarget* **8**, 11809-11826, doi:10.18632/oncotarget.14683 (2017).

208 Gao, Q. & Zheng, J. microRNA-323 upregulation promotes prostate cancer growth and docetaxel resistance by repressing p73. *Biomed Pharmacother* **97**, 528-534, doi:10.1016/j.biopha.2017.10.040 (2018).

209 Zeka, F. *et al.* Circulating microRNA biomarkers for metastatic disease in neuroblastoma patients. *JCI Insight* **3**, doi:10.1172/jci.insight.97021 (2018).

210 Bray, I. *et al.* Widespread dysregulation of MiRNAs by MYCN amplification and chromosomal imbalances in neuroblastoma: association of miRNA expression with survival. *PLoS One* **4**, e7850, doi:10.1371/journal.pone.0007850 (2009).

211 Schulte, J. H. *et al.* Deep sequencing reveals differential expression of microRNAs in favorable versus unfavorable neuroblastoma. *Nucleic Acids Res* **38**, 5919-5928, doi:10.1093/nar/gkq342 (2010).

212 Molenaar, J. J. *et al.* Cyclin D1 and CDK4 activity contribute to the undifferentiated phenotype in neuroblastoma. *Cancer Res* **68**, 2599-2609, doi:10.1158/0008-5472.CAN-07-5032 (2008).

213 Bienvenu, F. *et al.* Transcriptional role of cyclin D1 in development revealed by a genetic-proteomic screen. *Nature* **463**, 374-378, doi:10.1038/nature08684 (2010).

214 Barbieri, E. *et al.* Histone chaperone CHAF1A inhibits differentiation and promotes aggressive neuroblastoma. *Cancer Res* **74**, 765-774, doi:10.1158/0008-5472.CAN-13-1315 (2014).

215 Gohard, F. H., St-Cyr, D. J., Tyers, M. & Earnshaw, W. C. Targeting the INCENP IN-box-Aurora B interaction to inhibit CPC activity in vivo. *Open Biol* **4**, 140163, doi:10.1098/rsob.140163 (2014).

216 Watts, J. K. & Corey, D. R. Clinical status of duplex RNA. *Bioorg Med Chem Lett* **20**, 3203-3207, doi:10.1016/j.bmcl.2010.03.109 (2010).

217 Aartsma-Rus, A. & Krieg, A. M. FDA Approves Eteplirsen for Duchenne Muscular Dystrophy: The Next Chapter in the Eteplirsen Saga. *Nucleic Acid Ther* **27**, 1-3, doi:10.1089/nat.2016.0657 (2017).

218 Agency, E. M. *New medicine for hereditary rare disease*, <https://www.ema.europa.eu/en/news/new-medicine-hereditary-rare-disease> (2018).

219 Gebert, L. F. *et al.* Miravirsen (SPC3649) can inhibit the biogenesis of miR-122. *Nucleic Acids Res* **42**, 609-621, doi:10.1093/nar/gkt852 (2014).

220 Xue, H. Y., Liu, S. & Wong, H. L. Nanotoxicity: a key obstacle to clinical translation of siRNA-based nanomedicine. *Nanomedicine (Lond)* **9**, 295-312, doi:10.2217/nnm.13.204 (2014).

221 Bellis, S. L. Advantages of RGD peptides for directing cell association with biomaterials. *Biomaterials* **32**, 4205-4210, doi:10.1016/j.biomaterials.2011.02.029 (2011).

222 Jokerst, J. V., Lobovkina, T., Zare, R. N. & Gambhir, S. S. Nanoparticle PEGylation for imaging and therapy. *Nanomedicine (Lond)* **6**, 715-728, doi:10.2217/nnm.11.19 (2011).

223 Ardizzone, A. *et al.* Highly Stable and Red-Emitting Nanovesicles Incorporating Lipophilic Diketopyrrolopyrroles for Cell Imaging. *Chemistry* **24**, 11386-11392, doi:10.1002/chem.201801444 (2018).

224 González-Mira, E. (International Conference on Nanomedicine and Nanobiotechnology 2017, 2017).

225 Cabrera, I. *Nanovesicle-bioactive conjugates to be used as nanomedicines, prepared by one-step scalable method using CO2-expanded solvents.*, Universitat de Barcelona, (2013).

226 Isomaa, B. & Bjondahl, K. Toxicity and pharmacological properties of surface-active alkyltrimethylammonium bromides in the rat. *Acta Pharmacol Toxicol (Copenh)* **47**, 17-23, doi:10.1111/j.1600-0773.1980.tb02019.x (1980).

227 Gu, Z., Chang, M., Fan, Y., Shi, Y. & Lin, G. NGR-modified pH-sensitive liposomes for controlled release and tumor target delivery of docetaxel. *Colloids Surf B Biointerfaces* **160**, 395-405, doi:10.1016/j.colsurfb.2017.09.052 (2017).

228 Liang, L., Fu, J. & Qiu, L. Design of pH-Sensitive Nanovesicles via Cholesterol Analogue Incorporation for Improving in Vivo Delivery of Chemotherapeutics. *ACS Appl Mater Interfaces* **10**, 5213-5226, doi:10.1021/acsami.7b16891 (2018).

229 Lechanteur, A. *et al.* Cationic Liposomes Carrying siRNA: Impact of Lipid Composition on Physicochemical Properties, Cytotoxicity and Endosomal Escape. *Nanomaterials (Basel)* **8**, doi:10.3390/nano8050270 (2018).

230 Tam, Y. Y., Chen, S. & Cullis, P. R. Advances in Lipid Nanoparticles for siRNA Delivery. *Pharmaceutics* **5**, 498-507, doi:10.3390/pharmaceutics5030498 (2013).

231 Semple, S. C. *et al.* Rational design of cationic lipids for siRNA delivery. *Nat Biotechnol* **28**, 172-176, doi:10.1038/nbt.1602 (2010).

232 Foroozandeh, P. & Aziz, A. A. Insight into Cellular Uptake and Intracellular Trafficking of Nanoparticles. *Nanoscale Res Lett* **13**, 339, doi:10.1186/s11671-018-2728-6 (2018).

233 Mahmoudi, M. *et al.* Interaction of stable colloidal nanoparticles with cellular membranes. *Biotechnol Adv* **32**, 679-692, doi:10.1016/j.biotechadv.2013.11.012 (2014).

234 Kulig, W. *et al.* How well does cholesteryl hemisuccinate mimic cholesterol in saturated phospholipid bilayers? *J Mol Model* **20**, 2121, doi:10.1007/s00894-014-2121-z (2014).

235 Xia, Y., Tian, J. & Chen, X. Effect of surface properties on liposomal siRNA delivery. *Biomaterials* **79**, 56-68, doi:10.1016/j.biomaterials.2015.11.056 (2016).

236 Hillaireau, H. & Couvreur, P. Nanocarriers' entry into the cell: relevance to drug delivery. *Cell Mol Life Sci* **66**, 2873-2896, doi:10.1007/s00018-009-0053-z (2009).

237 Salatin, S., Maleki Dizaj, S. & Yari Khosroushahi, A. Effect of the surface modification, size, and shape on cellular uptake of nanoparticles. *Cell Biol Int* **39**, 881-890, doi:10.1002/cbin.10459 (2015).

238 Wang, Y., Miao, L., Satterlee, A. & Huang, L. Delivery of oligonucleotides with lipid nanoparticles. *Adv Drug Deliv Rev* **87**, 68-80, doi:10.1016/j.addr.2015.02.007 (2015).

239 Gumi-Audenis, B. *et al.* Pulling lipid tubes from supported bilayers unveils the underlying substrate contribution to the membrane mechanics. *Nanoscale* **10**, 14763-14770, doi:10.1039/c8nr03249a (2018).

240 Hosta-Rigau, L., Zhang, Y., Teo, B. M., Postma, A. & Stadler, B. Cholesterol--a biological compound as a building block in bionanotechnology. *Nanoscale* **5**, 89-109, doi:10.1039/c2nr32923a (2013).

241 Kolasinac, R., Kleusch, C., Braun, T., Merkel, R. & Csiszar, A. Deciphering the Functional Composition of Fusogenic Liposomes. *Int J Mol Sci* **19**, doi:10.3390/ijms19020346 (2018).

242 Pozzi, D. *et al.* Mechanistic evaluation of the transfection barriers involved in lipid-mediated gene delivery: interplay between nanostructure and composition. *Biochim Biophys Acta* **1838**, 957-967, doi:10.1016/j.bbamem.2013.11.014 (2014).

243 Rodriguez-Pulido, A., Ortega, F., Llorca, O., Aicart, E. & Junquera, E. A physicochemical characterization of the interaction between DC-Chol/DOPE cationic liposomes and DNA. *J Phys Chem B* **112**, 12555-12565, doi:10.1021/jp804066t (2008).

244 Chauhan, A. S., Diwan, P. V., Jain, N. K. & Tomalia, D. A. Unexpected in vivo anti-inflammatory activity observed for simple, surface functionalized poly(amidoamine) dendrimers. *Biomacromolecules* **10**, 1195-1202, doi:10.1021/bm9000298 (2009).

245 Frohlich, E. The role of surface charge in cellular uptake and cytotoxicity of medical nanoparticles. *Int J Nanomedicine* **7**, 5577-5591, doi:10.2147/IJN.S36111 (2012).

246 Kong, B., Seog, J. H., Graham, L. M. & Lee, S. B. Experimental considerations on the cytotoxicity of nanoparticles. *Nanomedicine (Lond)* **6**, 929-941, doi:10.2217/nnm.11.77 (2011).

247 Wang, J., Lu, Z., Wientjes, M. G. & Au, J. L. Delivery of siRNA therapeutics: barriers and carriers. *AAPS J* **12**, 492-503, doi:10.1208/s12248-010-9210-4 (2010).

248 Ozpolat, B., Sood, A. K. & Lopez-Berestein, G. Liposomal siRNA nanocarriers for cancer therapy. *Adv Drug Deliv Rev* **66**, 110-116, doi:10.1016/j.addr.2013.12.008 (2014).

249 Omedes Pujol, M., Coleman, D. J., Allen, C. D., Heidenreich, O. & Fulton, D. A. Determination of key structure-activity relationships in siRNA delivery with a mixed micelle system. *J Control Release* **172**, 939-945, doi:10.1016/j.jconrel.2013.10.013 (2013).

250 Zhu, C. *et al.* Co-delivery of siRNA and paclitaxel into cancer cells by biodegradable cationic micelles based on PDMAEMA-PCL-PDMAEMA triblock copolymers. *Biomaterials* **31**, 2408-2416, doi:10.1016/j.biomaterials.2009.11.077 (2010).

251 Alshehri, A., Grabowska, A. & Stolnik, S. Pathways of cellular internalisation of liposomes delivered siRNA and effects on siRNA engagement with target mRNA and silencing in cancer cells. *Sci Rep* **8**, 3748, doi:10.1038/s41598-018-22166-3 (2018).

252 Gujrati, M. *et al.* Multifunctional cationic lipid-based nanoparticles facilitate endosomal escape and reduction-triggered cytosolic siRNA release. *Mol Pharm* **11**, 2734-2744, doi:10.1021/mp400787s (2014).

253 Murugan, K. *et al.* Parameters and characteristics governing cellular internalization and trans-barrier trafficking of nanostructures. *Int J Nanomedicine* **10**, 2191-2206, doi:10.2147/IJN.S75615 (2015).

254 Guo, P. *et al.* Nanoparticle elasticity directs tumor uptake. *Nat Commun* **9**, 130, doi:10.1038/s41467-017-02588-9 (2018).

255 Zhang, X. X., McIntosh, T. J. & Grinstaff, M. W. Functional lipids and lipoplexes for improved gene delivery. *Biochimie* **94**, 42-58, doi:10.1016/j.biochi.2011.05.005 (2012).

256 Sahay, G., Alakhova, D. Y. & Kabanov, A. V. Endocytosis of nanomedicines. *J Control Release* **145**, 182-195, doi:10.1016/j.jconrel.2010.01.036 (2010).

257 Dowdy, S. F. Overcoming cellular barriers for RNA therapeutics. *Nat Biotechnol* **35**, 222-229, doi:10.1038/nbt.3802 (2017).

258 Jones, C. H., Chen, C. K., Ravikrishnan, A., Rane, S. & Pfeifer, B. A. Overcoming nonviral gene delivery barriers: perspective and future. *Mol Pharm* **10**, 4082-4098, doi:10.1021/mp400467x (2013).

259 Casey, J. R., Grinstein, S. & Orlowski, J. Sensors and regulators of intracellular pH. *Nat Rev Mol Cell Biol* **11**, 50-61, doi:10.1038/nrm2820 (2010).

260 Varkouhi, A. K., Scholte, M., Storm, G. & Haisma, H. J. Endosomal escape pathways for delivery of biologicals. *J Control Release* **151**, 220-228, doi:10.1016/j.jconrel.2010.11.004 (2011).

261 Cardarelli, F., Pozzi, D., Bifone, A., Marchini, C. & Caracciolo, G. Cholesterol-dependent macropinocytosis and endosomal escape control the transfection efficiency of lipoplexes in CHO living cells. *Mol Pharm* **9**, 334-340, doi:10.1021/mp200374e (2012).

262 Astrada, S., Fernandez Masso, J. R., Vallespi, M. G. & Bollati-Fogolin, M. Cell Penetrating Capacity and Internalization Mechanisms Used by the Synthetic Peptide CIGB-552 and Its Relationship with Tumor Cell Line Sensitivity. *Molecules* **23**, doi:10.3390/molecules23040801 (2018).

263 Eggimann, G. A. *et al.* Designed cell penetrating peptide dendrimers efficiently internalize cargo into cells. *Chem Commun (Camb)* **50**, 7254-7257, doi:10.1039/c4cc02780a (2014).

264 Pozzi, D. *et al.* Transfection efficiency boost of cholesterol-containing lipoplexes. *Biochim Biophys Acta* **1818**, 2335-2343, doi:10.1016/j.bbamem.2012.05.017 (2012).

265 Lu, J. J., Langer, R. & Chen, J. A novel mechanism is involved in cationic lipid-mediated functional siRNA delivery. *Mol Pharm* **6**, 763-771, doi:10.1021/mp900023v (2009).

266 Robson, A. L. *et al.* Advantages and Limitations of Current Imaging Techniques for Characterizing Liposome Morphology. *Front Pharmacol* **9**, 80, doi:10.3389/fphar.2018.00080 (2018).

267 Ivanov, A. I. Pharmacological inhibition of endocytic pathways: is it specific enough to be useful? *Methods Mol Biol* **440**, 15-33, doi:10.1007/978-1-59745-178-9_2 (2008).

268 Vercauteren, D. *et al.* The use of inhibitors to study endocytic pathways of gene carriers: optimization and pitfalls. *Mol Ther* **18**, 561-569, doi:10.1038/mt.2009.281 (2010).

269 Zhang, J., Zhu, X., Jin, Y., Shan, W. & Huang, Y. Mechanism study of cellular uptake and tight junction opening mediated by goblet cell-specific trimethyl chitosan nanoparticles. *Mol Pharm* **11**, 1520-1532, doi:10.1021/mp400685v (2014).

270 Russell, D. G., Vanderven, B. C., Glennie, S., Mwandumba, H. & Heyderman, R. S. The macrophage marches on its phagosome: dynamic assays of phagosome function. *Nat Rev Immunol* **9**, 594-600, doi:10.1038/nri2591 (2009).

271 Mauthe, M. *et al.* Chloroquine inhibits autophagic flux by decreasing autophagosome-lysosome fusion. *Autophagy* **14**, 1435-1455, doi:10.1080/15548627.2018.1474314 (2018).

272 Wolfram, J. *et al.* A chloroquine-induced macrophage-preconditioning strategy for improved nanodelivery. *Sci Rep* **7**, 13738, doi:10.1038/s41598-017-14221-2 (2017).

273 Jang, M., Kim, J. H., Nam, H. Y., Kwon, I. C. & Ahn, H. J. Design of a platform technology for systemic delivery of siRNA to tumours using rolling circle transcription. *Nat Commun* **6**, 7930, doi:10.1038/ncomms8930 (2015).

274 Bartlett, D. W., Su, H., Hildebrandt, I. J., Weber, W. A. & Davis, M. E. Impact of tumor-specific targeting on the biodistribution and efficacy of siRNA nanoparticles measured by multimodality in vivo imaging. *Proc Natl Acad Sci U S A* **104**, 15549-15554, doi:10.1073/pnas.0707461104 (2007).

275 Ruponen, M., Yla-Herttuala, S. & Urtti, A. Interactions of polymeric and liposomal gene delivery systems with extracellular glycosaminoglycans: physicochemical and transfection studies. *Biochim Biophys Acta* **1415**, 331-341, doi:10.1016/s0005-2736(98)00199-0 (1999).

276 Raja, M. A., Katas, H. & Jing Wen, T. Stability, Intracellular Delivery, and Release of siRNA from Chitosan Nanoparticles Using Different Cross-Linkers. *PLoS One* **10**, e0128963, doi:10.1371/journal.pone.0128963 (2015).

277 Persi, E. *et al.* Systems analysis of intracellular pH vulnerabilities for cancer therapy. *Nat Commun* **9**, 2997, doi:10.1038/s41467-018-05261-x (2018).

278 Webb, B. A., Chimenti, M., Jacobson, M. P. & Barber, D. L. Dysregulated pH: a perfect storm for cancer progression. *Nat Rev Cancer* **11**, 671-677, doi:10.1038/nrc3110 (2011).

279 Hanahan, D. & Weinberg, R. A. Hallmarks of cancer: the next generation. *Cell* **144**, 646-674, doi:10.1016/j.cell.2011.02.013 (2011).

280 Anselmo, A. C. & Mitragotri, S. Nanoparticles in the clinic. *Bioeng Transl Med* **1**, 10-29, doi:10.1002/btm2.10003 (2016).

281 Hua, S., de Matos, M. B. C., Metselaar, J. M. & Storm, G. Current Trends and Challenges in the Clinical Translation of Nanoparticulate Nanomedicines: Pathways for Translational Development and Commercialization. *Front Pharmacol* **9**, 790, doi:10.3389/fphar.2018.00790 (2018).

282 Shi, J., Kantoff, P. W., Wooster, R. & Farokhzad, O. C. Cancer nanomedicine: progress, challenges and opportunities. *Nat Rev Cancer* **17**, 20-37, doi:10.1038/nrc.2016.108 (2017).

283 Ernsting, M. J., Murakami, M., Roy, A. & Li, S. D. Factors controlling the pharmacokinetics, biodistribution and intratumoral penetration of nanoparticles. *J Control Release* **172**, 782-794, doi:10.1016/j.jconrel.2013.09.013 (2013).

284 Bhattacharya, S. & Haldar, S. Interactions between cholesterol and lipids in bilayer membranes. Role of lipid headgroup and hydrocarbon chain-backbone linkage. *Biochim Biophys Acta* **1467**, 39-53, doi:10.1016/s0005-2736(00)00196-6 (2000).

285 Carrillo-Carrion, C., Carril, M. & Parak, W. J. Techniques for the experimental investigation of the protein corona. *Curr Opin Biotechnol* **46**, 106-113, doi:10.1016/j.copbio.2017.02.009 (2017).

286 Kharazian, B., Hadipour, N. L. & Ejtehadi, M. R. Understanding the nanoparticle-protein corona complexes using computational and experimental methods. *Int J Biochem Cell Biol* **75**, 162-174, doi:10.1016/j.biocel.2016.02.008 (2016).

287 Ritz, S. *et al.* Protein corona of nanoparticles: distinct proteins regulate the cellular uptake. *Biomacromolecules* **16**, 1311-1321, doi:10.1021/acs.biomac.5b00108 (2015).

288 Longmire, M., Choyke, P. L. & Kobayashi, H. Clearance properties of nano-sized particles and molecules as imaging agents: considerations and caveats. *Nanomedicine (Lond)* **3**, 703-717, doi:10.2217/17435889.3.5.703 (2008).

289 Griffin, B. T. *et al.* Pharmacokinetic, pharmacodynamic and biodistribution following oral administration of nanocarriers containing peptide and protein drugs. *Adv Drug Deliv Rev* **106**, 367-380, doi:10.1016/j.addr.2016.06.006 (2016).

290 Martina, M. S. *et al.* The in vitro kinetics of the interactions between PEG-ylated magnetic-fluid-loaded liposomes and macrophages. *Biomaterials* **28**, 4143-4153, doi:10.1016/j.biomaterials.2007.05.025 (2007).

291 Decuzzi, P. *et al.* Size and shape effects in the biodistribution of intravascularly injected particles. *J Control Release* **141**, 320-327, doi:10.1016/j.jconrel.2009.10.014 (2010).

292 Huang, J. L. *et al.* Lipoprotein-biomimetic nanostructure enables efficient targeting delivery of siRNA to Ras-activated glioblastoma cells via macropinocytosis. *Nat Commun* **8**, 15144, doi:10.1038/ncomms15144 (2017).

293 Golombek, S. K. *et al.* Tumor targeting via EPR: Strategies to enhance patient responses. *Adv Drug Deliv Rev* **130**, 17-38, doi:10.1016/j.addr.2018.07.007 (2018).

294 Youn, Y. S. & Bae, Y. H. Perspectives on the past, present, and future of cancer nanomedicine. *Adv Drug Deliv Rev* **130**, 3-11, doi:10.1016/j.addr.2018.05.008 (2018).

295 Bazak, R., Houri, M., El Achy, S., Kamel, S. & Refaat, T. Cancer active targeting by nanoparticles: a comprehensive review of literature. *J Cancer Res Clin Oncol* **141**, 769-784, doi:10.1007/s00432-014-1767-3 (2015).

296 Brignole, C. *et al.* Immune cell-mediated antitumor activities of GD2-targeted liposomal c-myb antisense oligonucleotides containing CpG motifs. *J Natl Cancer Inst* **96**, 1171-1180, doi:10.1093/jnci/djh221 (2004).

297 Gholamin, S. *et al.* GD2-targeted immunotherapy and potential value of circulating microRNAs in neuroblastoma. *J Cell Physiol* **233**, 866-879, doi:10.1002/jcp.25793 (2018).

298 Wondimu, A. *et al.* Peptides mimicking GD2 ganglioside elicit cellular, humoral and tumor-protective immune responses in mice. *Cancer Immunol Immunother* **57**, 1079-1089, doi:10.1007/s00262-007-0439-4 (2008).

299 Sait, S. & Modak, S. Anti-GD2 immunotherapy for neuroblastoma. *Expert Rev Anticancer Ther* **17**, 889-904, doi:10.1080/14737140.2017.1364995 (2017).

300 Riemer, A. B. *et al.* Induction of IgG antibodies against the GD2 carbohydrate tumor antigen by vaccination with peptide mimotopes. *Eur J Immunol* **36**, 1267-1274, doi:10.1002/eji.200535279 (2006).

8. PUBLICATIONS AND PATENTS

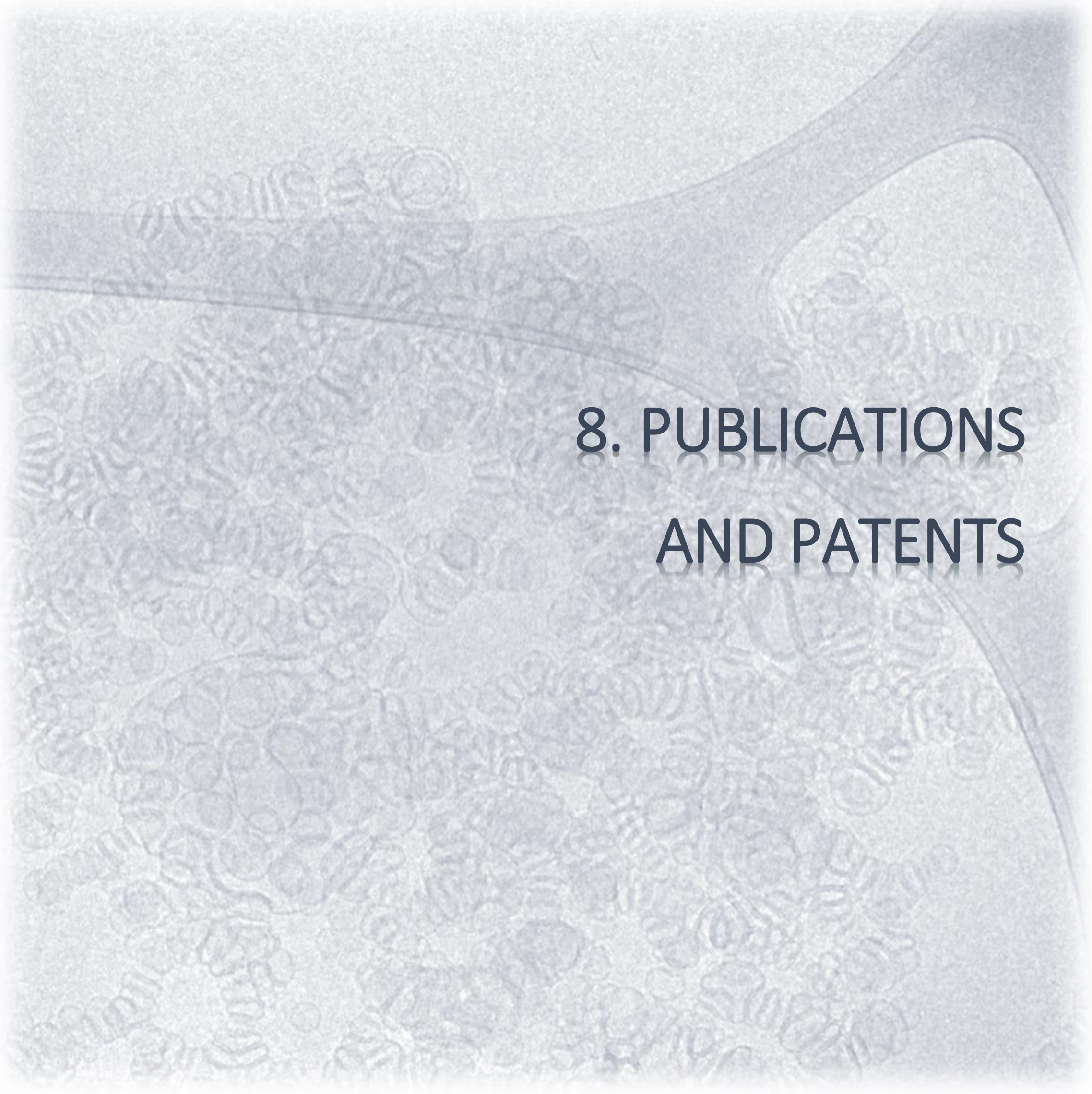

8. PUBLICATIONS

- **Boloix A**, Feiner-Gracia N, Segovia N, Köber M, Soriano A, Roma J, Sánchez de Toledo J, Gallego S, Veciana J, Albertazzi L, Segura MF, Ventosa N. Quatsomes as novel nanocarrier for clinical delivery of small RNAs. 2019. *Manuscript in preparation*.

- Soriano A, Masanas M, **Boloix A**, Masiá N, París-Coderch L, Piskareva O, Jiménez C, Henrich KO, Roma J, Westermann F, Stallings RL, Sábado C, de Toledo JS, Santamaria A, Gallego S, Segura MF. Functional high-throughput screening reveals miR-323a-5p and miR-342-5p as new tumor-suppressive microRNA for neuroblastoma. Cell Mol Life Sci. 2019 Jun;76(11):2231-2243.

- **Boloix A**, París-Coderch L, Soriano A, Roma J, Gallego S, Sánchez de Toledo J, Segura MF. Novel micro RNA-based therapies for the treatment of neuroblastoma. An Pediatr (Barc). 2016 Aug;85(2):109.e1-109.e6. Review.

- **Boloix A**, Masanas M, Jiménez C, Antonelli R, Soriano A, Roma J, Sánchez de Toledo J, Gallego S, Segura MF. Potential use of the lncRNA PVT1 as a prognostic and therapeutic target in pediatric cancer. Frontiers in Oncology. 2019. *Under revision*.

Papers in preparation:

- “Cellular dynamics of Quatsomes and miRNA conjugates”.

PATENTS

- Inventors: Ventosa N, Veciana J, Boloix A, Segura MF, Soriano A, Gallego S, Sánchez de Toledo J, Segovia N. Title: Nanovesicles and its use in cancer treatment. Application nº EP19382372.1. Priority date: 13/05/2019. Holder entity: VHIR/CSIC/CIBER.

9. ANNEXES

9. ANNEXES

Supplementary Figures

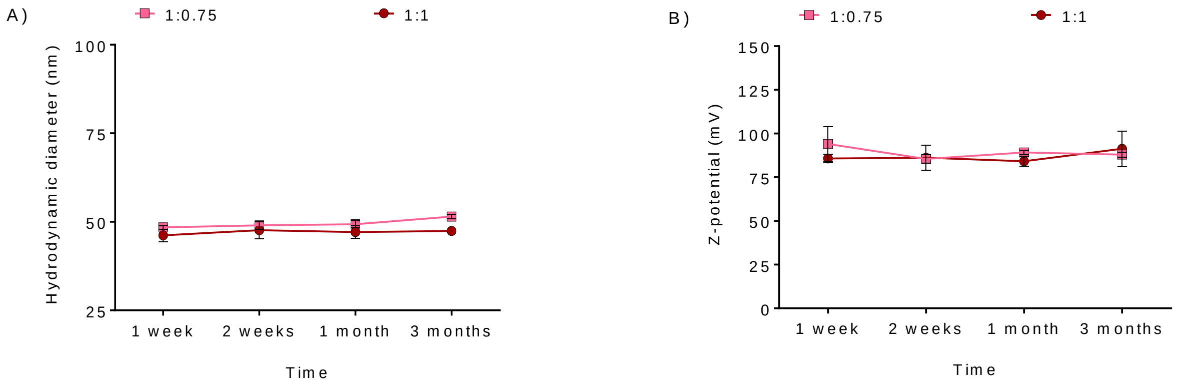

Figure A1. Both QS_0 systems produced at molar ratios 1:0.75 and 1:1, between the sterol and the surfactant, had good physicochemical properties after DELOS-SUSP. A-B) Hydrodynamic diameter **(A)** and Z-potential **(B)** of QS_0 prepared at two molar ratios. Graph represents the average of three different preparations ± SD.

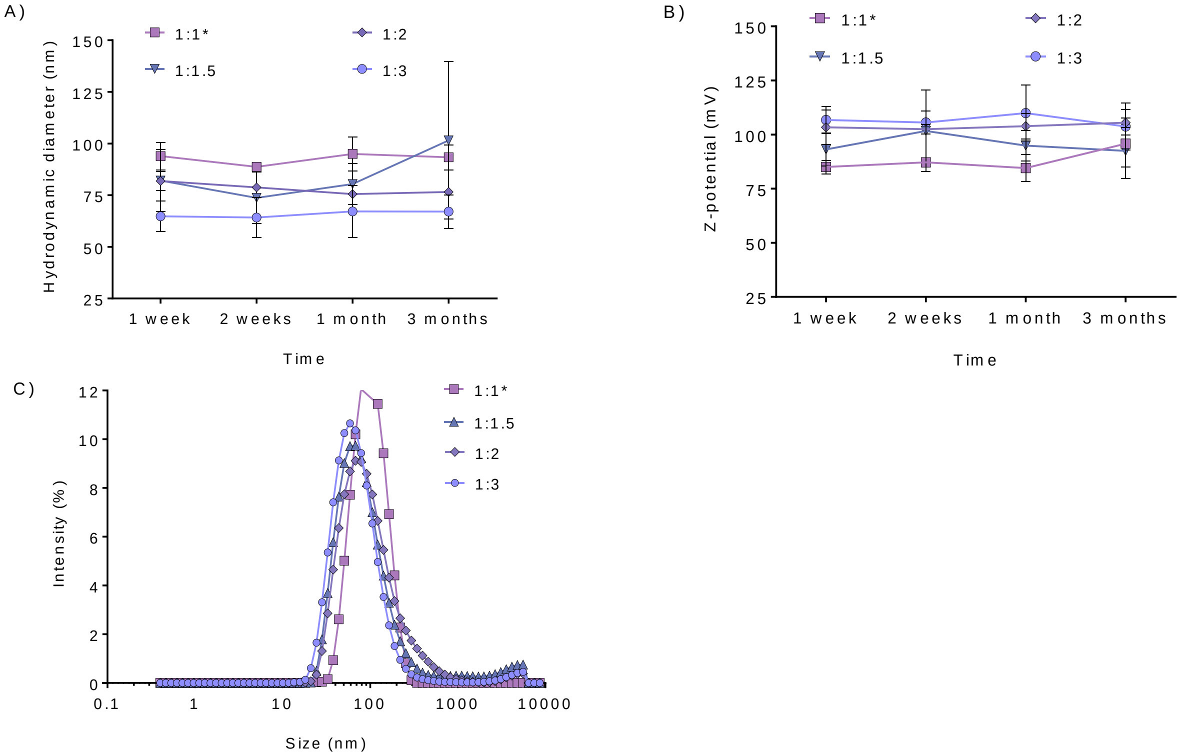

Figure A2. Comparison of the physicochemical properties of QS_1 at molar ratios 1:1.5, 1:2 and 1:3, between the sterol and the surfactant, produced by DELOS-SUSP and the nanostructures produced by sonication (at molar ratio 1:1). A-B) Hydrodynamic diameter **(A)** and Z-potential **(B)** of QS_1 prepared at various molar ratios by DELOS-SUSP or sonication. **C)** Particle size distributions measured by DLS after one week of QS_1 preparation. Graph represents the mean of triplicate samples ± SD.

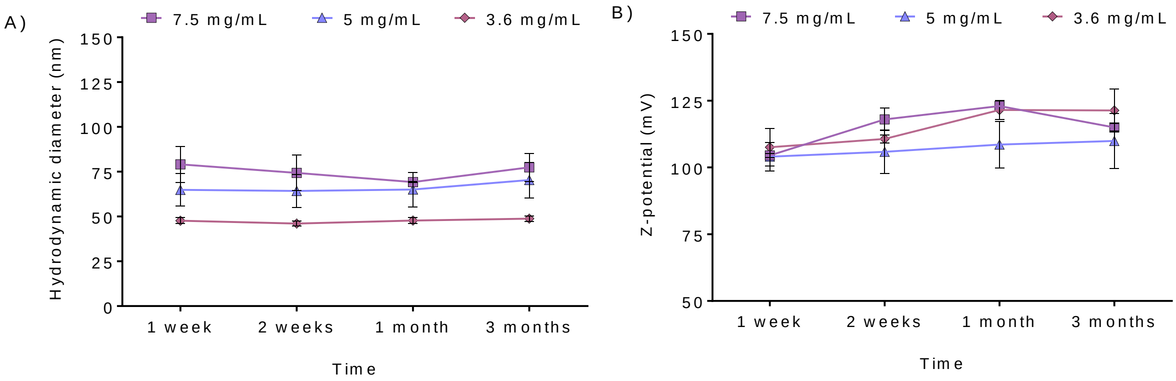

Figure A3. Physicochemical properties (hydrodynamic diameter (A) and Z-potential (B)) of QS$_1$ over time, after DELOS-SUSP preparation. Graph represents the mean of at least triplicate samples ± SD.

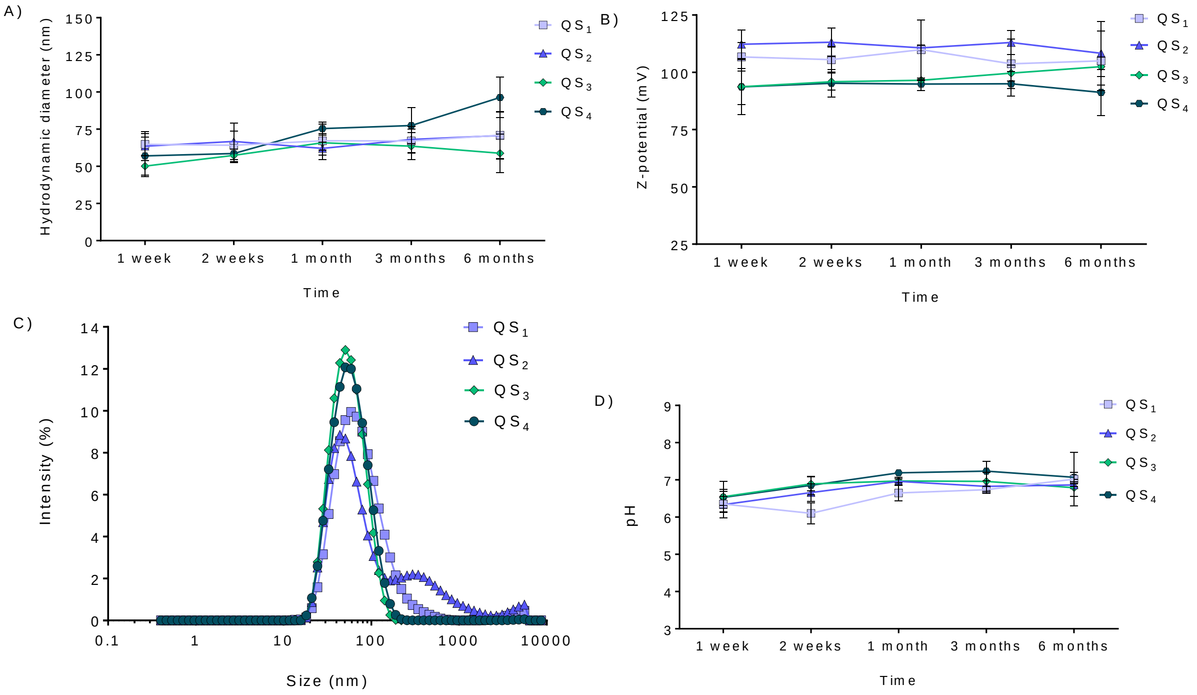

Figure A4. QS presented good physicochemical properties over time, such as small size, positive charge and slightly acidic-neutral pH after DELOS-SUSP preparation. A-B) Hydrodynamic diameter **(A)** and surface charge density (Z-potential) stability **(B)** of the indicated QS$_{1-4}$ systems determined through DLS technique over time. Each line represents the mean ± SD from the three independent samples. **C)** Particle size distribution of QS$_{1-4}$. Each curve are the mean of at least triplicate experiments. **D)** pH stability of the QS$_{1-4}$ systems over time. Error determined by the standard deviation of at least duplicate samples.

Supplementary Tables

Table A1. Polidispersity index of QS_1 prepared at different initial concentrations after DELOS-SUSP, diafiltration and then concentrationd.

Polidispersity index (PDI)		1 week	2 weeks	1 month	3 months
QS_1 at 7.5 mg/mL	DELOS-SUSP	0.34 ± 0.02	0.35 ± 0.01	0.36 ± 0.003	0.36 ± 0.01
	Diafiltrated	0.30 ± 0.00	0.33 ± 0.02	0.29 ± 0.00	0.28 ± 0.02
	Concentrated (5X)	0.50 ± 0.03	0.48 ± 0.03	0.45 ± 0.02	0.48 ± 0.01
QS_1 at 5 mg/mL	DELOS-SUSP	0.25 ± 0.05	0.25 ± 0.05	0.26 ± 0.05	0.29 ± 0.06
	Diafiltrated	0.28 ± 0.05	0.26 ± 0.02	0.29 ± 0.06	0.37 ± 0.07
	Concentrated (10X)	0.47 ± 0.05	0.47 ± 0.09	0.49 ± 0.06	0.50 ± 0.06
QS_1 at 3.6 mg/mL	DELOS-SUSP	0.20 ± 0.01	0.33 ± 0.92	0.29 ± 0.00	0.28 ± 0.02
	Diafiltrated	0.30 ± 008	0.30 ± 0.06	0.34 ± 0.04	0.43 ± 0.02
	Concentrated (10X)	0.47 ± 0.20	0.50 ± 0.10	0.48 ± 0.10	0.49 ± 0.18

Table A2. Polidispersity index stability over time of QS_0 prepared by DELOS-SUSP, diafiltration and then concentration.

Polidispersity index (PDI)		1 week	2 weeks	1 month	3 months
QS_0 at 6.1 mg/mL	DELOS-SUSP	0.16 ± 0.01	0.17 ± 0.02	0.15 ± 0.00	0.19 ± 0.01
	Diafiltrated	0.36 ± 0.08	0.38 ± 0.06	0.40 ± 0.08	0.36 ± 0.08
	Concentrated (9X)	0.62 ± 0.11	0.64 ± 0.21	0.56 ± 0.20	0.58 ± 0.27

Table A3. Polidispersity index stability over time of QS_{1-4} prepared by DELOS-SUSP and diafiltration.

PDI stability		1 week	2 weeks	1 month	3 months	6 months
QS_1	DELOS-SUSP	0.24 ± 0.02	0.24 ± 0.02	0.24 ± 0.02	0.23 ± 0.11	0.24 ± 0.03
	Diafiltrated	0.28 ± 0.04	0.27 ± 0.02	0.29 ± 0.06	0.33 ± 0.07	0.61 ± 0.13
QS_2	DELOS-SUSP	0.40 ± 0.14	0.48 ± 0.13	0.4 ± 0.04	0.34 ± 0.01	0.37 ± 0.15
	Diafiltrated	0.48 ± 0.09	0.43 ± 0.05	0.39 ± 0.06	0.39 ± 0.03	0.46 ± 0.14
QS_3	DELOS-SUSP	0.15 ± 0.01	0.15 ± 0.01	0.14 ± 0.02	0.14 ± 0.02	0.13 ± 0.01
	Diafiltrated	0.27 ± 0.02	0.25 ± 0.01	0.26 ± 0.01	0.24 ± 0.03	0.25 ± 0.02
QS_4	DELOS-SUSP	0.19 ± 0.05	0.15 ± 0.02	0.22 ± 0.14	0.19 ± 0.12	0.14 ± 0.04
	Diafiltrated	0.29 ± 0.04	0.24 ± 0.02	0.23 ± 0.05	0.29 ± 0.07	0.27 ± 0.04

MINISTERIO
DE INDUSTRIA, ENERGÍA
Y TURISMO

Oficina Española
de Patentes y Marcas

Acknowledgement of receipt

We hereby acknowledge receipt of your request for grant of a European patent as follows:

Submission number	300318252	
Application number	EP19382372.1	
File No. to be used for priority declarations	EP19382372	
Date of receipt	13 May 2019	
Your reference	P4830EP00	
Applicant	FUNDACIÓ HOSPITAL UNIVERSITARI VALL D'HEBRON - INSTITUT DE RECERCA	
Country	ES	
Title	NANOVESICLES AND ITS USE FOR NUCLEIC ACID DELIVERY	
Documents submitted	package-data.xml	ep-request.xml
	application-body.xml	ep-request.pdf (5 p.)
	OLF-ARCHIVE.zip\00 P4830EP00 memories.zip	SPECTRANONEP.pdf\Título y resumen en castellano P4830EP00.pdf (1 p.)
	SPECEPO-1.pdf\20190510105207-P4830EP00 v FINAL10052019.pdf (51 p.)	SEQLTXT.txt\P4830EP00 sequence listing 09052019_ST25.txt
	OTHER-1.pdf\20190513 To EUROPEAN PATENT OFFICE.pdf (1 p.)	f1002-1.pdf (2 p.)
Submitted by	CN=Mireia Cama 33265	
Method of submission	Online	
Date and time receipt generated	13 May 2019, 13:21:54 (CEST)	

/Madrid, Oficina Receptora/

Form 1002 - 1: Public inventor(s)

Designation of inventor

User reference: P4830EP00
Application No:

Public

Inventor	
Name:	SEGURA GINARD Francisco Miguel
Address:	Passeig Vall d'Hebron, 119-129 08035 BARCELONA Spain
The applicant has acquired the right to the European patent:	As employer
Inventor	
Name:	GALLEGO MELCON Soledad
Address:	Passeig Vall d'Hebron, 119-129 08035 BARCELONA Spain
The applicant has acquired the right to the European patent:	As employer
Inventor	
Name:	SÁNCHEZ DE TOLEDO CODINA Josep
Address:	Passeig Vall d'Hebron, 119-129 08035 BARCELONA Spain
The applicant has acquired the right to the European patent:	As employer
Inventor	
Name:	SORIANO FERNÁNDEZ Aroa
Address:	Passeig Vall d'Hebron, 119-129 08035 BARCELONA Spain
The applicant has acquired the right to the European patent:	As employer
Inventor	
Name:	VENTOSA RULL Nora
Address:	Institut de Ciència de Materials de Barcelona (ICMAB - CSIC) Campus de la UAB 08193 BELLATERRA Spain
The applicant has acquired the right to the European patent:	As employer

Inventor	
Name:	VECIANA MIRÓ Jaume
Address:	Institut de Ciència de Materials de Barcelona (ICMAB - CSIC) Campus de la UAB 08193 BELLATERRA Spain
The applicant has acquired the right to the European patent:	As employer
Inventor	
Name:	BOLOIX AMENÓS Ariadna
Address:	Institut de Ciència de Materials de Barcelona (ICMAB - CSIC) Campus de la UAB 08193 BELLATERRA Spain
The applicant has acquired the right to the European patent:	As successor in title
Inventor	
Name:	SEGOVIA RAMOS Nathaly Verónica
Address:	Passeig Camp del Roure 8 Esc. E, 4º 3ª 08227 TERRASSA Spain
The applicant has acquired the right to the European patent:	As employer

Signature(s)

Place:	Barcelona
Date:	13 May 2019
Signed by:	Mireia Cama 33265
Association:	ZBM Patents - Zea, Barlocci & Markvardsen
Representative name:	Mireia Cama
Capacity:	(Representative)